

The Development of Smart 4D Materials Utilising Smart Temperature Responsive Polymers

A thesis submitted to the Technological University of the Shannon:

Midlands Midwest

For the degree of Doctor of Philosophy

By

Shuo Zhuo, BSc.



Based on the research performed under the supervision of
Mr. Gavin Keane, Dr. Joe Geever & Dr. Luke Geever

Polymer, Recycling, Industrial, Sustainability and Manufacturing Centre
Technological University of the Shannon: Midlands Midwest,
Athlone Campus,
University Road,
Ireland.

DECLARATION

I hereby declare that this thesis, submitted to the Technological University of the Shannon: Midlands Midwest for consideration for the degree of Doctor of Philosophy, is a result of my own work and has not in the same or altered form, been presented to this university or any other university in support for any degree other than for which I am now a candidate.

Shuo Zhuo

Acknowledgements

The work presented in this thesis has been carried out under the direction of Dr. Luke Geever in the Material Research Institute group. The research was supported by a grant from Athlone Institute of Technology's President Seed Fund and is gratefully acknowledged. First and foremost, I wish to acknowledge the patience and guidance of my supervisory team: Dr. Luke Geever, Dr. Joe Geever, and Mr. Gavin Keane. Thanks for allowing me the opportunity to carry out this work. As my principal supervisor, Luke was the first person I encountered when I began my polymer research journey. As a Chinese student, it has been a challenge to meet the criteria for a doctorate. A really big thanks for his kindness and patience which always motivated me to overcome the difficulties and spurred me forward in my studies. Luke, you are absolutely stunning, thank you for everything — thank you for helping me reach the top of the mountain.

I also want to thank all the members of our group — Elaine, Billy, Declan, Maya, Shane, Gilberto, Colette and all the other postgraduates I met in the Hub — for all the memories and assistance. I would like to give a special thanks to my best Irish friend, the little girl Elaine Halligan; thank you for all the proof-reading she had to endure, thank you for making me feel at home, and I will never forget the fun moments when you were learning Chinese. Special thanks to Dr. Zhi Cao and Guangming Yan for all the training and guidance. I also want to show appreciation for Dr. Crevan O'Donnell and Dr. Mark Lynch, for their patience and help with all issues resolved in the lab.

Finally, my family, my mom and dad — Lihong Jiang and Pinghong Zhuo — for their moral, financial and spiritual support throughout the years. Thank you for giving me the opportunity to study abroad. It gave me an amazing life in Ireland. I would most like to thank my girlfriend, Xiaoning Wang, and my cat Vava. Thank you for letting me discover

the joy of life, and thank you for your companionship and encouragement throughout the sleepless nights and anxiety during this thesis. I love you guys! Thank you all.

Abstract

This study involved the preparation and optimisation of novel temperature-sensitive hydrogel copolymer and terpolymer systems, and also the development and evaluation of smart hydrogels with the potential for 4D printing and shape-shifting behaviours.

In this work, N-vinylcaprolactam (NVCL) was chosen as the base polymer. NVCL is a temperature-responsive polymer which is often used for biomedical applications due to its biocompatibility, solubility and non-toxic features. However, studies of the use of NVCL for developing 4D material have been limited. This polymer was bonded with different types and concentrations of photoinitiators, crosslinkers, and other polymers to obtain the optimum ratio, with the most suitable properties and performance for 3D printing. UV polymerisation, a process with similar mechanisms to Stereolithography (SLA) printing, was first employed for the preparation of samples. The cured polymers were characterised by the following techniques: The chemical structure of the hydrogels was confirmed using Fourier transform infrared spectroscopy (FTIR). Four techniques were used to determine the lower critical solution temperature (LCST) of the polymers in aqueous solution: i) cloud point analysis, ii) UV-spectrometry, iii) differential scanning calorimetry and iv) rheology. Pulsatile swelling studies were performed to investigate the effect of the transition temperature, monomer feed ratio and crosslinker content on the swelling size and quality. The mechanical properties of the polymers were detected by tensile tests. Goniometry was used to probe the water absorption capacity of the samples. Results indicated that the physically and chemically crosslinked NVCL based polymers exhibited a tuneable LCST by modifying the contents with regard to the material composition and concentration. The LCST could be raised to 54°C and was validated by four different techniques. FTIR showed that the samples were successfully synthesised. After incorporating with the monomer N, N-dimethylacrylamide (DMAAm), the mechanical

properties improved. The copolymer P (70NVCL-30DMAAm) exhibited potential for the next stages of 4D printing trials. It exhibited outstanding swelling capabilities and was flexible to changes in size as the temperature increased or decreased.

By changing structures that can be converted in a pre-programmed manner in response to a stimulus, 3D printed materials can be modified to impart flexibility and boost utility. Four-dimensional (4D) printing is a relatively new concept that was initially reported in 2013. 4D printing refers to the idea that the shape or properties of a printed object can be changed again when an external stimulus is applied. In this study, by using a modified P (NVCL-DMAAm) candidate formulation, containing 2 wt% H-Nu 400IL, 2 wt% PEGDMA, 30 wt% DMAAm and 70 wt% NVCL, 4D printing was achieved. The same characterisation tests were applied to the 3D printed samples to compare the differences in the properties of materials between samples prepared using SLA and those prepared with UV chamber photopolymerisation.

Due to the superior properties of the shape memory polymers, a number of scholars have used the material to produce 4D printed objects in multi-material 3D printers. The printed objects are capable of demonstrating complex and magnificent changes when stimulated. However, smart hydrogels are only able to expand/contract in water. In addition, the printer used in this study was an inexpensive one and could only apply one material at a time for printing. It is difficult to develop flexible shape-shifting behaviours by using a single hydrogel material and a single material 3D printer. This study exploited a new method to utilise bilayer structures and a UV chamber system to allow hydrogel-based materials to exhibit controllable shape shifting behaviours (such as self-curving and self-bending behaviours). Although other researchers have developed similar smart structures, none have use a NVCL based polymers developed in a UV chamber system. Based on the different ways of transformation, diverse demonstrators were developed.

In summary, by constantly modifying and improving the formulation of NVCL solutions, a new ‘NVCL-based resin’ that can be used in an SLA 3D printer has been successfully synthesised. In the presence of water, the 4D printed parts were able to switch their sizes as the temperature rises and falls. In addition, by using bilayer structures, the shape shifting behaviours have also been successfully developed for hydrogel-based materials. This research not only opens up new applications for NVCL materials, but also provides a simple and fast method for the preparation of 4D materials.

Table of Contents

1	Literature Review	1
1.1	Problem statement	1
1.2	Aims and objectives of this study	3
1.3	Definition and history of hydrogels.....	4
1.3.1	Physically and chemically crosslinked hydrogels	6
1.3.2	Preparation and characteristics of hydrogels	9
1.3.3	Applications of hydrogels	11
1.4	Stimuli-responsive polymers	13
1.4.1	Temperature-responsive polymers/gels	15
1.4.2	Lower and upper critical solution temperature	16
1.4.3	Adjustment of LCST.....	19
1.5	Main polymers used in this study	20
1.5.1	N-vinylcaprolactam	20
1.5.2	Poly (N-vinylcaprolactam)	21
1.5.3	Photoinitiators.....	23
1.6	Photopolymerisation.....	25
1.7	Three-dimensional (3D) printing.....	26
1.7.1	Stereolithography (SLA)	28
1.8	Fourth-dimensional printing	30
1.8.1	Shape-shifting materials & materials used for 4D printing	32

1.8.2 The deformation mechanisms of the shape-shifting behaviours for hydrogel-based materials	36
1.9 4D printing state-of-the-art	40
2 Experimental details	43
2.1 Materials' selection.....	43
2.2 Preparation of hydrogels.....	44
2.2.1 Photopolymerisation 1	45
2.2.2 Photopolymerisation 2	46
2.2.3 Photopolymerisation 3	46
2.3 Form 2 SLA 3D printing parameters.....	47
2.4 Patterns design.....	48
2.4.1 Development of mould for complex-shaped samples	49
2.5 4D printing.....	51
2.5.1 4D printing trial with increasing Irgacure 2959 concentration.....	52
2.5.2 4D printing trial with different types of photoinitiators	52
2.5.3 4D printing trial with a stepwise increase in H-Nu 400IL concentration.....	53
2.6 Preparation of aqueous polymer and copolymer solutions.....	53
2.7 Characterisation techniques	54
2.7.1 Attenuated total reflectance Fourier Transform Infrared Spectroscopy	54
2.7.2 Phase transition temperature analysis for physically crosslinked samples.....	55
2.7.3 Phase transition temperature analysis for chemically crosslinked hydrogels	57
2.7.4 Swelling studies	57

2.7.5 Gel fraction measurement	58
2.7.6 Pulsatile swelling studies	58
2.7.7 Goniometry	59
2.7.8 Tensile test	59
2.8 Preparation of bilayer structures	60
2.8.1 The strips prototype design 1	60
2.8.2 The strips prototype design 2	61
2.8.3 The strips prototype design 3	62
2.9 Fabrication of the demonstrators	64
2.9.1 Automatic demonstrator	64
2.9.2 Toy train puller	64
2.9.3 Gripper	65
2.10 Statistical Analysis	65
3 Results and Discussion	67
3.1 Formulation development I: Synthesis, characterisation, phase transition and swelling of temperature-responsive polymers based on poly (N-vinylcaprolactam).....	67
3.1.1 Preface	67
3.1.2 Preparation of physically crosslinked xerogels	70
3.1.3 Preparation of chemically crosslinked xerogels	72
3.1.4 Attenuated total reflectance Fourier Transform Infrared Spectroscopy	74
3.1.5 Phase transition determination in solution.....	80
3.1.6 Swelling studies	85

3.1.7 Tensile test	89
3.1.8 Goniometry	89
3.1.9 Summary	91
3.2 Formulation development II: Synthesis, characterisation, phase transition and swelling of temperature-sensitive copolymer/terpolymer hydrogels	92
3.2.1 Preface	92
3.2.2 Preparation of physically and chemically crosslinked terpolymer samples	94
3.2.3 Attenuated total reflectance Fourier transform infrared spectroscopy	97
3.2.4 Phase transition determination.....	102
3.2.5 Pulsatile swelling studies	106
3.2.6 Rheological analysis	110
3.2.7 Gel fraction measurement.....	111
3.2.8 Tensile test.....	112
3.2.9 Goniometry	112
3.2.10 Summary.....	115
3.3 Synthesis of complex shaped “4D objects” and shape shifting capabilities exploration through 3D printing and photopolymerisation techniques	116
3.3.1 Preface	116
3.3.2 Photopolymerisation of the complex shaped objects with moulds.....	117
3.3.3 The synthesis of complex shaped objects via a 3D printing technique using novel formulation	119
3.3.4 Comparison of the properties of UV-cured and 4D printed samples	127
3.3.5 Attenuated total reflectance Fourier transform infrared spectroscopy	127

3.3.6	Differential scanning calorimetry	129
3.3.7	Pulsatile swelling studies on cured and printed complex shaped samples	130
3.3.8	Gel fraction measurement	134
3.3.9	Tensile tests	135
3.3.10	Goniometry	135
3.3.11	Summary	137
3.4	Use of bilayer structures in UV chamber system to develop shape shifting materials	138
3.4.1	Preface	138
3.4.2	The development of first-generation bilayer strips.....	140
3.4.3	Shape shifting behaviours detection of first-generation bilayer strips	143
3.4.4	The development of second-generation bilayer strips	146
3.4.5	Shape shifting behaviours detection of second-generation bilayer strips.....	148
3.4.6	The development of third-generation bilayer strips.....	149
3.4.7	Shape shifting behaviour detection of third-generation strips	152
3.4.8	The development of bilayer flowers	156
3.4.9	Shape shifting behaviours of bilayer flowers	158
3.4.10	Demonstration I: TUS Demonstration.....	159
3.4.11	Demonstration development II: Toy train puller	160
3.4.12	Demonstration development III: Gripper	161
3.4.13	Summary	163
4	Conclusion and Future work.....	165
4.1	Conclusion	165

4.2	Future Works	169
5	Appendices	171
5.1	Appendix A-Literature Supplement	171
5.2	Appendix B –Experimental Figures and Tables.....	180
5.2.1	DSC results	180
5.2.2	Rheology results	182
5.2.3	Swelling studies	184
5.2.4	UV spectroscopy.....	189
5.2.5	Gel fraction measurement.....	190
5.2.6	Goniometry	191
5.2.7	Tensile tests	192
5.3	Appendix C- Gantt chart workplan and works display and publish during the PhD ..	193
5.3.1	Poster	193
5.3.2	Publications.....	194
6	Bibliography	201

Abbreviations

ABS	Acrylonitrile butadiene styrene
AM	Advanced manufacture
BAPO	Bis-acylphosphine oxide
BIS	N, N-methylenebisacrylamide
BMA	Benzyl methacrylate
BPA	Bisphenol A ethoxylate dimethacrylate
C60	Carbon 60
CAD	Computer-aided design software
CMC	Carboxymethyl cellulose
CQ	Camphorquinone
CST	Critical solution temperature
DCM	Dual-component mechanism
DDS	Drug delivery system
DEGDA	Di (ethylene glycol) diacrylate
DEGDMA	Di (ethylene glycol) dimethacrylate
DGEDA	Diglycidyl ether diacrylate
DLS	Dynamic light scattering
DSC	Differential scanning calorimetry
DSM	Dual-state mechanism
FDA	Food and drug administration
FDM	Fuse deposition modelling
GRAS	Generally recognised as safe
IBOA	Isobornyl ether diacrylate

IPN	Interpenetrating polymer
KBr	Potassium bromide
KF	Potassium fluoride
KCL	Potassium chloride
KI	Potassium iodide
LCST	Lower critical solution temperature
MAA	Methacrylic acid
NFC	Nanofibrillated cellulose
NMR	Nuclear magnetic resonance
NNMBA	N, N'-methylene bis acrylamide
NVP	N-vinylpyrrolidone
P2VP	2-vinylpyridine
PA66	Polyamide 66
PAAc	Poly (acrylic acid)
PC	Polycarbonate
PCLDMA	Polycaprolactone dimethacrylate
PDMAAm	Poly (N,N-dimethylacrylamide)
PE	Polyethylene
PEG	Poly (ethylene glycol)
PEGDMA	Poly (ethylene glycol) dimethacrylate
PEO	Poly (ethylene oxide)
PHA	Poly (hydroxy alkanoates)
PHEMA	Poly (2-hydroxyethyl methacrylate)
PI	Photoinitiator
PLA	Poly(lactic acid)
PNIPAAm	Poly (N-isoropylacrylamide)

PNVCL	Poly (N-vinylcaprolctam)
PPO	Poly (propylene oxide)
PS	Polystyrene
PTM	Partial-transition mechanism
PU	Polyurethane
PUA	Polyurethane acrylate
PVA	Poly (vinyl alcohol)
RAFT	Reversible addition fragmentation chain transfer
RP	Rapid prototyping
SCPs	Shape-changing polymers
SLA	Stereolithography
SLS	Selective laser sintering
SMA	Shape memory alloy
SMC	Shape memory ceramics
SME	Shape memory effect
SMPs	Shape memory polymers
SMPCs	Shape memory polymer composites
SP	Spirobenzopyran
T _g	Glass transition temperature
T _m	Melting temperature
tBA	tert-Butyl acrylate
TPE	Thermoplastic elastomer
UCST	Upper critical solution temperature
UV	Ultraviolet
VAc	Vinyl acetate
3D	Three dimensions

List of Figures

Figure 1-1 Classification of hydrogels by different factors (Ullah et al., 2015).	6
Figure 1-2 The principle of physical and chemical crosslinking (Fajardo et al., 2013).	8
Figure 1-3 Example of mechanisms for hydrogel preparation by free radical polymerisation (Ullah et al., 2015).	10
Figure 1-4 Drug release from matrix systems (Caló & Khutoryanskiy, 2015).	12
Figure 1-5 The stimulus and responses to stimuli-responsive polymers (Schmaljohann, 2006).	14
Figure 1-6 The chemical structure of typical temperature responsive polymers: (a) Poly(N-isopropylacrylamide); (b) Poly(N,N'-diethylacryamide);(c) Poly(N-vinylcaprolactam); (d) Poly(ethylene glycol); (e) Poly(propylene oxide).	16
Figure 1-7 A plot of typical phase behaviour of polymer binary solution (Mao et al., 2016).	17
Figure 1-8 The state of the molecular chain below and above LCST (Alarcón et al., 2005)..	18
Figure 1-9 (L) Structure of NVCL determined by quantum-chemical calculation; (R) Structure of NVCL determined by x-ray (H. B. Sun et al., 2008).	21
Figure 1-10 The preparation of PNVCL by free radical polymerisation.....	22
Figure 1-11 Poly(N-vinylcaprolactam) (PNVCL) in different architectures (Norma A Cortez-Lemus & Licea-Claverie, 2016).	23
Figure 1-12 General presentation of photoinitiated polymerisation (Pan et al., 2016).	26
Figure 1-13 Schemes of two types of stereolithography setups. (L): a bottom-up system with a scanning laser & (R): a top-down setup with digital light (Melchels et al., 2010).....	29
Figure 1-14 The difference between 3D and 4D printing (Momeni et al., 2017).....	31
Figure 1-15 A summary of the types of printers, stimuli, materials and applications that have been used for 4D printing (Kuang et al., 2019).	34

Figure 1-16 Schematic illustrations of (L) one-way and two-way SME & (R) Dual and Triple-SME (Hager et al., 2015).....	35
Figure 2-1 (L) Jigsaw and (R) flower shape models designed in Solidwork.	48
Figure 2-2 (L) The printed jigsaw shape prototype & (R) the jigsaw type silicone mould.....	50
Figure 2-3 (L) The designed flower shape set in the Preform software & (R) flower shape silicone mould.	51
Figure 2-4 Polymer dissolved in the distilled water.	54
Figure 2-5 Perkin Elmer Spectrum One ATR-FTIR (left side) and FTIR spectrometer layout (right side).	55
Figure 2-6 UV-spectroscopy Synergy HT BioTek plate reader.	56
Figure 2-7 The dimensions of the dumbbell tensile bars.....	59
Figure 2-8 The first generation of strips designed in Solidworks.	61
Figure 2-9 The second generation of strips designed in Solidworks.....	62
Figure 2-10 The third generation of strips designed in the Solidworks.	63
Figure 3-1 Scheme of photopolymerisation of poly (N-vinylcaprolactam) using Irgacure 2959 and N-vinylcaprolactam.	68
Figure 3-2 Work breakdown structure for the evaluation of the effects of the different concentrations of photoinitiators and crosslinkers.	69
Figure 3-3 PNVCL xerogels fabricated using different concentrations of Igracure 2959 initiator: a) 0.1 wt%; b) 0.2 wt%; c) 0.5 wt%; d) 1 wt%; e) 2 wt%; f) 3 wt%; g) 5 wt%.	71
Figure 3-4 PNVCL xerogels fabricated using different concentrations of VA-086 initiator: a) 0.1 wt%; b) 0.5 wt%; c) 1 wt%; d) 2 wt%; e) 3 wt%.	72
Figure 3-5 Polymerisation of NVCL with PEGDMA.	73
Figure 3-6 Chemically crosslinked PNVCL polymers fabricated using different concentrations of PEGDMA: a) 0.1 wt%; b) 1 wt%; c) 2 wt%; d) 5 wt%.	74

Figure 3-7 FTIR spectra of NVCL and PNVCL. Block marks the C=C and vinyl group in NVCL monomer. These are absent in PNVCL polymer. n=2.	76
Figure 3-8 FTIR spectra of NVCL, PEGDMA and PNVCL. Block marks the C=C and vinyl group in NVCL monomer. These are absent in the PNVCL base polymers. n=2.	78
Figure 3-9 Cloud point of PNVCL samples at 10 wt% in solution with different concentrations of photoinitiator at 32°C: A. 5wt% Irgacure 2959, B. 2 wt% Irgacure 2959, C. 1 wt% Irgacure 2959, D 0.5 wt% Irgacure 2959, E 0.2wt% Irgacure 2959, F. 0.1 wt% Irgacure 2959.....	81
Figure 3-10 Cloud point analysis of PNVCL with different concentrations of photoinitiator (Irgacure 2959). n=3, P<0.05.	81
Figure 3-11 Cloud point of samples (L) PNVCL 5 wt% at 32.3°C, (R) 10 wt% at 33°C. n=3, p>0.05.....	82
Figure 3-12 UV Spectrometry illustrating the LCST of PNVCL homopolymer at different aqueous solution concentrations. n=3, p>0.05.	83
Figure 3-13 A representative thermogram illustrating the LCST of PNVCL (5 and 10 wt%) aqueous solution. n=3, p>0.05.....	84
Figure 3-14 Rheological data illustrating the LCST and gelation point of PNVCL (10 wt%) aqueous solution. n=3.	85
Figure 3-15 Swelling studies of PNVCL-PEGDMA hydrogels with 0.1-5 wt% PEGDMA crosslinker concentration at ambient temperature. n=3, p<0.05.	87
Figure 3-16 PNVCL-PEGDMA 2 wt% (C3) samples submerged in distilled water at times: A 0 hours, B 2 hours, C 24 hours, D 48 hours and E 72 hours at ambient temperature.	87
Figure 3-17 Swelling studies of PNVCL-PEGDMA hydrogels with 0.1-5 wt% PEGDMA crosslinker concentration at 50°C. n=3, p>0.05.	88
Figure 3-18 PNVCL-PEGDMA 2 wt% (C3) samples submerged in distilled water at times: A 1 hour, B 2 hours, C 6 hours, D 24 hours and E 48 hours at 50°C.....	88

Figure 3-19 The representative contact angles figures of P1 and C3 samples at 0 and 115 seconds. n=3, p<0.05.....	90
Figure 3-20 Work breakdown structure for the evaluation of the effects of the different copolymers and terpolymers.....	94
Figure 3-21 The chemical structure of NVCL based physically crosslinked copolymers and terpolymers:(a) NVCL/NVP; (b) NVCL/DMAAm; (c) NVCL/NVP/DMAAm & (d) NVCL/NVP/NIPAAm.....	95
Figure 3-22 Representative chemical structures of NVCL based chemically crosslinked copolymers: (a) NVCL/NVP & (b) NVCL/DMAAm.....	95
Figure 3-23 The appearance of (L) S7 (30DMAAm/70NVCL/2PEGDMA), (M) S18 (25NVP/25NVCL/50NIPAAm/0.1PEGDMA), &(R) S11 (65DMAAm/20NIPAAm/15NVCL) samples.	96
Figure 3-24 FTIR spectra of the constituent monomers and the S6 and S7 hydrogel copolymer. n=2.....	98
Figure 3-25 FTIR spectra of the constituent monomers and the S14, S16 and S18 hydrogel terpolymers. n=2.....	101
Figure 3-26 The cloud point of terpolymers 10 wt% aqueous solutions. n=3, p<0.05.	103
Figure 3-27 UV-spectrometry illustrating the LCST of PNVCL based copolymers and terpolymers. n=3, p<0.05.....	105
Figure 3-28 A representative thermogram illustrating the LCST of PNVCL based copolymer S2 (30DMAAm/70NVCL) aqueous solution. n=3.....	105
Figure 3-29 Pulsatile swelling behaviours of chemically crosslinked NVCL/DMAAm copolymer hydrogels with different concentrations of PEGDMA (S6 0.1 wt% and S7 2 wt%) at temperatures between 20°C and 50°C. n=3, p<0.05.	107

Figure 3-30 Pulsatile swelling behaviours of chemically crosslinked NVCL/DMAAm/NVP hydrogels with different polymeric compositions and 2 wt% PEGDMA at temperatures between 20°C, 50°C and 80°C. n=3, p<0.05.....	108
Figure 3-31 The appearance of the disc samples of S7 sample at times: A 0 hour; B 6 hours; C 72 hours; D 216 hours; E 336 hours; F 384 hours.....	108
Figure 3-32 Pulsatile swelling behaviours of chemically crosslinked NVCL/NVP/NIPAAm terpolymer hydrogels with different polymeric compositions and 2 wt% PEGDMA at temperature between 20°C and 50°C. n=3, p<0.05.....	109
Figure 3-33 A representative graph of rheological analysis demonstrating the onset temperature and crossover point of S2 (30DMAAm/70NVCL). n=3.....	111
Figure 3-34 The appearance of swollen samples. The gel codes from left to right are S5, S9, S15, S17 and S19. n=3.	111
Figure 3-35 The representative contact angles figures of S5, S7, S9, S15, S17 and S19 at 0 and 115 seconds. n=3, p<0.05.....	114
Figure 3-36 Work breakdown structure for the development of the smart 4D objects.....	117
Figure 3-37 Mould printed using Form 2 3D printer.....	118
Figure 3-38 The above mould was made with Flexible Form 2 resin, and fracture was caused by bending when removing the sample.	118
Figure 3-39 <i>The puzzle shape samples developed using the UV curing chamber.....</i>	119
Figure 3-40 The flower shape sample developed using the UV curing chamber.....	119
Figure 3-41 (L) printing without support & (R) printing with support.	120
Figure 3-42 Recrystallisation of NVCL based solution occurs on the printer resin tank.....	121
Figure 3-43 (L) the BAPO sample printed flower shape model stuck on the resin-filling tank; (R) flower-shaped sample printed with 2 wt% BAPO resin.	122
Figure 3-44 Flower-shaped parts printed using 2 wt% H-Nu 400IL resin.....	123

Figure 3-45 The flower-shaped parts printed using 1~5 wt% H-Nu 400IL homemade resin.	124
Figure 3-46 (L) The new flower-shaped part printed on the platform & (R) the new flower-shaped part after remove from the platform.	125
Figure 3-47 (L) Support-bases built on the platform, (M) the flower model printed on the support structure & (R) the flower model after removing the support and post-cure.	126
Figure 3-48 The appearance of printed samples (L) Flower & (R) Jigsaw.	127
Figure 3-49 FTIR spectra of the photopolymerised and printed samples. n=2.	128
Figure 3-50 A thermogram illustrating the LCST of printed and cured P(70NVCL-30DMAAm); Green: S7(photocured); Blue: F2(photocured) and Red: F2(printed). n=3, p>0.05.	130
Figure 3-51 The Pulsatile swelling behaviours of photocured chemically crosslinked NVCL/DMAAm copolymer hydrogels with different shapes at temperatures 20°C, 50°C and 80°C. n=3.	131
Figure 3-52 The appearance of the photopolymerised puzzle and flower samples at times: A 0 hour; B 2 hours; C 4 hours; D 6 hours; E 72 hours; F 216 hours; G 336 hours.	132
Figure 3-53 The Pulsatile swelling behaviours of photocured and printed chemically crosslinked flowers NVCL/DMAAm copolymer hydrogels at temperatures 20°C and 50°C. n=3.	133
Figure 3-54 The appearance of the 4D printed puzzle and flower samples at times: A 0 hour; B 6 hours; C 24 hours; D 72 hours; E 168 hours; F 240 hours; G 408 hours.	133
Figure 3-55 The gel fraction of printed samples, S7 and H-Nu UV cured samples. n=3, p>0.05.	134
Figure 3-56 The comparison of tensile properties between S7, H-Nu photocured and H-Nu printed samples. n=5, p>0.05(maximum load), p>0.05(tensile strength), p>0.05(Young's modulus).	135

Figure 3-57 (L) The representative contact angles figures of F2 printed and UV-cured samples at 0 and 115 seconds; (R) The comparison of contact angles between S7, F2 UV-cured and 3D printed samples. n=3, p>0.05(0s), p<0.05(115s).....	136
Figure 3-58 Work breakdown structure for the development of the bilayer smart 4D objects.	139
Figure 3-59 The Flexible and Elastic 50A resin cartridge obtained from formlabs.	141
Figure 3-60 The first-generation strips types of silicone mould.....	142
Figure 3-61 (L) Bilayer strips made using Elastic resin + NVCL; (R) Bilayer strips made using Flexible resin + NVCL.	142
Figure 3-62 At room temperature, the appearances of the different types of flexible bilayer strips at the times: (L-R) 0 hours, 1 hour, 2 hours, 6 hours and 24 hours.	144
Figure 3-63 The appearances of the different types of elastic bilayer strips at the times: (L-R) 0 hour, 2 hours, 6 hours, 24 hours and 48 hours (oven).	146
Figure 3-64 (L) The second-generation silicone mould of strips & (R) The scheme of direction control for strips in water.....	147
Figure 3-65 (L) The thickness of proportioned strip samples & (R) the appearances of proportioned strip samples.....	148
Figure 3-66 At room temperature, the appearances of swollen proportioned bilayer samples at the times: 0 hour, 2 hours, 4 hours and 24 hours.....	149
Figure 3-67 (L) The 3D printed strips & (R) The third-generation silicone mould of strips.	151
Figure 3-68 The appearances of third-generation bilayer strips.	151
Figure 3-69 The appearances of swollen type ‘a’ and ‘d’ bilayer samples at the times (L-R): 0 hour;1 hour; 2 hours; 6 hours; 24 hours and 48 hours (50°C).....	153
Figure 3-70 The appearances of swollen type ‘b’, ‘c’ and ‘e’ bilayer samples at the times:0 hour;1 hour; 4 hours; 24 hours; 48 hours (Oven);72 hours (Oven); 144 hours; 192 hours (Oven) and 216 hours.	155

Figure 3-71 The 1.5 mm and 3 mm flower shaped silicone mould.....	157
Figure 3-72 The appearances of bilayer flower samples.....	157
Figure 3-73 The appearance of swollen bilayer flowers samples at the time (L to R): 0 hours, 2 hours, 4 hours, 6 hours, 20 hours (14 hours in oven), 24 hours, 30 hours (6 hours in oven).	158
Figure 3-74 The TUS automatic displays achieved by using self-curving strips.....	160
Figure 3-75 The toy train automatic puller achieved by using self-curving strips.....	161
Figure 3-76 The flower gripper achieved by using bilayer self-curving flowers.....	162
Figure 5-1 DSC graph of S1 PNVCL based polymer sample.....	180
Figure 5-2 DSC graph of S3 PNVCL based polymer sample.....	180
Figure 5-3 DSC graph of S10 PNVCL based polymer sample.....	181
Figure 5-4 DSC graph of S12 PNVCL based polymer sample.....	181
Figure 5-5 DSC graph of S13 PNVCL based polymer sample.....	182
Figure 5-6 The rheology graph shows the phase transition and gelation point of 5 wt% PNVCL sample.....	182
Figure 5-7 The rheology graph shows the phase transition and gelation point of S3 sample.	183
Figure 5-8 Best material research institute poster in AIT seminar in 2019.....	193

List of Tables

Table 1-1 Approaches for synthesising physically and chemically crosslinked hydrogels (Ebara et al., 2014).	9
Table 1-2 Common photoinitiators with their corresponding wavelength peak and properties (Mondschein et al., 2017).	25
Table 1-3 Assessment criteria for each printing technique used for manufacturing (Hwa et al., 2017).	27
Table 1-4 Summary of the recent developments with novel materials in 3D printing (Lee & Chua, 2017).	28
Table 1-5 Mechanical analysis of each shape deformation (Nam & Pei, 2019).	38
Table 1-6 Summary of the applications of 4D printing that exists in the literature.	41
Table 2-1 Name and chemical structure of selected materials.	43
Table 2-2 Formulated polymer composition of NVCL physically crosslinked with varying concentrations of Irgacure 2959, VA-086 and Camphorquinone.	45
Table 2-3 Formulated polymer composition of NVCL chemically crosslinked with varying concentrations of PEGDMA.	46
Table 2-4 Formulated NVCL terpolymers physically and chemically crosslinked with varying concentrations of NVP, DMAAm, and NIPAAm.	47
Table 2-5 Formulated polymer composition of physically and chemically crosslinked NVCL with varying concentrations of Irgacure 2959.	52
Table 2-6 Formulated polymer composition of NVCL with varying photoinitiators.	52
Table 2-7 Formulated composition of NVCL copolymers with varying concentrations of H-Nu 400IL.	53
Table 2-8 The mixing details of the bilayer structure.	60
Table 3-1 Functional groups in NVCL and PNVCL following FTIR analysis.	77

Table 3-2 Functional groups in NVCL, PEGDMA and PNVCL-PEGDMA following FTIR analysis.	79
Table 3-3 The LCST of PNVCL homopolymer detected by four techniques.	85
Table 3-4 Mechanical properties of P1 and C3 samples. n=5, p<0.05.	89
Table 3-5 Functional groups in NVCL, DMAAm, PEGDMA, S6 and S7 analysed by FTIR.	99
Table 3-6 Functional group in NIPAAm, NVCL, NVP, PEGDMA, S14, S16 and S18 analysed by FTIR.	100
Table 3-7 LCST of selected PNVCL-based samples which were established using cloud point, UV-spectrometry, DSC and rheological analysis.	102
Table 3-8 Tensile properties of C3 and S7 samples. n=5, p<0.05.	112
Table 3-9 Functional groups in NVCL, DMAAm, PEGDMA, S6 and S7 analysis using FTIR.	129
Table 5-1 Below and above LCST swelling wt% ratios for the chemically crosslinked samples.	184
Table 5-2 Pulsatile swelling study performed on the PNVCL based polymer samples and swelling wt% ratio in below and above LCST condition.	185
Table 5-3 Pulsatile swelling study performed on the H-Nu 4D printed and UV-cured samples and swelling wt% ratio in below and above LCST condition.	187
Table 5-4 UV spectroscopy data for LCST studies on PNVCL and its copolymers.	189
Table 5-5 Gel fraction results of S7, H-Nu printed and UV-cured samples.	190
Table 5-6 The contact angles result of PNVCL homopolymers, co/terpolymers, H-Nu printed and UV-cured samples.	191
Table 5-7 The tensile tests data of P1, C3, S7, H-Nu printed and UV-cured samples.	192
Table 5-8 Gantt chart workplan Sept. 2017-June 2022.	196

Chapter 1:

Literature Review

1 Literature Review

1.1 Problem statement

Reviewing the literature on the development of auto-deformation using temperature-sensitive polymers, nearly all the reports suggest used Poly (N-isopropylacrylamide) (PNIPAAm) derivatives. Lee *et al.* (2018) created a bilayer structure that exhibited unique altered bending behaviour by combining NIPAAm with poly (vinyl alcohol) (PVA). The direction and extent of bending can be controlled by combining NIPAAm and PVA films with different swelling ratios. Also, Lee *et al.* have developed a motion of grasping and releasing in response to temperature which was demonstrated in the starfish structures (Lee & Jho, 2018). Zheng *et al.* (2018) composed of a PNIPAAm layer (featuring a lower critical solution temperature, LCST) and a poly (acrylic acid-coacrylamide) (P(AAc-co-AAm)) layer (featuring an upper critical solution temperature, UCST), produced a reversible thermo-responsiveness bilayer composite structure. The actuation of this hydrogel can be operated under non-aqueous conditions (Zheng *et al.*, 2018).

Although a large number of 4D printed concepts have been pioneered in recent years, experts are undecided about the market growth potential of this recent technology. 4D printing opportunities are vast, especially in the biomedical, aerospace, lifestyle, robotics and military fields, however, there still exist several challenges which need to be overcome before it becomes widely adopted technology.

4D printing technology can be considered to be still in its early stage of development with the materials in use being one of the limiting factors with regards to its widespread use. The materials used in 4D printing must be responsive and not all responsive materials are capable of being printed, resulting in only a small number of materials being available for selection (Ding *et al.*, 2019). Additionally, the majority of

these materials can generally be activated with only a single type of external stimulus which may be unable to satisfy the requirements of complicated constructs (Otrokov, *et al.*, 2018). The development of new formulations for existing reactive materials to provide them with printability and multi-sensitivity is a future challenge for 4D printing.

The second factor limiting the development of 4D printing is the lack of complex and appropriate deformation mechanisms and high precision multi-material 3D printers. 4D printing is a high-precision, rapid and customisable way to prepare monolayer/bilayer smart hydrogels (Wu *et al.*, 2018). The mathematical modelling supports for multilateral design ensure the quality and responsiveness of the printed objects (Saritha & Boyina, 2021). However, complicated manufacturing process and diversity of materials seems to be a difficult task for an ordinary 3D printer. As a result of the high price and advanced technology of multi-layer 3D printers, they are not readily available. Currently, for some complex 3D models, the existing multi-materials 3D printer is unable to supply suitable support structures for intricate geometrical objects, resulting in printed structures or objects that exhibit low geometric accuracy and fidelity.

Moreover, the existing deformation of 4D-printed parts is confined to a single deformation. For many fields, only complex multi-dimensional variations can fulfil their requirements. Hence, the design and fabrication of advanced 3D printers and the mastery of new deformation mechanisms will be important directions to explore in the field of 4D printing in the future (Ayushi *et al.*, 2021). Designing 4D printing structures is another important aspect of the 4D printing process. The lack of computational design and simulation software to program time into structures in a systematic and controlled manner is another issue that needs to be addressed in the field of 4D printing (Demoly *et al.*, 2021). These tools require a combination of information on material properties, the printing process and designed structures. The current methods rely on several practical trials before the desired deformation can be obtained, which is time-consuming (Otrokov, *et al.*, 2018).

Besides the challenge involved in materials, printing equipment and technologies, other issues, including slow printing and response times, slow and inaccurate actuation, high set-up costs and the inability to have control over intermediate states have all acted as barriers to the adoption of 4D printing (Shahrubudin *et al.*, 2020).

1.2 Aims and objectives of this study

Having extensively reviewed the literature for 4D printing, several limitations have been identified. It is these limitations such as lack of multi-materials 3D printer and printable responsive materials etc. that have allowed for clear and concise aims to be proposed for this research study. Thus, for the development of a feasible scheme to achieve 4D printing and shape-shifting behaviour using temperature-responsive hydrogels the key aims are as follow:

1. To develop a new temperature-responsive hydrogel formulations (differentiation of NIPAAm) as a candidate for 4D printing;
2. To develop formulations for the temperature-responsive hydrogels with reasonable properties and printability, which allows the formulations to be used with traditional 3D printing;
3. Without using multi-layer 3D printers, to develop more complex autonomous shape-shifting behaviours for the temperature-responsive hydrogel.

Based on the proposed the aims of this study. The objectives of this body of research are summarised below:

1. To prepare both physically and chemically crosslinked photopolymerisable NVCL smart hydrogels;
2. To characterise the thermal, mechanical and swelling behaviour of the synthesised hydrogels and select formulations that can potentially be used for 4D printing;

3. To design and create complex shaped objects via 3D printing techniques and to detect the change of state for the printed object as the temperature rises and falls;
4. To examine the effect of NVCL properties prepared via stereolithography and UV chamber polymerisation;
5. To implement the shape shifting behaviours using NVCL-based gels and develop demonstrators for those deformable objects.

1.3 Definition and history of hydrogels

“Hydrogels as three-dimensional crosslinked hydrophilic polymer networks are capable of swelling or de-swelling reversibly in water and retaining large volume of liquid in swollen state.” (Ahmed, 2015)

As a polymeric material, hydrogels are defined as water-swollen, cross-linked polymeric three-dimensional network structure established by the response of one or more monomers. Hydrogels may be resistant to chemicals, or they can deteriorate, disintegrate, and dissolve (Caló & Khutoryanskiy, 2015). “Hydrogel”, as a term, was first used in print in 1894 to describe a "colloidal gel of inorganic salts". Because of the good biocompatibility and good degradability, hydrogels have received widespread attention and are widely used in biomedical engineering (Su *et al.*, 2023). The present knowledge of hydrogels for biological applications was discovered in 1960 (Lee *et al.*, 2013; Liu *et al.*, 2022). As mentioned in the introductory quote of this paragraph, hydrogels are capable of absorbing large volumes of water due to crosslinking between the hydrophilic functional groups linked to the polymer backbone (Shin *et al.*, 2010; Michalik & Wandzik, 2020). Since the beginning of human activity on the planet, hydrogels have been discovered in nature (Ratner & Zhang, 2020).

The classification of hydrogels is quite a broad area of categorisation and is displayed graphically in **Figure 1-1**. The categorisation of hydrogels may be performed

based on their configuration, physical appearance, network electrical charge or origin (Khansari *et al.*, 2017). They may be further subdivided into being homopolymeric hydrogels, copolymeric hydrogels, and multipolymer interpenetrating polymer networks (IPNs) on the polymer composition. Commonly, hydrogels may be classified as one of two categories corresponding to the types of crosslinking agent — physically or chemically crosslinked (Bustamante-Torres *et al.*, 2021). The configuration can be a criterion for classification as well — they may be amorphous, semi-crystalline, and crystalline. Hydrogels can be cationic, anionic, or neutral, depending on the charges on the bonded groups (Ullah *et al.*, 2015; Ahmed, 2015; Sánchez *et al.*, 2021).

By definition, hydrogels are regarded as a hydrophilic network with an elastic structure produced by crosslinking; thus, crosslinking is the primary method of hydrogel preparation. To synthesise the crosslinks, the polymer chains may attach via a chemical reaction or ionising radiation to build main-chain free radicals and physical interactions such as entanglement or crystalline formation (Ahmed, 2015). Hydrogels have been used since their discovery to the present day (Kim & Park, 1998; Juan Liu *et al.*, 2015; Yuanfen Liu *et al.*, 2022). They are generally biocompatible, and the breakdown products produced have a minimal toxicity potential. The qualities of degradation products produced can also be altered by choosing the right starting ingredients for hydrogels (Akhtar *et al.*, 2016).

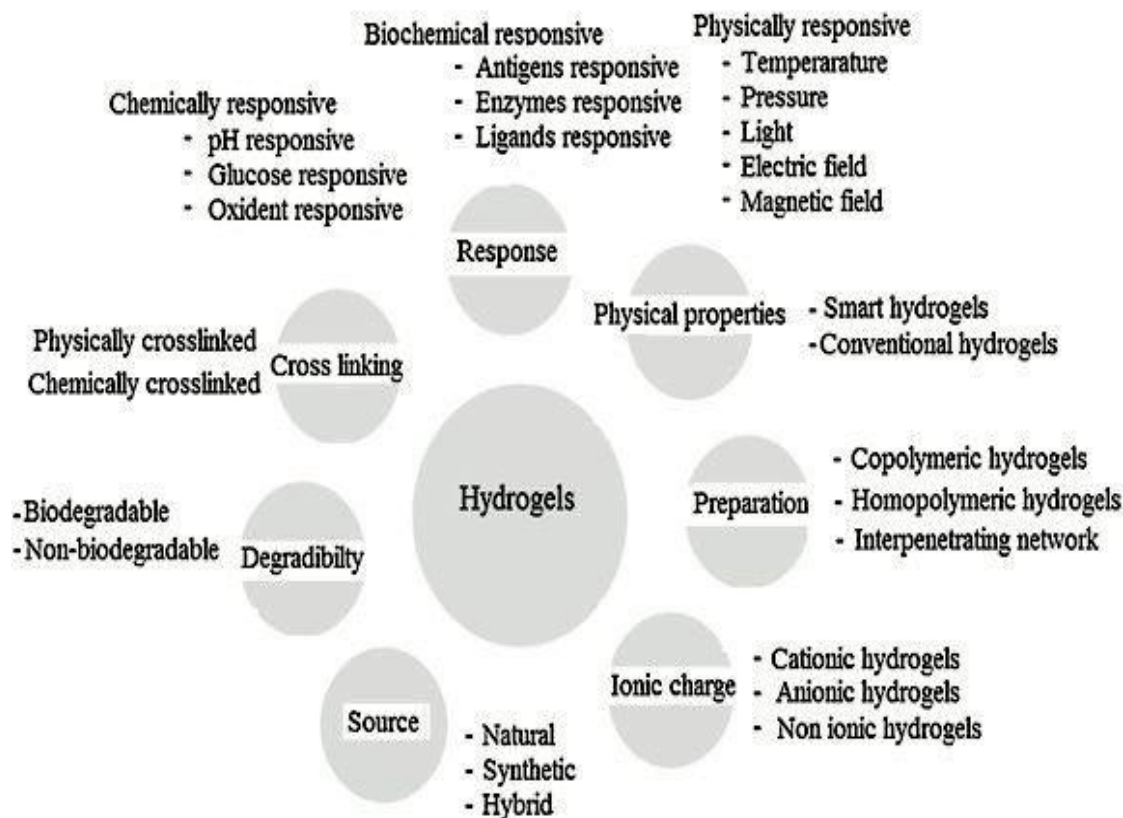


Figure 1-1 Classification of hydrogels by different factors (Ullah *et al.*, 2015).

1.3.1 Physically and chemically crosslinked hydrogels

An innovative trend in the polymer industry is that of polymerising the monomer with various initiators to create a new polymer which possesses different structures and performances (Nowak *et al.*, 2017). Crosslinking is a connection that connects one molecular chain to another. It is a steady process in polymer chemistry that results in the multi-dimensional expansion of polymeric chains to construct mesh structures (Maitra & Shukla, 2014). Akhtar *et al.* (2016) and Ebara *et al.* (2014) summarised several approaches to forming physical or chemical crosslinking.

Figure 1-2 demonstrates the principle of physical and chemical crosslinking. The transient junctions of physically crosslinked hydrogels are always achieved due to molecular entanglements or secondary forces — such as ionic interactions, H-bonding, or hydrophobic forces (Ahmed, 2015; Soni *et al.*, 2021). These gels are always degradable and the interaction can be collapsed in response to the temperature, pH and solution

concentration etc. (Hoffman, 2012; Caló & Khutoryanskiy, 2015). Controlling degradability is desirable for many applications, such as a drug delivery system (DDSs). Additionally, the dissolution can be prevented by physical interactions between the polymeric chains (Varaprasad *et al.*, 2017). Freeze-thawing can achieve physical crosslinking as well and under repeat freezing and thawing cycle conditions microcrystals are generated. The relative ease of production and the absence of crosslinking agents during synthesis are among the advantages of physical crosslinking. Compared with other physical crosslinkers with the presence of strong hydrogen bonds, polyurethanes (PUs) possess significant biocompatible and mechanical properties (Xie *et al.*, 2019). PUs can be used as excellent physical crosslinking agents in the synthesis of hydrogels to enhance mechanical integrity (Patel & Mequanint, 2011; Claudio-Rizo *et al.*, 2021). In summary, without any addition or chemical modification, physically crosslinked gels can be formed by interactions. However, because of the difficulties in decoupling the variables, flexibility and mechanical strength are limited (Ebara *et al.*, 2014; Xia *et al.*, 2018).

To initiate chemical crosslinking, low molecular weight (M_w) crosslinking agents and polymers are chosen for incorporation into the reaction mixture (Ullah *et al.*, 2015; Wegrzynowska-Drzymalska *et al.*, 2020). Furthermore, the covalent connection between polymer chains can be built by the reaction of the functional groups. These two methods are called radical polymerisation. Moreover, enzymes can be used as catalysts to synthesise chemically crosslinked hydrogels. Compared with physical methods, the chemical route provides very good regioselectivity to hydrogels, particularly via the Michael addition reaction (Hennink & van Nostrum, 2012; Stojkov *et al.*, 2021). Chemically crosslinked gels are permanent and stable and, due to the existence of covalent bonds, cannot be dissolved in any solvent (Varaprasad *et al.*, 2017). On the contrary, they swell due to the thermodynamic compatibility (Brannon-Peppast, 1991; Lusina & Cegłowski, 2022). Solubility counteracts the balance by the elastic retraction force of the

crosslinking points in the network. The swelling stops when these forces are equal (Ullah *et al.*, 2015). Depending on the type of the chemical bonds and the crosslinks, chemical crosslinking provides a relatively robust mechanical property and stability for hydrogels, but the chemical agents are generally toxic (Akhtar *et al.*, 2016). The chemical agents link the two molecules together and are usually obtained via reacting with other entities, including proteins, peptides, active pharmaceutical ingredients (APIs), nucleic acids and solid particles (Back *et al.*, 2003). The chemical hydrogels are able to be produced by crosslinking the water-soluble polymer or, alternatively, by transferring the hydrophobic polymers to hydrophilic form in a crosslinking network (Hoffman, 2012; Asghar *et al.*, 2018). A successful crosslinking has to retain several circumstances — side-chain groups must be acceptable to the agent, such as carboxylic acids and primary amines; besides, the distance span of them must be in crosslinker spacer chains and generate a special or limited number of conjunctions (Maitra & Shukla, 2014).

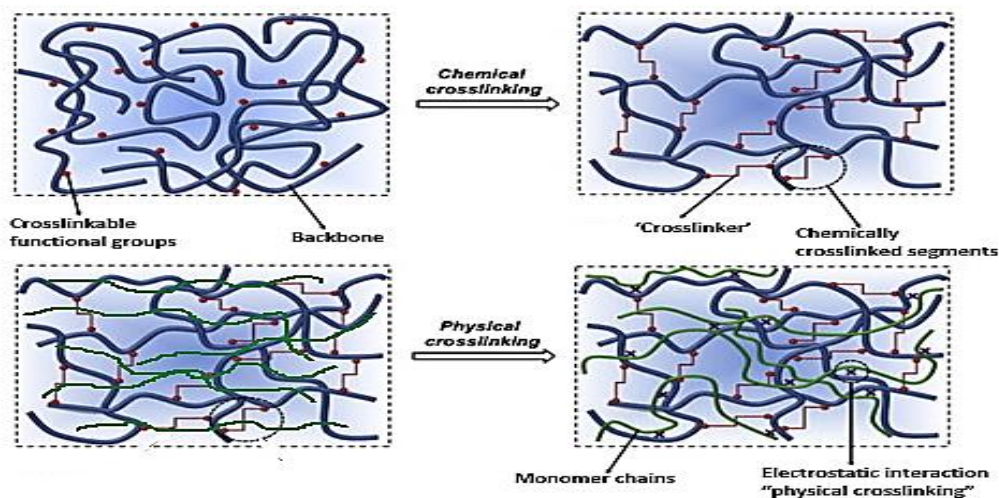


Figure 1-2 The principle of physical and chemical crosslinking (Fajardo *et al.*, 2013).

Table 1-1 demonstrates the typical physical and chemical crosslinking processes. For physically crosslinked hydrogels, due to the diminished capacity of the individual chain movement, a liquid or sol state polymer is capable of being transferred to a solid or gel state. Additionally, with increasing molecular weight, the chemically crosslinked polymer will have high mechanical strength and the ability to resist heat, wear and solvent

erosion (Liu *et al.*, 2001; Chen *et al.*, 2022). However, the hydrogels synthesised by crosslinking have poor cell adhesion performance. At the same time, it is difficult to find a non-toxic crosslinker to eliminate the toxicity of crosslinking agents for application to the medical industry (Patel & Mequanint, 2011). In addition, another restriction of photo-crosslinking is that light cannot penetrate deeply into a material, resulting in an incomplete or failure crosslinking (Bhattacharjee & Ahearne, 2021).

Table 1-1 Approaches for synthesising physically and chemically crosslinked hydrogels (Ebara *et al.*, 2014).

Physically crosslinked hydrogels
<ul style="list-style-type: none"> • Ionic interaction (alginate, etc.) • Hydrophobic interactions (PEO-PPO-PEO, etc.) • Hydrogen bonding interactions (PAAc, etc.) • Stereocomplexation (enantiomeric lactic acid, etc.) • Supramolecular chemistry (inclusion complex, etc.) • Freeze-thawing (PVA, etc.)
Chemically crosslinked hydrogels
<ul style="list-style-type: none"> • Polymerisation (acryloyl group, etc.) • Chemical/Radiation grafting (Chitosan, NVCL etc.) • Small-molecule crosslinking (glutaraldehyde, etc.) • Polymer-polymer crosslinking (condensation reaction, etc.)

1.3.2 Preparation and characteristics of hydrogels

There are two general schemes used to establish hydrogels; (i) Polymerisation of hydrophilic monomers and (ii) Modification or functionalisation of existing polymers (natural or artificial) (Ullah *et al.*, 2015; Ahmed, 2015).

Hydrogels can exist as either natural or synthetically derived materials. The two most commonly used natural materials utilised for the synthesis of hydrogels are polysaccharides and polypeptides. **Figure 1-3** shows example of mechanisms for hydrogel preparation by free radical polymerisation. The natural-based hydrogels are usually

synthesised by synthetic parts with the natural substrate — for example, graft copolymerisation of vinyl monomers on polysaccharides (Ahmed *et al.*, 2013). The free-radical multifunctional vinyl monomers are the best-known and most widely used means of producing synthetic hydrogels. Each monomer has an active carbon double bond centre that can propagate to form polymer chains. The way to produce active centres depends on the solvents, reaction conditions, and specific monomers, and can be achieved by heat (thermal-initiators), light (photo-initiators), enzymes (bio-initiators) or electron beams (Saxena, 2010; Chen *et al.*, 2016; Ribas-Massonis *et al.*, 2022).

In an equilibrium state, the synthetic-based hydrogel structures can contain varying quantities of water (Zainal *et al.*, 2021). As synthetic hydrogels have greater gel strength, high water absorption, and longer service life, they have gradually replaced the natural hydrogels to become the leading product. In addition, the structure of synthetic hydrogel can be amorphous, semi-crystalline and crystalline which can be modified to produce unique performance and function (Ahmed, 2015).

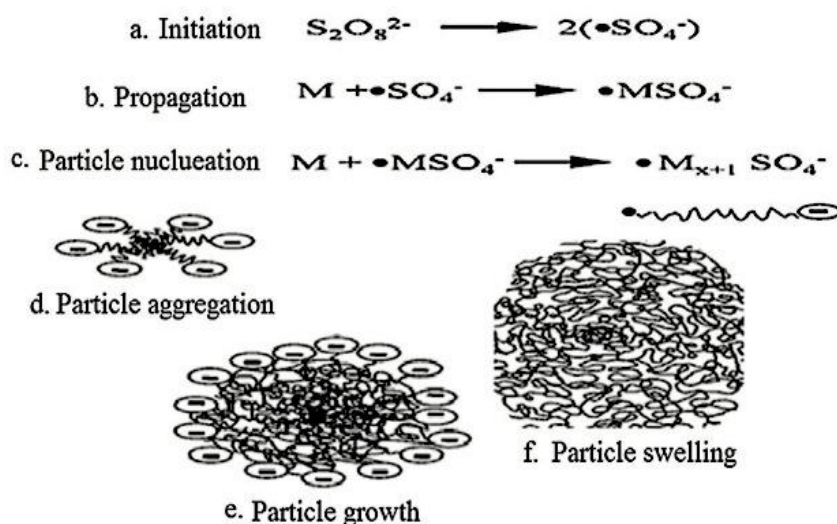


Figure 1-3 Example of mechanisms for hydrogel preparation by free radical polymerisation (Ullah *et al.*, 2015).

1.3.3 Applications of hydrogels

During the reaction process of hydrogel synthesis, a portion of monomer remains unreacted. This unreacted monomer may lead to hydrogel toxicity and, as such, these hydrogels should undergo a purification process. This purification is commonly performed by extraction into excess water (Caló & Khutoryanskiy, 2015). There are several approaches by which the purification process may be enhanced or avoided altogether. One such method is to add a new process and maximise the degree of monomer conversion — for example, irradiation or heat treatment of products. Alternatively, it is possible to choose non-toxic monomers, such as poly(acrylic acid) (PAA) and poly(vinyl alcohol) (PVA), to avoid purification (Park & Nho, 2003; Mao *et al.*, 2022).

However, due to their characteristics, hydrogels are most frequently used in the biomedical field in wound dressings, medication delivery, tissue engineering (Caló & Khutoryanskiy, 2015; Aswathy *et al.*, 2020), dyes for encapsulating cells (Akhtar *et al.*, 2016) and diagnostics (Taylor & Dua, 2020). Hydrogels can also be used for sealing, coal dewatering, artificial snow, and the agriculture industry (Varaprasad *et al.*, 2017), and they can be used to make contact lenses and hygienic products (Chen *et al.*, 2020). In addition, there is a lot of literature available on natural hydrogels prepared from food biopolymers (proteins and polysaccharides) (Ahmad *et al.*, 2019; Y. Cao & Mezzenga, 2020). Due to the diversity of hydrogel structures, it brings a wider scope for functional modulation, which opens the door to the application of hydrogels in the food sector (Li *et al.*, 2021). For instance, Wang *et al.* (2019) formed a 2D molecularly imprinted photonic crystal hydrogel sensor for the detection of oxytetracycline in milk (Wang *et al.*, 2019).

A drug release model is exhibited graphically in **Figure 1-4**. A major aim of drug delivery research is to investigate innovative drug delivery methods or devices to treat and support patients (Lee *et al.*, 2013). The loading and subsequent release of API from

hydrogels is due to their porous structure which may be adjusted through alteration of the crosslinking density of the polymer matrix and the affinity for water.

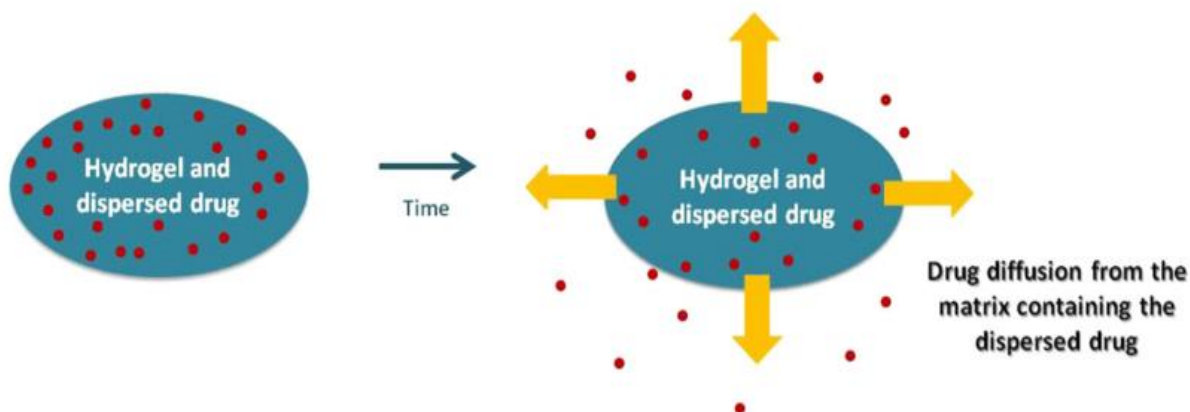


Figure 1-4 Drug release from matrix systems (Caló & Khutoryanskiy, 2015).

The advantages of hydrogels for drug delivery applications include the possibility of sustained release, which leads to the consistent maintenance of high local concentrations of active pharmaceutical ingredients (Hoare & Kohane, 2008). The release of API from hydrogel-based DDSs can be a result of several mechanisms such controlled diffusion, controlled swelling of the hydrogel matrix or, chemically controlled or environmentally-responsive (Caló & Khutoryanskiy, 2015). An example of a hydrogel-based DDS is a self-regulating insulin delivery system. A self-regulating insulin delivery system or the creation of an artificial pancreas would be good examples of this in practice. (Lee *et al.*, 2013). Such self-regulating DDSs are comprised of “smart” hydrogels. The family of smart hydrogels are those of which have the ability to react to small changes in the surrounding environment and subsequently undergo a large change in physicochemical properties, degradation, sol–gel phase transition, and transformation in morphology. The properties can be optimised for safety reasons, biodegradability, drug-loading ability and control of drug release. The creation of unique formulations that controls release rate of API or adjusts itself to the environment has become an area of significant interest for new smart hydrogels.

An excellent example of the future outlook of DDSs is the aforementioned self-regulating insulin delivery system. The release of insulin depends on the glucose (Glu) concentration in the blood-balanced environment. If Glu concentration increases, the right amount of insulin must be released to reduce the Glu concentration. Once Glu has dropped to normal levels, the system should be switched off to avoid hypoglycaemia. Therefore, controlling the time, speed and amount of insulin release are crucial (Lee *et al.*, 2013). To date, 3D bioprinting using hydrogels ushers in a new age of tissue engineering and regenerative medicine. Although some human-scale tissues have been successfully generated, 3D bioprinting is still in its early stages of development. Currently, the selection of printing materials is based mostly on their biocompatibility with cell growth, function, and printing qualities such as viscosity, extrudability, and post-printing stability. The most recent achievement in chemical synthesis is the development of a functionally adaptable material that reprograms its structure and functioning in response to external stimuli — however, current discoveries of "4D bioprinting" are far from producing a practical human-scale tissue construct (Unagolla & Jayasuriya, 2020).

1.4 Stimuli-responsive polymers

Polymers offer many uses for humans. Stimuli-sensitive polymers are one type of smart polymer, where properties are altered (e.g. solubility or shape) according to changes in the surrounding environment, including temperature (Nastyshyn *et al.*, 2022), electrical field (Mokhtar *et al.*, 2021), PH (Deirram *et al.*, 2019), solvent (Meng & Li, 2013) and light (Stoychev *et al.*, 2019). The stimulus can first be observed at the molecular level. As many molecules change, the performance of the material changes to a different state. The response time of different materials to the stimulus is also different, and the response occurs at different levels, usually involving multiple processes. Not all materials are capable of responding to stimuli. In some cases, the material requires passing through a physical process to obtain stimuli-responsiveness (Roth & Lowe, 2017).

The potential stimuli and responses for the stimuli-responsive polymers are represented in **Figure 1-5**. In the last ten years, a series of smart materials have been developed. Sun *et al.* (2019) critically evaluated the state-of-the-art synthetic strategies that enable stimuli-responsive polymers and summarised the various stimuli that can induce transformation as well as examining recent advancements and future directions (Sun *et al.*, 2019). Moad *et al.* (2017) introduced a reversible addition-fragmentation chain transfer (RAFT) method, which is a process of free radical polymerisation to form stimuli-responsive polymers. One major application branch of stimuli-sensitive polymers is the biomedical field, where changes in conformation or solubility would alter the hydrophilic/hydrophobic balance or release of a bioactive molecule (Schmaljohann, 2006; Sarwan *et al.*, 2020; Husseiny *et al.*, 2022).

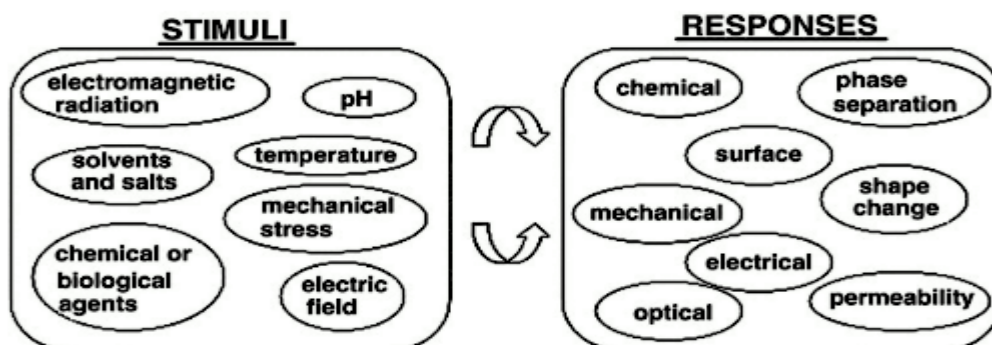


Figure 1-5 The stimulus and responses to stimuli-responsive polymers (Schmaljohann, 2006).

There has been a lot of interest in pH-sensitive hydrogels for medication targeting and controlled-release applications among other stimuli-sensitive hydrogels. Changes in ambient pH can alter the ionisation of pH-dependent hydrogels, causing swelling/deswelling, which can then be employed as a drug release regulator (Bazban *et al.*, 2017).

1.4.1 Temperature-responsive polymers/gels

Temperature-responsive polymers are polymers whose physical or chemical properties are changed with temperature (Brighenti & Cosma, 2022). Water-soluble polymers have been extensively investigated due to their wide range of applications in medicine, biotechnology, ecology and pharmacology. H-bonding between the hydrophilic regions of the polymer chain and water molecules is effective at low temperatures. When the temperature is increased, there is a partial displacement of water from the polymer coil. Water displacement weakens the H-bonds and improves interactions between the hydrophobic segments of the polymer macromolecules. The internal and intermolecular hydrogen connections between the hydrophobic portions of the polymer molecules cause polymer collapse, aggregation, and phase separation. H-bonds are reorganised around the non-polar polymer. The polymers form a separate phase in solution and change their conformation from the coil to globule (Quoika *et al.*, 2020). The temperature at which phase separation occurs is taken as the critical solution transition temperature. Hydrogels as a prototype are most frequently applied in biomedical applications where they swell/shrink in water when they meet the desired temperature (Killion *et al.*, 2013; Sarwan *et al.*, 2020).

Poly (N-isopropylacrylamide) (PNIPAAm) is the most commonly researched temperature-responsive polymer as its phase transition temperature is close to physiological temperature (Alarcón *et al.*, 2005; Ortega-García *et al.*, 2022). When the temperature increases beyond the transition point, the stored API is released. In recent years, temperature-responsive polymers have been formed into nano and hyperbranched sizes. Wang *et al.* (2017) reported two different approaches to synthesise hyperbranched temperature responsive polymers:

- 1) Modification moieties resulting in temperature sensitivity;

- 2) The dendritic polymer's backbone can be designed to be temperature sensitive by adjusting the hydrophobic/hydrophilic balance and distribution.

Other polymers such as poly(N-vinylcaprolactam) (PNVCL), poly(ethylene glycol) (PEG) or poly(ethylene oxide) (PEO) and poly(propylene oxide) (PPO) can exhibit the temperature-responsive nature (Marsili *et al.*, 2021), the chemical structures of which are shown in **Figure 1-6**. In an aqueous solution, the performance of smart polymers which are sensitive to temperature become active at the lower critical solution temperature (LCST) (Roth & Lowe, 2017). This means that the hydration is high in the low temperature region and phase separation occurs upon heating (Messing & Schmidt, 2011).

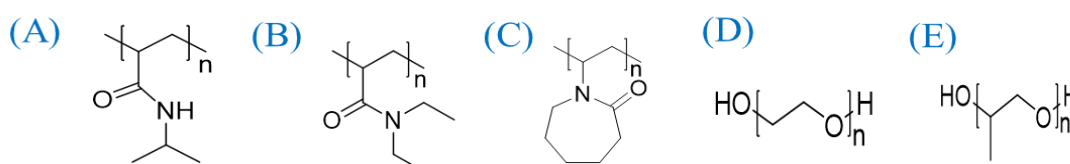


Figure 1-6 The chemical structure of typical temperature responsive polymers: (a) Poly(*N*-isopropylacrylamide); (b) Poly(*N,N'*-diethylacrylamide); (c) Poly(*N*-vinylcaprolactam); (d) Poly(ethylene glycol); (e) Poly(propylene oxide).

1.4.2 Lower and upper critical solution temperature

At a certain temperature, polymers are compatible with a solvent. The critical solution temperature (CST) is the temperature at which the polymer solution undergoes phase separation. As can be seen in **Figure 1-7**, the temperature, at which the polymer dissolves and subsequently undergoes phase separation, is deemed the Lower Critical Solution Temperature (LCST). Conversely, should the polymer dissolve above a specific temperature, this point is deemed the Upper Critical Solution Temperature (UCST) (Bordat *et al.*, 2019).

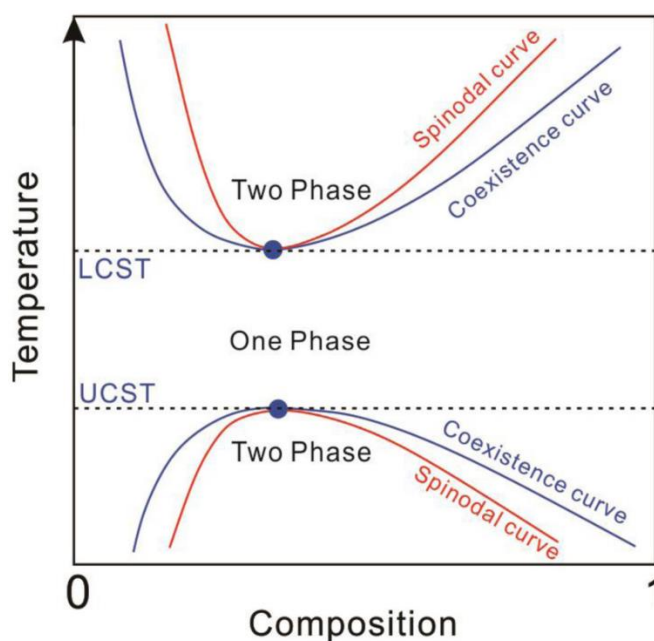


Figure 1-7 A plot of typical phase behaviour of polymer binary solution (Mao *et al.*, 2016).

This phenomenon can be explained as follows. Gibbs presents an equation applied to the phase behaviour of any mixture at a constant pressure P and temperature T (Lemanowicz *et al.*, 2014; Takeuchi, 2020).

$$\Delta G = \Delta H - T\Delta S \quad \text{Equation (1)}$$

Where: ΔH and $T\Delta S$ are the enthalpy and entropy of mixing respectively.

Typically **Figure 1-8** displays the state change of a molecular chain below and above LCST. Water loses entropy when it is hydrated to the polymer chains, which results in the free energy (ΔG) of dissolving the polymer in water becoming negative at lower temperatures. As the temperature increases, the enthalpic interaction will decrease. More importantly, however, the entropy term ($-T\Delta S$) will become dominant, thereby leading to positive free energy of mixing and, thus, to phase separation (Hoogenboom, 2014). For example, when the temperature exceeds the critical point, the LCST response polymer solution changes from transparent to opaque. As the temperature increases, water is repelled from the polymer chains and the H-bonds collapse (positive enthalpy) (Lemanowicz *et al.*, 2014), and the increase of water molecules leads to the increase of entropy. In general, a homogenous and transparent solution can be observed below LCST

while higher temperatures cause the polymer to become insoluble in water and change to milky white (García-Peñas *et al.*, 2019).

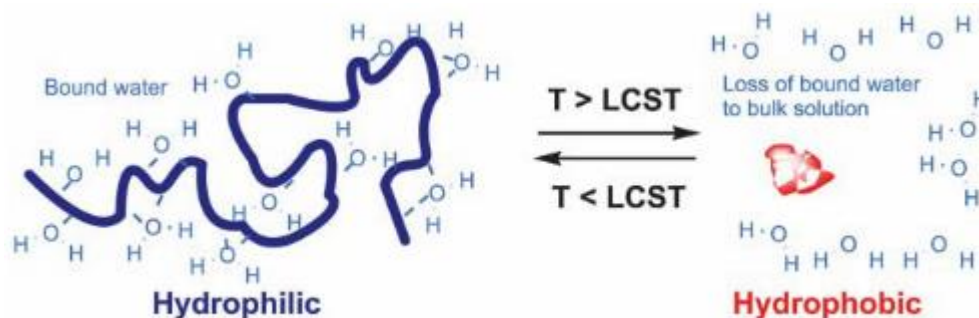


Figure 1-8 The state of the molecular chain below and above LCST (Alarcón *et al.*, 2005).

When $T > T_{LCST}$, polymer transfers spontaneously from a soluble and elongating chain to an insoluble shrunken mass curl (Messing & Schmidt, 2011). Differential scanning calorimetry (DSC) and turbidimetric detection are commonly used techniques for detecting phase transition temperatures in aqueous solutions. The specific phase transition temperature is also called cloud point temperature (T_{cp}) (Pelosi *et al.*, 2021). The LCST of temperature-sensitive polymers may additionally be determined utilising technique such as transmittance, viscosimetric (Can *et al.*, 2015), dynamic light scattering (DLS) (Ramírez-Jiménez *et al.*, 2019) and pH measurement (Lemanowicz *et al.*, 2014). Other methods, such as nuclear magnetic resonance spectroscopy (NMR), or fluorescence spectroscopic and X-ray scattering methods, are frequently utilised to gather specific information on the nature of the transition (Thompson *et al.*, 2019). NVCL exhibits a well-defined LCST in water and each chain shows a sharp coil-to-globule transition when heated to 33°C (Mohammed *et al.*, 2018). By integrating comonomer units, the LCST can be increased to 37°C (Gonzalez-Urias *et al.*, 2022). Due to the local structural transformation of water molecules around a specific part of the polymer, LCST type systems are far more concentrated than those showing UCST transitions (Strandman & Zhu, 2015).

LCST and UCST transitions differ in that the LCST transition is a cooperative entropy driven process whereas the UCST transition is an enthalpic process (Pietsch *et al.*, 2010). Zwitterionic polymers, which consist of strong intermolecular H-bonds, would shrink at a temperature \leq UCST and swell at a higher temperature (Zhang & Hoogenboom, 2015). The phase transition temperature of UCST polymer is sensitive to external environment factors which has led to such materials not finding widespread use as of yet.

1.4.3 Adjustment of LCST

Due to the aforementioned issue, there are substantially fewer reports on the UCST-type systems in aqueous solutions than on polymers displaying the LCST transition. As a rule of thumb, it can be taken that better hydrated polymers have a higher T_{cp} than poorly hydrated polymers (Hoogenboom, 2014). Indeed, depending on the polymer functionality and application field, the value of LCST can be tailored. The LCST transition behaviour can be explained by a local structural transition involving water molecules surrounding a specific segment of the polymer (Strandman & Zhu, 2015), which depends on the delicate balance between polymer-solvent H-bonding and hydrophobic and hydrophilic polymer-polymer interactions (Nigro *et al.*, 2017). Furthermore, the LCST can be adjusted by other factors, such as M_w , polymer architecture, end groups (Furyk *et al.*, 2006; Mohammed *et al.*, 2018), neighbouring blocks and possible linkers in the case of block copolymers, concentration, spatial separation between the co-monomers, and the presence of salts or additives (Strandman & Zhu, 2015). In general, the LCST for temperature-responsive polymers will decrease when polymerised with a more hydrophobic monomer and increase with a more hydrophilic monomer (Frazar *et al.*, 2020).

The phase transition behaviour of PNVCL can be modified by various methods. Anufrieva *et al.* (2001) found that utilising N-vinylpyrrolidone (NVP) as a comonomer led to an increase of LCST of PNVCL from 33°C to 80°C while, for NVCL copolymers with the concentration from 15 to 66 mol% vinyl acetate (VAc), the LCST gradually decreased

from 30 to 5°C (Norma A Cortez-Lemus & Licea-Claverie, 2016). This alternation in the LCST of polymers has similarly been shown when incorporating various salts into the formulation. Maeda *et al.* (2002) found that the transition temperature decreases with the addition of KCl or KF and increases with the addition of KBr or KI. Another interesting result was obtained by Kirsh *et al.* (2001), who reported that n-propanol and tertbutanol will decrease the LCST even further, to 10-12°C. However, the same alcohol at concentrations >20 mol% will improve the PNVCL solubility and increase the LCST to >60-80°C (Norma A Cortez-Lemus & Licea-Claverie, 2016).

Sabrina *et al.* (2005) reported that saccharide molecules will affect the LCST polymer system and will induce the disruption of the H-bonding between polymer and water molecules in solution and, therefore, will decrease both inter- and intra-molecular hydrophobic interactions; in other words, the phase transition temperature is being altered (Belbekhouche *et al.*, 2013). Alternation in the balance of hydrophilic/hydrophobic molecular fragments is not the sole method of controlling the LCST. It also depends on M_w , polymer pattern, functional groups, neighbouring blocks and possible linkers (Strandman & Zhu, 2015). Furyk *et al.* (2006) found that the LCST of temperature-responsive polymers with M_w above 50,000 are affected by changes in polydispersity and M_w ; for lower M_w specimens, the change can be seen by altering end-group structure and polarity.

1.5 Main polymers used in this study

1.5.1 N-vinylcaprolactam

N-vinylcaprolactam (NVCL) is a temperature-sensitive monomer with an amphiphilic performance composed of a vinyl group and seven ring members. It consists of six carbon atoms (C) and one nitrogen atom (N), the only N atom connected to a vinyl group. Additionally, a seven-member NVCL ring includes the rigid amide group connected

to the double bond — therefore, for the combination, the “chair” conformation is the most favourable one (**Figure 1-9**). Kirsch *et al.* (1999) used the quantum-chemical method and x-ray analysis to express confirmation of a type of NVCL (Kozanoğlu, 2008). Polymerisation occurs at the carbon-carbon double bond of the vinyl group, which ensures the balance of hydrophobic (the presence of the vinyl group) and hydrophilic (the presence of carboxylic and amide group).

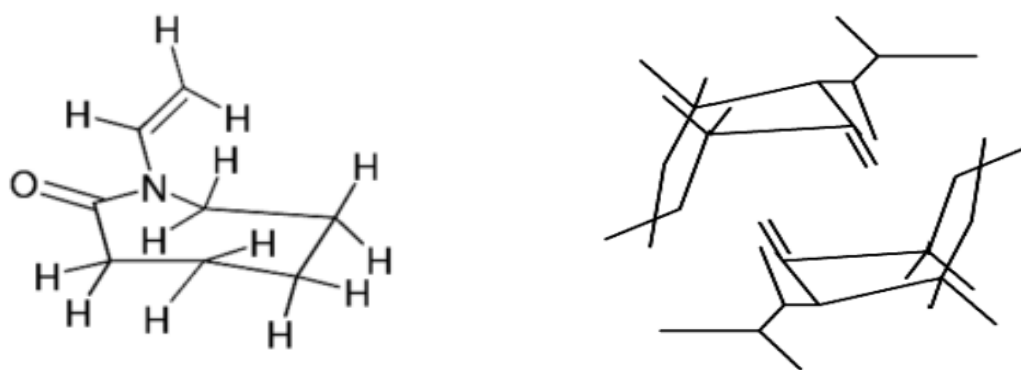


Figure 1-9 (L) Structure of NVCL determined by quantum-chemical calculation; (R) Structure of NVCL determined by x-ray (H. B. Sun *et al.*, 2008).

1.5.2 Poly (N-vinylcaprolactam)

Poly (N-vinyl caprolactam) (PNVCL) is a temperature-responsive polymer. It is well-known for its exceptional biocompatibility, solubility, thermosensitivity, and non-ionic and non-toxic properties. PNVCL presents a LCST in solution (32-34°C). Due to this, PNVCL is fabricated into hydrogels by both chemical and physical crosslinking and researched extensively for drug delivery applications (Halligan *et al.*, 2017). PNVCL is compared with the most commonly used temperature-responsive polymer poly PNIPAAm. PNVCL is hydrophilic and water-soluble at room temperature, gradually becoming hydrophobic and insoluble as the temperature increases (Alarcón *et al.*, 2005). However, due to the difficulty of synthesising copolymer via NVCL monomer, PNVCL has received less attention compared with PNIPAAm (Norma A Cortez-Lemus & Licea-Claverie, 2016).

In the case of LCST-types polymers, the amphiphilic groups cause the temperature sensitive behaviour. Polymer chains are soluble in an aqueous medium at low temperatures but become insoluble while heating, and the transition from coil-to-globule occurred (Nizardo *et al.*, 2022). In an aqueous solution, chemically crosslinked hydrogel-based PNVCL exhibits swelling or de-swelling phenomena when the temperature is increased to a critical point. Free radical polymerisation is a well-established method for preparing PNVCL homopolymers and copolymers (**Figure 1-10**)(Halligan *et al.*, 2017; Fallon *et al.*, 2019; González-Ayón *et al.*, 2020; Gonzalez-Urias *et al.*, 2022). Furthermore, it has been indicated that PNVCL is biocompatible and thermosensitive. Thus, it may be widely applied in the biomedical and environmental field (Norma A Cortez-Lemus & Licea-Claverie, 2016).

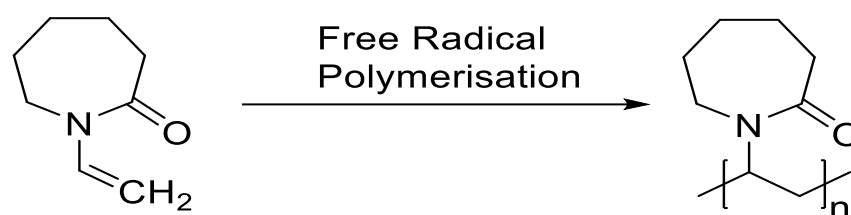


Figure 1-10 The preparation of PNVCL by free radical polymerisation.

For the preparation of PNVCL, NVCL is an soluble amphiphilic monomer, which is soluble in both polar and non-polar solvents (Vihola *et al.*, 2008). Its free radical synthesis has been performed in different media — bulk, toluene, benzene and water provide outstanding media for it. The concentration of the solution determines the M_w and dispersity of the sample post-synthesis. Nevertheless, due to its degradable performances, PNVCL has been blended with other additives or materials to form a new temperature-sensitive copolymer, such as poly (ethylene glycol) (PEG) (Halligan *et al.*, 2017), vinyl acetate (VAc), methacrylic acid (MAA) (Liu *et al.*, 2016) and α -azide terminated poly (oligo(ethylene oxide) methyl ether methacrylate (N₃-POEOMA) (Góis *et al.*, 2016). This

series of composites have been used in DDSs. Ultraviolet (UV) light is usually capable of creating the physical or chemical crosslink between monomers, crosslinkers and initiators.

PNVCL is fabricated to produce different forms with other substances to form various copolymers. The different forms of PNVCL are displayed graphically in **Figure 1-11**. Henna *et al.* (2007) reported that, when compared with pure PNVCL, a copolymer PNVCL- $C_{11}EO_{42}$ allows for more opportunities for H-bond generation due to the CEO. This in turn allows for creation of a more stable structure, which results in a steady and sustained drug release.

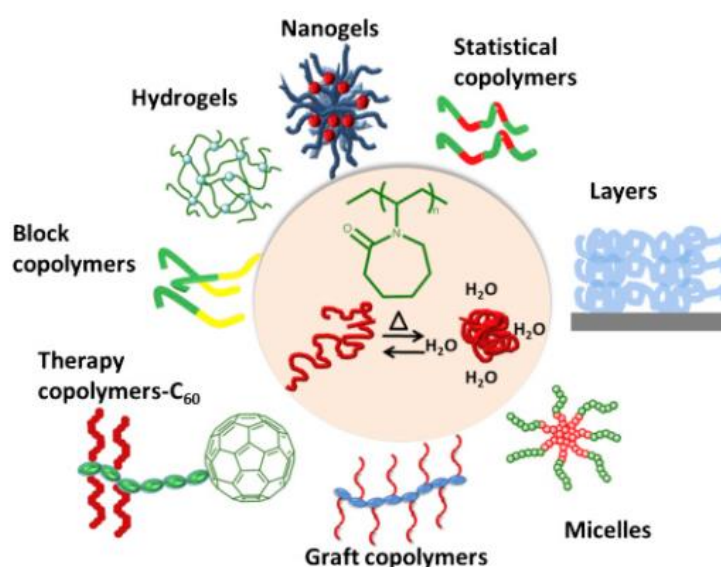


Figure 1-11 *Poly(N-vinylcaprolactam) (PNVCL) in different architectures* (Norma A Cortez-Lemus & Licea-Claverie, 2016).

1.5.3 Photoinitiators

The technology of radiation curing has evolved from an esoteric research speciality into a major industrial development and is now a core sector in polymer science and technology. Applications include barrier coatings, paper, board and metal coatings, dentistry, imaging science and printing. Inherent in these technologies is the use of a photoactivation system which is capable of absorbing the incident ultraviolet (UV) or visible radiation wavelengths employed for converting a monomer or prepolymer system into a crosslinked network (Wang *et al.*, 2021). The key property of a photoinitiator is that

it will not react with the monomer itself — the photoinitiator must first absorb UV light to form free radicals/ions. The UV curable resin must be exposed to light of the correct wavelength and of sufficient intensity to ensure the photoinitiator reacts correctly (Huang *et al.*, 2015). Photoinitiators (PI) are necessary for the photopolymerisation processes. They absorb light and are typically added as additives into the solution (Xiao *et al.*, 2015). The selected PI is unique, depending on the wavelength and application area. Mondschein *et al.* found that the photoinitiator Irgacure 2959 had minimal toxicity compared to Irgacure 184 and Irgacure 651, when employing these PI in six cell populations (Mondschein *et al.*, 2017). Knowlton *et al.* (2017) evaluated the effect of various wavelengths in the crosslinked polymer chain on photocuring efficiency. The authors found that, as the wavelength increases from 295 to 635 nm, the efficiency decreased. Radical photoinitiating systems are commonly classified according to the nature of the mechanism that produces the free-radical intermediates upon irradiation of the initiators. The mechanisms characterising the classes of photoinitiators are photofragmentation that generates radical pairs through a highly efficient α -cleavage process (type I) and hydrogen abstraction from donor molecules (type II) (Kabac, 2017). The Norrish type I initiators are typically compounds containing benzoyl groups. The carbonyl group of the initiator absorbs a photon and is converted into an excited state. Two other common Norrish type I initiators are 1-hydroxycyclohexylphenyl-ketone and 2-hydroxy-2-methyl-1-phenylpropanone. Both are soluble in many solvents (monomers) and can be used in combination with other initiators. Common type II photoinitiator systems include benzophenone and its derivatives, and isopropyl thioxanthone in combination with a synergist such as tertiary amines. The amines function as active hydrogen donors for the excited photoinitiators (Bastani & Mohseni, 2015).

Table 1-2 Common photoinitiators with their corresponding wavelength peak and properties (Mondschein *et al.*, 2017).

Photoinitiator	Wavelength Peak	Properties
Irgacure 2959	257–276 nm	<ul style="list-style-type: none"> • One of most common initiators • Least toxic of Irgacures
Irgacure 184	246, 280, 333 nm	<ul style="list-style-type: none"> • More cytotoxic than Irgacure 2959
Irgacure 651 DMPA	250, 340 nm	<ul style="list-style-type: none"> • More cytotoxic than Irgacure 2959
Irgacure 369	233, 324 nm	<ul style="list-style-type: none"> • More cytotoxic than Irgacure 2959
Camphorquinone	285, 400–500 nm	<ul style="list-style-type: none"> • Can absorb blue light
LAP	375 nm	<ul style="list-style-type: none"> • Relatively high water solubility • Initiate in visible light region
Lucirin TPO-L	380 nm	<ul style="list-style-type: none"> • Low yellowing • Water miscible
VA-086	385 nm	<ul style="list-style-type: none"> • Narrow activation range
eosin Y Disodium salt	514 nm	<ul style="list-style-type: none"> • Usable with green light • Less toxic than Irgacure 2959

1.6 Photopolymerisation

Photopolymerisation, a ubiquitous free radical polymerisation method, was widely used in the preparation of materials in the 1940s such as coatings, adhesives and printing ink (Nowak *et al.*, 2017). The primary materials that can be utilised in photopolymerisation are liquids, such as radiation-curable resin and photopolymer solutions. It is a complex process involving many chemical participants. Upon irradiation in the specific wavelength range of UV light or visible light, such polymers undergo a chemical reaction and solidify into a solid. This kind of response is called photopolymerisation (Gibson *et al.*, 2010). A UV curable mixture must contain a photoinitiator which is used to initiate the photopolymerisation of chemically multifunctional oligomers or prepolymers (Huang *et al.*, 2015).

Figure 1-12 shows the process of the photopolymerisation method. Compared to the thermal polymerisation method, photopolymerisation occurs with a high cure rate at ambient temperature. In addition, some temperature sensitive molecules — such as pharmaceutical compounds, enzymes, peptides or proteins — can safely penetrate the polymer during photopolymerisation (Pan *et al.*, 2016). Additionally, compared to other coating treatments, the use of free solvents, low energy consumption, low space consumption, low cost and environmental friendliness are the main advantages of photopolymerisation (Bastani & Mohseni, 2015). Currently, as different types of monomers and initiators are developed, the curable composites can be processed by free radical and cationic photopolymerisation mechanisms. Many free radical photoinitiators can be selected and combined into several free radical photo curable formulations. However, one paper pointed out that, for a free radical polymerisation, the reaction can be inhibited by oxygen. Covering the coated surface with nitrogen or other inert gas allows for fast cure rates and non-stick surfaces (Nowak *et al.*, 2017).

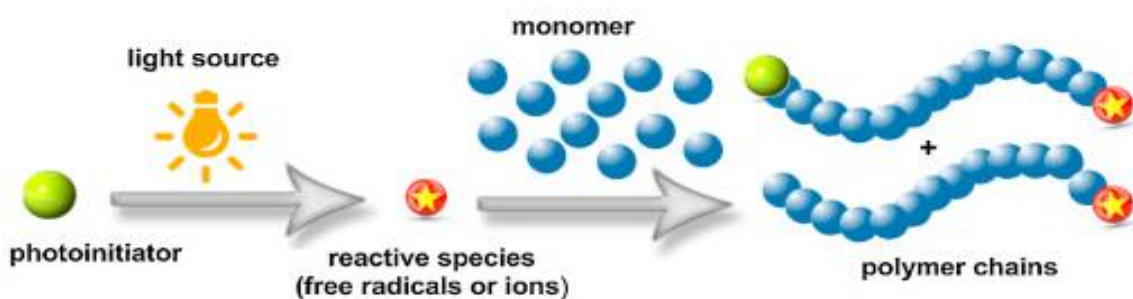


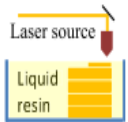

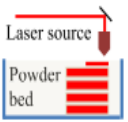
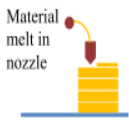
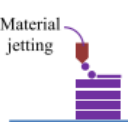
Figure 1-12 General presentation of photoinitiated polymerisation (Pan *et al.*, 2016).

1.7 Three-dimensional (3D) printing

Three-dimensional printing (3D) technique, which is also known as additive fabrication and rapid prototyping, is a fast way to create objects based on pre-designed shapes and sizes. These processes may lead to the toolless production of finished goods and the mass production of individually customised parts (Niaki *et al.*, 2019). 3D printing

has slowly evolved to create one-of-a-kind devices. Everything from small machine components to large automotive and aerospace equipment can be created by 3D printing. In the biomedical field, 3D printing technology can even be used to create therapeutic devices that fit individual patient, such as customised implants, diagnostic platform, scaffolds for tissue engineering and DDSs (Chia & Wu, 2015). With the continuous development of science and technology, the 3D printer has evolved an ability to work with a variety of types, from liquid resin to thermoplastic solid material. Each 3D printer employs different methods and principles to process the entity model. The size, shape and performance of the objects produced by each 3D printer are varied.

Table 1-3 Assessment criteria for each printing technique used for manufacturing (Hwa *et al.*, 2017).

	Techniques	SLA	SLS	SLM	FDM	3DP
	Technique schematic					
	Operating principle	Photo polymerization	Powder sintering	Powder melting	Melt extrusion	Power + binder deposition
Characterizations	Surface quality	Average	Good	Poor	Average	Good
	Post-finish	Average	Good	Average	Average	Good
	Accuracy	Excellent	Good	Poor	Average	Average
	Resistance to impact	Average	Good	Good	Good	Low
	Flexural strength	Low	Excellent	Excellent	Excellent	Low
	Prototype cost	High	High	High	Low	Medium
	Post cure	Yes	Yes	No	No	No

The first 3D printing technology for pharmaceuticals used an ink-jet printer to jet a liquid binder onto a powder bed, adhering particles together to form an agglomerated mass (Martinez *et al.*, 2017). Realising the multi-functionality and ductility of the 3D structure created, researchers sought to improve the 3D printing technique by adding other materials such as smart materials, biomaterials and nanomaterials (Lee & Chua, 2017). In contrast with conventional manufacturing methods, 3D printing has the ability to hierarchically construct intricate 3D patterns. However, material applicability is still a limiting factor for additive manufacturing technology (Zhang *et al.*, 2017). In the future,

improvements in 3D printing will be sought to process higher dimensional accuracy and improve the surface finish of production. In addition, utilising super sources (nanoscale material, faster speed and lower energy consumption) to construct larger volume models will be a challenge for the future development of 3D printing (Lee & Chua, 2017).

Table 1-4 Summary of the recent developments with novel materials in 3D printing (Lee & Chua, 2017).

	Specific material	Process (ASTM)	Application
Digital and smart materials	shape memory polymers	Vat Photopolymerization	Actuator, sensor, jewelry, gripper
Ceramic materials	UV curable monomers	Vat Photopolymerization	Thermal protection
Electronic materials	Silver nanoparticle	Material jetting	Thin-film translator, antenna emitter
	Conductive polymer	Material jetting	Resistors
	Quantum dot	Material jetting	Light emitting diodes
Biomaterials	Hydrogels	Material Extrusion	Tissue engineering
	Functional inks	Material Extrusion	Cardiac micro-physiological devices
Composite materials	CB/PCL	Material Extrusion	Sensors
	VeroWhite Plus & TangoBlack Plus	Material Jetting	Fracture resistant composites
	Barium titanate nanoparticle/polyethylene glycol diacrylate	Vat Photopolymerization	3D piezoelectric polymers

1.7.1 Stereolithography (SLA)

Stereolithography (SLA) is a solid free formation technology and was first exposed to the public in the early 1970s by a Japanese researcher Hideo Kodama (Sood *et al.*, 2010). Stereolithography (SLA) is a type of 3D-printing technique which works by solidifying light-sensitive photocurable resin. Optical fabrication provides the capability to print a part with high accuracy (Melchels *et al.*, 2010). An ultraviolet (UV) laser can solidify the photopolymer to create a link chain between molecules. The product is created layer by layer following the shape and size of a virtual model, which is drawn in the computer-aided design software (CAD) in advance (Chia & Wu, 2015). Following the pre-designed model, the photopolymer resin is solidified by UV light to form a single layer onto the surface of the photopolymer vat, then the elevator platform descends and repeats the process to form a new layer until the actual object is built from bottom to top. Removing the residual resin on the surface and the auxiliary layer used for building, the

object is formed (Mondschein *et al.*, 2017). A decade ago, a top-down system process approach was also gradually applied to the technique of stereolithography (**Figure 1-13**). This method did not require a large amount of resin and created a smooth surface on the manufactured piece (Melchels *et al.*, 2010).

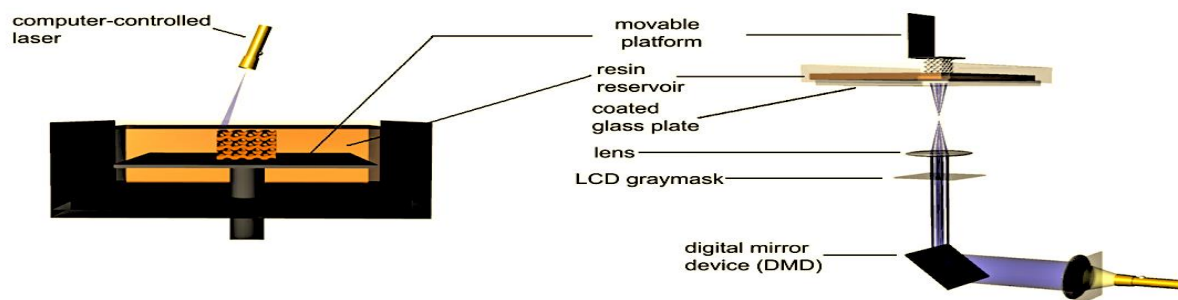


Figure 1-13 Schemes of two types of stereolithography setups. (L): a bottom-up system with a scanning laser & (R): a top-down setup with digital light (Melchels *et al.*, 2010).

The solid freeform technique has been expertly applied in electronics components, jewellery manufacturing and the automotive and biomedical industries. Mondschein *et al.* (2017) listed the limitations and requirements for fabricating scaffolds used for patient tissue necrosis and reviewed the recent developments and prospects in tissue engineering. The main benefit of SLA technique is the capability to print a part with high resolution. Also, compared to the fused-deposition modelling (FDM) 3D printing, nozzle jamming does not occur during the process (Wang *et al.*, 2017). In addition, due to the complex consolidation behavior and molecular diffusion of selective laser sintering (SLS) process, SLA have relatively wider the choice of materials (Goodridge *et al.*, 2011). Currently, commercial SLA 3D printers do not allow the operator to program the printer's parameters; only specific resins can be used in specific printers. However, some studies have shown that the quality of printed parts can be improved by replacing components or modifying the parameters of the printers (Martínez-Pellitero *et al.*, 2017). The intensity of the laser, laser scan speed and the content of oxygen can all affect the curing responses and quality of the final objects (Manapat *et al.*, 2017). The depth and efficiency of the polymerisation

are impacted by adding varying photoinitiators or crosslinkers (Pereira & Bártolo, 2015). In the future, the development of a resin that could be applied to all SLA printers will be a big challenge for all the 3D printer companies.

1.8 Fourth-dimensional printing

“The process of building a physical object using appropriate additive manufacturing technology, laying down successive layers of stimuli-responsive composite or multi-material with varying properties. After being built, the object reacts to stimuli from the natural environment or through human intervention, resulting in a physical or chemical change of state through time.”

(Pei, 2014)

Smart materials are those materials that can change their shape or properties under the influence of external stimuli (Khoo *et al.*, 2015). With the introduction of smart materials, the AM-fabricated components are able to alter their shape or properties over time (the 4th dimension) as a response to the applied external stimuli (Momeni *et al.*, 2017). 4D printed objects can be adjusted by exposing them to an environment in which pressure, moisture, temperature, magnetic field, etc., changes (Gao *et al.*, 2016).

4D printing was first initiated and described by a research group at MIT (Skylar Tibbits, 2013). The fundamental building requirements of 4D printing are mathematical modelling, smart material, stimulus, 3D printing facility, and interaction mechanism. Mathematical modelling: the material and structural design relies on math to achieve the desired change in shape, property, or functionality. Theoretical and numerical models need to be developed to build the connections between four core elements: material structure, desired final shape, material properties, and stimulus properties (Momeni *et al.*, 2017). The difference between the 3D and 4D printing is exhibited in **Figure 1-14**. Smart or stimuli-responsive material: In an era of lack of multi-material 3D printers, smart material is one of the most crucial components for 4D printing. These materials possess a number

of capabilities, such as self-sensing, decision making, responsiveness, shape memory, self-adaptability, self-repair and multi-functionality (Khoo *et al.*, 2015). Stimulus: a stimulus is required to induce the alterations of shape/property/functionality of a 4D printed structure. The selection of the stimulus depends on the requirements of the specific application which, in turn, determine the types of smart materials used in the 4D printed structure. 3D printing facility: A 4D printed structure is usually created by integrating several materials in the appropriate distribution into a single structure (Raviv *et al.*, 2014). The differences in material properties, such as swelling ratio and thermal expansion coefficient, will lead to the desired behaviour. Therefore, 3D printing is necessary for the fabrication of multi-material structures with straightforward geometry (Roy *et al.*, 2010). Interaction mechanism: In some cases, the desired shape of a 4D printed structure is not directly achieved by merely exposing the materials to the stimulus. The stimulus is required to be employed in a particular sequence for an appropriate amount of time, and this is called an interaction mechanism (Momeni *et al.*, 2017).

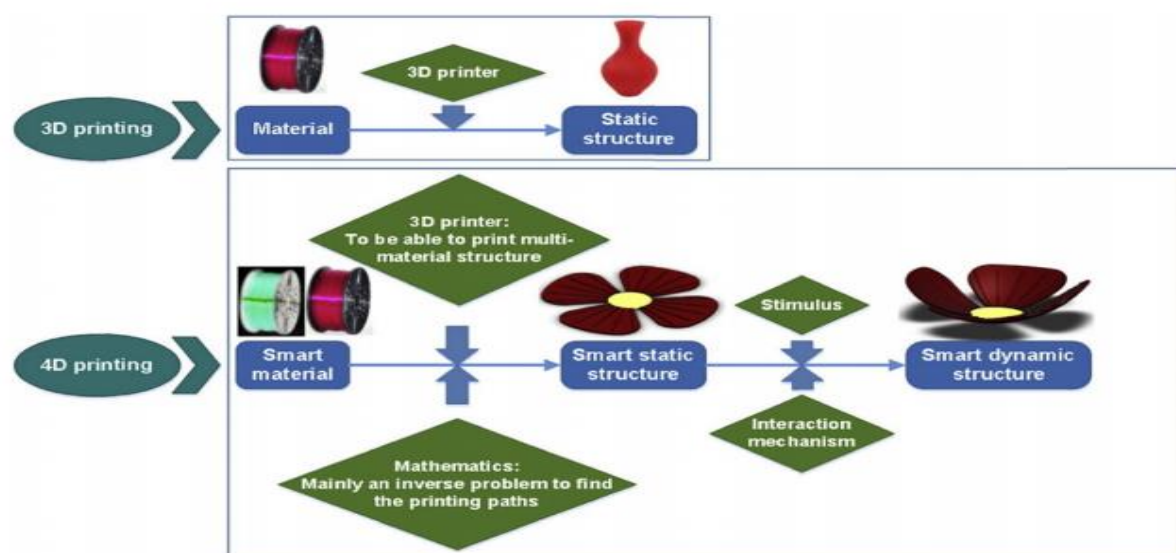


Figure 1-14 The difference between 3D and 4D printing (Momeni *et al.*, 2017).

4D printing is a new technology with possibilities for development in the bio-industry (Gao *et al.*, 2016; Chua & Mironov, 2016; Sydney Gladman *et al.*, 2016),

including cell encapsulation, tissue regeneration, drug delivery (Bakarich *et al.*, 2015) and functional heterogeneity (Kokkinis *et al.*, 2015). Additionally, Zarek *et al.* (2016) have successfully used a type of SMP called methacrylate semicrystalline oligomer melts to form flexible and changeable geometries for electronic device parts by SLA (Zarek *et al.*, 2016). Yang *et al.* (2016) pointed out the appropriate parameters for the manufacture of high-class SMP filament and examined the influence of different printing parameters on the quality of printed parts in FDM (Yang *et al.*, 2016). In the future, shoes may become intelligent — such that when the user exercises, they provide additional support to ankles or knees to avoid strain, or provide additional non-slip performance when walking in wet weather. Such shoes would be able to transform their mode via changes induced by the surrounding environment, such as force, pressure, temperature and humidity (Kayla Matthews, 2016). However, the materials' printable performance and satisfactory properties (Khoo *et al.*, 2015), the right ingredient ratio, mathematical model design and complex preparation process are all necessary and would need to be explored continuously (Momeni *et al.*, 2017).

1.8.1 Shape-shifting materials & materials used for 4D printing

Shape-shifting of flat materials into programmed 3D configurations is an emerging area of research that holds a lot of promise for the development of complex materials with unprecedented functionalities and properties. A wide range of shapeshifting phenomena is seen in nature and often originate from the spatial arrangement of the structural elements and their differential responses to the various types of stimuli (van Manen *et al.*, 2018). Many plants (such as pine cone (Studart, 2015) and mimosa pudica (Volkov *et al.*, 2010)) use the principle of cellulose orientation to guide water-driven deployment. The complex transformation behaviours is produced with more elaborate cellulose arrangements (Oliver *et al.*, 2016). Integration of 3D printing and active polymers, together with the necessary mathematical modelling and sequential stimulation,

allows the printed objects to transform between multiple configurations. These sorts of geometrically changeable polymers are not new. In fact, active polymers have been extensively investigated before 4D printing came into being. Three main classes of stimuli-responsive polymers have been used in shape-shifting materials. First, the reversible volumetric expansion or contraction of polymer gels has been widely used as a driving force for changing the shape of materials (Ionov, 2014). Many swellable polymers have good biocompatibility as well as biodegradability, which makes them suitable materials for biomedical applications (Liu & Urban, 2010). However, 4D behaviours can only occur when such smart hydrogels are combined with soft and elastic materials. Dielectric elastomers (DEs) and liquid crystal elastomers (LCEs) are also active materials that have the shape morphing capability upon triggering. LCE materials are composed of a liquid crystalline material aligned inside a polymeric network. In contrast to most swellable polymers, the response time of LCE is much shorter (Ohm *et al.*, 2010). A third widely reported class of active materials are shape memory polymers (SMP). Two key attributes of SMPs are their ability to fix a temporary programmed shape (fixity) and to subsequently recover the initial shape upon activation by a stimulus (recover) (Ge *et al.*, 2016). Both SMPs and LCEs can be printed to form a single-material structure and undergo morphing afterwards. To date, SMPs and hydrogels are the two main active polymers used in 4D printing. The most important feature that distinguishes SMPs from hydrogels is that the shape shifting pathway for SMPs can be programmed after they are printed, a feature that makes SMP attractive. However, most of the early studies on 4D printing focused on multi-material structures which can either be a mixture of different active materials or a combination of active materials and non-active materials (Wu *et al.*, 2018).

Figure 1-15 gives a comprehensive summary of types of printers, stimuli, materials and applications that have been used for 4D printing. In addition to the materials mentioned above, a number of other materials have the potential to be used for 4D printing

— such as wood, wax, fibres, plant cellulose, thermoplastic polyurethane (TPU) and ferrofluids (Sharma & Singholi, 2019). Polylactic acid (PLA) is a biodegradable plastic that is made into filaments for use in fused deposition moulding (FDM) 4D printing systems (Deshmukh *et al.*, 2019). In order to improve the shape memory effect of PLA, Lai & Lan (2013) melt-blended TPU with PLA to form a shape memory bio-based mixture. They found that the peak of the recovery stress largely corresponded to the predeformation temperatures. As the temperature increased, the recovery stress was enhanced.

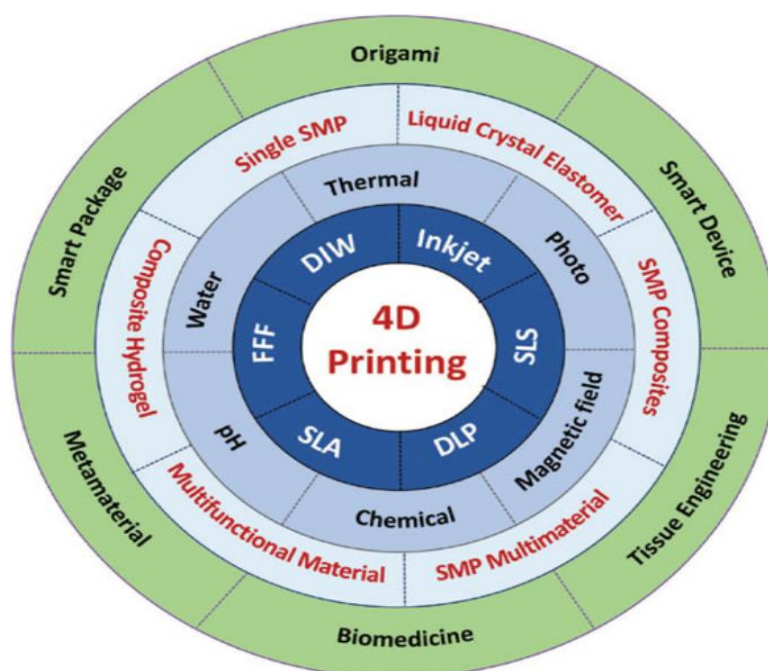


Figure 1-15 A summary of the types of printers, stimuli, materials and applications that have been used for 4D printing (Kuang *et al.*, 2019).

1.8.1.1 Shape memory polymers

“Shape memory polymers (SMPs) represent responsive polymers which can fix deformed temporary shape and recover their original shape upon the external stimulus.”

(Liu *et al.*, 2010)

SMPs are easily confused with shape-changing polymers (SCPs). Compared with the SMP, the shape change in SCP can only be converted to several stable states. In other words, this shape change cannot be controlled externally after it is formed. It is a non-programmable changing behaviour — however, under the influence of shape memory

effect (SME), SMP possesses the ability to transfer the shape from a temporary to a permanent state (Zhao *et al.*, 2015). **Figure 1-16** displays the common shape memory effects of shape memory materials. In theory, this is a programmable cycle and the SMP can recover its original shape several times (Hager *et al.*, 2015). SMPs also possess some distinct properties, such as that the density range must be between 900-1000 kg/m³, and 1-3 MPa stress is required for the deformation and recovery process. In addition, SMPs are able to withstand the deformation and can be processed into other polymer structures (Liu *et al.*, 2017). The literature shows that scientists have applied SMP in many areas, such as biomedical installations, aerospace, textile, civil engineering, energy, electrical engineering and daily necessities (Stuart *et al.*, 2010; Zhao, Qi & Xie, 2015; Liu *et al.*, 2017).

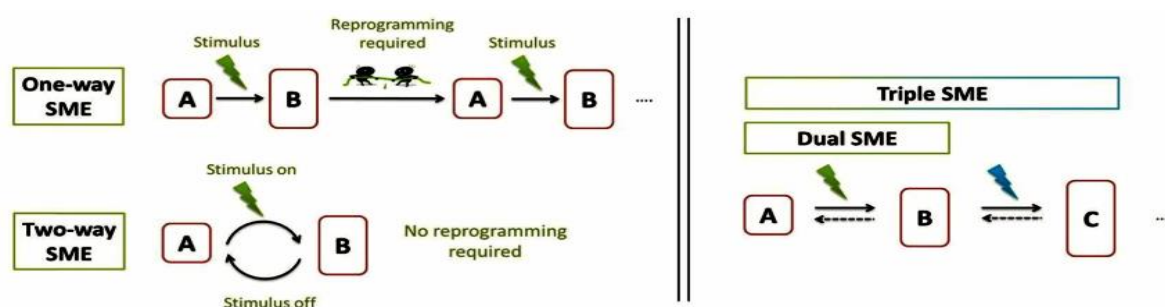


Figure 1-16 Schematic illustrations of (L) one-way and two-way SME & (R) Dual and Triple-SME (Hager *et al.*, 2015).

SMPs consist of net points and molecular switches which are formed by either chemical or physical crosslinking. These crosslinks contribute to the thermal transition as switching domains. For thermoplastics, the formation of phase-segregated morphology is the fundamental mechanism behind the SME of the material. For thermosets, the switch segments of chemical crosslinks are the network chains between net points, and the thermal transition of polymer segments is used as the shape memory switch. In comparison with thermoplastics, thermosets usually display better chemical, thermal, mechanical, and shape memory properties than thermoplastics (Lee & Chua, 2017).

For applications, SMPs tend to be reversible multiple times without any human intervention, which means that the temporary shape must reorganise itself and return the shape to its initial stage (Hager *et al.*, 2015). A new development trend in recent years is multi-shape memory polymers (multi-SMPs) (Zhao *et al.*, 2015). Liu *et al.* (2010) examined the shape memory performance of polymers including polyurethanes, polynorbornenes, styrene-butadiene copolymers, crosslinked polyethylenes and epoxy-based polymers with shape memory performances. Generally, depending on the synthesis route, the glass transition temperature (T_g) and melting temperature (T_m) are the two typical phase shift temperatures of SMPs. According to Hager *et al.* (2015), the conversion temperatures of different types of general SMPs are usually expressed in T_m or T_g . Scientists have found that, by blending with metal, ceramics or inorganics, SMP performance can be enhanced to form shape memory polymer composites (SMPCs). In addition, polymorphic memory effects, space control shape memory effects, and two-way shape memory effects have been the subject of the most innovative studies in the past few years (Meng & Li, 2013). Temperature and extended light are reported to be the two standard stimuli (Hager *et al.*, 2015). In the future, scientists may look for alternative stimuli to trigger shape changes. Exploring the new molecular structure or morphology of SMPs and discovering new shape memory effects constitute the main direction of future research (Khalid *et al.*, 2022).



1.8.2 The deformation mechanisms of the shape-shifting behaviours for hydrogel-based materials









Stimuli-sensitive hydrogels are named as one type of smart or intelligent polymer, where size, shape, solubility, conductivity, permeability, viscosity, mechanics can be altered, according to changes in the surrounding environment. Given the inherent water absorption/release behaviour of hydrogels, the swelling and shrinking behaviour of hydrogels have attracted a broad range of interest. However, since hydrogels are typically

isotropic materials that normally undergo uniform volume swelling and shrinking under stimulation, it is difficult to achieve asymmetric shape changes such as bending, curving and buckling. This poses a challenge to achieve shape-changing behaviours using environmentally sensitive hydrogels (He *et al.*, 2019). Bending and buckling are two basic deformation types. However, to date, scientists have created new transformations by combining different arrangements of materials, such as folding, rolling, twisting, helixing, curving, and waving. The strategies to achieve these changes are summarised in **Table 1-5**. To address this issue, researchers designed hybrid hydrogels with different (or even opposite) compositions and network structures, which introduces a new strategy for achieving complex shape-shifting for intelligent hydrogels. The deformation occurs when force is generated. Normally, an anisotropic deformation is often accomplished by fabrication of two materials (Zhang *et al.*, 2019). One is the active layer, made of stimuli-responsive materials; the other is a passive layer and is often the layer with low stiffness (for example rigid or soft materials). Once triggered by the activation stimulus, the deformation is generated on the active layer and spurs the passive change which leads to the change in the planer dimensions and curvature (Champeau *et al.*, 2020). The curvature of the multi-layer structures can be controlled based on the swelling ratio of the hydrogels, thickness ratio, the stiffness of the materials and the shape and size of the designs, etc. By inducing stress only in the desired directions, one additional programming parameter could be included in the form of anisotropic material properties so that more complex transformations could be achieved (Chen *et al.*, 2016). The multilayer structure enables accurate control in both directions and the amount of curving depends on the dimensions and material properties. However, the high shear stress levels at the interface between the layers and the multi manufacturing steps required are disadvantages of this type of structure (van Manen *et al.*, 2018).

Noteworthy, the strategy of using a single-layer structure has also been proposed. Instead of incorporating multiple different materials into a multilayer structure, a gradient in the material properties of a single-layer structure can be used to produce a stress gradient along the thickness of the material (Otero & Valero, 2017; van Manen *et al.*, 2018; Chen *et al.*, 2022;). The gradient could be achieved by exposing the light from one side while being partially absorbed by the polymer. In addition, non-homogenous exposure of the material to the activating stimulus can also generate a stress gradient. This strategy is typically more suitable for shape memory polymers (SMPs). SMPs can be retained with a temporary shape without an external stimulus and return to its original shape when exposed to a suitable external stimulation, which allows SMPs achieve the self-changing independently (Xia *et al.*, 2021). Compared with the multilayer structures, the high shear stress levels at the interface of two different materials can be avoided in a monolayer structure so that the risk of delamination is eliminated. However, complex manufacturing processes and limited forms of transformation limit the use of monolayers. Moreover, precisely controlling the location of the stimulus is also a huge challenge for monolayer structures (van Manen *et al.*, 2018). Therefore, it is of great significance to develop an intelligent mono-gel that can achieve autonomous deformation.

Table 1-5 Mechanical analysis of each shape deformation (Nam & Pei, 2019).

Shape Changing Behaviour		Mechanical Analysis
	Folding	Folding deformation is caused by a stress mismatch between rigid and active materials, which is possible with various swelling ratios (Drahansky <i>et al.</i> , 2016)
	Bending	Bending deformation is the swelling/shrinkage mismatch between both layers in response to activation stimuli, while sustaining the same strain at the interface between both layers, could result in different types of deformation (Cendula <i>et al.</i> , 2009)

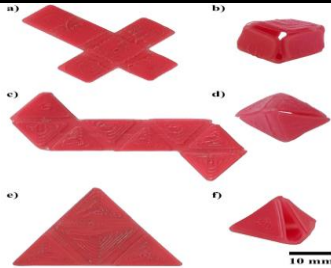
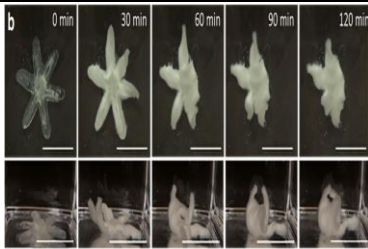
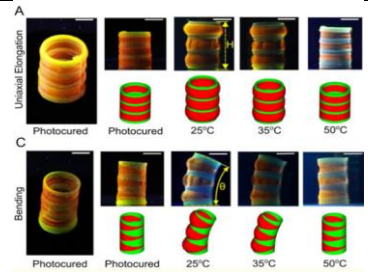
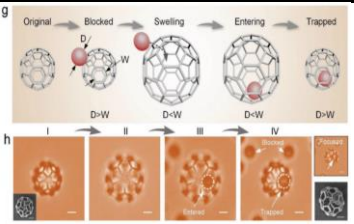
	Rolling	Rolling deformation is a normalized curvature that varies depending on both the expansion mismatch and the thickness, which is a nonlinear relationship between the rolling radius of one hand and the ratio of expansion and the sample thickness (Byun, Santangelo & Hayward, 2013)
	Twisting	Twisting deformation printed the fibres with certain angles to induce twisting, and by adjusting the print angles of active fibres, the final twist angle would be changed (Zhang & Hu, 2016)
	Helixing	Helixing deformation is made by a uniaxial expanding/shrinking active layer for a nonzero angle between the main straining direction of the active layer and the main axis of the bilayer strip (Janbaz, Hedayati & Zadpoor, 2016)
	Buckling	Buckling deformation that compressive stresses above a certain critical value will induce out-of-plane buckling of the flat structure (van Manen, Janbaz & Zadpoor, 2018)
	Curving	Based on the light intensity gradient along the thickness of material, a stress gradient could be created, which results in spontaneous curving of the structure after release from the substrate (Z. Zhao et al., 2017)
	Expansion/contraction	This mechanism is driven by a variety of expansion ratios between active and rigid materials, which consist of scalable, hydrophobic active materials and rigid materials (Bakarich et al., 2016)
	Waving	Wave shape deformation could occur in bilayers with comparable stiffness and layer thickness through swelling/shrinkage mismatch in response to activation stimuli (Cendula et al., 2009)
	Curling	Curling deformation is enabled by a stress mismatch between rigid and active materials from their different swelling properties (Tibbits et al., 2014)

1.9 4D printing state-of-the-art

The state-of-the-art commercial printable materials are mainly formulated to be tough, elastic, transparent, colourful, or recyclable, to satisfy various end applications. The current State-of-the-Art in the field of 4D printing is summarised in **Table 1-6**. Also, further applications are shown in Appendix A. There is definitely more that can be done to make the printed parts more useful, especially with the rapid development of active or smart materials. The initial conceptualisation of 4D printing was presented by Skylar Tibbits (in collaboration with StratasysTM). This marked the beginning of the 4D printing concept, where the fourth dimension is time. Since then, 4D printing has become a new and exciting evolution of 3D printing, increasingly gaining substantial attention from scientists and engineers from various disciplines. The essential characteristic of 4D printing is that the printed objects are no longer static. Instead, they can reshape in a pre-programmed and active manner over time, and may be accompanied with function evolution in the process. Beyond such a somewhat vague description, there is currently no standard definition of 4D printing. Even if there were a strict definition now, it would be challenged by future groundbreaking developments.

4D printing as an advanced concept opens a new field for applications in which a structure may be activated for self-transformation, reconfiguration, and reproduction through environmental free energies (Tibbits *et al.*, 2014). This solves several limitations, such as the significant volume requirement for storage, reduced flexibility in terms of product design and manufacture and lack of diversity and functionality (Choong *et al.*, 2017).

Table 1-6 Summary of the applications of 4D printing that exists in the literature.

Material(s)	Stimuli	Reaction time	Printing method	Prototype developed	Function	Reference
TecophilicTPU (HP-93A-100), NinjaFlex 85A	H ₂ O	> 11-h	FFF		Self-fold	(Baker <i>et al.</i> , 2019)
HEA, EPOX, BA, HDDA PEGDA, TAS, Irgacure 819, hydroquinone	H ₂ O	2-h	DLP UV printer		Sea star self-change	(Schwartz & Boydston, 2019)
DI water, NIPAM, AAM, Irgacure 2959, Laponite	H ₂ O & Heat	24-h	3D bioprinter		Bioinspired tubes	(Liu <i>et al.</i> , 2019)
AAc, NIPAAm, PVP, ethyl lactate	pH	0.39s	Illumination light		Drug load	(Hu <i>et al.</i> , 2019)

Chapter 2:

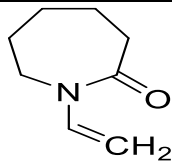
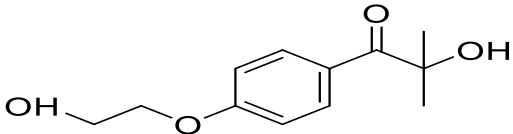
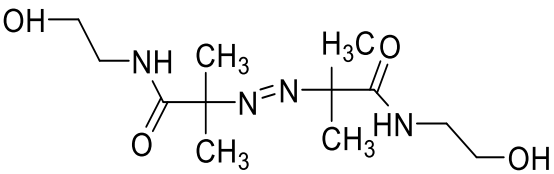
Experimental details

2 Experimental details

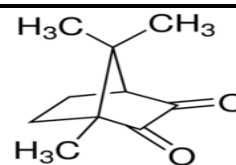
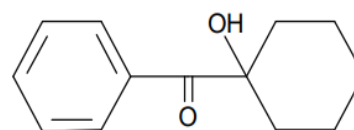
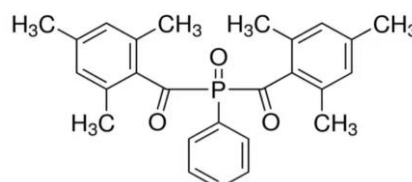
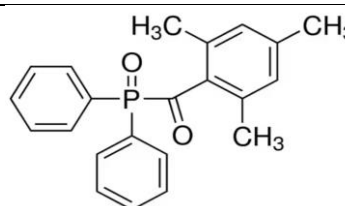
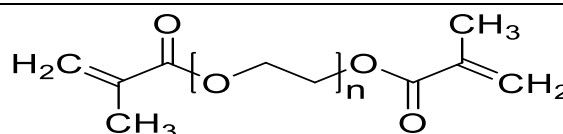
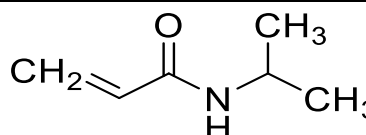
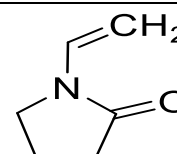
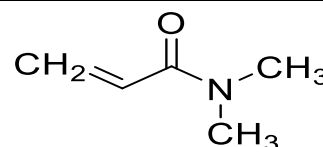
2.1 Materials' selection

The monomers employed throughout this research were N-Vinylcaprolactam (139.19 g/mol NVCL, Sigma Aldrich), N-vinyl-2-pyrrolidone (111.14 g/mol NVP, Sigma Aldrich), N, N-dimethylacrylamide (99.13 g/mol DMAAm, Sigma Aldrich), N-isopropylacrylamide >98% (NIPAAm, Tokyo Chemical Industry). The UV light-sensitive initiators used were 4-(2-hydroxyethoxy) phenyl-(2-hydroxy-2-propyl) ketone (Irgacure 2959, Siba Specialty Chemicals), the 1-Hydroxycyclohexyl phenyl ketone (Irgacure 184), 2,2'-Azobis[2-methyl-N-(2-hydroxyethyl) propionamide] (VA-086, Wako Chemicals GmbH Germany), 2,3-Bornanedione (Camphorquinone, Sigma Aldrich), Phenylbis(2,4,6-trimethyl-benzoyl)phosphine oxide (BAPO, Sigma Aldrich), Diphenyl(2,4,6-trimethyl-benzoyl)phosphine oxide (TPO, Sigma Aldrich) and H-Nu 400 IL (Spectra Photopolymers Industry). Polyethylene glycol 550 dimethacrylate (PEGDMA 550, Sigma Aldrich) was used as crosslinking agent. Flexible and elastic 50A (Formlabs) was used for fabricating the bilayer structures.

Table 2-1 Name and chemical structure of selected materials.

N-vinylcaprolactam (NVCL)	
4-(2-hydroxyethoxy)phenyl-(2-hydroxy-2-propyl)ketone (Irgacure 2959)	
2,2'-Azobis[2-methyl-N-(2-hydroxyethyl) propionamide] (VA-086)	

2,3-Bornanedione (Camphorquinone)

1-Hydroxycyclohexyl phenyl ketone
(Irgacure 184)Phenylbis(2,4,6-trimethyl-benzoyl)
phosphine oxide (BAPO)Diphenyl(2,4,6-trimethyl-benzoyl)
phosphine oxide (TPO)Poly (ethylene glycol) Dimethacrylate
(PEGDMA)*N*-isopropylacrylamide (NIPAAm)*N*-vinylpyrrolidone (NVP)*N,N*-dimethylacrylamide (DMAAm)

2.2 Preparation of hydrogels

The polymeric mixtures investigated in this study were prepared by combining the photoinitiator, monomers and crosslinker via free-radical polymerisation using ultraviolet (UV) light. The UV irradiation chamber (Dr. Gröbel UV- Elektronik GmbH) is a controllable light source with 20 UV-tubes, providing a spectral range of 315-400 nm

wavelength at an average intensity of 10-13.5 mW/cm². The monomer was put into a 100mL beaker and, using a pipette, was added to the other solution to form a mixture and formulate the different concentrations. To achieve homogeneity, a magnetic stirrer was used to stir the mixture for 20 minutes at 50°C heat. The solution was pipetted (1 mL) directly into silicone moulds containing disc impressions (23 mm diameter × 2.2 mm thickness) in preparation for photopolymerisation. The moulds were placed into the UV chamber for 10 minutes per side to ensure the gels had full exposure to the UV source during the process.

2.2.1 Photopolymerisation 1

NVCL was selected as the homopolymer because of its non-ionic, water-soluble, non-toxic, thermosensitive and biocompatible properties. The initial study was carried out to determine the effects of different photoinitiators and concentrations on hydrogels' properties. The samples were prepared by incorporating different concentrations of Irgacure 2959, VA-086 and Camphorquinone with NVCL to form the different monomeric compositions. The **Table 2-2** lists the composition details for the samples.

Table 2-2 Formulated polymer composition of NVCL physically crosslinked with varying concentrations of Irgacure 2959, VA-086 and Camphorquinone.

Sample	Irgacure 2959 (wt%)	VA-086 (wt%)	Camphorquinone (wt%)	NVCL (wt%)
P1	0.1	--	--	100
P2	--	0.1	--	100
P3	--	--	0.1	100
P4	0.2	--	--	100
P5	0.5	--	--	100
P6	1	--	--	100
P7	2	--	--	100
P8	3	--	--	100
P9	5	--	--	100

P10	--	0.5	--	100
P11	--	1	--	100
P12	--	2	--	100
P13	--	3	--	100

2.2.2 Photopolymerisation 2

After initial characterisation, the subsequent study investigated the effect on polymers' swelling properties by incorporating different concentrations of chemical crosslinker PEGDMA with NVCL. All xerogels were fixed at 0.1 wt% Irgacure 2959 and formed by photopolymerisation, See **Table 2-3** for the composition details of hydrogel samples with differing feed ratios.

Table 2-3 Formulated polymer composition of NVCL chemically crosslinked with varying concentrations of PEGDMA.

Sample	Irgacure 2959 (wt%)	NVCL (wt%)	PEGDMA (wt%)
C1	0.1	100	0.1
C2	0.1	100	1
C3	0.1	100	2
C4	0.1	100	5

2.2.3 Photopolymerisation 3

The third element of research investigated the effect on performance when incorporating different concentrations of other hydrophilic polymers. Based on the previous studies, the content of the photoinitiator was kept constant. See **Table 2-4** for formulation details.

Table 2-4 Formulated NVCL terpolymers physically and chemically crosslinked with varying concentrations of NVP, DMAAm, and NIPAAm.

Sample	Irgacure 2959 (wt.%)	NVP (wt.%)	DMAAm (wt.%)	NIPAAm (wt.%)	NVCL (wt.%)	PEGDMA (wt.%)
S1	0.1	30	-	-	70	-
S2	0.1	-	30	-	70	-
S3	0.1	15	15	-	70	-
S4	0.1	30	-	-	70	0.1
S5	0.1	30	-	-	70	2
S6	0.1	-	30	-	70	0.1
S7	0.1	-	30	-	70	2
S8	0.1	15	15	-	70	0.1
S9	0.1	15	15	-	70	2
S10	0.1	65	-	20	15	-
S11	0.1	-	65	20	15	-
S12	0.1	30	-	30	40	-
S13	0.1	25	-	50	25	-
S14	0.1	65	-	20	15	0.1
S15	0.1	65	-	20	15	2
S16	0.1	30	-	30	40	0.1
S17	0.1	30	-	30	40	2
S18	0.1	25	-	50	25	0.1
S19	0.1	25	-	50	25	2

2.3 Form 2 SLA 3D printing parameters

Form 2 is a stereolithography 3D printer developed by Formlab. Items are constructed on the platform from bottom to top in an upside-down posture. Only files in STL format can be accepted and uploaded to the printer. Based on a model designed in advance in computer-aided design software (CAD), the photopolymer resin is solidified by the provided UV laser (405 nm) to form a single layer onto the surface of the photopolymer vat, then the elevator platform descends and repeats the process to form a new layer until the object is built. The laser spot size of the 3D printer is 140 microns and the maximum printing size is $14.5 \times 14.5 \times 17.5 \text{ cm}^3$, with a range from 25-300 microns per

layer. A range of materials can be used for printing, including standard materials, tough & durable materials, flexible & elastic materials, rigid & structural materials, dental materials, biomedical materials, castable and specialty materials. The specific resin cartridge and tank and build platform should be correctly installed on the printer before the printing begins. During the printing process, the resin can be automatically filled into the self-heating resin tank. Depending on the material, the resin would be heated and kept at a constant temperature until the print is complete. Independently developed resins can also be used on this printer, but open mode needs to be activated. In this mode, the cartridge or tank detection function, resin heating, resin wiper, and resin dispensing are disabled. The resin also needs to be filled manually in the resin tank.

2.4 Patterns design

In order to explore whether further scenarios and patterns of 4D objects are able to display the same intelligent behaviour, more complex three-dimension objects were designed and prepared. The model of a jigsaw and flower shape were designed in Solidworks software, the size and patterns are shown in **Figure 2-1**. The thickness of the models is 2 mm. In order to prepare the silicone mould for photopolymerisation, the jigsaw and flower prototypes were printed using the SLA Form 2 3D printer with V2 High Temperature resin (Formlab company, Berlin, Germany). The prototype made of High Temperature resin has tough properties to avoid adhesion during the mould processing.

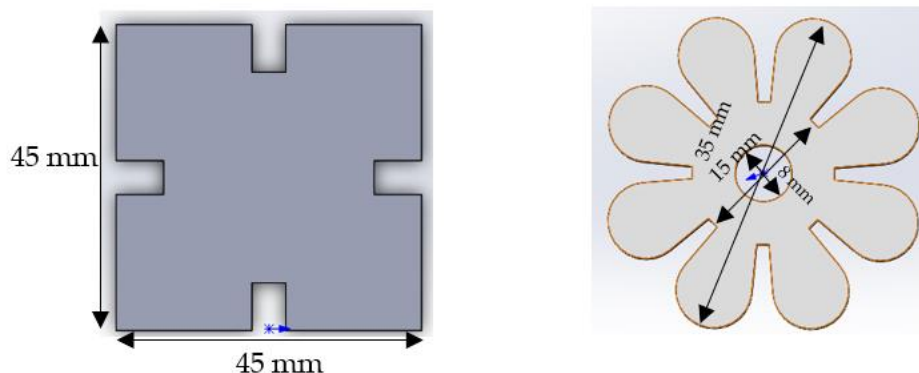


Figure 2-1 (L) Jigsaw and (R) flower shape models designed in Solidwork.

2.4.1 Development of mould for complex-shaped samples

2.4.1.1 Development Phase I: 3D printed mould

As a starting point, the model of the jigsaw shape was designed. It consists of a square (4.5 cm×4.5 cm) with a 0.5 cm intermediate groove in the middle (**Figure 2-1L**). Prior to the photopolymerisation commencing, a suitable mould should be produced to contain the solution under the UV irradiation. The technique of 3D printing is a rapid processing method that can quickly create custom components and products. Thus, the first puzzle mould was fabricated with support using Form 2 SLA 3D printer with V2 Flexible resin. The mould was first designed in Solidworks software and set in the Preform software. The support part was constructed at the base to ensure the quality of the practical part. Finally, the printed mould was immersed in an IPA solution for 20 minutes to remove the residual resin and exposed to UV light for 30 minutes to guarantee the residual resin was fully cured. According to the previous formulation, the solution was prepared and pipetted into the prepared mould and cured in the UV chamber for 10 minutes on each side.

2.4.1.2 Development Phase II: Silicone mould

The earlier study revealed that silicone mould is suitable for containing the UV curable liquid base material. The cured materials can be easily removed from the mould and possess an excellent appearance. Due to this reason, it was decided to make the next generation mould of silicone. As can be seen in **Figure 2-2L**, the puzzle prototype was printed with support using SLA Form 2 3D printer with V3 white resin. The model made of white resin has tough properties to avoid adhesion during the second processing. Then, after removal of the support, the printed puzzle model was immersed in the IPA solution for 20 minutes to remove the residual resin and exposed to UV light for 30 minutes to ensure the residual resin was fully cured. After that the printed and treated puzzle model was placed at the bottom of a clean glass petri dish. To prepare the silicone, the BASE and Red catalyst are mixed at a ratio of 9:1 in the plastic beaker (total 200 g) and stirred until

homogeneous. Subsequently, the mixture was allowed to stand until no more bubbles were produced and then poured into the petri dish until the container was fully filled. After 24 hours of self-solidification, the puzzle shape mould was successfully established (**Figure 2-2R**).



Figure 2-2 (L) The printed jigsaw shape prototype & (R) the jigsaw type silicone mould.

Using the same method, other complex shape components can be easily fabricated. A flower shape pattern was designed on the CAD software (2 mm thick) and modified in the Preform software (**Figure 2-3L**). Subsequently, the flower model was printed with support using SLA Form 2 3D printer with V2 high temperature resin. Using the same treating, processing, and manufacturing method, the final flower prototypes were created. It is worth noting that, since the angle between each of the petals was small, it was necessary to fill all the small angles when making the silicone moulds (**Figure 2-3R**). In addition, the samples had to be carefully removed from the mould to ensure their integrity.

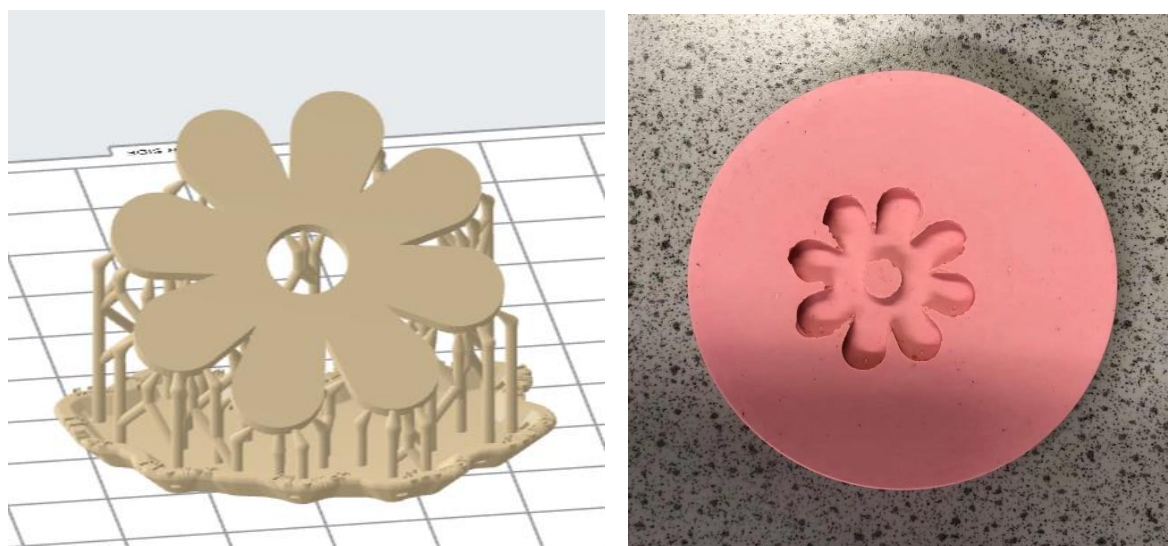


Figure 2-3 (L) The designed flower shape set in the Preform software & (R) flower shape silicone mould.

2.5 4D printing

In this study, 4D printing was carried out using the SLA 3D printer (Formlabs, Form 2) to print homemade resin. The prototype is created layer-by-layer following the model designed in advance using computer-aided design software (CAD). Preform software is the specific application to upload the model to the printer. The orientation and numbers of the model can be adjusted in Preform software automatically or manually and the support structure can also be created automatically in the software. The printer should switch to the open mode for third party resin use. After the model was uploaded to the printer, the homemade solution was prepared in the same way as the hydrogels in section 2.2.1. Based on the formulations, the monomer was first placed into a 250 mL beaker and other solutions were added to the beaker using a pipette to prepare a mixture of different concentrations. To achieve homogeneity, a magnetic stirrer was used to stir the mixture for 20 mins at 50°C heat. All in all, 50 g of solutions were prepared and poured directly into the resin tank in preparation for printing. After printing, any residue remaining on the printed objects was removed with a tissue containing IPA. The finished parts were placed into a UV box to post cure for 20 minutes.

2.5.1 4D printing trial with increasing Irgacure 2959 concentration

The formulations used for 4D printing were based on the formula (S7) of the photopolymerisation 3 trials. The initial study was carried out to determine the effects of different concentrations of photoinitiator on the printing. The influence of crosslinking methods on printing was also explored. The sample details are shown in **Table 2-5**.

Table 2-5 Formulated polymer composition of physically and chemically crosslinked NVCL with varying concentrations of Irgacure 2959.

Sample	Photoinitiator	Monomer	Crosslinker
	Irgacure 2959 (wt%)	NVCL (wt%)	PEGDMA (wt%)
D1	2	100	-
D2	3	100	-
D3	4	100	-
D4	5	100	-
D5	2	100	2
D6	3	100	2
D7	4	100	2
D8	5	100	2

2.5.2 4D printing trial with different types of photoinitiators

The second trial was designed to determine the effects of different photoinitiators on printing. All wavelengths of the photoinitiators had been found in the literature (Jing Zhang & Xiao, 2018). All samples were fixed at 2 wt% content of the photoinitiator and formed by 3D printing technique. The sample details are shown in **Table 2-6**.

Table 2-6 Formulated polymer composition of NVCL with varying photoinitiators.

Monomers (wt%)		Crosslinker (wt%)		Photoinitiators (wt%)		
NVCL	DMAAm	PEGDMA	Irgacure 184 (~246 nm)	TPO (~380 nm)	BAPO (~370 nm)	H-Nu 400IL (300~430 nm)
70	30	2	2	-	-	-
70	30	2	-	2	-	-
70	30	2	-	-	2	-
70	30	2	-	-	-	2

2.5.3 4D printing trial with a stepwise increase in H-Nu 400IL concentration

After the samples containing 2 wt% H-Nu 400 IL from the second trial showed a promising performance after printing, a subsequent study was performed to investigate the effect on polymers' properties by incorporating different concentrations of photoinitiator H-Nu 400 IL with NVCL. The preparation of the H-Nu 400IL based solutions was performed in a dark environment. Aluminium paper was used to surround the beaker to avoid prepolymerisation. See **Table 2-7** for the details of H-Nu 400IL samples with differing feed ratios.

Table 2-7 Formulated composition of NVCL copolymers with varying concentrations of H-Nu 400IL.

Samples	Monomers (wt %)		Crosslinkers (wt%)	Photoinitiators (wt %)
	NVCL	DMAAm	PEGDMA	H-Nu 400IL (300~430 nm)
F1	70	30	2	1
F2	70	30	2	2
F3	70	30	2	3
F4	70	30	2	4
F5	70	30	2	5

2.6 Preparation of aqueous polymer and copolymer solutions

Homogeneous solutions of the physically crosslinked gels were prepared by weighing appropriate amounts of the polymers and distilled water in a plastic tube. The mixtures were placed at room temperature for hours/days until the samples completely dissolved. The aqueous polymer and copolymer solutions were prepared for subsequent phase transition temperature measurements using cloud point measurement, differential scanning calorimetry (DSC), UV-spectroscopy, and rheological techniques.



Figure 2-4 *Polymer dissolved in the distilled water.*

2.7 Characterisation techniques

2.7.1 Attenuated total reflectance Fourier Transform Infrared Spectroscopy

Fourier Transform Infrared Spectroscopy (FTIR) offers quantitative and qualitative analysis for organic and inorganic samples. FTIR is an effective analytical instrument for detecting functional groups and characterising covalent bonding information. ATR-FTIR equipment consisted of a Perkin Elmer Spectrum One component with a conventional ATR accessory sampling. All data was obtained at ambient temperature ($<25^{\circ}\text{C}$), within the wavelength of $4000\text{-}650\text{ cm}^{-1}$ with a resolution of 0.5 cm^{-1} . Four scans for each sample cycle were used, with a compression force of 85 N. Subsequent analysis was performed using Spectrum One and the original software. The tests were performed in duplicate for each sample.

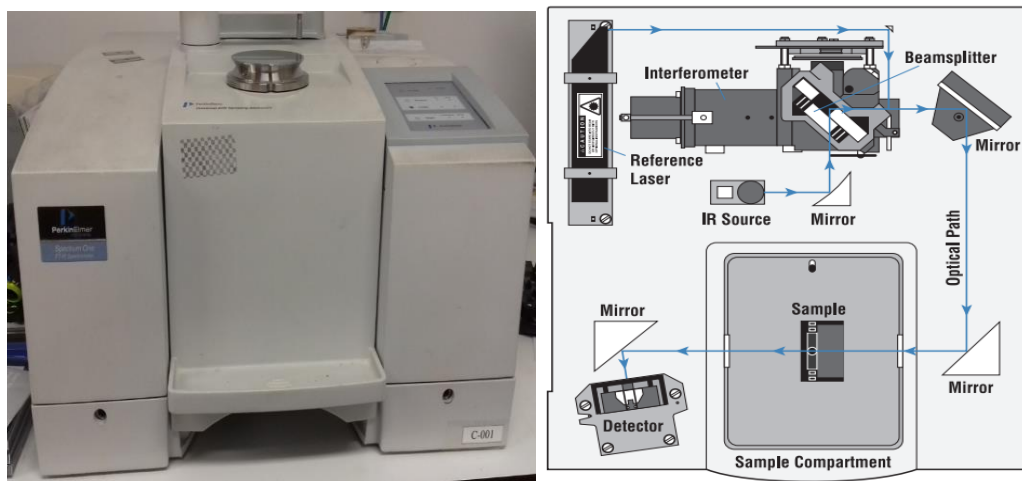


Figure 2-5 Perkin Elmer Spectrum One ATR-FTIR (left side) and FTIR spectrometer layout (right side).

2.7.2 Phase transition temperature analysis for physically crosslinked samples

2.7.2.1 Cloud point measurement

Cloud point measurement was used to investigate the transition temperature of the physically crosslinked gels. The aqueous polymer solution, which was prepared in advance (see Section 2.6), was put into a 10 mm diameter sealed glass test tube and placed in a thermostable bath. The temperature was gradually increased at a rate of less than 1°C per minute. After the temperature reached a few degrees below the pre-estimated transition temperature, cloud point was determined visually at the first sign of turbidity with an accuracy of $\pm 0.2^\circ\text{C}$. All tests were performed in triplicate. Photographs were taken of samples to show the contrasting visual appearance of the solutions above and below the phase transition temperature.

2.7.2.2 UV-spectroscopy

The LCST behaviour of samples was analysed using a UV-spectroscopy synergy HT BioTek plate reader. The temperature was increased by 1°C/min from 22°C to 50°C. The transmittance of samples in aqueous polymer solutions was measured at 500 nm. The solution was allowed to equilibrate at each temperature before transmittance was measured.

Each sample was measured in triplicate, with the average measurement used as the final absorbance.



Figure 2-6 *UV-spectroscopy Synergy HT BioTek plate reader.*

2.7.2.3 Differential scanning calorimetry of aqueous solutions

The DSC method was among the techniques used for the examination of the phase transition phenomenon exhibited by the temperature-sensitive polymers. Analysis was performed using a DSC 2920 DSC (TA Instruments). Samples of between 8-12 mg were transferred by micropipette and weighed using a Sartorius scale. A constant nitrogen gas flow at 20 mL/min was applied while performing all tests. Samples were ramped from 10 to 60°C at a rate of 1°C/min, referenced against an empty pan. The tests were performed in triplicate.

2.7.2.4 Rheology

Dynamic rheological tests were conducted on the physically crosslinked gel solution with a TA DISCOVERY HR-2 hybrid rheometer. In all cases, the instrument was calibrated for inertia and mapped before use. The gap between the plates was zeroed prior to loading of samples. To determine the phase transition temperature of the selected sample solutions, temperature ramp tests were performed. In this study, the storage modulus (G') and loss modulus (G'') were examined with a change in temperature from 15-50°C at the rate of 1°C/min. A 20 mm diameter stainless-steel parallel plate was used for testing all

samples. The test was conducted at a constant 0.5% strain and 0.1Hz frequency. The tests were performed in triplicate.

2.7.3 Phase transition temperature analysis for chemically crosslinked hydrogels

The LCST of the chemically crosslinked hydrogels was performed on the TA instruments 2920 apparatus. The hydrogel samples were allowed to swell until equilibrium in distilled water at room temperature. The sample's surface was wiped with moistened filter paper to remove free water and placed into the aluminium pans and weighed out, ranging from 8 to 12 mg, using a Sartorius scale with 0.01 mg resolution. DSC measurement was performed on swollen samples from 10°C to 60°C at a rate 1°C/min, referenced against an empty pan. The results were plotted as a function of heat flow (W/g) against temperature (°C). All tests were carried out in triplicate.

2.7.4 Swelling studies

The 20 mm diameter xerogel samples were placed in a vacuum oven for 24 hours at 50°C and their apparent dry weights (W_o) were measured. Samples were temperature tested below (ambient temperature) and above (50 Degree Celsius) the LCST. The disc samples were placed into Petri dishes containing 30mL distilled water (18ΩM). These Petri dishes were stored in the oven at 50°C or at room temperature, to ensure the correct LCST conditions. Petri dish lids were placed on the Petri dishes while in the oven to prevent evaporation. Periodically, the excess polymer solution was removed after predetermined time intervals by pouring the solution through a funnel. The samples were then blotted free of surface water with filter paper, and the weight of the sample was measured at room temperature after specific intervals (W_t) to determine water uptake until the swelling equilibrium was reached. All tests were carried out in triplicate. The swelling weight percentage for each time was calculated using Equation 2,

$$\text{Swelling ratio } \% = \frac{W_t - W_o}{W_o} \times 100 \% \quad \text{Equation 2}$$

where W_o is the weight of the dry and, W_i is the weight of hydrogel in the swollen state at a particular time during testing.

2.7.5 Gel fraction measurement

Gel fraction measurement may be used as a quantitative indicator of the efficiency of hydrogels network formation (Killion *et al.*, 2013). The gel fraction of all batches was measured using a round disc. The xerogel samples were placed into covered Petri dishes of distilled water at room temperature until equilibrium swelling was achieved. Once equilibrium swelling was attained, samples were dried in the vacuum oven at 100 Pa and 50°C until no change in weight was observed. Each sample was measured in triplicate. Gel fraction (%) was calculated using Equation 3,

$$\text{Gel fraction}\% = \frac{W_d}{W_o} \times 100\% \quad \text{Equation 3}$$

where W_o is the weight of the xerogel after photopolymerisation, and W_d represents the dried weight of the sample after extraction of soluble parts.

2.7.6 Pulsatile swelling studies

The apparent dry weight (W_0) of the samples was measured first. The samples were placed into Petri dishes containing distilled water (18ΩM). Samples were tested under switching conditions between ambient temperature and 50 degrees Celsius. The Petri dishes were first stored at room temperature and weighed after specific intervals (W_t) to determine water uptake until the swelling equilibrium was reached. Then these Petri dishes were placed into the oven to raise the temperature to 50°C (above LCST) and the weight of samples was measured again. After the new equilibrium state was reached, these Petri dishes were restored to room temperature. Before each measurement, the excess distilled water was dried with filter paper. The measurement was conducted in triplicate for each sample. The expanding percentage for each time was calculated using Equation 2.

2.7.7 Goniometry

Contact angle goniometry is used to assess a solid substrate's capacity to resist liquids (Mahltig, 2016). The 20 mm diameter xerogels were placed onto the stage area and a dynamic sessile droplet of water was placed on the sample surface while simultaneously photographing the spread of the drop over the surface of the xerogel. The angle measurement can be automatically performed on the photo screen. In this study, photos at 0 second and 115 seconds were used to analyse the wettability of the xerogels. All samples were measured in triplicate.

2.7.8 Tensile test

Tensile testing is a destructive test process that provides information about the tensile strength, yield strength, and ductility of the materials. It measures the force required to break a composite or plastic specimen and the extent to which the specimen stretches or elongates up to that breaking point (Saba *et al.*, 2018). The tensile strength at break of samples was analysed in line with ASTM standard D 638 Type V, using a Lloyd LRX tensometer set up in tensile mode. A $< 0.005\%$ of load cell is provided (resolution). Each sample was measured in quintuplet. Specimens were mounted and strained at a rate of 20 mm per minute until failure occurred. The dimensions of the dumbbell samples are shown in **Figure 2-7**.

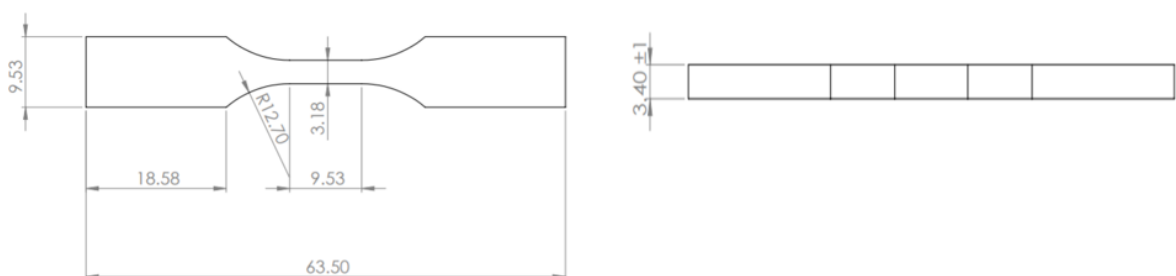


Figure 2-7 The dimensions of the dumbbell tensile bars.

2.8 Preparation of bilayer structures

The trial of bilayer structures was prepared in the shape of a rectangle strip and flower. The prototype of the strip and flower was 3D printed with high temperature V4 (Formlabs Company, Berlin, Germany) based on the designs shown in **Figure 2-1R**, **Figure 2-8**, **Figure 2-9** and **Figure 2-10** for silicone mould preparation. The bilayer structures were fabricated by the Dr. Gröbel UV chamber system for the detection of self-changing behaviours. The formulation S7 was used to form the active layer. The passive layer was prepared with commercial resin. For the flower samples and first and second-generation strips, the active layer was first prepared by pipetted the S7 solution into the shaped mould. The mould was exposed to UV light for 10 minutes to cure. After curing, the commercial resin was pipetted on the top of the cured active layer and cured in the UV chamber system for a further 10 minutes. For the third-generation strips, the passive layer was first generated by pipetted the commercial resin onto the shaped mould. The mould was placed into the UV chamber for 10 minutes to cure. After curing, the S7 solution was pipetted onto the prepared elastic shaped layer and cured for a further 10 minutes.

The passive layer was constructed using commercial flexible and elastic 50A resins obtained from the Formlabs Company. These types of resin are UV curable and can be used directly. The details of each layer are listed in the table below.

Table 2-8 *The mixing details of the bilayer structure.*

Bilayer structure		
Samples	Active layer	Passive layer
1	S7	Flexible resin
2	S7	Elastic 50A resin

2.8.1 The strips prototype design 1

Five types of strips were designed for the preparation of the bilayer structures. The strips were first designed in Solidworks software and converted to STL format. The

STL profiles were modified in Preform software and uploaded to the Form 2 3D printer for silicone mould manufacturing. Each strip is 75 mm in length and 20 mm in width. Further details of the parameters are explained in the following diagram.

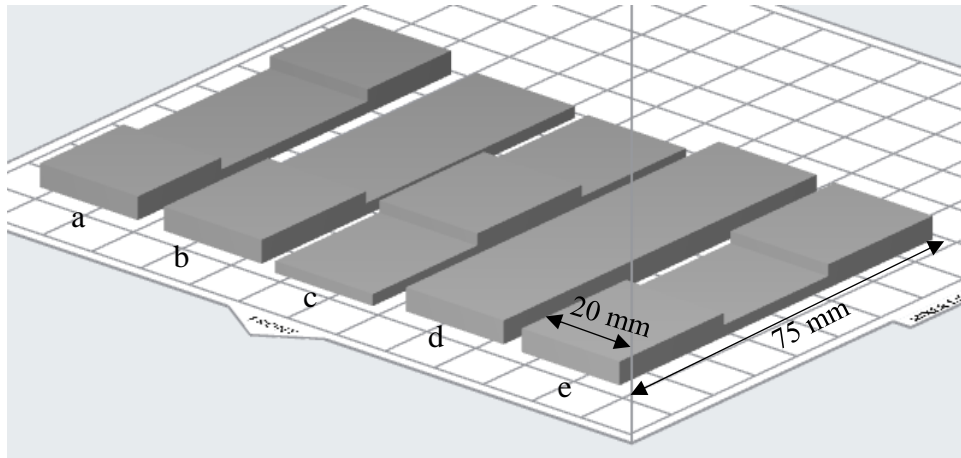


Figure 2-8 *The first generation of strips designed in Solidworks.*

- a) The two rectangles are designed on both sides of the long strip, with a length of 20 mm and a thickness of 1.5 mm. The thickness of the strip is 3 mm.
- b) The normal rectangle strip prototype thickness is 3 mm.
- c) The rectangle is designed in the middle of the long strip, with a length of 25 mm and a thickness of 1.5mm. The thickness of the strip is 3 mm.
- d) The rectangle is designed on one side of the long strip, with a length of 20 mm and a thickness of 1.5 mm. The thickness of the strip is 3 mm.
- e) The two rectangles are designed on both sides of the long strip, with a length of 15 mm and a thickness of 1.5 mm. The thickness of the strip is 3 mm.

2.8.2 The strips prototype design 2

The design for the second type of strips was carried out in Solidworks. All three types of design strips are 75 mm in length, 20 mm in width and 3 mm in thickness. In order to control the ratio between the passive and active layers, one end of these strips has been designed in a stepped shape. The stepped structure is designed to be 10 mm wide and 1 mm, 1.5 mm and 2 mm thick respectively. This effectively ensures that the ratio between

the active and passive layers is 0.5, 1 and 2. The designs were converted to STL files for modification and uploaded to the Form 2 3D printer for moulding with high temperature resin.

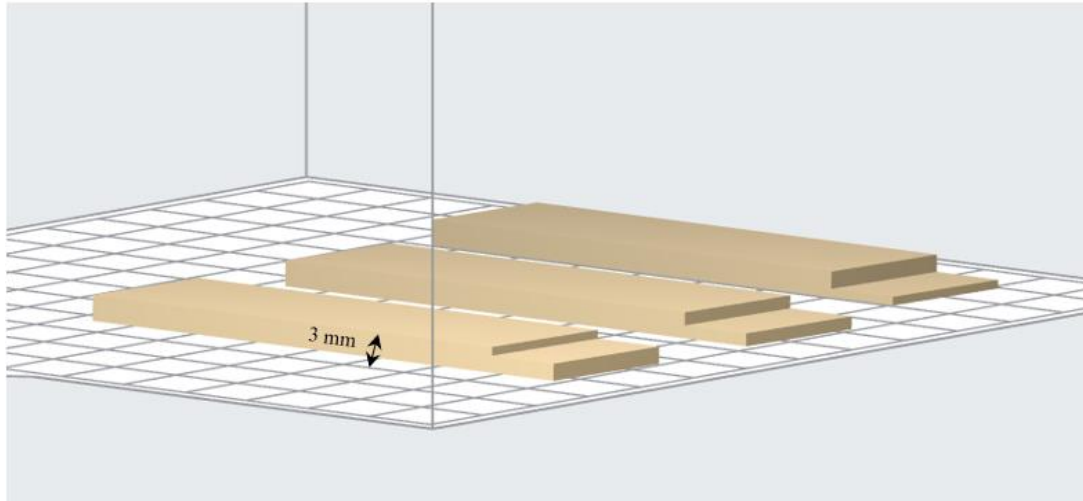


Figure 2-9 *The second generation of strips designed in Solidworks.*

2.8.3 The strips prototype design 3

More complex third types of strip pattern were also designed in Solidwork software in STL format and uploaded to Preform software for silicone mould preparation. Unlike the first design, the elastic resin is first dropped into the mould and cured under UV light to form the corresponding pattern. The S7 solution is then pipetted into the reserved rectangular slot for secondary curing to form double layer structures. All the strips are 85 mm in length and 15 mm in width. The details of dimensions for each strip is presented below.

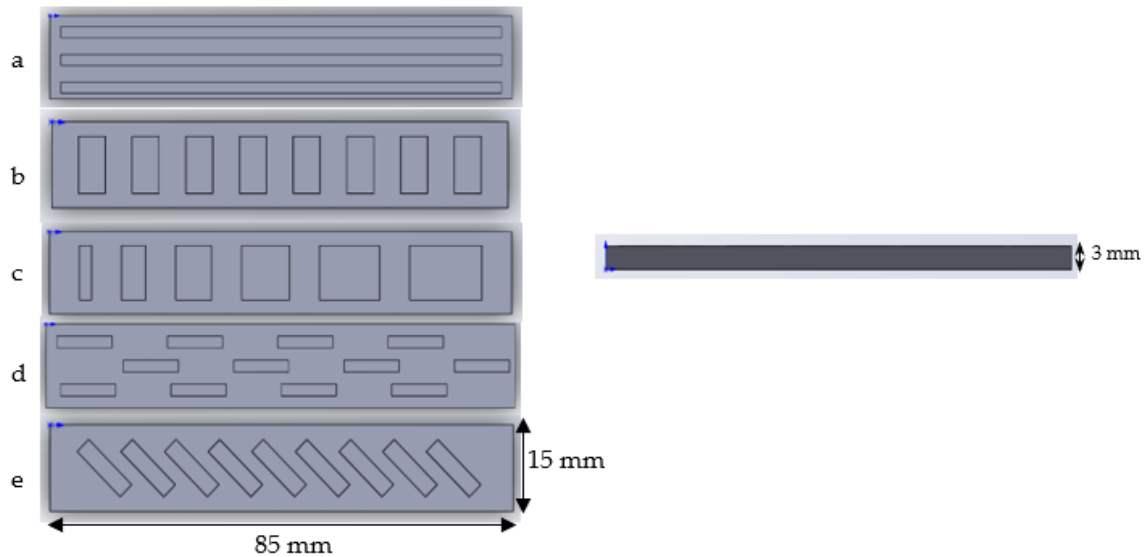


Figure 2-10 *The third generation of strips designed in the Solidworks.*

All strips in the third design are 3 mm thick.

- a) The strip consists of 3 long rectangular recesses, 2 mm in width, 81 mm in length 1.5 mm in thickness, spaced 5 mm apart from each other.
- b) The strip consists of 8 identically size rectangular recesses, 10 mm in width, 5 mm in length and 1.5 mm in thickness, spaced 5 mm apart from each other.
- c) The strip consists of 6 rectangular recesses. The length is increased by 2 mm each, from 2 mm to 12 mm. The width and thickness are maintained at 10 mm and 1.5 mm respectively.
- d) The strip consists of 12 rectangular recesses, 2 mm in width, 10 mm in length and 1.5 mm deep arranged in three rows. 4 recesses are arranged in each row 20 mm apart from each other.
- e) The strip consists of 9 identically size rectangular recesses placed at a 45-degree angle, 11 mm in width, 3 mm in length and 1.5 mm in thickness, spaced 3 mm apart from each other.

2.9 Fabrication of the demonstrators

To explore the practicality of layered samples, three different kinds of demonstrators were fabricated. The specific production process is as follows.

2.9.1 Automatic demonstrator

Initially, the AIT, LIT and TUS letters were designed in CAD software and uploaded to a Form 2 3D printer and printed using high temperature resin. The printed letters were then placed in a UV system for 20 minutes post-cure and painted in different colours. In the meantime, the type 'b' bilayer strips were prepared based on the method in Section 2.8.3. LOCTITE® 401 adhesive is a highly absorbent and water resistant. This adhesive has previously been used to bond superelastic polymers to shape memory polymers to construct bilayer structures (Janbaz *et al.*, 2016). Therefore, in order to avoid the letters falling off the strip during the experiment, they were glued to one side of the double layered strips. Subsequently, the strips with the letters were aligned neatly and fixed to the bottom of a transparent box by means of LOCTITE® 401 adhesive. Each strip was positioned 2 mm apart to ensure that the strips did not interfere with each other in the event of curving. Finally, when all the preparations had been completed, a large quantity of water was added to the container until the strips were submerged.

2.9.2 Toy train puller

The wooden toy locomotive was purchased from Smith's Toys (Ireland). The train head is fitted with magnets on both sides. Due to the light weight of the wooden train, two small pieces of iron were attached to the magnets to ensure that the train remained submerged throughout the experiment. A type 'b' double layer strip was prepared according to the method in Section 2.8.3. In order to clearly observe any changes, the type 'b' strip was coloured orange. A small hole was drilled in one end of the strip to connect the rope to the strip. The other end of the rope was tied to the chimney of the train. This created a simple connection between the train and the strip. The other end of the strip was

glued to the bottom of the container with LOCTITE® 401 adhesive. When all the preparations had been completed, a large quantity of water was added to the container until the train and strip were submerged.

2.9.3 Gripper

The bilayer flower was mounted on a long plastic burette. In order to connect the flower to the burette, a stretchable film was inserted into the burette. Thereafter, LOCTITE® 401 adhesive was applied around the hole in the centre of the flower so that the flower model could be mounted on the stretchable elastic film. This ensured that the flower would not fall off during the experiment. In addition, the outlet of the burette was sealed with tape. Subsequently, the burette with the flower model was then mounted on a burette clamp. This allowed the flower to be suspended and the height of the flower to be flexibly adjusted. For this work, an automatic heating water bath system was used so that the temperature could accurately be controlled over time. A thumb-sized bolt was placed at the bottom of the water bath. Finally, when all the preparations had been completed, a large quantity of water was poured into the water bath until the bolt was submerged.

2.10 Statistical Analysis

A statistical comparison of results was performed using a one-way ANOVA with Turkey post-tests to determine differences between each batch. Differences were considered significant when $p < 0.05$. The software package used to perform statistical analysis was IBM SPSS Statistics.

Chapter 3:

Results and Discussion

3 Results and Discussion

3.1 Formulation development I: Synthesis, characterisation, phase transition and swelling of temperature-responsive polymers based on poly (N-vinylcaprolactam)

3.1.1 Preface

Stimuli-responsive polymers, also known as smart, intelligent or environmentally sensitive polymers, have recently received increased attention (Hoffman, 2013; Moad, 2017; Wurm *et al.*, 2021). Stimuli-responsive polymers are polymers that react abruptly to small changes in physical or chemical conditions with relatively large phase or property changes. Physical stimuli, such as temperature, electric or magnetic fields, and mechanical stress, will affect the level of various energy sources and alter molecular interactions at critical onset points. Chemical stimuli, such as pH, chemical agents and ionic factors, change the interactions between polymer chains or solvents at molecular levels (Gil & Hudson, 2004). Among the stimuli-responsive polymers investigated; temperature is the most frequently used. Temperature-responsive materials can fold, shrink or swell in response to a change in temperature (Gao *et al.*, 2016). These behaviours enable temperature-responsive polymers to be used in biomedical applications such as diagnostics and cell culture.

Hydrogels are cross-linked hydrophilic polymer networks formed by the reaction of one or more monomers (Ahmed, 2015). They have the capability of imbibing significant amounts of fluid from the aqueous media in which they are placed, causing them to swell, while retaining their overall structure (Jakubiak *et al.*, 2003; Maitra & Shukla, 2014; Akhtar, Hanif & Ranjha, 2016; Vandenhoute *et al.*, 2017). Therefore, these polymer materials have extensive application capabilities in various areas, such as sealing (A. Singh

et al., 2010), coal dewatering (Ahmed, 2015), artificial snow (A. Singh et al., 2010), drug delivery systems and tissue engineering (Qiu & Park, 2012).

NVCL monomer contains a tertiary amine with a carbonyl group and methylene group which has bonds that separate during free radical polymerisation (**Figure 3-1**). PNVCL is a temperature-responsive polymer which was first investigated in 1968 (Norma A Cortez-Lemus & Licea-Claverie, 2016). The lower critical solution temperature (LCST) of PNVCL is close to physiological temperature (Maeda *et al.*, 2002), and has been acknowledged for its superior characteristics such as biocompatibility (Vihola *et al.*, 2008) and solubility (Anufrieva *et al.*, 2001) and also for its non-ionic and non-toxic features (Liu *et al.*, 2016). PNVCL is an ideal material for biomedical and industrial applications. In both theoretical and experimental studies, copolymerisation has been used to tune the desired functionalities of PNVCL. The incorporation of ionic monomers and hydrophilic or hydrophobic functional groups into the NVCL polymer chains can add new properties to the polymer while preserving the temperature-responsive properties (Norma A Cortez-Lemus & Licea-Claverie, 2016).

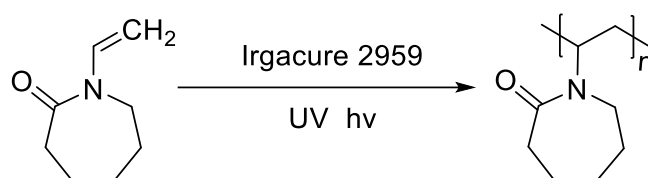


Figure 3-1 Scheme of photopolymerisation of poly (*N*-vinylcaprolactam) using Irgacure 2959 and *N*-vinylcaprolactam.

Research was undertaken to assess the polymers' potential suitability for 4D printing applications. The samples were initially synthesised using photopolymerisation in a UV chamber as it employs the same mechanism as the stereolithography (SLA) technique, whereby UV radiation is used to cure liquid-based materials. In addition, photopolymerisation has a higher curing efficiency than SLA, and can produce a large number of samples for characterisation in a short timeframe. Therefore, the sensing

wavelength of the selected photoinitiators is required to be within the range of the laser provided by the UV chamber and SLA printer.

UV photopolymerisation is a common and safe free radical polymerisation method widely used to prepare materials (Nowak *et al.*, 2017). The initial formulation development concentrated on examining the effect of different photoinitiators and crosslinkers with different feed ratios on the material behaviours. The effects on the three selected photoinitiators were based on the wavelengths used with different concentrations in the synthesis of novel hydrogels. The crosslinker PEGDMA was employed with different contents to prepare chemically-crosslinked hydrogels. The chemical structure of the xerogels was explored by ATR-FTIR. The characterisation methods DSC, cloud point measurement, UV spectrometry, and rheology were used to investigate the LCST of the aqueous polymer solutions. Gel fraction measurement and swelling analysis were performed to detect the potential change at critical temperatures, both below and above LCST. The goniometry and tensile tests were carried out to explore the mechanical properties and hydrophilicity of the chemical xerogels.

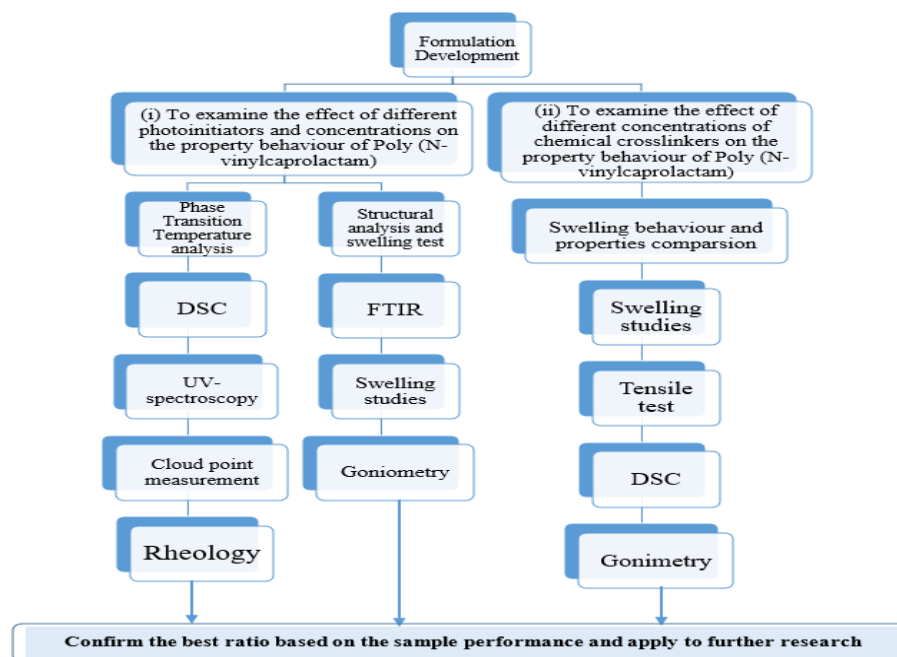


Figure 3-2 Work breakdown structure for the evaluation of the effects of the different concentrations of photoinitiators and crosslinkers.

3.1.2 Preparation of physically crosslinked xerogels

Based on the crosslinking mechanism, hydrogels can be formed to be either physically or chemically crosslinked. These are synthesised from hydrophilic monomers by either chain or step-growth, along with a functional crosslinker to promote network formulation (Maitra & Shukla, 2014). Physically crosslinked hydrogels have become significant as they are relatively easy to produce and have the advantage of not requiring crosslinking agents during their synthesis (Varaprasad *et al.*, 2017).

Physically crosslinked hydrogels can absorb water. However, inhomogeneities or network defects may occur due to free chain ends or chain loops (Maitra & Shukla, 2014). The physically crosslinked xerogels were prepared by polymerising NVCL into PNVCL using Irgacure 2959, VA-086 and CQ initiators at different feed ratios for photopolymerisation. In photocurable systems, photoinitiators mainly impact curing speed, yellowing and cost (Yagci *et al.*, 2010). The photoinitiators are substances which can be decomposed and cleave when exposed to a UV or visible light source which initiates the polymerisation of the monomers.

In this research, the three different photoinitiators: **Irgacure 2959**, **VA-086**, and **Camphorquinone (CQ)** were applied to initiate polymerisation of the NVCL monomers. Irgacure 2959 undergoes cleavage from the excited triplet state, which generates two radicals for initiating polymerisation (Occhetta *et al.*, 2015). Irgacure 2959 is water-soluble and tolerated by many cell types over a range of mammalian species (Duquette & Dumont, 2019). Moreover, Irgacure 2959 has low toxicity when compared to other Irgacure initiators (Mondschein *et al.*, 2017). VA-086 is an azo initiator having two hydroxyl groups. It was selected due to its outstanding biocompatibility and low cytotoxicity (Park *et al.*, 2010). The low cytotoxicity photosensitiser camphorquinone is ubiquitously used in visible-light-curing systems (Jakubiak *et al.*, 2003; Singh *et al.*, 2017). It is a powder with an intense yellow colour which remains after light irradiation

(Kowalska *et al.*, 2021). Based on the method provided in Section 2.2, the quantified solutions were pipetted into silicone moulds and cured under UV irradiation. Cured samples were dried in a 50°C oven for 24 hours.

All xerogel samples which were formed using different concentrations of Irgacure 2959 exhibited a bright, transparent appearance and had a glossy surface. This indicates that the chains are arranged randomly and present no actual boundaries or discontinuities from which light can be reflected (Ward, 2009). After drying in the oven, no shrinkage or swelling occurred. However, they were slightly brittle and had a pungent odour (**Figure 3-3**).



Figure 3-3 *PNVCL xerogels fabricated using different concentrations of Irgacure 2959 initiator: a) 0.1 wt%; b) 0.2 wt%; c) 0.5 wt%; d) 1 wt%; e) 2 wt%; f) 3 wt%; g) 5 wt%.*

In comparison, the xerogels developed using VA-086 displayed a worse appearance than Irgacure 2959 samples. As can be seen in **Figure 3-4**, bubbles appeared in the synthesised samples. This escalated as the concentration of photoinitiator was increased. Such bubbles filled the entire sample when the concentration increased to 3 wt%. At high concentration, UV radiation results in an increase in the contribution of the diffusion relaxation process. At the freshly solidified interface, the initiator concentration of the post-cured solution is higher than that of the non-cured solution, causing a decrease in the dynamic surface tension. Thus, bubbles were produced (Jiang *et al.*, 2018). Though the samples were fully intact, the surface was rough and uneven. Additionally, the gels had a pungent odour and were slightly brittle.

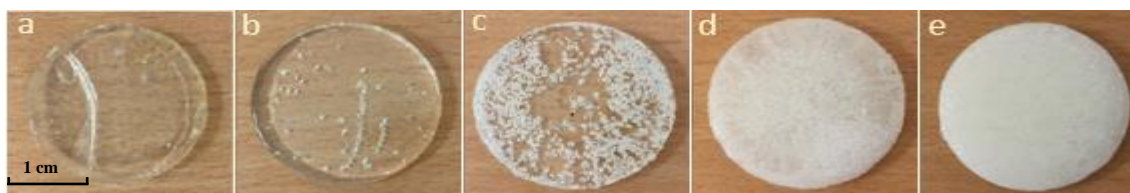


Figure 3-4 PNVCL xerogels fabricated using different concentrations of VA-086 initiator: a) 0.1 wt%; b) 0.5 wt%; c) 1 wt%; d) 2 wt%; e) 3 wt%.

The samples blended with CQ were unable to cure at all when exposed to UV radiation. Based on the literature, Camphorquinone, a blue light photoinitiator, is commonly used in dental resin formulation. However, since the 3D printer light source of this project is UV, the sample made by CQ was not considered further.

Comparison of the samples showed that the PNVCL xerogels formed using Irgacure 2959 exhibited the best performances and were considered for further study to develop the chemical crosslinking hydrogels. In order to possess the lowest cytotoxic potential in the same group sample, **0.1 wt%** was considered for use in the preparation of smart chemically crosslinked materials.

3.1.3 Preparation of chemically crosslinked xerogels

Hydrophilic polymers such as PNVCL can be crosslinked by either physical or chemical means to form hydrogels (Varaprasad *et al.*, 2017). Chemical crosslinks are formed by creating a permanent junction (covalent bond) between molecule chains, which provides excellent mechanical strength and a stable three-dimensional network structure for hydrogels (Hennink & van Nostrum, 2012; Ahmed, 2015).

PNVCL is a temperature-sensitive polymer. Most literature has reported that PNVCL is an outstanding material for biomedical applications due to its biocompatibility and acceptable cytotoxicity (Liu *et al.*, 2016). When a crosslinker is added to the solution, the LCST behaviour can be tailored, the network structure and mechanical strength can be heightened, and the longevity of the polymers increased. To date, monomers such as N-vinylpyrrolidone (NVP) (Norma Aidé Cortez-Lemus & Licea-Claverie, 2018),

methacrylic acid (MAA) (Liu *et al.*, 2016), 2-hydroxyethylacrylate (HEA) (Kenessova *et al.*, 2019) and poly(ethylene oxide) (PEO) (Vihola *et al.*, 2007) have been used for copolymerisation. PEGDMA is commonly used as a crosslinker, which serves to enhance the internal molecule network strength and is added into the solution to form the chemically crosslinked gels. It has attracted broad interest as a material for tissue engineering due to its biocompatibility, non-toxicity, variable degradability and its ability to be formed readily *in situ* (Beamish *et al.*, 2010; Aldana *et al.*, 2017; Burke *et al.*, 2019).

Chemically crosslinked gels can be obtained by radical polymerisation in the presence of the crosslinked agent. The crosslinked polymers were achieved by adding crosslinker PEGDMA into NVCL monomer solution, which creates the chemical bonds between the linear molecules, forming a network structure to increase the strength and elasticity of the samples. Using wet chemistry methods, monomer mixtures of NVCL-PEGDMA were prepared by using 0.1 wt% Irgacure 2959 photoinitiator which was based on the earlier study, and various concentrations of PEGDMA crosslinker. The mixture solution was pipetted into the silicone mould and cured under UV irradiation. The cured samples were dried in a 50°C oven for 24 hours. **Figure 3-5** illustrates the photopolymerisation reaction occurring in NVCL-PEGDMA mixtures.

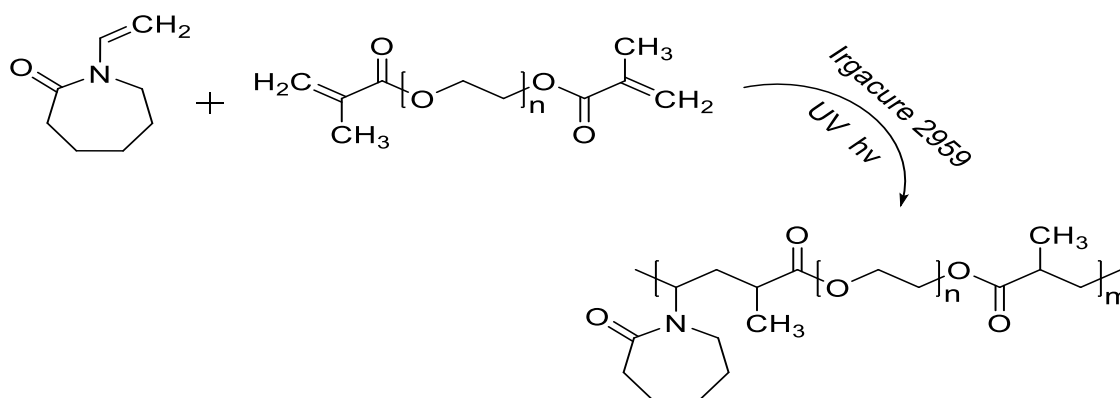


Figure 3-5 Polymerisation of NVCL with PEGDMA.

0.1 wt% Irgacure 2959 was employed to initiate the polymerisation with 0.1 wt%, 1 wt%, 2 wt% and 5 wt% of PEGDMA to form chemically crosslinked gels. As **Figure 3-**

6 shows, the polymers exhibited a clear, transparent appearance. The disc samples were non-brittle due to the chemical bonds produced between the linear molecules. After drying in the oven, no shrinkage or swelling of the sample occurred. All samples showed a consistent shape without noticeable impurities. Due to the presence of covalent bonds, the chemically crosslinked hydrogels are able to absorb water and swell. As 4D printed objects require the ability to change shape or properties when acted on by a stimulus, the swelling ability of the samples is the most critical factor in achieving 4D transformation. The size, integrity and properties of the sample before and after expansion need to be considered. Therefore, an array of analytical techniques was used in selecting the best sample and application of the formulation into the next phase of the research.

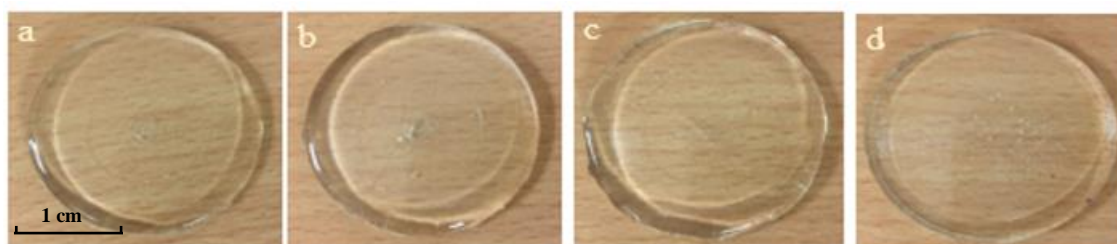


Figure 3-6 Chemically crosslinked PNVCCL polymers fabricated using different concentrations of PEGDMA: a) 0.1 wt%; b) 1 wt%; c) 2 wt%; d) 5 wt%.

3.1.4 Attenuated total reflectance Fourier Transform Infrared Spectroscopy

ATR-FTIR was used to determine if PNVCCL was successfully photopolymerised. Both physical and chemical crosslinking was explored. When infrared radiation passes through the sample, some of the radiation is absorbed by the sample and some radiation is passed (i.e., transmitted). The signal generated at the detector represents the spectral “fingerprint” of the molecule. Different structures or chemical bonds can be distinguished following the spectral curve.

Figure 3-7 shows the spectra of NVCL and PNVCCL, and **Table 3-1** identifies the peaks. Functional groups in NVCL and PNVCCL found by FTIR show a carbonyl (C=O) absorption band, which depends on the degree of hydrogen bonding and the physical state

of the compound (Dalton *et al.*, 2018). In the NVCL spectrum, the characteristic carbonyl peak is seen at 1622 cm^{-1} , a C=C peak was observed at 1649 cm^{-1} , while the aliphatic C-H stretching peak is observed at 2933 cm^{-1} and 2850 cm^{-1} . The peaks at 3108 cm^{-1} and 992 cm^{-1} correspond to the characteristic vinyl peaks ($=\text{CH}$ and $=\text{CH}_2$), similar to those reported in the literature (Dalton *et al.*, 2018).

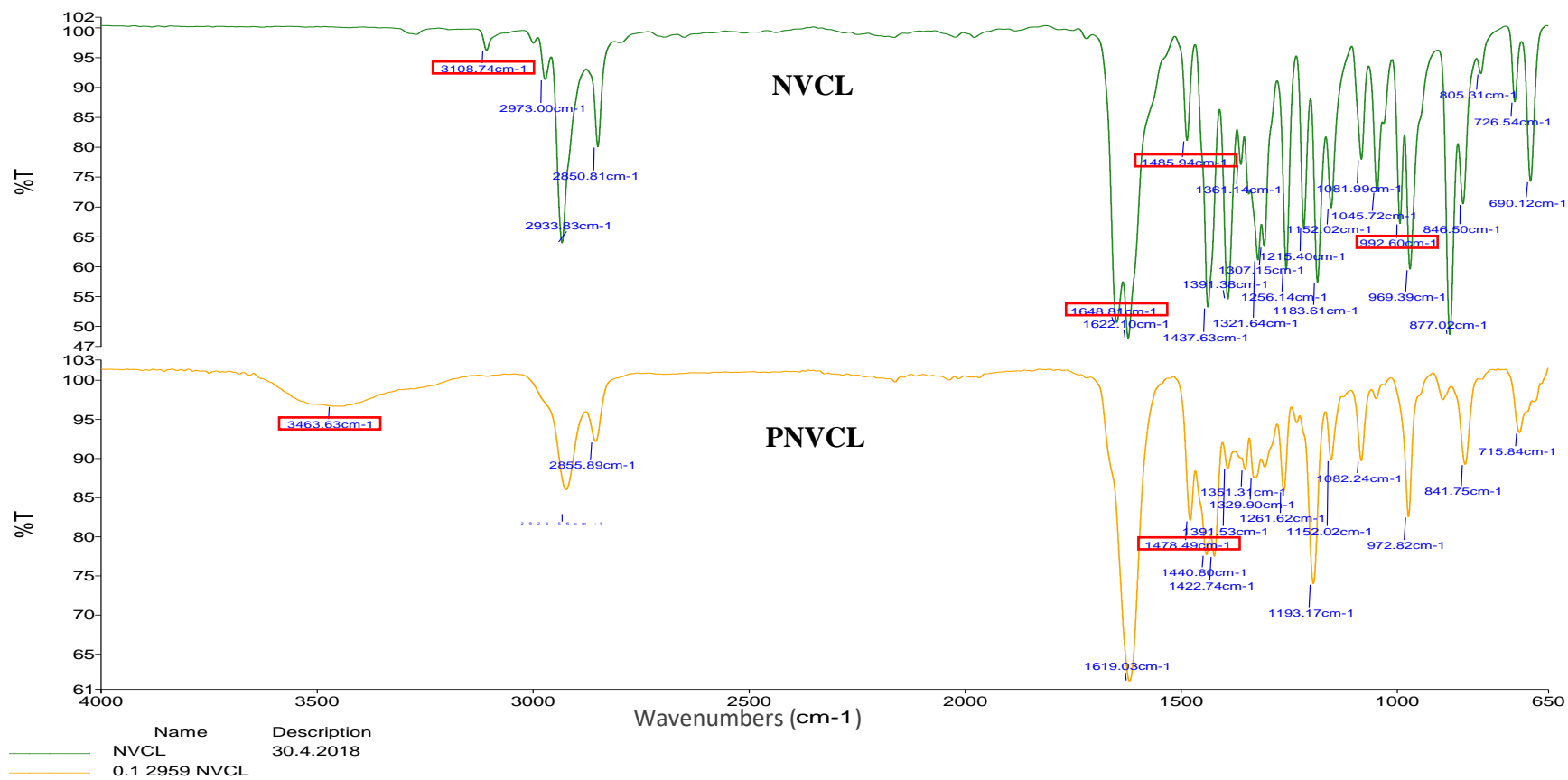


Figure 3-7 FTIR spectra of NVCL and PNVCCL. Block marks the C=C and vinyl group in NVCL monomer. These are absent in PNVCCL polymer. $n=2$.

Table 3-1 Functional groups in NVCL and PNVCL following FTIR analysis.

Functional Group	Shift(cm^{-1})	
	NVCL	PNVCL
Aliphatic C-H	2933, 2850	2924, 2855
C=O	1622	1619
C-N	1486	1478
-CH ₂ -	1438	1440
C=C	1649	---
=CH and =CH ₂	3108, 992	---
O-H	---	3463

In the spectrum of PNVCL, a carbonyl peak was located at 1619 cm^{-1} , as in the monomer. The carbon double bond peak disappeared in the PNVCL spectrum. The aliphatic C-H stretching peak was observed at 2924 cm^{-1} and 2855 cm^{-1} , close to that of the monomer. The $-\text{CH}_2-$ peak is situated at 1440 cm^{-1} . The stretching and bending vibration peaks of the C-H bond in the vinyl group ($=\text{CH}$ and $=\text{CH}_2$) were seen at 3108 cm^{-1} and 992 cm^{-1} in the monomer, and disappeared in the spectrum of PNVCL. These results indicate that polymerisation was a success without any change in the caprolactam ring. As **Figure 3-7** shows, a new broad peak arose at 3463 cm^{-1} , related to O-H stretching. This may be associated with the polymer hydrophilic character and ability to absorb moisture from the air or have been brought about by the photoinitiator, which has O-H bonds in its structure (Kozanoğlu, 2008; Lee *et al.*, 2013; Halligan *et al.*, 2020).

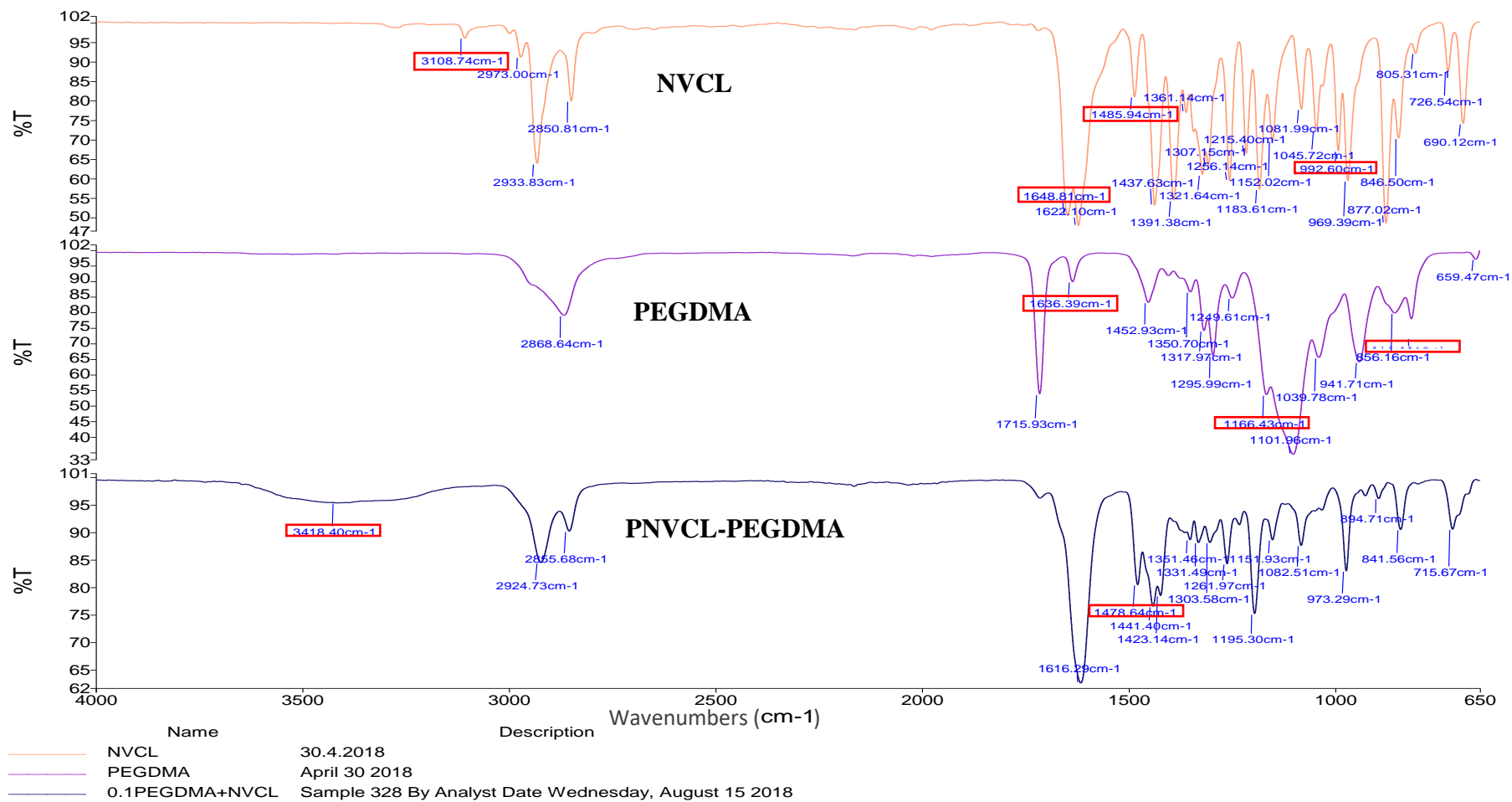


Figure 3-8 FTIR spectra of NVCL, PEGDMA and PNVL. Block marks the C=C and vinyl group in NVCL monomer. These are absent in the PNVL base polymers. $n=2$.

Table 3-2 Functional groups in NVCL, PEGDMA and PNVCL-PEGDMA following FTIR analysis.

Functional Group	Shift(cm^{-1})		
	NVCL	PEGDMA	PNVCL-PEGDMA
Aliphatic C-H	2933, 2850	2868	2924, 2855
C=O	1622	1716	1616
C-N	1486	---	1478
-CH ₂ -	1438	1453	1441
C=C	1649	1637	---
C-O	---	1166	---
=CH and =CH ₂	3108, 992	815	---
O-H	---	---	3418

Figure 3-8 shows the spectra of NVCL, PEGDMA and chemically crosslinked gels PNVCL-PEGDMA, and **Table 3-2** identifies the associated peaks. In the NVCL spectrum, the characteristic carbonyl peak is seen at 1622 cm^{-1} , a C=C peak was recognised at 1649 cm^{-1} while the aliphatic C-H stretching peak is observed at 2933 cm^{-1} and 2850 cm^{-1} . The peaks at 3108 cm^{-1} and 992 cm^{-1} correspond to the characteristic vinyl peaks (=CH and =CH₂).

In the PEGDMA spectrum, the ester groups were identified at 1716 cm^{-1} and 1166 cm^{-1} , represented as the carbonyl peak (C=O) and C-O stretching respectively. The peak at 2868 cm^{-1} corresponds to the aliphatic C-H stretching, and =CH and =CH₂ peaks were located at 815 cm^{-1} and 1453 cm^{-1} (Killion *et al.*, 2011). In the PNVCL-PEGDMA spectrum, the C=O peak is observed at 1616 cm^{-1} and a C-N stretching was observed at 1478 cm^{-1} , similar to NVCL monomer. The caprolactam ring was not changed due to the aliphatic C-H peaks as seen at 2924 cm^{-1} and 2855 cm^{-1} , and -CH₂- was located at 1441 cm^{-1} . This evidence indicated that the chemically crosslinked gels were successfully synthesised in the absence of C=C, C-O peaks, which exist in NVCL and PEGDMA monomers respectively. The stretching and bending vibration peaks of the C-H bond in the vinyl group (=CH and =CH₂) observed at 3108 cm^{-1} and 992 cm^{-1} in the monomer

disappeared as well. This is in agreement with reports in the literature (Wu *et al.*, 2010; Halligan *et al.*, 2020).

3.1.5 Phase transition determination in solution

3.1.5.1 Cloud point analysis

The covalent bonds in chemically crosslinked hydrogels are strong, and these types of polymers cannot dissolve in solution. The phase transition in solution was thus determined using only physically crosslinked hydrogels (Chai *et al.*, 2017). In this study, cloud point was used for analysing different concentrations of the homopolymer in an aqueous solution. The cloud point is defined as the temperature at which the first sign of opacity appear in the solution (Idris *et al.*, 2017). At ambient temperature, the aqueous polymer solutions were transparent. Due to the effect of the hydrophobic chain, the polymers precipitated gradually, resulting in the solutions becoming opaque as the temperature increased. At a certain temperature, the growing internal energy breaks the hydrogen bonds. The water molecules are released to generate polar polymer conformation, leading to an increased entropy in the system. In order to maintain the balance of entropy, the prevalence of hydrophobic molecules tends to aggregate, leading to phase transition (Wu *et al.*, 2007). Essentially, LCST behaviour is dependent on the enthalpy and entropy of the mixture of the polymer with water. **Figure 3-9** illustrates the appearance of polymers at 5% in solution with different concentrations of photoinitiator in solution at 32°C. There was a clear difference in the degree of whiteness in each tube. The turbidity from left to right decreased. Moreover, white precipitates can be observed at the bottom of tube “A” and “B”, which contained 5 wt% and 2 wt% Irgacure 2959 photoinitiator. However, the solution with 0.1 wt% Irgacure 2959 (F) was almost transparent. **Figure 3-10** summarises the cloud point result for PNVCL samples containing different concentrations of photoinitiator. In conclusion, increasing initiator concentrations resulted in a decrease in LCST. However, no relevant papers were found in the literature relating to this finding.

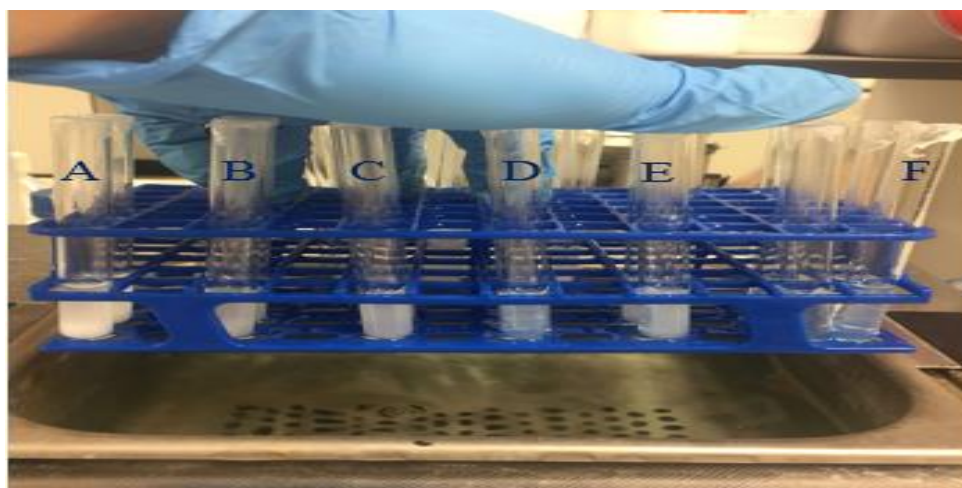


Figure 3-9 Cloud point of PNVCL samples at 10 wt% in solution with different concentrations of photoinitiator at 32°C: A. 5wt% Irgacure 2959, B. 2 wt% Irgacure 2959, C. 1 wt% Irgacure 2959, D 0.5 wt% Irgacure 2959, E 0.2wt% Irgacure 2959, F. 0.1 wt% Irgacure 2959.

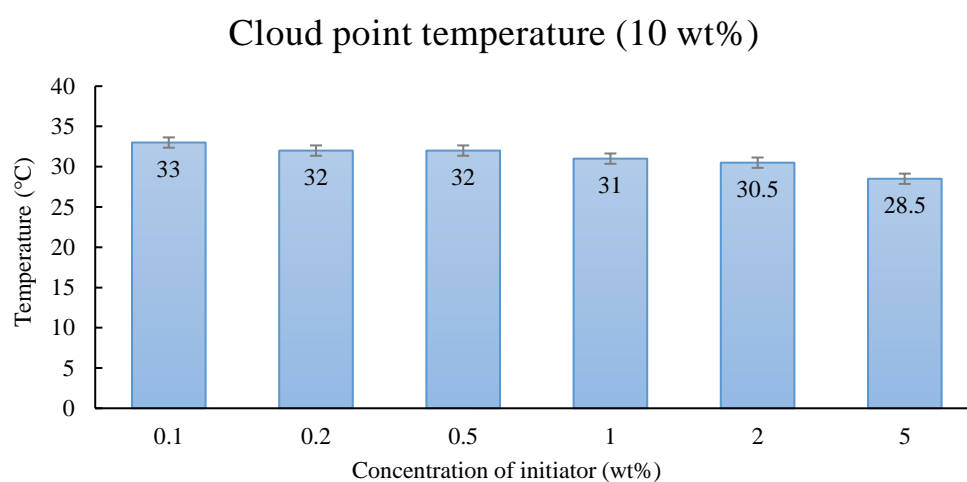


Figure 3-10 Cloud point analysis of PNVCL with different concentrations of photoinitiator (Irgacure 2959). $n=3$, $P<0.05$.

Additional testing was carried out on specific aqueous solution concentrations of homopolymer. Based on the initial study, the sample which contained 0.1 wt% Irgacure 2959 was considered for further testing. Solutions consisting of 5 wt% and 10 wt% homopolymers were used. The polymer solutions were transparent at 25°C. As the temperature increased close to its LCST, a precipitate began to appear in the solution. The cloud point of the 5 wt% PNVCL solution was determined to be 32.5°C, while the cloud

point of the 10 wt% PNVCL solution was 33°C, with similar results being reported in the literature (Gaballa *et al.*, 2013; Halligan *et al.*, 2017). Corresponding to the literature, the LCST increases as the polymer concentration in solution increases. This is attributed to endothermic enthalpy; an increase is required to break a number of hydrogen bonds according to the solute increasing (Halligan *et al.*, 2017; Marsili *et al.*, 2021).

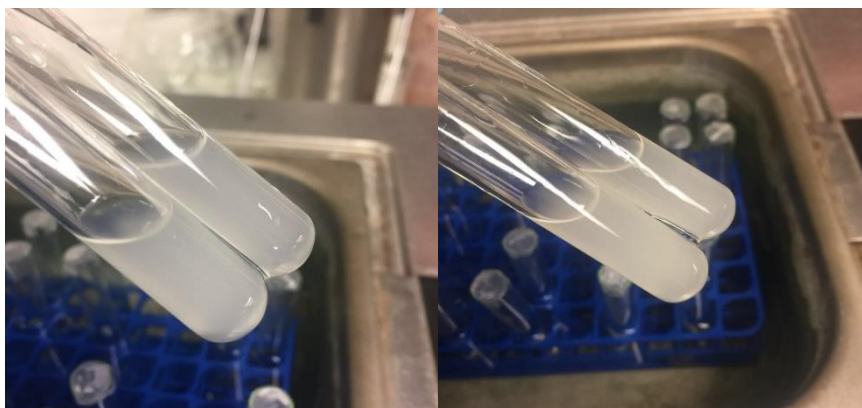


Figure 3-11 Cloud point of samples (L) PNVCL 5 wt% at 32.3°C, (R) 10 wt% at 33°C. $n=3$, $p>0.05$.

3.1.5.2 UV-spectroscopy

The phase separation temperature of aqueous solutions of PNVCL homopolymer (5 wt%) and (10 wt%) was investigated using UV-spectroscopy. This technique measured the absorbance of the sample, which is a universally used technique for determination of the LCST (Lee *et al.*, 2013). All samples were analysed over a temperature range of 22°C–50°C. **Figure 3-12** illustrates the phase transition behaviour of PNVCL. The change in absorbance is attributed to the transfer of the solution state — optically transparent below the LCST and opaque above the LCST (Halligan *et al.*, 2017). The inflexion point in the S-shaped curve corresponds to the LCST. The solution which contained 5 wt% homopolymer was shown to have a LCST at 33°C, whereas, the 10 wt% sample experienced the phase transition at 35°C. The phase transition temperature obtained for PNVCL was within the range already reported in the literature (Lee *et al.*, 2013; Ferraz *et al.*, 2014).

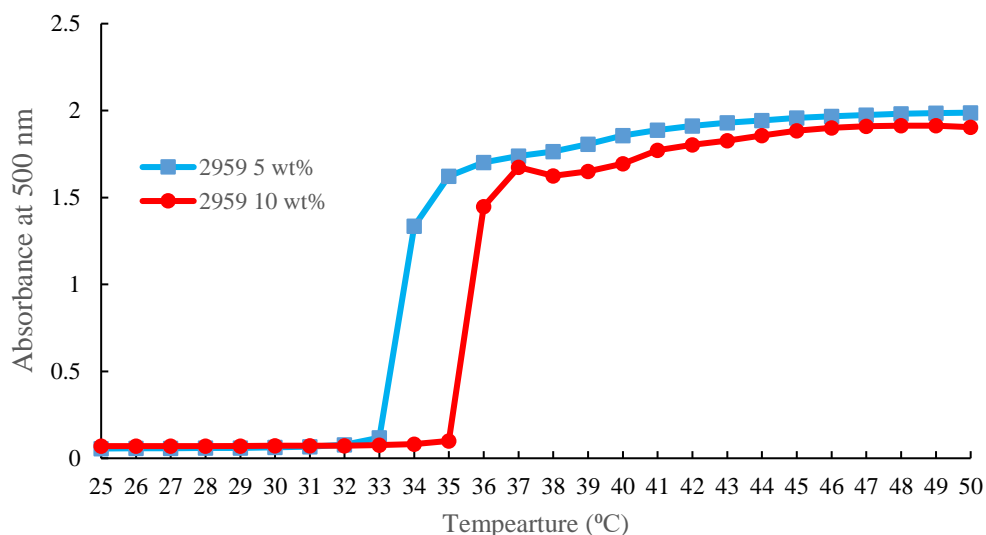


Figure 3-12 UV Spectrometry illustrating the LCST of PNVCCL homopolymer at different aqueous solution concentrations. $n=3$, $p>0.05$.

3.1.5.3 Differential scanning calorimetry

Differential scanning calorimetry is a thermal analytical technique used to measure a heat capacity of a material, its endothermic and exothermic transitions, and relationship to change in temperature (Dalton *et al.*, 2014). It was used to analyse the LCST behaviour in this body of work. As the temperature rises slowly, it facilitates the separation of adjacent peaks or adjacent weightless platforms while displaying a small peak. Mohammed (2018) *et al.* reported that the LCST of PNVCCL was around 32°C (Mohammed *et al.*, 2018). In all cases, the onset value of the endothermic peak was used to establish the LCST value. The relatively strong hydrogen bonds formed between water molecules and N-H and C=O groups in dilute solutions become weaker and break as the temperature is raised, resulting in the endothermic heat of phase separation. One transition was identified at 32.1°C during the heating scan of the 10 wt% homopolymer sample. This transition was related to the LCST, in accordance with the values achieved by previous research (Ferraz *et al.*, 2014). The LCST detected using DSC exhibited a similar result and trend as that of UV-spectroscopy.

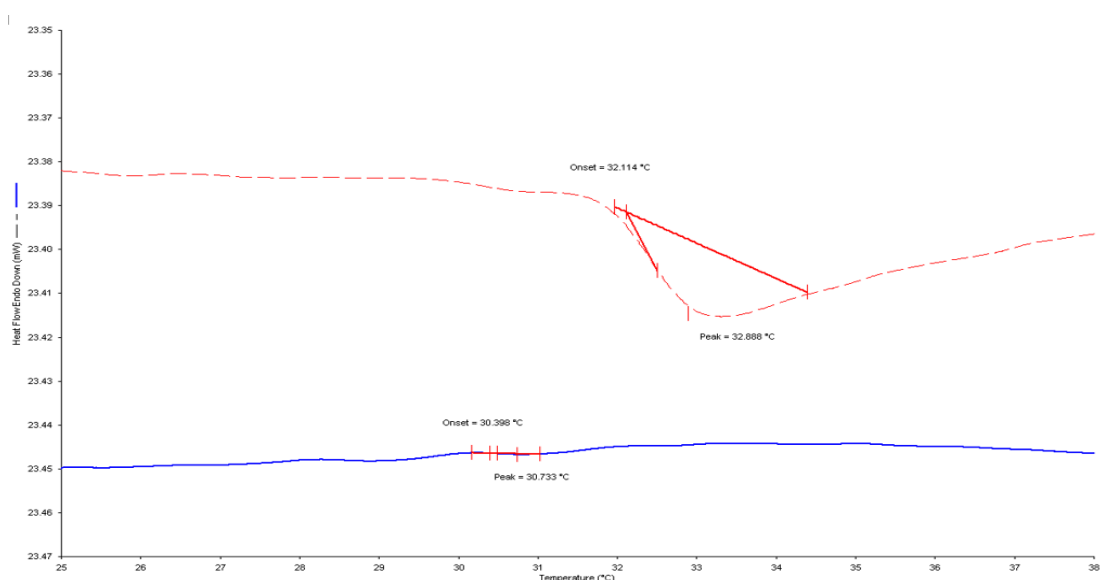


Figure 3-13 A representative thermogram illustrating the LCST of PNVCCL (5 and 10 wt%) aqueous solution. $n=3$, $p>0.05$.

3.1.5.4 Rheology

Rheology is the study of flow and deformation of matter. The rheological analysis was performed in an aqueous solution. It is known that there is an absolute relationship between the average molar mass of a polymer in a solution and a relative increase in viscosity (Wu *et al.*, 2022). As the temperature ramps, the solution changes from transparent to opaque, resulting in a change in viscosity. The onset point of the viscosity transition is the phase transition temperature. The elastic component (G') and storage modulus (G'') were measured as a function of temperature within the range of 15-50°C. It is known that the G' dominates the LCST when it first responds and is more sensitive to temperature change than the G'' (Halligan *et al.*, 2017). **Figure 3-14** illustrates the behaviours of storage and loss modulus. As the graph shows, the transition temperature appears at 32.9°C. As the LCST is approached, the values for G' and G'' increase until $G'=G''$ — this is known as the gelation point (Laupheimer *et al.*, 2015).

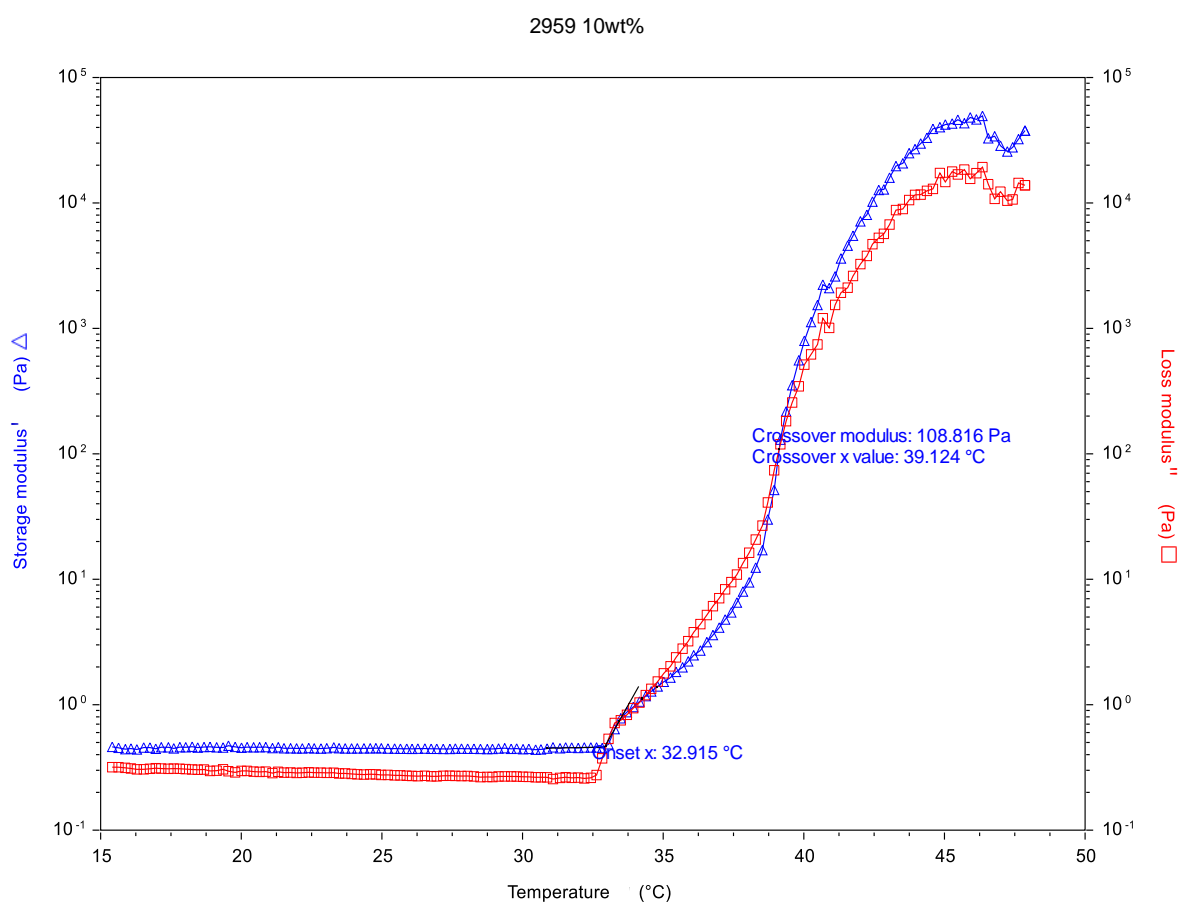


Figure 3-14 Rheological data illustrating the LCST and gelation point of PNVCN (10 wt%) aqueous solution. $n=3$.

In summary, the results detected using the four techniques illustrated a similar trend: the greater the concentration of PNVCN in solution, the higher LCST that was achieved.

Table 3-3 The LCST of PNVCN homopolymer detected by four techniques.

	Cloud point measurement (°C)	DSC (°C)	UV-spectroscopy (°C)	Rheology (°C)
5 wt.%	32.5	30.9	33	33.2
10 wt.%	33	32.2	35	32.9

3.1.6 Swelling studies

A hydrogel-based sample placed in distilled water will absorb the solvent until the elasticity of the network and osmotic pressure is balanced until an equilibrium state is reached (Neffe *et al.*, 2011). Swelling from water absorption is a characteristic property of

hydrophilic groups in a polymer. The form and degree of the crosslinking impacts the swelling properties of hydrogels, The mechanical properties of a hydrogel, however, decrease as the degree of swelling increases (Killion *et al.*, 2013).

PEGDMA is hydrophilic in nature. Swelling studies were performed on the samples developed by physical crosslinking: P1 (0.1wt% Irgacure 2959/100 wt% NVCL), and chemically crosslinked: C1 (0.1 wt%), C2 (1 wt%), C3 (2 wt%) and C4 (5 wt%). All studies were carried out above and below LCST.

The weight of the hydrogels was measured at hourly intervals. The swelling percentage of the hydrogel at a given time was calculated by subtracting the weight of the dry polymer. The final swelling ratio was calculated using Equation 2. The results of this study are shown graphically in **Figure 3-15** while **Figure 3-17** displays images of the samples during the analysis. All samples below LCST softened and became sticky after 1-hour. After 6-hours, due to the lack of insufficient covalent bonds present, the physically crosslinked gels and chemically crosslinked gels formed at both 0.1 and 1 wt.% crosslinker started to break down. After 24-hours, the hydrogels were fully dissolved and lost their structure. However, the swollen weight of 2 and 5 wt.% samples continued to increase. Contrasting swelling behaviour was observed for PNVCL samples above LCST. Millimetre grid paper was used to observe the gels' volume change during the experiment. All samples displayed a similar trend, with peak swelling achieved around 48-hours. It was noticed that the amount of water absorbed by the gels was not substantial.

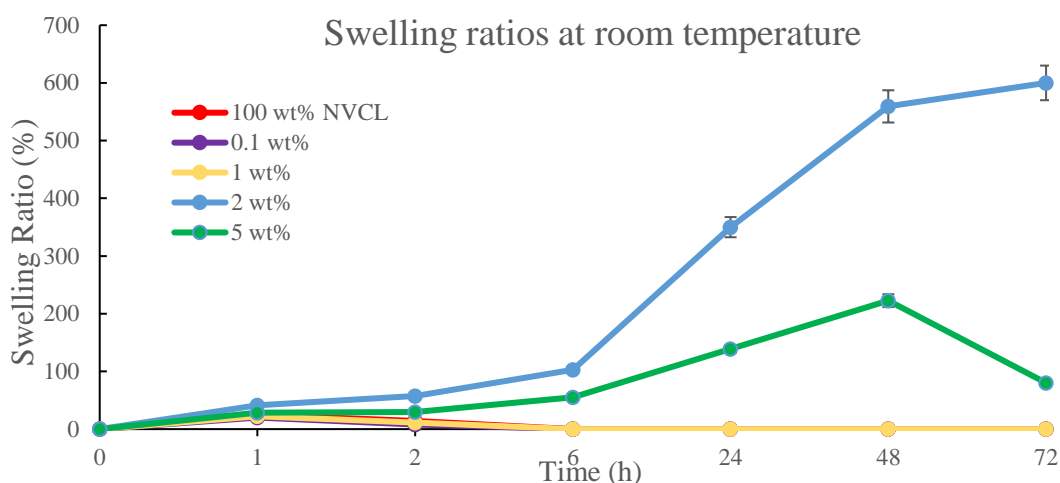


Figure 3-15 Swelling studies of PNVCLE-PEGDMA hydrogels with 0.1-5 wt% PEGDMA crosslinker concentration at ambient temperature. $n=3$, $p<0.05$.

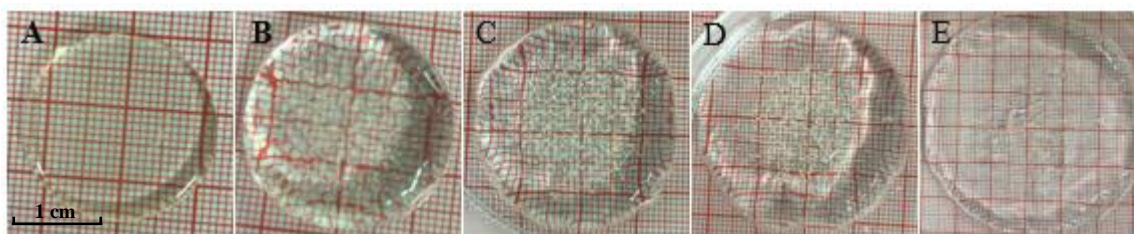


Figure 3-16 PNVCLE-PEGDMA 2 wt% (C3) samples submerged in distilled water at times: A 0 hours, B 2 hours, C 24 hours, D 48 hours and E 72 hours at ambient temperature.

When the temperature is \leq LCST, the hydrogen-bonding of the hydrophilic segments dominates the interaction between water and the polymer chains — the gel absorbs water which dissolves the polymer chains and forms the swollen state. When the temperature increases \geq LCST, the polymer chains shrink and expel water molecules through hydrophobic segments, which results in the precipitation of polymer, so a globular state appears (Li *et al.*, 2014). At room temperature, the C3 samples achieved swelling equilibrium at 72 hours of submersion. The swelling weight was recorded as being on average six times heavier than the dry weight. Though the samples had maintained shape and integrity, they were soft and easily broken with manual handling after submersion. When the temperature rose above the LCST, the samples' swelling become not substantial. In addition, as the gel absorbs the increased amount of water, cracks begin to appear in the

C5 type samples after 24-hours at room temperature. This resulted in a loss of weight in the C5 samples during drying and measurement. The chemically cross-linked gels prepared from 2 wt.% PEGDMA exhibited greater water absorption and were able to maintain their integrity after swelling compared to samples prepared from 5 wt.% PEGDMA.

According to the literature, due to the water assimilation, a hydrogel's mechanical properties decrease as the percentage of swelling increases (Iyer *et al.*, 2008). The results for the homopolymers in this study correlate with such findings. Therefore, although the C3 chemically crosslinked NVCL homopolymer displays smart behaviour, its weak mechanical properties are a significant drawback.

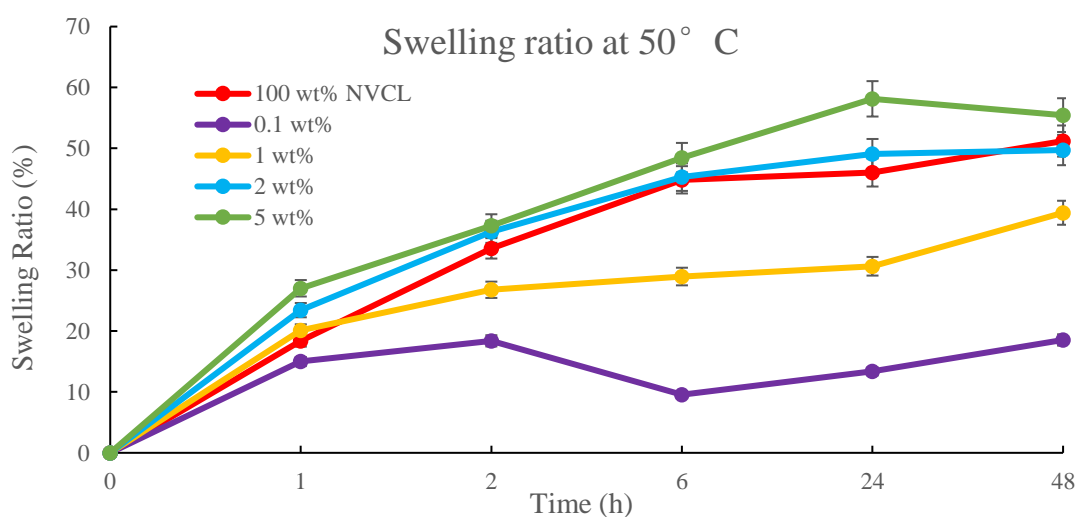


Figure 3-17 Swelling studies of PNVCL-PEGDMA hydrogels with 0.1-5 wt% PEGDMA crosslinker concentration at 50°C. $n=3$, $p>0.05$.

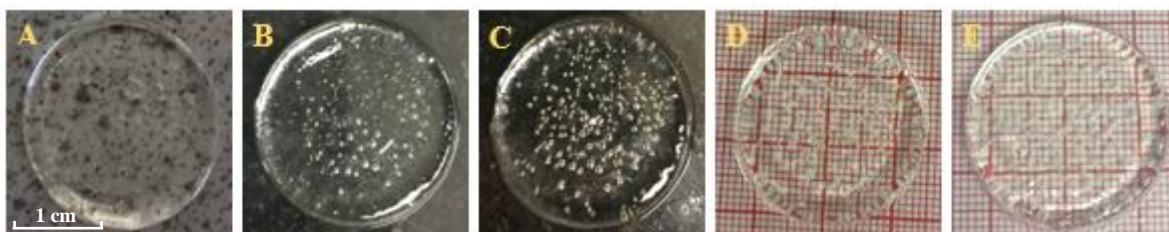


Figure 3-18 PNVCL-PEGDMA 2 wt% (C3) samples submerged in distilled water at times: A 1 hour, B 2 hours, C 6 hours, D 24 hours and E 48 hours at 50°C.

3.1.7 Tensile test

The tensile test is used to find out how strong a material is and also how much it can be stretched before breaking. Tensile tests were performed on the P1 and C3 samples that showed the most suitable swelling behaviour for 4D printing. The results are listed in **Table 3-4**.

Table 3-4 Mechanical properties of P1 and C3 samples. $n=5$, $p<0.05$.

Properties	P1	C3
Maximum load (N)	81.58±3.37	117.64±9.91
Tensile strength (MPa)	8.80±0.54	12.12±1.06
Elongation at maximum load (mm)	2.89±0.13	2.47±0.36
Young's modulus (MPa)	27.65±3.1	46.2±4.5

Tensile tests show the tensile strength of the basic P1 and C3 chemical crosslinked polymer, providing an understanding of the behaviour of the chemical crosslinked gels. During the crosslinking process, the formation of three-dimensional networks can lead to an increase in tensile strength properties, though highly crosslinked structures can become more brittle (elongation decreased) (Murray *et al.*, 2013). Understanding the base polymer behaviour will help identify changes which occur with the addition of monomers and/or additives.

3.1.8 Goniometry

The hydrophilicity of the polymeric material was determined using goniometry at room temperature, to measure the wettability of the surface of the samples by measuring the angle of drop of water and its contact with the dry surface of the xerogel. The more the liquid spreads across the solid surface of the material, the more attracted to the material it is. The closer the contact angle is to 0°, the greater the hydrophilicity of the sample material. Materials with contact angle up to 90° are considered hydrophilic, those with contact angle greater than 90° are considered hydrophobic, and surfaces with contact angle greater

than 150° are considered to be superhydrophobic, as the liquid droplet meets the surface without significant wetting (Förch *et al.*, 2009). In this section, the contact angle measurements were performed on the homopolymer (0.1 wt% Irgacure 2959) and C3 samples.

The homopolymer PNVCCL prepared at 0.1 wt% Irgacure 2959 has a mean contact angle of 46.97° at zero seconds, dispersing into a drop with mean contact angle of 31.73° , characterising it as a hydrophilic material. The same trend was observed in C3 samples, which had a mean contact angle of 50.74° at zero seconds, spreading into a drop with mean contact angle of 40.02° at 115 seconds. In comparison, both physical and chemical crosslinked samples are considered hydrophilic, with the contact water angle being less than 90° . As the homopolymer contact dispersing angle was closer to 0° , PNVCCL is more hydrophilic than P(NVCL-PEGDMA).

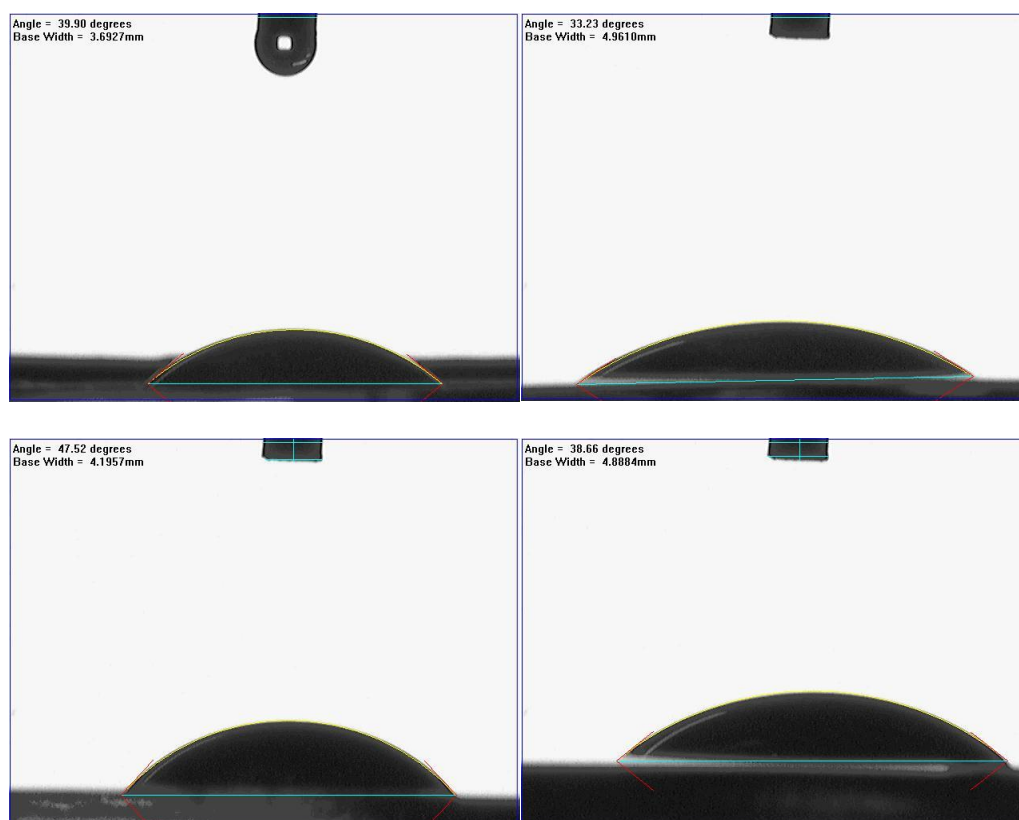


Figure 3-19 The representative contact angles figures of P1 and C3 samples at 0 and 115 seconds. $n=3$, $p<0.05$.

3.1.9 Summary

In this chapter, physically and chemically crosslinked PNVCL based polymers were synthesised to investigate their potential for shape shifting applications. The successful polymerisation of the polymers has been confirmed by FTIR analysis. Phase transition behaviour was investigated by cloud point, DSC, UV-spectroscopy and rheology. Based on the contact water angle detection, the homopolymer and C3 samples are hydrophilic. Swelling studies were performed to detect water uptake below and above LCST. The chemically crosslinked polymers which were prepared using **0.1 wt% Igracure 2959** photoinitiator and **2 wt% PEGDMA** crosslinker exhibited promising water absorption capabilities. However, the samples became soft and flaccid after expansion, which results in the structural integrity and disc shape of the sample being easily disrupted.

3.2 Formulation development II: Synthesis, characterisation, phase transition and swelling of temperature-sensitive copolymer/terpolymer hydrogels

3.2.1 Preface

The samples developed in the first section displayed outstanding expansion capabilities and maintained LCST close to physiological temperature (samples: 30.9-35 °C, physiological: ~37 °C). Unfortunately, the developed samples displayed such a reduction in mechanical strength in their swollen state, thereby rendering them unusable. In order to circumvent this issue of poor mechanical properties and improve the properties of the samples, it was decided to copolymerise the NVCL with additional polymers. As mentioned previously, smart polymers such as PNVCL can be crosslinked either physically or chemically to form hydrogels. Through altering the degree of crosslinking, the LCST and properties of the samples may be changed (Guo *et al.*, 2019). Further to this, the hydrogel properties may also be optimised through incorporating other monomers.

This section primarily investigates the thermal and swelling properties of different PNVCL-based polymers. Thermal and swelling studies determine the rate and amount of water uptake, which determines the final performance and size of the objects for potential 4D applications. Due to their specific characteristics, the monomers NVP, DMAAm, and NIPAAm were chosen to be combined with PNVCL.

NVP is a synthetic, non-ionic polymer soluble in water and many organic liquids. It is a highly amorphous polymer with a glass transition temperature of around 150°C (Ahmad *et al.*, 2022). PVP repeating unit contains a highly polar amide group (which determines its hydrophilic and polar-attraction properties) and polar methylene groups (which confer the hydrophobic properties of PVP) (Lewandowska, 2014). Its absorptivity, biocompatibility and non-toxicity have resulted in the application of PVP in food,

pharmaceutical, cosmetics, detergent and adhesive industries (Raimi-Abraham *et al.*, 2014). DMAAm is composed of two methyl groups that increase the electron density on the nitrogen atom and form the polarity on the amide structure, causing the property of electron donation (Akin & Işiklan, 2016). The scientific and practical interest in PDMAAm is steadily growing. There are some reports that the LCST of PDMAAm is estimated to be higher than 200°C (Pagonis & Bokias, 2004). The non-ionic temperature-sensitive polymer Poly (N-isopropylacrylamide) (PNIPAAm) has received particular attention and is widely used in the research field. PNIPAAm is composed of amide(-CONH-) and propyl(CH(CH₃)₂) sections in the monomer structure (Haq *et al.*, 2017). PNIPAAm exhibits a sharp phase transition at its LCST of 32°C in an aqueous solution (Nagase *et al.*, 2018). This enhances the appeal of PNIPAAm for biomedical applications, such as drug and gene delivery systems and regulation of cell attachment (Zhang *et al.*, 2015).

In this section, with the addition of other polymers, the synthetic hydrogels are expected to obtain improved mechanical properties. Due to the thermal sensitivity of NIPAAm, the reaction time for swelling is expected to decrease. The UV chamber was used for polymerisation of the polymers, and the samples were made based on the batch discussed in Section 2.2.3. The samples developed were characterised using the following techniques: molecule structures (Fourier transform infrared spectroscopy), thermal properties (cloud point analysis, UV-spectrometry, differential scanning calorimetry and rheology), mechanical properties (tensile test and goniometry) and shape changing pulsatile performances (swelling studies) (Geever *et al.*, 2006; Gaballa *et al.*, 2013; Halligan *et al.*, 2017).

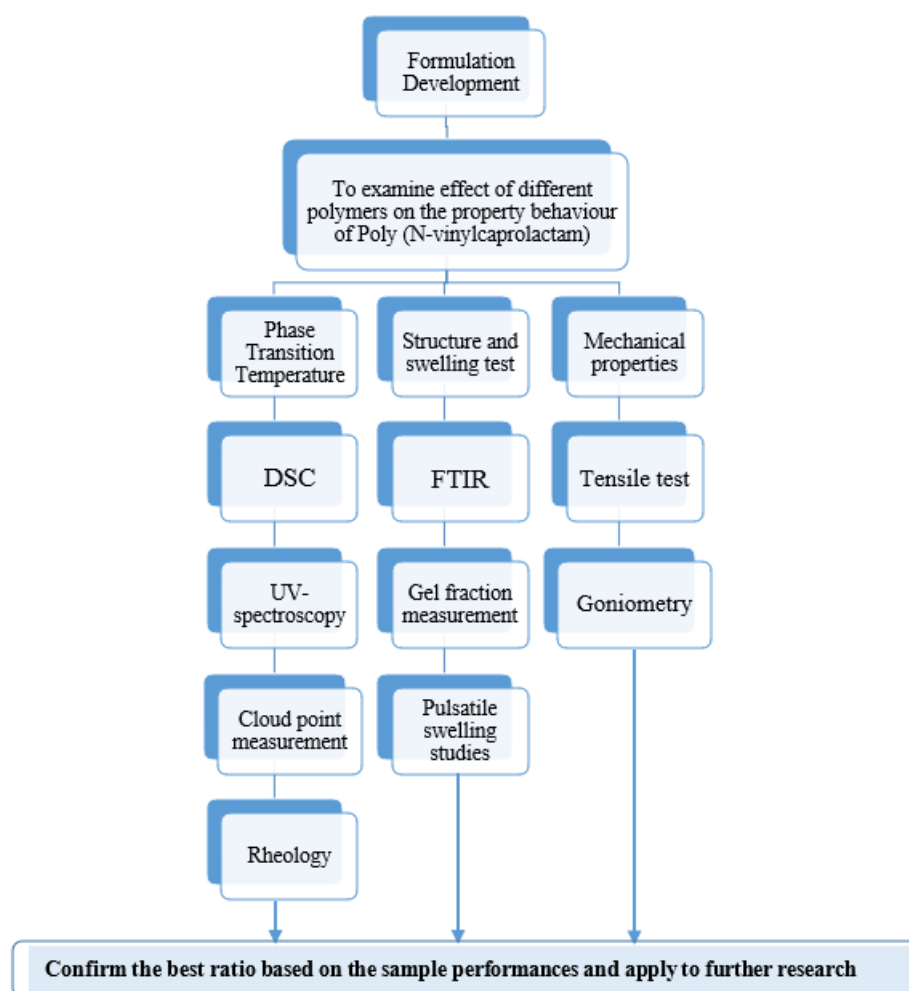


Figure 3-20 Work breakdown structure for the evaluation of the effects of the different copolymers and terpolymers.

3.2.2 Preparation of physically and chemically crosslinked terpolymer samples

Though the samples produced previously in Section 3.1 displayed satisfying properties for 4D printing, some limitations remained. One such limitation is that the produced samples were not sensitive enough to the environmental conditions and the reaction time was, therefore, too long. Additionally, the produced samples were overly soft and sticky to touch which in turn caused the samples to lack mechanical strength, rendering them unusable.

In order to improve the performance of samples, the homopolymers *N*, *N*-dimethylacrylamide (DMAAm), *N*-vinylpyrrolidone (NVP) and *N*-isopropylacrylamide (NIPAAm) were selected to polymerise with the NVCL. NIPAAm is the most popular

temperature-responsive polymer and exhibits a sharp phase transition at its LCST of 32°C in an aqueous solution (Nagase *et al.*, 2018). The hydrophilic monomers DMAAm and NVP were used to raise the LCST of the samples (Pagonis & Bokias, 2004; Lewandowska, 2014), and to satisfy 4D processing requirements. Both physically and chemically, crosslinked copolymers and terpolymers were synthesised based on the previous formulation using 0.1 wt% Irgacure 2959 photoinitiator. The representative corresponding chemical structures of physically and chemically crosslinked copolymers and terpolymers are shown in **Figure 3-21** and **Figure 3-22**.

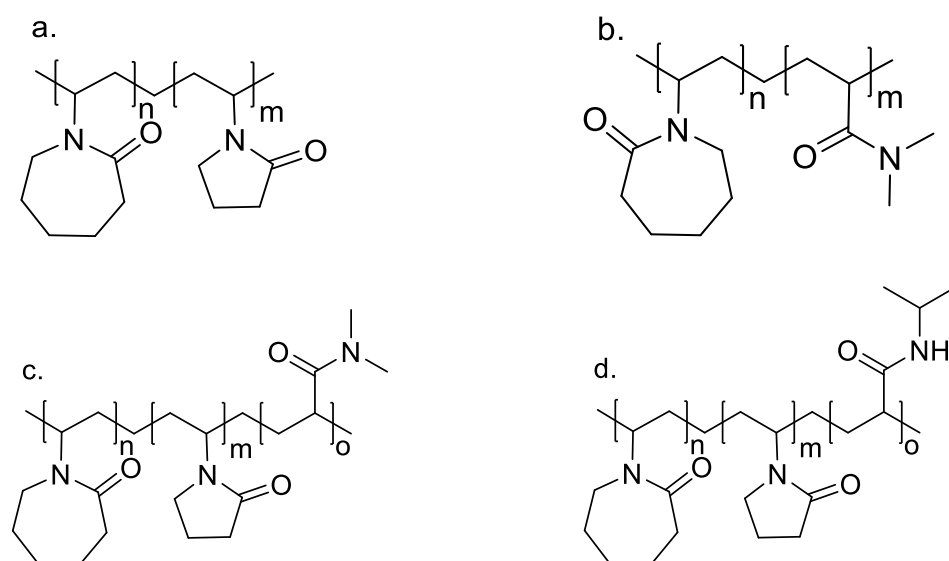


Figure 3-21 The chemical structure of NVCL based physically crosslinked copolymers and terpolymers: (a) NVCL/NVP; (b) NVCL/DMAAm; (c) NVCL/NVP/DMAAm & (d) NVCL/NVP/NIPAAm.

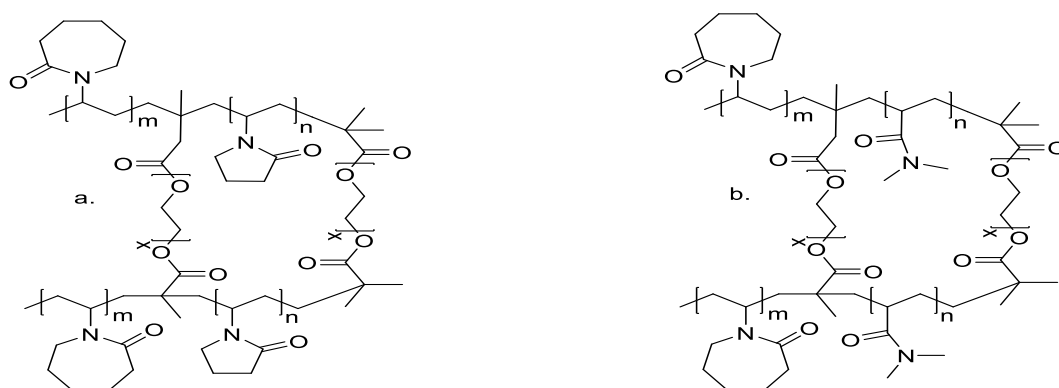


Figure 3-22 Representative chemical structures of NVCL based chemically crosslinked copolymers: (a) NVCL/NVP & (b) NVCL/DMAAm.

It has been reported that the swelling characteristics of hydrogel samples can be positively affected by decreasing the concentration of crosslinker utilised in the formulation (Chavda & Patel, 2011). Thus, PEGDMA as a crosslinker was again added into the solution at two different concentrations (0.1 wt%, 2 wt%) to observe the variance in the swelling performance. The mixture solution must be heated and stirred for at least 20 minutes before curing, to ensure the crosslinking has fully occurred. The cured samples were dried in a 50°C vacuum oven for 24 hours before testing. Disc samples were prepared based on **Table 2-4**. Without NIPAAm monomer (from S1 to S9), all samples cured well. The polymers were transparent and glass-like. In terms of colour, when taken in comparison to the previously prepared samples, the samples herein displayed a slightly yellow colour. Samples maintained their shape and integrity, and had a shiny, smooth surface.

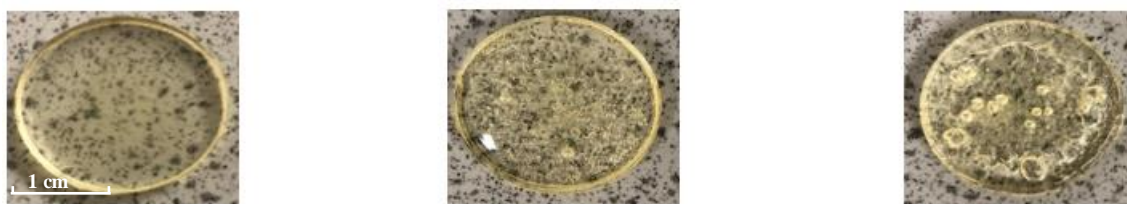


Figure 3-23 The appearance of (L) S7 (30DMAAm/70NVCL/2PEGDMA), (M) S18 (25NVP/25NVCL/50NIPAAm/0.1PEGDMA), &(R) S11 (65DMAAm/20NIPAAm/15NVCL) samples.

The chemically crosslinked terpolymer samples which were synthesised without NIPAAm — **Figure 3-23(L)** — displayed a better appearance than the copolymer samples prepared with NIPAAm as shown in **Figure 3-23 (M and R)**. Though the samples made with NIPAAm are promising, some bubbles appeared on the sample surfaces after curing. The surface of some NIPAAm-based samples is also uneven, with some of them protruding upward. **Figure 3-23 (R)** shows the appearance of physically crosslinked sample S11 (65DMAAm/20NIPAAm/15NVCL). As the image shows, the worst appearance was exhibited by this sample. This sample was defective, with many holes and

big bubbles, which affected its weight and shape integrity. Many attempts to simultaneously mix the NIPAAm and DMAAm with NVCL resulted in poor performance and aesthetics of the samples. This may have been caused by photopolymerisation in an air environment where oxygen in the air reacted with the sample. However, because the 3D printing will be performed in an oxygen-based environment, this type of NIPAAm/DMAAm/NVCL batch was not considered appropriate for this research.

3.2.3 Attenuated total reflectance Fourier transform infrared spectroscopy

The materials in this work were analysed using FTIR to confirm the structure of monomers NVCL, DMAAm, PEGDMA, as well as the copolymers. The monomers displayed characteristic absorption bands at 1622/1649 cm^{-1} (NVCL) (Kozanoğlu, 2008; Lee *et al.*, 2013) 1611/1648 cm^{-1} (DMAAm) (Alpaslan *et al.*, 2021) and 1715/1636 cm^{-1} (PEGDMA) (Wu *et al.*, 2010; Killion *et al.*, 2011). These bands were assigned to the carbonyl group C=O bond stretching vibration, and the C=C bond stretching vibration. However, in the P(NVCL/DMAAm) spectra, only an intense peak at 1619/1619 cm^{-1} in S6 and S7 samples is attributed to the characteristic absorption of C=O stretching. The disappearance of the C=C peaks in the S6 and S7 sample spectra indicates successful polymerisation. The absorbance bands at 2933 cm^{-1} /2850 cm^{-1} for NVCL monomer and 2934 cm^{-1} for DMAAm are attributed to the aliphatic C-H bending (Babu *et al.*, 2008). The bands discernible at 3109 cm^{-1} /992 cm^{-1} and 981 cm^{-1} have previously been reported to be associated with =CH or =CH₂ bending (Chen *et al.*, 2009). The bands at 1486 cm^{-1} (NVCL), 1493 cm^{-1} (DMAAm) and 1478 cm^{-1} (S6, S7) are attributed to the stretching of C-N bonds in both monomers and copolymers (Chen *et al.*, 2009). The O-H bending arises at 3422 cm^{-1} and 3456 cm^{-1} in S6 and S7, is providing further evidence that the polymerisation has succeeded (Killion *et al.*, 2011; Fallon *et al.*, 2019).

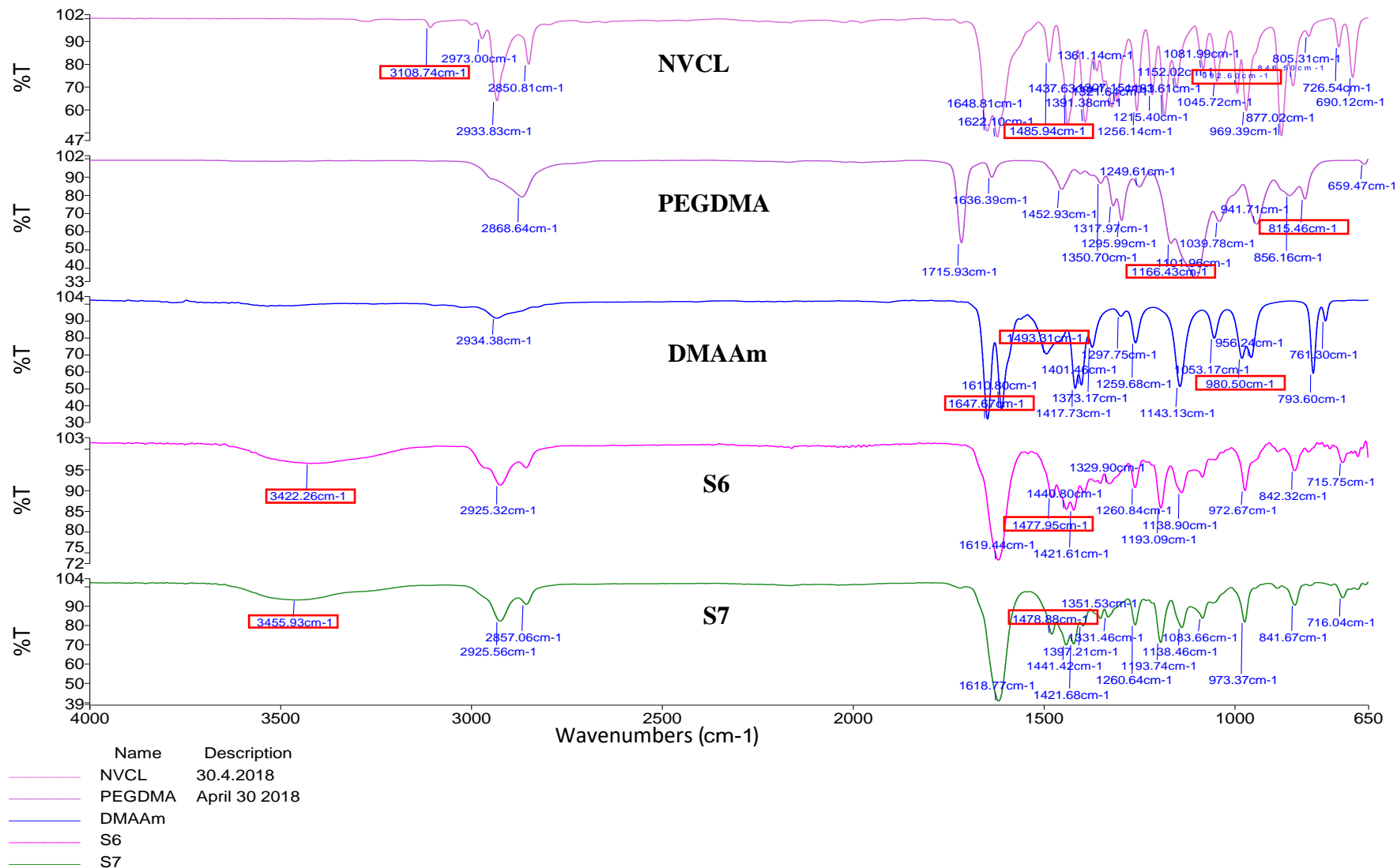


Figure 3-24 FTIR spectra of the constituent monomers and the S6 and S7 hydrogel copolymer. $n=2$.

Table 3-5 Functional groups in NVCL, DMAAm, PEGDMA, S6 and S7 analysed by FTIR.

Functional Group	Wavelength (cm ⁻¹)				
	NVCL	DMAAm	PEGDMA	S6	S7
Aliphatic C-H	2933, 2850	2,934	2868	2925, 2857	2926, 2857
C=O	1622	1611	1716	1619	1619
C-N	1486	1493	---	1478	1479
-CH ₂ -	1438	1418	1453	1422	1422
C=C	1649	1648	1636	---	---
C-O	---	---	1166	---	---
=CH and =CH ₂	3109, 992	981	815	---	---
O-H	---	---	---	3422	3456

The spectra of chemically crosslinked terpolymers were also explored by the FTIR as displayed in **Figure 3-25**. The similarity of the backbone structure of both monomers is obvious, displaying characteristic peaks at 1619 cm⁻¹ and 1656 cm⁻¹ (Cao *et al.*, 2005; Kurečić, Majda & Karin, 2012) in the NIPAAm spectrum and exhibiting bands at 1625 cm⁻¹ and 1695 cm⁻¹ (Száráz & Forsling, 2000) in the NVP spectrum, and 1622 cm⁻¹ and 1649 cm⁻¹ (Kozanoğlu, 2008; Lee *et al.*, 2013) peaks in the NVCL spectrum. These absorption bands are assigned to the C=O (carbonyl group) and the olefin C=C bond stretching vibration, respectively. However, in the terpolymers spectra, an intense peak exists only at 1655 cm⁻¹, 1624 cm⁻¹ and 1641 cm⁻¹ in each sample, confirming polymerisation through the C=C bond.

The specific absorbance bands at 3282 cm⁻¹ and 1546 cm⁻¹ for NIPAAm are attributed to the secondary amide and amide II N-H bond (Száráz & Forsling, 2000). The characteristic double band for the isopropyl group is at 1387 and 1368 cm⁻¹. These bands appeared in the terpolymer spectra, confirming the presence of NIPAAm in the structure. The NIPAAm spectrum also revealed absorption bands at approximately 2970/2876/1410 cm⁻¹, previously reported to be associated with the C-H bond (Cao *et al.*, 2005; Kurečić,

Majda & Karin, 2012), which are also located in the NVCL and NVP monomer at 2933/2850/1438 cm^{-1} and 2976/2886/1423 cm^{-1} respectively (Száráz and Forsling, 2000; Halligan *et al.*, 2017). Vinyl groups in the NIPAAm monomer could be identified at peaks between 3072 and 987 cm^{-1} (Kim *et al.*, 2003) while the NVP monomer exhibited sharp peaks at 981 and 842 cm^{-1} , in agreement with reports that it shows strong peaks in the range of 800-1000 cm^{-1} corresponding to the mode of vinyl double bonds ($\text{CH}_2=\text{CHR}$) (Száráz & Forsling, 2000). This also arises in the NVCL monomer situated at 3109 and 992 cm^{-1} (Kozanoğlu, 2008). Such characteristic monomeric peaks subsequently failed to appear in the S14, S16 and S18 terpolymer spectra — a further indication of polymerisation of the terpolymer. Also in the terpolymer spectra, the broad peaks at 3465 cm^{-1} , 3462 cm^{-1} and 3462 cm^{-1} for S14, S16 and S18 samples respectively are characteristic of O-H vibration of water molecules, associated with polymer molecules through hydrogen bonds (Száráz & Forsling, 2000).

Table 3-6 Functional group in NIPAAm, NVCL, NVP, PEGDMA, S14, S16 and S18 analysed by FTIR.

Functional Group	Wavelength (cm^{-1})						
	NIPAAm	NVCL	NVP	PEGDMA	S14	S16	S18
Aliphatic C-H	2970, 2876	2933, 2850	2976, 2886	2868	2925	2928	2971, 2931
C=O	1619	1622	1625	1715	1655	1624	1641
C-N	1454	1486	1487	---	1458	1458	1458
-CH ₂ -	1410	1438	1423	1453	1423	1424	1424
C=C	1656	1649	1695	1636	---	---	---
C-O	---	---	---	1166	---	---	---
=CH and =CH ₂	3072, 987	3109, 992	981, 842	815	---	---	---
O-H	---	---	---	---	3465	3462	3462
N-H stretching of secondary amide	3282	---	---	---	3290	3289	3290
N-H stretching of amide II bond	1546	---	---	---	1544	1543	1542
isopropyl C-H	1387, 1368	---	---	---	1389, 1366	1389, 1366	1388, 1366

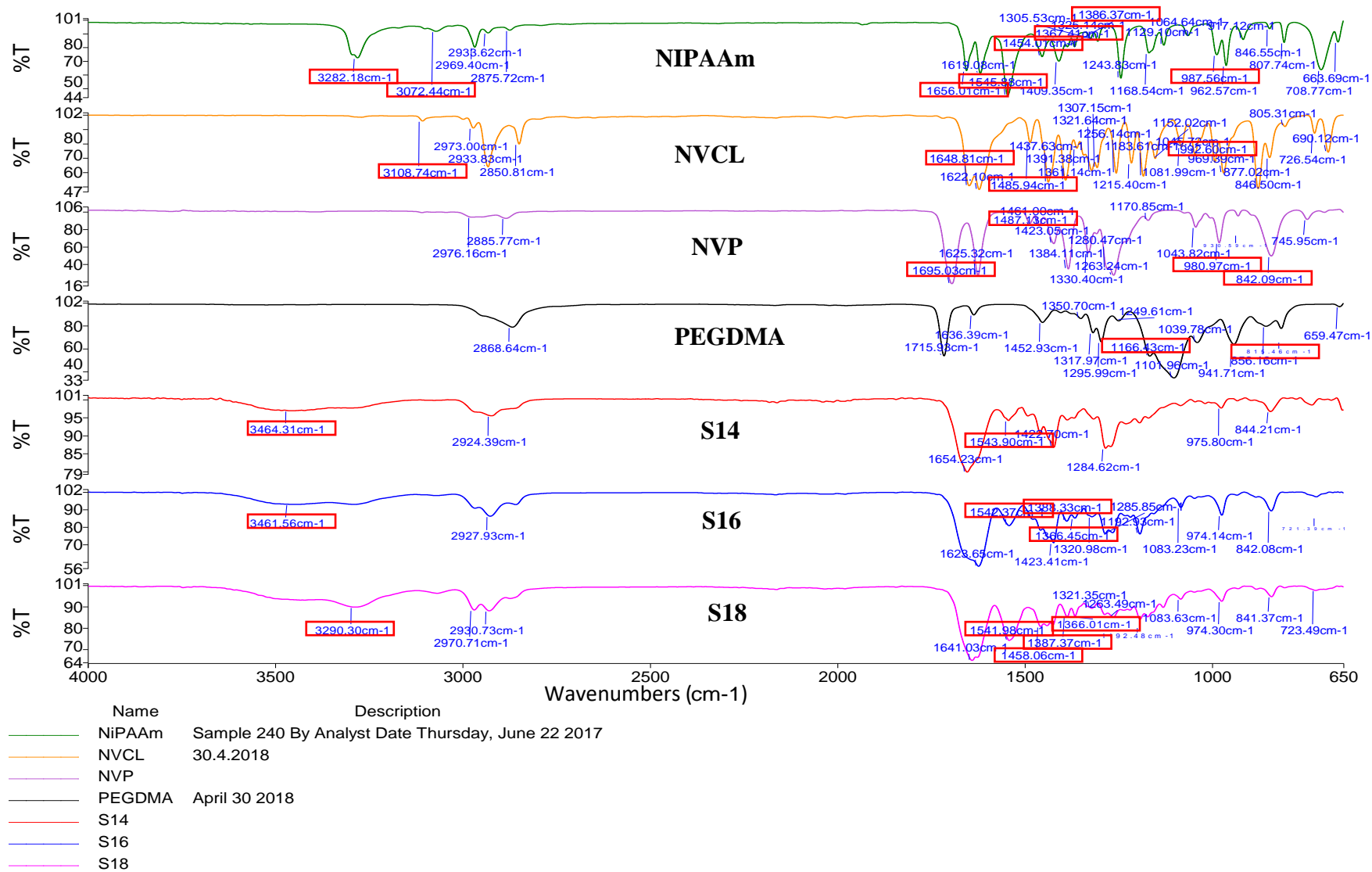


Figure 3-25 FTIR spectra of the constituent monomers and the S14, S16 and S18 hydrogel terpolymers. n=2.

3.2.4 Phase transition determination

Temperature-sensitive polymers provide excellent flexibility in tailoring transitions to suit temperature, inheriting great potential in 4D printing. Therefore, the LCST of temperature-responsive polymers plays an essential role in designing smart 4D behaviours, as the phase transition temperature is the point at which change occurs. In order to manipulate the LCST, hydrophilic or hydrophobic monomers can be incorporated into the polymer. In this study, hydrophilic monomers have been used. Due to the hydrophilicity of the monomers, the LCST of the synthesised polymers was expected to increase upon their incorporation. Phase transition was measured by employing four techniques to determine the LCST, as demonstrated in **Table 3-7**. The physically crosslinked hydrogels were dissolved in an aqueous solution before testing.

Table 3-7 LCST of selected PNVCL-based samples which were established using cloud point, UV-spectrometry, DSC and rheological analysis.

Gel code	Cloud point (°C)	DSC (°C)	UV-spectrometry (°C)	Rheological analysis (°C)
S1	49.0±0.5	49.4	>50	-
S2	33.0±0.5	32.3	32	33.7
S3	37.0±0.5	36.3	36	38.0
S10	55.0±0.5	54.1	>50	-
S12	43.0±0.5	42.9	43	-
S13	44.0±0.5	45.2	44	-

3.2.4.1 Cloud point analysis

As shown in **Table 2-4**, the cloud point measurement was carried out appropriately on prepared physical hydrogel copolymers. The cloud point was determined to be the point at which the solution changed from transparent to turbid at a specific temperature. While at low temperatures, the aqueous solutions were homogenous and transparent, at elevated temperatures approaching the transition temperature there was a conversion to an opaque appearance. **Figure 3-26** shows the phase transition point of selected samples. The behaviour of the temperature-sensitive gels was controlled by

adjusting the hydrophilicity. This was achieved by copolymerisation of hydrophilic monomers with PNVCL at varying ratios. Compared to the homopolymer, the LCST is increased after combination with hydrophilic monomers. In addition, as the concentration of hydrophilic monomer increases, the phase transition temperature increases steeply. The S10 sample, containing 65% NVP, 20% NIPAAm and 15% NVCL displayed a phase transition temperature at 55°C, revealing the correlation between the LCST and the hydrophilicity of the polymer. Furthermore, the NVP would appear to have a greater effect on LCST than DMAAm when combined with NVCL. The LCST is increased to 49°C and 33°C respectively when mixed with 30% NVP and DMAAm. NIPAAm is the most popular temperature sensitive polymer, with a LCST around 33°C (Haq *et al.*, 2017). Incorporating NIPAAm and NVP with NVCL had a noticeable effect on the cloud point temperature. The S12 sample, containing 30% NVP, 30% NIPAAm and 40% NVCL shows a cloud point at 43°C. Compared with S1 sample, when 30% of NIPAAm replaces NVCL, the phase transition temperature decreases by 6 degrees. These results correlate well with such findings, with the transition temperature increasing proportionally with hydrophilic polymer concentration (Anufrieva *et al.*, 2001). This temperature-responsive behaviour is a result of increased hydrogen bonding between water molecules, and polymer and hydrophilic aggregation of the polymer chains (Wilke *et al.*, 2015).

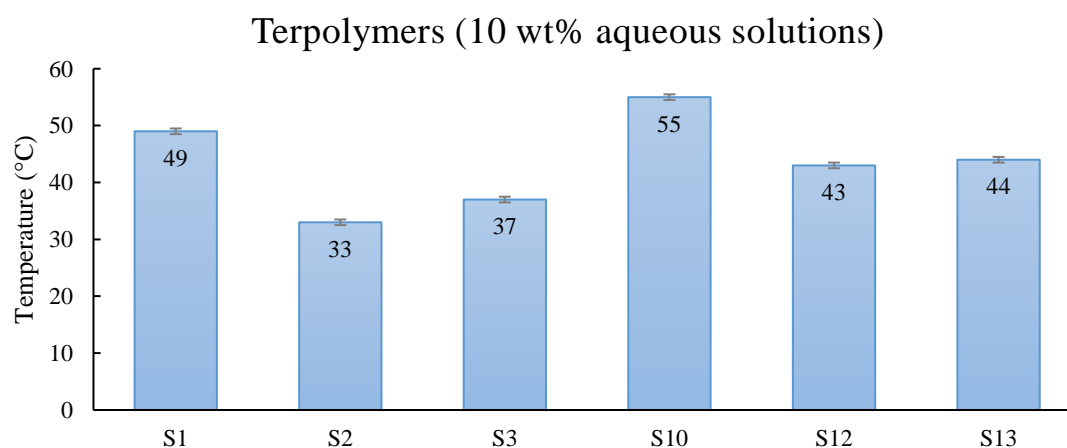


Figure 3-26 The cloud point of terpolymers 10 wt% aqueous solutions. $n=3$, $p<0.05$.

3.2.4.2 UV-spectroscopy

The phase transition point was quantitatively determined by measuring the turbidity of the samples in solution. The aqueous solution was analysed over a temperature range of 22-50°C, with 50°C being the maximum temperature that can be applied using this technique. **Figure 3-27** illustrates the LCST of the NVCL based polymers detected by UV-spectroscopy. The onset value of light absorption was used to establish the LCST value. The point at which LCST occurred during UV spectroscopy resulted in similar values to those obtained by cloud point analysis. Additionally, it was noticed that the absorption rate of S1 and S10 solutions progresses towards zero in the absorbance spectrum, which means these samples were unable to experience the transition from colourless to opaque within this limited range. Thus, with the incorporation of the NVP monomers, the LCST of S1 and S10 had been raised to >50°C. Furthermore, it can be observed that for homopolymers, the phase transition occurs instantaneously. In the case of copolymers or terpolymers, a temperature increase is required for the phase change to be completed. This regularity can be explained by the fact that a small portion of the gel initially undergoes phase change at the onset temperature, while the majority gradually undergoes phase change as the temperature raised (Scherzinger *et al.*, 2014). Due to the different polymerisation kinetic constants of the respective monomers and the concentration of the mixture, the water content increases the hydrogen bonding reaction between the water and the polymer, which requires more thermal energy to break the water structure, resulting in a delayed phase transition (Eeckman *et al.*, 2004).

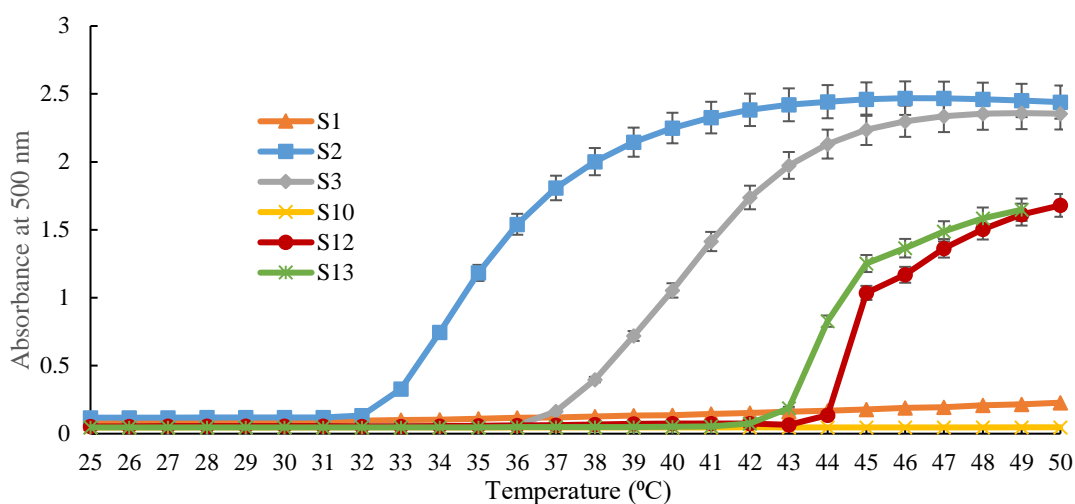


Figure 3-27 UV-spectrometry illustrating the LCST of PNVCL based copolymers and terpolymers. $n=3$, $p<0.05$.

3.2.4.3 Differential scanning calorimetry

Differential scanning calorimetry was also used to analyse the LCST behaviour of the PNVCL based materials. **Figure 3-28** illustrates a representative thermogram (S2), where the onset value recorded was 32.31°C. In some cases, it was found there was a difference of over 1°C between the calorimetric peak and onset values. It is understood that a small portion of the gel starts to undergo its phase transition at the onset temperature, while the major part experiences the transition at the peak value (Geever *et al.*, 2006).

Table 3-7 shows the summary of the results.

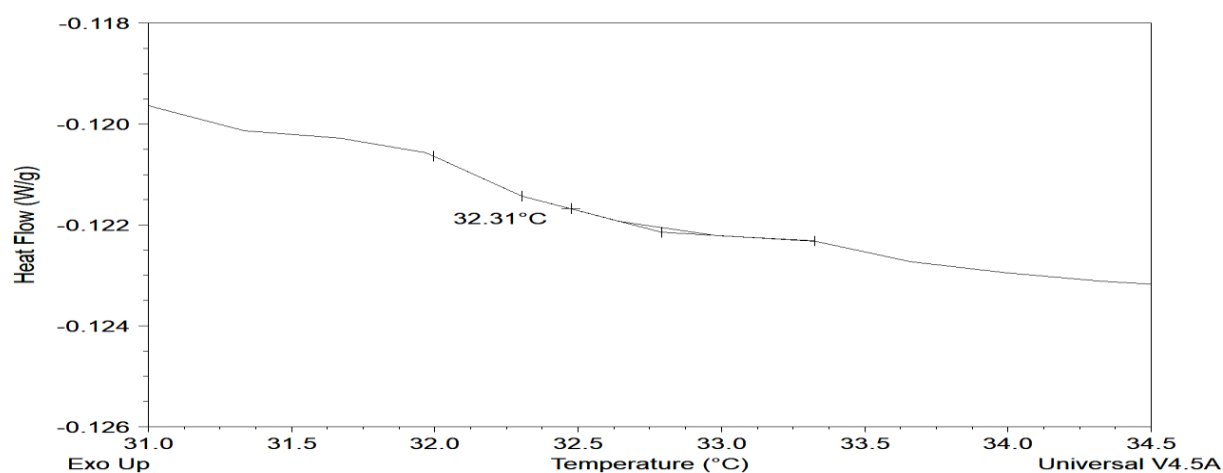


Figure 3-28 A representative thermogram illustrating the LCST of PNVCL based copolymer S2 (30DMAAm/70NVCL) aqueous solution. $n=3$.

The results detected using the three techniques illustrate the prevailing trend. According to the previous section, the LCST of 10 wt% homopolymer solution is approximately 32°C. After incorporation of different concentrations of hydrophilic monomers NVP and DMAAm, the LCST can be increased to as high as 50°C. This is favourable in relation to 4D printed objects, which may use different temperatures for different applications. Pulsatile swelling studies were subsequently performed on all of the relevant chemically crosslinked samples to investigate whether they possess suitable swelling behaviour for 4D printing potential.

3.2.5 Pulsatile swelling studies

Due to the presence of covalent bonds, the chemically crosslinked hydrogels are able to absorb water and swell. 4D printed objects require the ability to change their shape or properties when a stimulus act on them. Therefore, the swelling ability of samples is one of the most critical factors. A hydrogel-based sample placed in distilled water will absorb the solvent until the elasticity of the network and osmotic pressure is balanced. The constitution and degree of crosslinking affect the swelling properties of the hydrogels. The hydrogel's mechanical properties decrease as the percentage of swelling increases (Iyer *et al.*, 2008). Pulsatile swelling experiments were conducted to investigate the reversible response and thermo-sensitivity of these hydrogels to changes in environmental temperature. Pulsatile swelling studies were carried out on all chemically crosslinked circular smart polymer discs above and below the LCST, which was determined previously by phase transition experiments. At various time intervals, samples were removed from the distilled water and blotted with filter paper to absorb excess water on the surface, weighed, and submerged into fresh distilled water until equilibrium was established. The samples were then submerged into distilled water preheated to the required temperature and weighed as before until a new equilibrium was achieved.

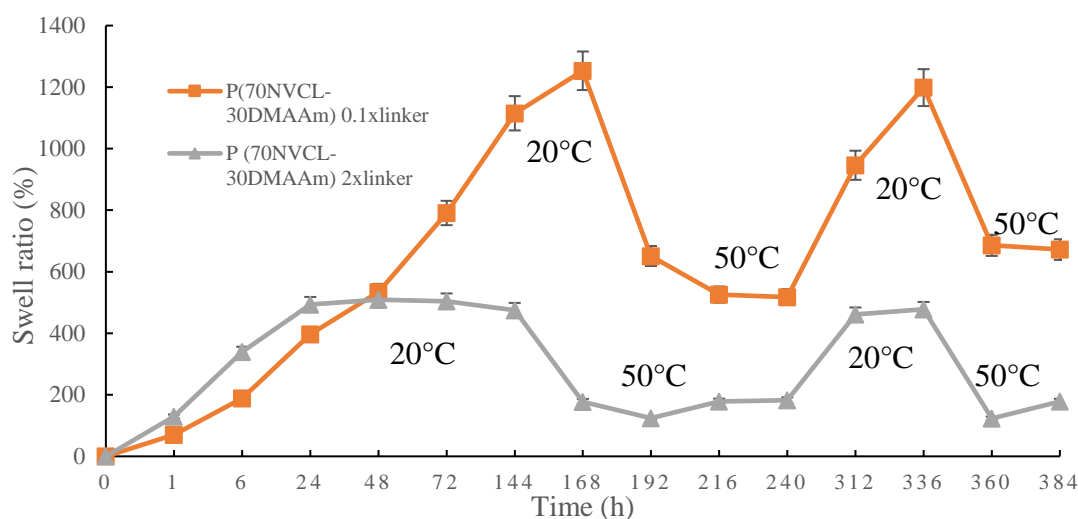


Figure 3-29 Pulsatile swelling behaviours of chemically crosslinked NVCL/DMAAm copolymer hydrogels with different concentrations of PEGDMA (S6 0.1 wt% and S7 2 wt%) at temperatures between 20°C and 50°C. $n=3$, $p<0.05$.

Figure 3-29 illustrates how the swelling ratio was affected by the concentration of crosslinker. The swelling degree had a gradual reduction based on the crosslinker increase (Iyer *et al.*, 2008). The different crosslinker concentrations led to similar expanding and shrinking kinetics, while there was a reduction in the sharpness of the volume transition along with an increasing concentration of crosslinker. Sample S6, which contained 30DMAAm/70NVCL/0.1PEGDMA, can expand 12-times more than xerogel. However, the maximum swollen weight of S7, which contained 30DMAAm/70NVCL/2PEGDMA, is only 5-fold compared to the xerogel. The gels can be described as chains of hydrophobic and hydrophilic groups interconnected by crosslinks to form regions of open and restricted free volume. At low crosslinker densities, the gel contains few restricted free volumes, or the number of hydrophilic groups restricted is low. This causes the copolymer gels to show sharp transition behaviour as the water is quickly expelled during gel collapse. At higher crosslinker densities, when the number of restricted free volumes is high, there is increased polymer chain rigidity and increased bound water retention resulting in loss of sharp phase transition behaviour (Iyer *et al.*, 2008).

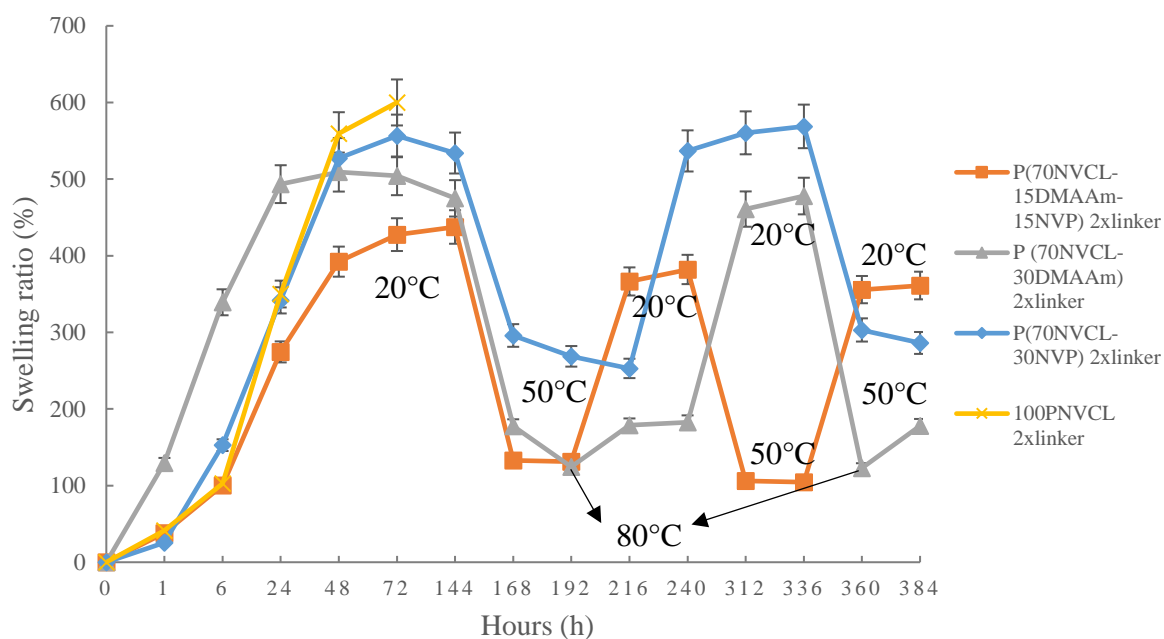


Figure 3-30 Pulsatile swelling behaviours of chemically crosslinked NVCL/DMAAm/NVP hydrogels with different polymeric compositions and 2 wt% PEGDMA at temperatures between 20°C, 50°C and 80°C. $n=3$, $p<0.05$.

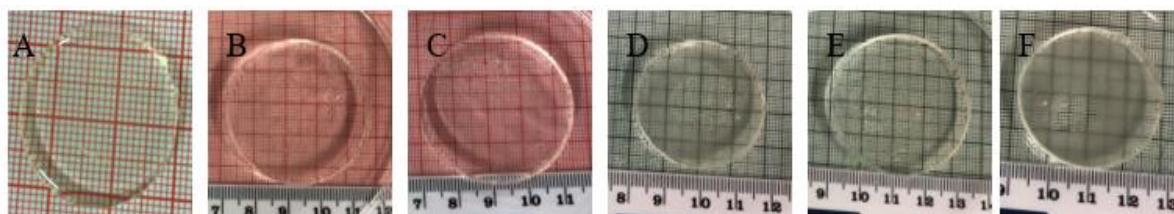


Figure 3-31 The appearance of the disc samples of S7 sample at times: A 0 hour; B 6 hours; C 72 hours; D 216 hours; E 336 hours; F 384 hours.

As **Figure 3-30** shows, Sample S5 (30NVP/70NVCL) can swell to nearly 5.5-times its original weight. However, the samples became soft and sticky after swelling and it was easy to destroy the structure during the experiment. S7 (30DMAAm/70NVCL) and S9 (15NVP/15DMAAm/70NVCL) only expanded 5-times and 4.5 times the original weight, respectively. But after absorbing water, these samples retained their toughness, shape and integrity. For all S7 samples below LCST, the maximum swollen weight had been reached after 24h. For homopolymer (C2) and other copolymers (S5, S9), the maximum swollen weight was achieved after 48h. Subsequent to the maximum swollen weight being achieved, when the temperature was above LCST, the samples started to

shrink and exhibit reversible shape change behaviour as the temperature rose and fell. As a result, when the 70% NVCL is mixed with 30% DMAAm, the swelling reaction time was reduced. In addition, for all S7 samples above LCST, as the temperature increased from 50 to 80 degrees, the weight of samples continued to shrink to a lower-level state. However, after adding the hydrophilic monomers, the size of the expansion of samples did not increase. This may be due to the high concentration of crosslinker that restricts the free volume of the sample.

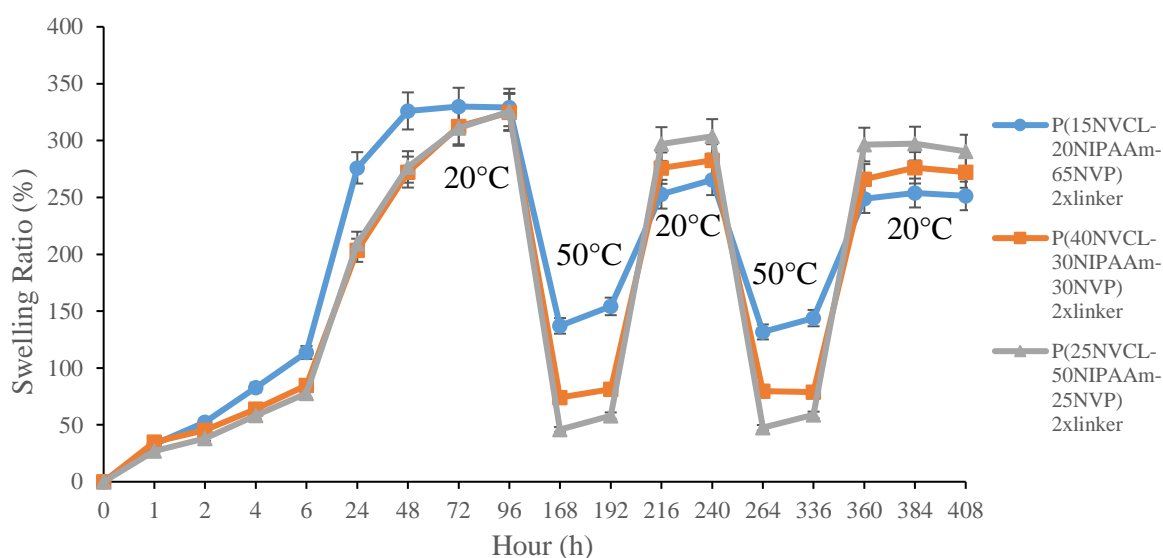


Figure 3-32 Pulsatile swelling behaviours of chemically crosslinked NVCL/NVP/NIPAAm terpolymer hydrogels with different polymeric compositions and 2 wt% PEGDMA at temperature between 20°C and 50°C. $n=3$, $p<0.05$.

As **Figure 3-32** shows, for samples below LCST, when NIPAAm monomer is added, the terpolymers require 72h to reach maximum swollen weight. This means the time it took to reach equilibrium and the magnitude of swelling ratio as the content of NIPAAm increases or decreases have no apparent effect. Additionally, the NIPAAm based samples in the swollen state were soft and easy to stick on the filter paper and crack when measuring. The samples above LCST showed reversible properties. With increased NVP incorporation during photopolymerisation, the degree of shrinkage is reduced. The swelling ratio of S15, which contained 65 percentage NVP, was 150%. However, the

swelling ratios of S17 and S19 decreased below 100%. When the temperature dropped again, the samples expanded back to maximum weight. This phenomenon can be explained by the hydrogen-bonding of the hydrophilic segments, which dominates the interaction between water and the polymer chains, and the polymers' absorption of water. When the temperatures increase above the LCST, the polymer chains shrink and expel water molecules through hydrophobic interactions because of the hydrophobic segments, which results in the precipitation of polymer and the appearance of a globular state (Li *et al.*, 2014).

In summary, the swelling properties have been affected by incorporating hydrophilic monomers. All samples exhibited reversible swellability. During expansion and shrinkage, all water-absorbed samples showed varying degrees of cracking, which explains the loss of quality of samples after several expansion and contraction processes. Only the hydrogels created by S7 formulation were able to maintain their shape and structural integrity. Those hydrogels showed a relatively fast reaction time, and suitable swelling and mechanical properties at both low and high temperatures. The outstanding reversible swelling properties suggest there is a possibility to change the final shape and apply such formulations to a 4D printing technique.

3.2.6 Rheological analysis

The rheological analysis was conducted to determine the LCST and gelation point of selected samples. G' and G'' were measured as a function of the temperature, within the range of 15-50°C. Stress sweeps were conducted, to confirm that rheological measurements were performed within the linear viscoelastic region. **Figure 3-33** illustrates a typical curve. As the LCST is approached, the values for G' and G'' increased until $G' = G''$ — this point is known as the gel point (Laupheimer *et al.*, 2015). As the temperature rises, G' becomes greater than G'' after the gel point. The crossover point for sample S2 (30DMAAm/70NVCL) was 38.6°C.

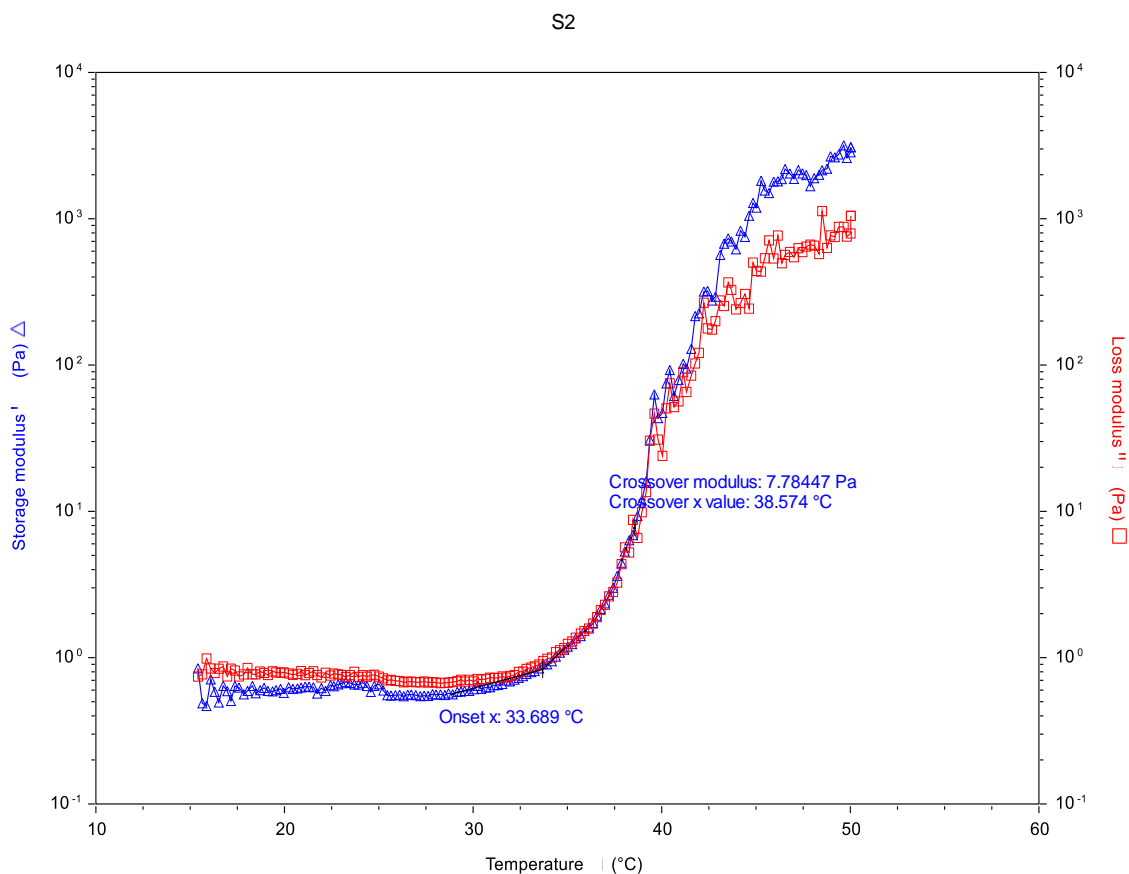


Figure 3-33 A representative graph of rheological analysis demonstrating the onset temperature and crossover point of S2 (30DMAAm/70NVCL). $n=3$.

3.2.7 Gel fraction measurement

In order to further investigate the selected sample (S7), gel fraction measurements have been carried out to compare differences in appearance and weight between the xerogels and swollen gels. Due to the poor mechanical properties of some samples following water absorption, a large number of tiny polymer pieces get stuck to the filter paper and are carried away during the drying process.



Figure 3-34 The appearance of swollen samples. The gel codes from left to right are S5, S9, S15, S17 and S19. $n=3$.

Gel fraction can be used as a qualitative indicator of the efficiency of network formation (Wu *et al.*, 2010). The greater the gel fraction percentage, the greater the covalent bonding. S7 had a gel fraction of $95.77 \pm 1.87\%$. The 5% weight loss indicates that formula of S7 is a suitable candidate for 4D printing techniques.

3.2.8 Tensile test

Tensile testing is used for detecting the mechanical strength of polymers. The tensile test results for homopolymer C3 and copolymer S7 are summarised in **Table 3-8**. The chemically crosslinked homopolymer had a maximum load of $117.64 \pm 9.91\text{N}$ compared to the P(NVCL-DMAAm) copolymer which had a maximum load of $197.3 \pm 42.6\text{N}$, increasing with 30% DMAAm monomer incorporation. In addition, the tensile modulus increased from $46.2 \pm 4.5\text{ MPa}$ to $77.6 \pm 2.8\text{ MPa}$ after 30% DMAAm was mixed with NVCL, which indicated the stiffness of samples is improved.

Table 3-8 Tensile properties of C3 and S7 samples. $n=5$, $p<0.05$.

Properties	C3	S7
Maximum load (N)	117.64 ± 9.91	197.3 ± 25.7
Tensile strength (MPa)	12.12 ± 1.06	19.63 ± 2.89
Elongation at Maximum Load (mm)	2.47 ± 0.36	2.35 ± 0.44
Young's modulus (MPa)	46.2 ± 4.5	77.6 ± 2.8

3.2.9 Goniometry

The contact angle provided the level of the hydrophobicity held by each hydrogel. The hydrophobicity of the copolymeric and terpolymeric hydrogels were determined using goniometry to measure the angle of a drop of water wetting the surface of the solid xerogel. The mean contact angle of chemically crosslinked C3 homopolymer was 50.74° (0 seconds), spreading into a drop with mean contact angle of 40.02° (115 seconds), characterising it as a hydrophilic material. **Figure 3-35** below shows the contact angles for S5, S7, S9, S15, S17 and S19 from 0-115 seconds of the water drop contacting the surface.

All tests were performed in triplicate. The mean contact angles of these copolymers and terpolymers was 77.97° (S5), 67.83° (S7), 84.15° (S9), 74.15° (S15), 82.77° (S17) and 53.53° (S19) at zero seconds, and 46.52° (S5), 45.26° (S7), 59.18° (S9), 56.15° (S15), 58.67° (S17), 45.91° (S19) at 115 seconds. Thus, hydrophobicity was found to increase with the addition of other polymers compared to the homopolymer.



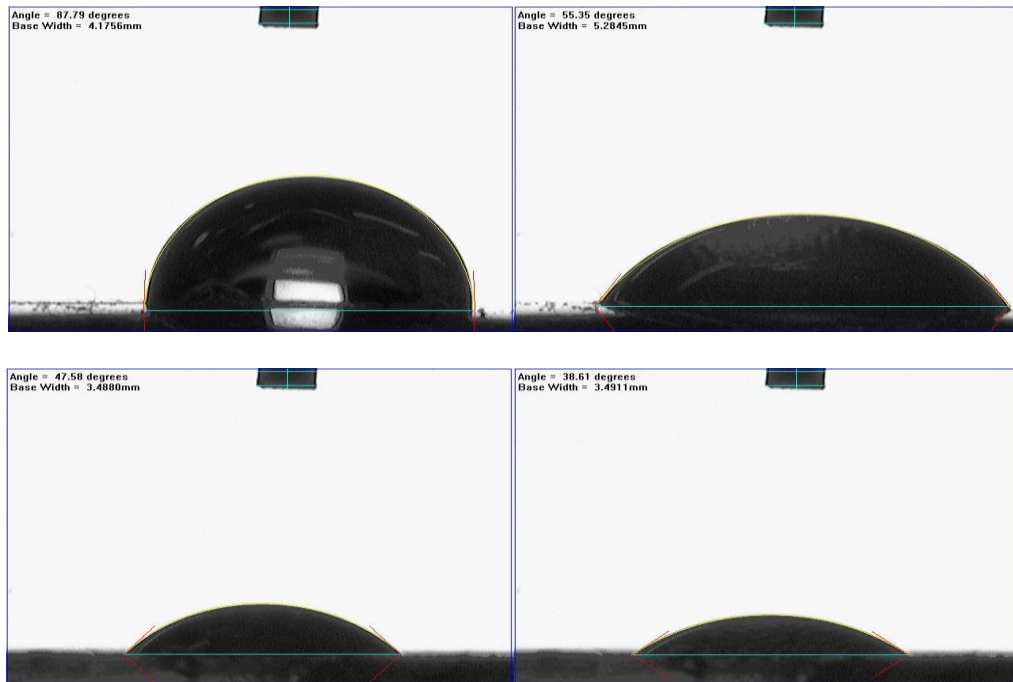


Figure 3-35 The representative contact angles figures of S5, S7, S9, S15, S17 and S19 at 0 and 115 seconds. $n=3$, $p<0.05$.

3.2.10 Summary

The physically and chemically crosslinked NVCL/NVP, NVCL/DMAAm, NVCL/NVP/DMAAm and NVCL/NIPAAm/NVP polymers were synthesised using UV-polymerisation.

The FTIR results revealed that the PNVCL based polymers were successfully polymerised. NVP and DMAAm, as the hydrophilic monomers, had a significant effect on phase transition temperature and swelling performance, as the phase transition point was increased by incorporation of NVP and DMAAm monomers. In addition, all chemically crosslinked samples exhibited reversible swelling behaviours. Only samples which contained 30 wt% DMAAm retained their shape and integrity, both below and above LCST. Also, the mechanical strength was improved, as confirmed by tensile testing studies. Based on the results, S7 chemically crosslinked gels containing **0.1 wt% Igracure 2959** initiator, **2 wt% PEGDMA** crosslinker, **70 wt% NVCL** and **30 DMAAm** monomers, which exhibited promising mechanical strength, suitable phase transition temperature and outstanding water absorption capabilities, were selected for the next phase of the research.

3.3 Synthesis of complex shaped “4D objects” and shape shifting capabilities exploration through 3D printing and photopolymerisation techniques

3.3.1 Preface

The previous section explained how the smart components were developed and displayed the ability to change their size after curing. The developed smart materials have the ability to expand when submerged in water at room temperature (~22 °C) while at elevated temperatures they are capable of shrinking. The mechanical properties of the samples were greatly enhanced compared to the earlier samples in chapter 3.1. It was, therefore, determined that the best performing formulation developed in the previous section may be used for fabricating the 4D objects.

As a technique, 4D printing utilises a 3D printer to create a sample (“4D objects”) with the added dimension of time to allow for an object to change its shape after removal from the printer. This allows for objects to self-assemble when exposed to external stimuli such as, water or heat due to the chemical interaction of the materials (Naficy *et al.*, 2017). UV photopolymerisation utilises UV radiation to cure liquid-based materials, the same mechanism employed by an SLA 3D printer. In this section, based on the best performing formulation developed previously, the personalised complex shaped models were produced via 3D printing technology. This section mainly describes the process and experience of 4D printing, summarising the reasons why 4D printing went from initial failure to success, and investigates how to continuously improve the quality of samples step by step. In addition, the differences in properties between UV-cured and 3D printed samples is also discussed.

The 3D printed and UV cured samples were characterised using the following techniques: molecule structures (Fourier transform infrared spectroscopy), thermal

properties (differential scanning calorimetry), shape changing pulsatile performances (swelling studies), and mechanical properties (tensile tests) (Geever *et al.*, 2006; Gaballa *et al.*, 2013; Halligan *et al.*, 2017). The 4D objects under development are expected to have suitable performances and swelling abilities, so that they can be used in practical applications.

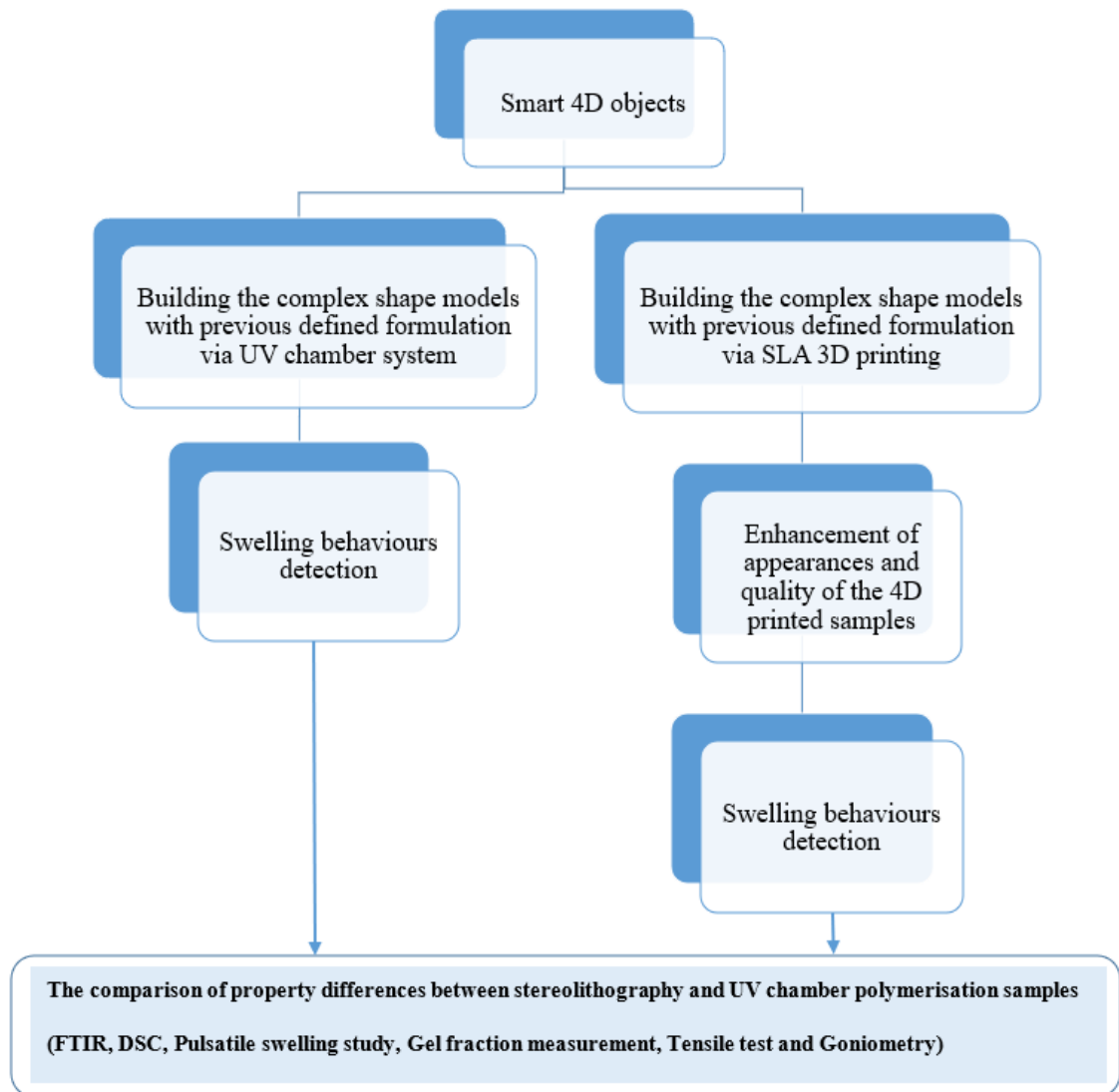


Figure 3-36 Work breakdown structure for the development of the smart 4D objects.

3.3.2 Photopolymerisation of the complex shaped objects with moulds

Based on the designed model, the mould was printed layer by layer from bottom to top with V2 Flexible resin. **Figure 3-37** shows the finished part which had been established in the build platform. Stainless-steel tools were used to remove the support.



Figure 3-37 Mould printed using Form 2 3D printer.

Based on the previous formulation, the liquid base monomeric solution was prepared and pipetted into the silicone mould. As seen in **Figure 3-38**, the puzzle shape sample was successfully cured in the mould. However, after ultraviolet irradiation, the cured part became stuck to the mould and unable to be separated. The entire mould became soft and broke after bending slightly. This may be due to the similar type of materials (the raw materials used to develop the mould and samples are liquid and UV curable) being treated after the same process (UV curing) resulting in adhesion or fusion between the two materials.

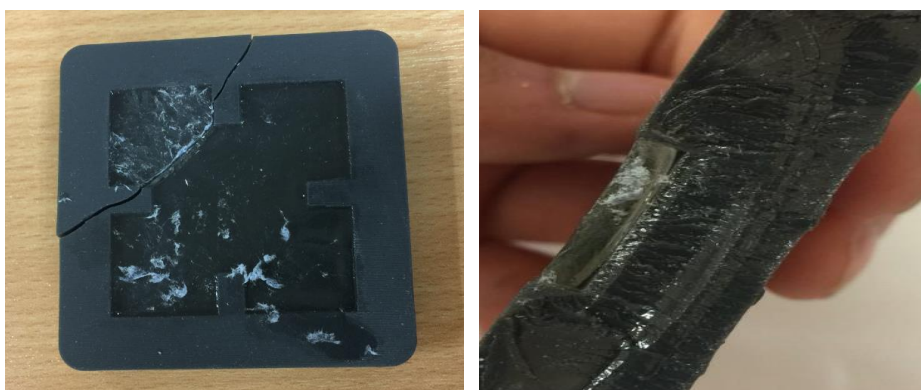


Figure 3-38 The above mould was made with Flexible Form 2 resin, and fracture was caused by bending when removing the sample.

Therefore, the silicone mould was subsequently considered for the second photopolymerisation trial. After the UV irradiation, the puzzle shape samples were made

and were easily removed from the mould. Just as with the disc samples, the puzzle samples displayed a shiny and transparent appearance (**Figure 3-39**).



Figure 3-39 *The puzzle shape samples developed using the UV curing chamber.*

Using the silicone mould, the flower shape sample, made with the same formula, was bright and transparent, and all the samples displayed the required flower shape (**Figure 3-40**). Subsequently, the swelling studies were performed on the synthesised jigsaw and flower samples to detect smart behaviour. This will be discussed in the subsequent sections.

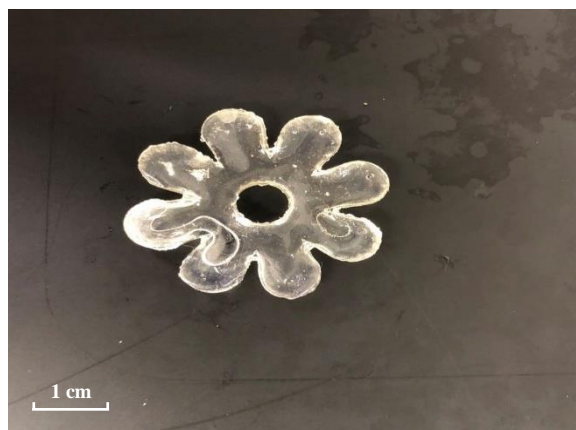


Figure 3-40 *The flower shape sample developed using the UV curing chamber.*

3.3.3 The synthesis of complex shaped objects via a 3D printing technique using novel formulation

In the previous section, the puzzle and flower pattern samples were successfully developed through the Dr. Gröbel UV curing system. Therefore, the resin used for 3D

printing was prepared with the same formulation, containing 0.1 wt% Irgacure 2959, 2 wt% PEGDMA, 70 wt% NVCL and 30 wt% DMAAm. The total amount of solution for each configuration was 50g. It was decided to use the flower models for the first printing trial. The flower model sits at a 45-degree angle to ensure the model after printing could be easily removed from the platform. Furthermore, in a conventional printing process, the support structure would be printed first to support the part throughout the printing process. However, considering the particular properties of the homemade resin, it was anticipated that it would be difficult to print the default complex support structure. The first sample was designed to print a without support. The difference in the printing method can be seen in **Figure 3-41**.

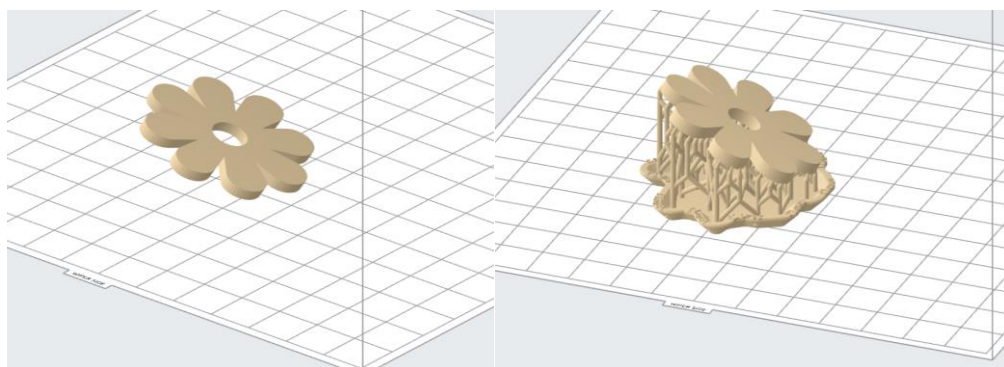


Figure 3-41 (L) printing without support & (R) printing with support.

A minimum cure size of 0.05 mm per each layer was selected for the printer. The total time taken for printing was 3 hours 22 min. However, after three attempts, the homemade resin was unable to print. No solid parts were observed. In order to ensure the accuracy of the experiment, the resin used in the printer was placed in a silicone mould and an attempt was made to cure it in the Dr. Gröbel UV system. As a result, the resin was fully cured via photopolymerisation. Comparing the differences between the two technologies, the reason why the homemade resin was unprintable may be that the laser scanning time for each layer is too short so that the new layer of resin cannot be cured on the basis of the previous layer. This may also be attributed to the fact that the intensity of the ultraviolet light provided by the printer is poor, resulting in the inability of the self-

made resin to cure. Furthermore, compared with commercially available resins, synthetic self-made resins often have a lower viscosity, so they cannot be attached on the inverted platform during printing. Therefore, with this in mind, new formulations were developed for the 4D printing trial.

3.3.3.1 New formulation development for 4D printing

In order to make 4D printing possible, the first consideration was to increase the content of photoinitiator, to make the solution more sensitive to UV light. Also, in order to explore the influence of crosslinking methods on printing, a physical crosslinking solution with the same ratio after removing the crosslinking agent was also prepared. The samples were prepared based on the blending details as shown in **Table 2-5**. However, for those chemically crosslinking solutions, as the initiator concentration increased, still no objects were printed. For those resins that are physically crosslinked, there were crystals that precipitate in the resin container during the printing process and, after a period of time, almost all of the liquid condenses into solid fragments. This phenomenon is due to the recrystallisation that occurs in the NVCL monomer when the NVCL mixture is exposed to room temperature for a long period of time, which prompts it back to its stored state. Therefore, in the subsequent research, solutions that are physically cross-linked were not considered for further use in producing 4D objects.



Figure 3-42 Recrystallisation of NVCL based solution occurs on the printer resin tank.

It was found that changes in concentration of the Irgacure 2959 and crosslinking method had no effect on printing. Therefore, for the next generation formulation it was decided to use other photoinitiators. In line with the relevant literature (Jing Zhang & Xiao, 2018), considering the price of the materials, the wavelength range of induction and the initial state of the materials, Irgacure 184, BAPO, TPO and H-Nu 400IL were selected to use for the new trial.

3.3.3.2 The effect of new photoinitiators on 3D printing

The solutions were prepared based on the details that are listed in **Table 2-6** and poured into the printer resin tank. The total amount of solution in each batch was 50 g. The flowers were successfully created with four new formulations. However, when Irgacure184 was used as a photoinitiator, the shapes of the printed flowers were incomplete — only a part of the flowers were successfully printed. Although a complete flower could be printed when using TPO and BAPO, the printed part did not satisfy the predetermined dimensions and pattern.



Figure 3-43 (L) the BAPO sample printed flower shape model stuck on the resin-filling tank; (R) flower-shaped sample printed with 2 wt% BAPO resin.

As **Figure 3-44** shows, when the NVCL solution contained 2 wt% H-Nu 400IL, the printed flowers were able to obtain the designed dimensions. However, there were still parts of the petals missing at the outer edge of the flower. Additionally, it can be noticed

that all printed parts were built on the bottom of the resin tank instead of the printing platform. This could be due to the fact that the parts were placed and created at a 45° angle and the layers created at the beginning failed to build up on the print platform due to the lack of contact area between the parts and the print platform.

In summary, comparing the flower parts made by the four different new photoinitiators, the flower printed using 2 wt% H-Nu 400IL demonstrated a relatively better appearance.



Figure 3-44 Flower-shaped parts printed using 2 wt% H-Nu 400IL resin.

In order to improve the quality of the prints, the next stage of the study investigates the effect of concentration on the quality. Resins that contained 1 to 5 wt% H-Nu 400IL were prepared in sequence. The details of these formulations are shown in **Table 2-7**. After printing was complete, a flower-like print could be found on the bottom of the resin tank. This means that all flower bodies were constructed on the resin tank. As **Figure 3-45** reveals, the flower shape can be basically printed as a thin layer when mixed with 1 wt% H-Nu 400IL. When using 3, 4 and 5 wt% H-Nu 400IL, only a part of the flower was printed with uneven edges. Only the 2 wt% H-Nu 400IL samples exhibited a relatively complete shape of flower. Therefore, it can be concluded that the samples obtained by printing with the resin containing 2 wt% H-Nu 400IL show a relatively better performance.

The sample is able to be established roughly in accordance with the design. However, the quality of prints is still inadequate to meet the criteria for use.

For the 2 wt% H-Nu 400IL resin, it can be observed that the thickness of printed models is inconsistent. Moreover, the surface of the samples after printing was incomplete and not smooth. There are even some details missing on the outside of the petals. The reasons can be summarised as follows. Firstly, it may be because the amount of resin used for printing is insufficient, resulting in the absence of resin to cure in the later stage of printing. Secondly, as the print's construction is carried out on the resin tank it is possible that the actual position of the print slightly differs from the designed position. This leads to different curing rates in different areas resulting in inconsistent thickness of the sample. Additionally, since the printed parts are directly printed on the platform, it is easy to cause damage to the sample during the process of removing the samples. It is also worth noting that during the printing process, due to the strong corrosiveness of NVCL, the printing platform shell is corroded and gradually fell off in the resin box. This leads to a reduction in the quality of the prints.

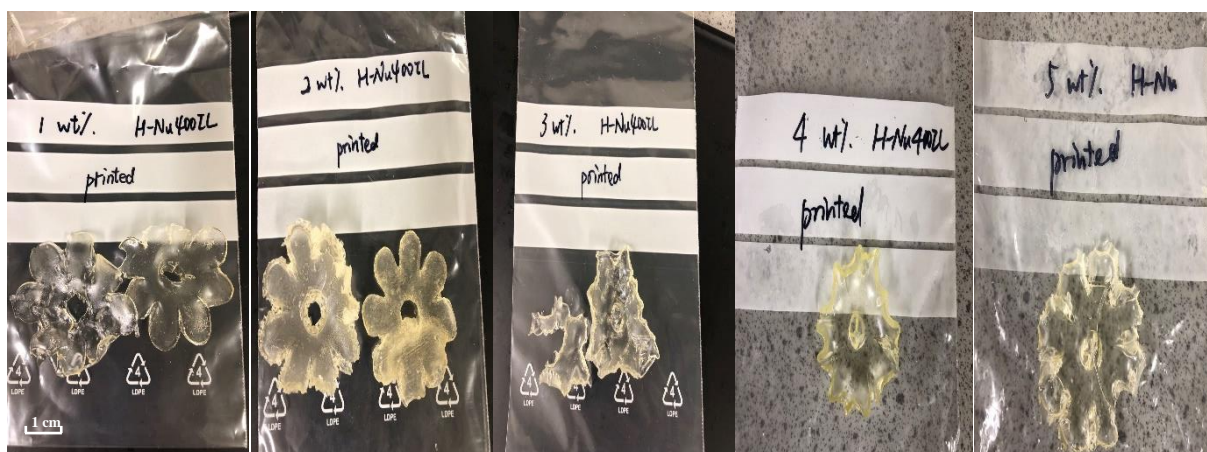


Figure 3-45 The flower-shaped parts printed using 1~5 wt% H-Nu 400IL homemade resin.

3.3.3.3 Further improvement of the 2 wt% H-Nu 400IL samples

Up to this point, the flower parts had been successfully printed with home-made resin but the appearance of the printed flowers was not ideal. Therefore, the next step in

the research was to address each of the issues listed above to further improve the quality of the 2 wt% H-Nu 400IL samples.

Initially, the total weight of the resin was increased from 50g to 150g. At the start of printing, the 100g prepared solution was poured into the resin tank and then the remaining 50g was gradually added to the tank during the printing process to ensure that there was sufficient resin for curing. The shells of the platform were wrapped with transparent tape to avoid contact with NVCL. As **Figure 3-46L** demonstrates, after increasing the content of the resin, the quality of the printed flower was significantly improved. The flower model was fully printed with an outstanding appearance and shape integrity. It could be established on the platform without any contaminants inside the sample. However, when removed from the platform, it can be observed that an extra amount of resin is cured on the side of the model to use for connecting with the platform, resulting in an uneven thickness of the printed sample.

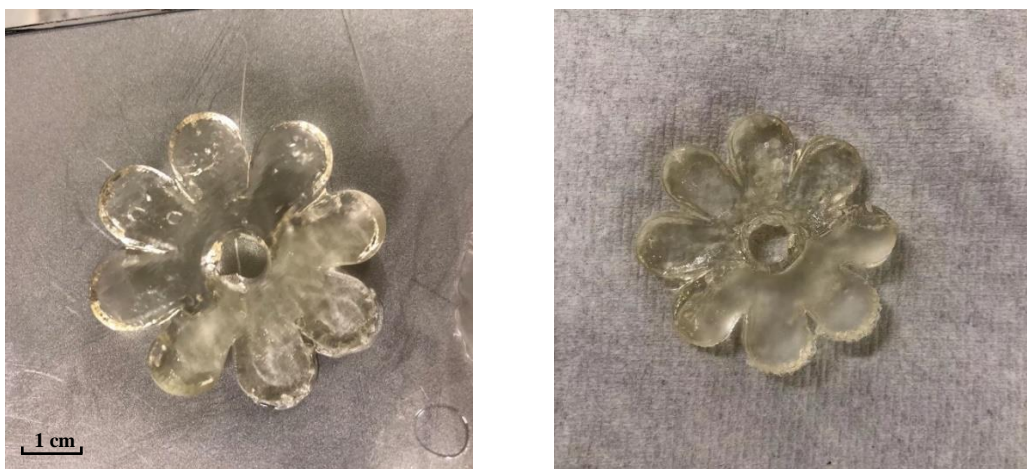


Figure 3-46 (L) *The new flower-shaped part printed on the platform & (R) the new flower-shaped part after remove from the platform.*

As mentioned above, for a common 3D printing process, a support structure is always built. This gives better assurance of the quality and integrity of the product. Therefore, the next generation of 4D objects were built on support structures. In order to investigate the impact of the printing angle on the printed samples, the flower model with

support was placed horizontally and at 45 degrees (**Figure 3-41**). After several attempts, the print was unable to build up on the stand. This was because the structure between the item and the base was too slim and dispersed (**Figure 3-47L**). By modifying the support structure, the structure becomes gathered and thick. It can be observed that the flower and support are successfully printed on the platform with a horizontal lay-out (**Figure 3-47M**). However, it was found that the flower printed on the support structure is soft and difficult to separate from the support structure. This is probably due to prolonged immersion in the solution, which causes both the support structure and the print to swell after printing. Although the sample hardened again after post-curing, there was resin filling in the voids between the petals giving the flower an imperfect appearance **Figure 3-47R**.

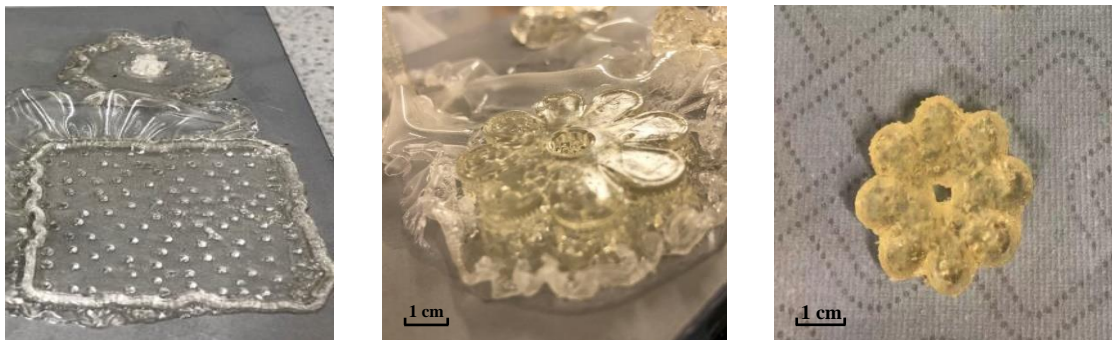


Figure 3-47 (L) Support-bases built on the platform, (M) the flower model printed on the support structure & (R) the flower model after removing the support and post-cure.

As the support structure cannot be built stably and guarantee the quality of the print, in the final iteration of the design, the model of the flower was designed to be built horizontally without supports. As a result, the prints can be built on the platform with an excellent appearance and can be easily removed from the platform by means of a small spatula. Furthermore, to verify the feasibility of this scheme, the jigsaw prototype was attempted to be printed with the same set-up. **Figure 3-48** shows the appearances of the printed items removed from platform. These prints were printed in accordance with the design. After post-curing, the parts exhibited a bright and flat surface. The size and pattern of the prints were also as required.

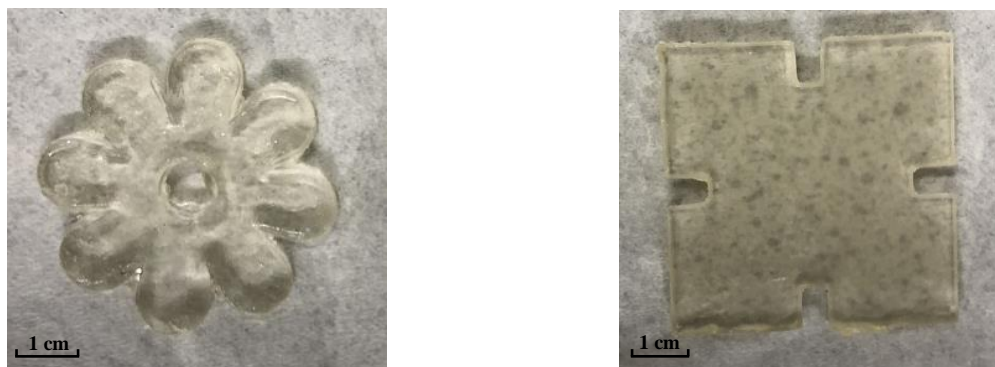


Figure 3-48 The appearance of printed samples (L) Flower & (R) Jigsaw.

In summary, using the Form 2 SLA 3D printer, the homemade resin could be successfully printed by preparing a 150 g solution containing 2 wt% H-Nu 400IL photoinitiator, 2 wt% PEGDMA, 30 wt% DMAAm and 70 wt% NVCL with a curing size of 0.05 mm per layer. Furthermore, the layout of designed components must be horizontal and constructed directly in the printer build platform.

3.3.4 Comparison of the properties of UV-cured and 4D printed samples

As discussed in the last section, the three-dimensional flower and puzzle have been manufactured via UV chamber system and 3D printer. The characterisation studies are carried out to further explore the properties of the prepared parts. The expand-shrink cycle behaviours are expected to be completed by cured and printed items so that the 4D printing can be successfully achieved in this study. In addition, the effects on material properties of NVCL samples prepared via stereolithography and UV chamber polymerisation are also investigated.

3.3.5 Attenuated total reflectance Fourier transform infrared spectroscopy

The chemical structure differences were detected on S7(photopolymerised), which has the best performance, and F2 (printed and photopolymerised) which is the most suitable formulation for a 3D printing. As can be seen in **Figure 3-49**, the displayed characteristic absorption bands of the three samples basically match one another. In the P(NVCL/DMAAm) spectra, only an intense peak at 1618/1615/1614 cm^{-1} in S7 and F2

cured and printed samples is attributed to the characteristic absorption of C=O stretching. Based on the previous studies, only one peak exists at the wavelength between 1600~1700 cm^{-1} in the printed and cured sample spectra, indicating successful printing and polymerisation (C=C bonds disappearance). The bands at 1479 cm^{-1} (S7), 1479 cm^{-1} (F2 UV-cured) and 1481 cm^{-1} (F2 printed) are attributed to the stretching of C-N bonds in both monomers (Chen *et al.*, 2009). The O-H bending arising at 3442 cm^{-1} and 3425 cm^{-1} in photopolymerised and printed samples provides further evidence that the polymerisation has succeeded (Killion *et al.*, 2011). It is worth noting that some of the peaks detected in the printed samples were lower or higher in intensity than the two photopolymerised samples. This suggests that the chemical bonds created in the printed samples may be slightly different compared with those created in the photocured samples (Hughes *et al.*, 2014). For example, photopolymerisation will produce more C=O bonds than the 3D printing process. However, the water content in the printed samples was greater than in the samples formed by photopolymerisation. Compared to light-cured samples, 4D printing is time consuming. As the part is built up layer by layer, the sample being printed and the solution are more exposed to moisture in the air, resulting in a sharp peak and large shift of the O-H peak in the printed samples.

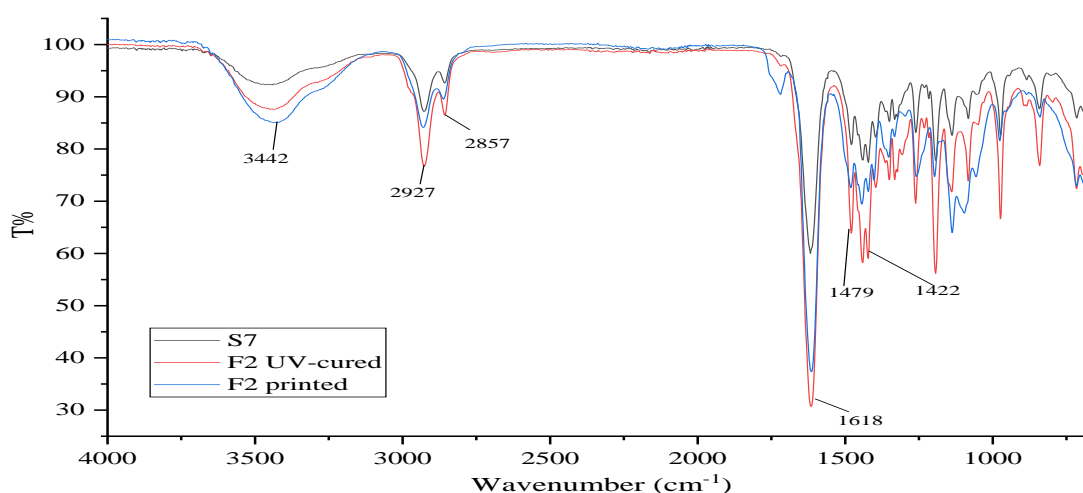


Figure 3-49 FTIR spectra of the photopolymerised and printed samples. $n=2$.

Table 3-9 Functional groups in NVCL, DMAAm, PEGDMA, S6 and S7 analysis using FTIR.

Functional Group	Wavelength (cm ⁻¹)		
	S7 photopolymerised	F2 photopolymerised	F2 printed
Aliphatic C-H	2927, 2857	2926, 2857	2930, 2857
C=O	1618	1615	1614
C-N	1479	1479	1481
-CH ₂ -	1422	1422	1422
O-H	3442	3442	3425

3.3.6 Differential scanning calorimetry

The LCST of those printed and photopolymerised chemically crosslinked P(NVCL/DMAAm) were detected by differential scanning calorimetry. The gel samples were immersed in distilled water at room temperature and allowed to swell to equilibrium before the DSC measurement. The onset point of the endothermal peak was defined as the LCST. The DSC profiles show that the LCST's of S7 photocured, F2 photocured and F2 printed are 40.7°C, 40.6°C, and 39.7°C respectively. There was no significant difference between polymerisation methods and photoinitiator types. As the temperature increased, all the samples exhibited similar LCSTs at around 40°C — this is because the chemical composition of the S7, F2 and F2 printed hydrogels were identical. The same hydrophilic/hydrophobic balance in the polymer side chains determines the gel's similar phase separation behaviour (Zhang *et al.*, 2005).

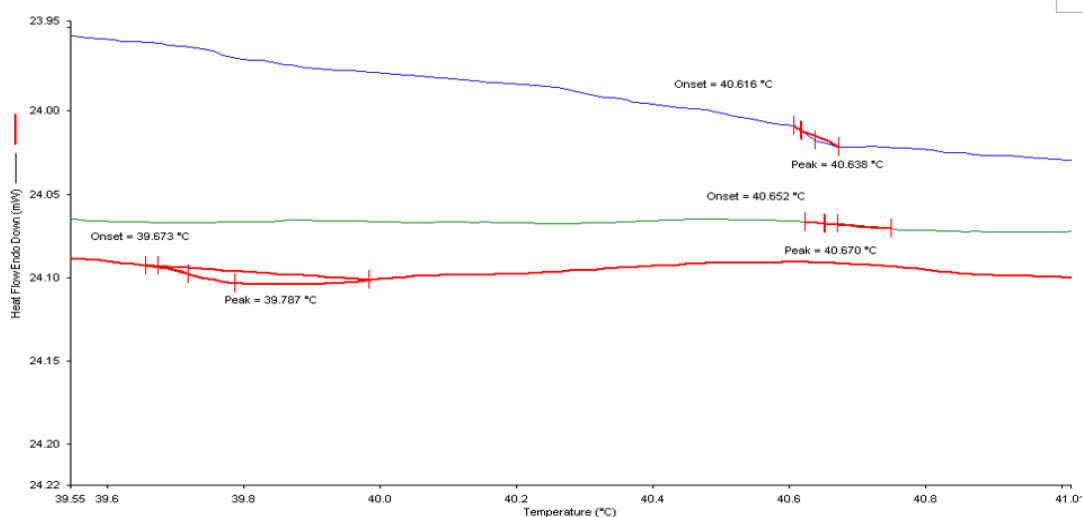


Figure 3-50 A thermogram illustrating the LCST of printed and cured P(70NVCL-30DMAAm); Green: S7(photocured); Blue: F2(photocured) and Red: F2(printed). $n=3$, $p>0.05$.

3.3.7 Pulsatile swelling studies on cured and printed complex shaped samples

The pulsatile swelling tests were carried out on both photocured and printed samples to further examine the smart 4D behaviours of the shaped samples and to compare the differences in dimensional expansion/shrinkage capabilities between the photopolymerised and printed samples. Taking into account the potential expanding dimensions of the samples, swelling analysis of samples was performed in a rectangular plastic container of $120 \times 80 \text{ cm}^2$ containing 350 mL of distilled water. The first part of this study aimed to investigate the swelling behaviour differences between the puzzle shapes, flower samples and disc samples. As can be seen in **Figure 3-51**, the curves of the formed samples and discs are fundamentally consistent. At temperatures below LCST, all samples reach their maximum swelling capacity in water and retained their structural integrity. For all NVCL/DMAAm samples, their dimensions can be nearly expanded by a factor of 5 compared to their original state. It is worth noting that the circle and flower samples can reach equilibrium after 24 hours, while the jigsaw samples take 48 hours to reach their maximum capacity. This phenomenon can be explained by the slow contact of the internal structure with water due to the greater thickness of the jigsaw samples. After

the temperature was raised above LCST, the polymers shrunk to an equilibrium state after 24h. The samples can continuously deswell and reach a new equilibrium level after the temperature reaches 80 degrees. This performance revealed the same trend as previously for chemical crosslinking discs. When the temperature was changed back to 20 degrees Celsius, all samples were able to return to their swollen state.

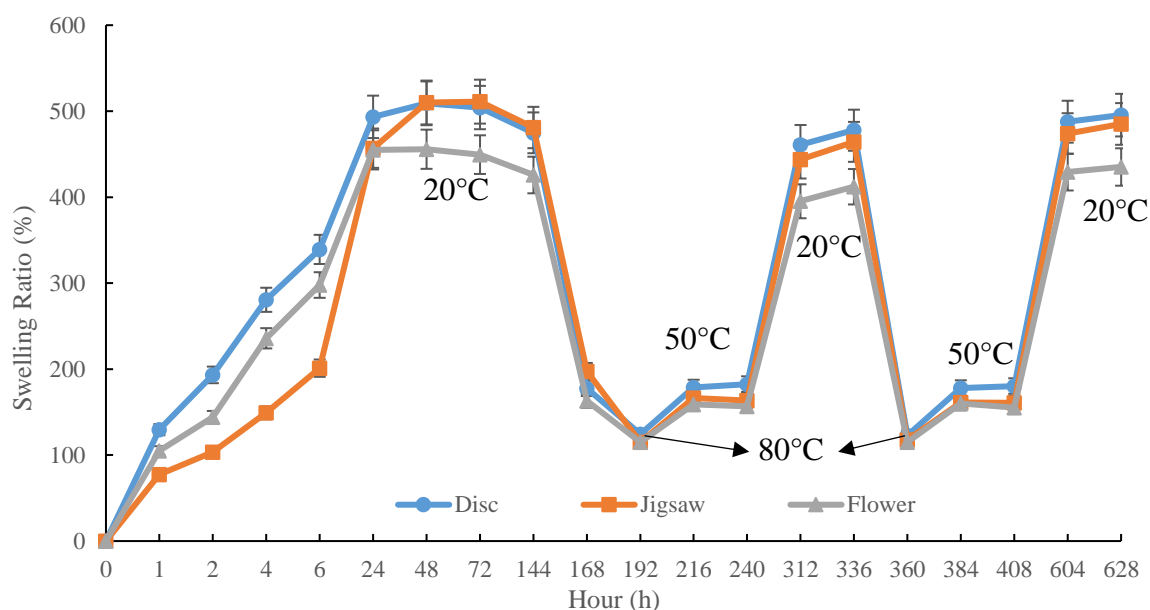


Figure 3-51 The Pulsatile swelling behaviours of photocured chemically crosslinked NVCL/DMAAm copolymer hydrogels with different shapes at temperatures 20°C, 50°C and 80°C. $n=3$.

The appearance of these samples exhibited a bright, transparent appearance throughout the swelling test. The flower and jigsaw shapes presented, with a smooth surface and well-defined edges after expansion and contraction. This indicates that the cyclable intelligent expansion behaviour can be successfully achieved using complex shaped designs.

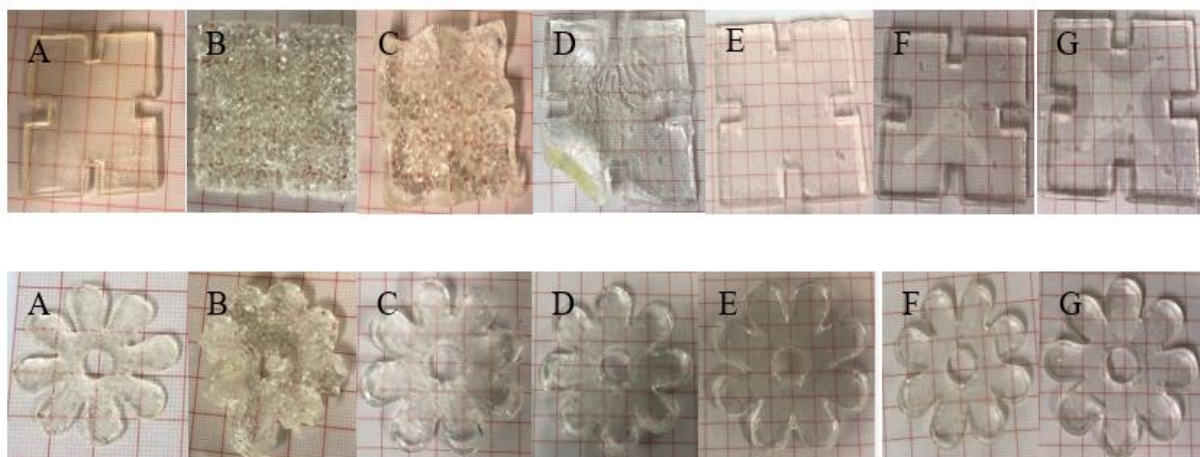


Figure 3-52 *The appearance of the photopolymerised puzzle and flower samples at times: A 0 hour; B 2 hours; C 4 hours; D 6 hours; E 72 hours; F 216 hours; G 336 hours.*

The second part of the swelling study investigated the differences in water absorption between the printed and photopolymerised samples. All NVCL/DMAAm samples were able to exhibit reversible shape change behaviour as the temperature rose and fell. At temperatures below LCST, it was observed that the maximum swollen weight had been reached after 24h. Those items that were photocured showed greater expansion than prints, they were five times (S7) and four times (H-Nu) larger than the size of the original parts, respectively, while the printed parts reached an expansion ratio of 320%. When the temperature was above LCST the samples began to shrink, but there was no significant difference in the expansion rate of the shrunken samples, which dropped to around 150% for both printed and cured parts. In the subsequent cycles, the expansion ratios of the photocured and printed samples were consistent with the results obtained in the first pulsatile swelling experiment.

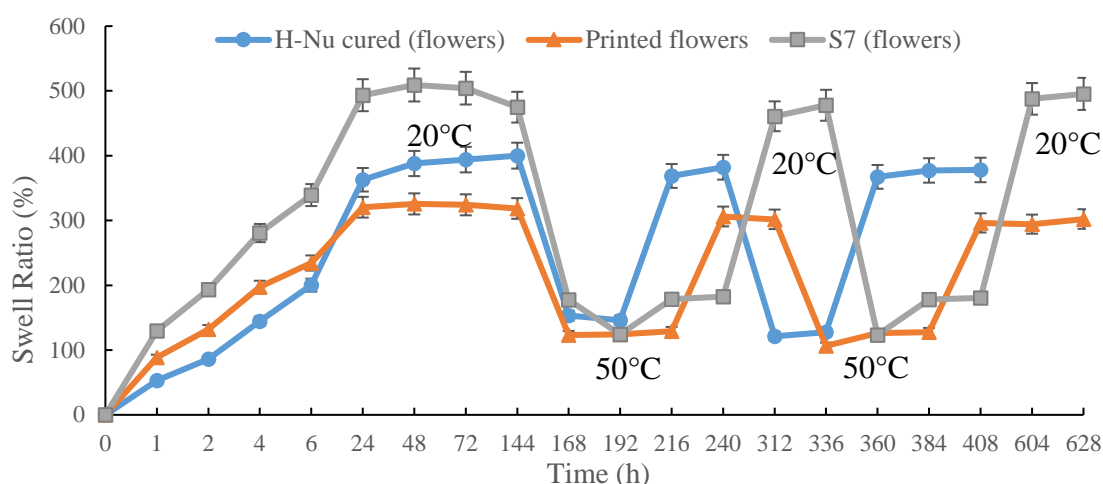


Figure 3-53 The Pulsatile swelling behaviours of photocured and printed chemically crosslinked flowers NVCL/DMAAm copolymer hydrogels at temperatures 20°C and 50°C. $n=3$.

As **Figure 3-54** shows, both swollen flower and puzzle shapes are able to maintain structural integrity in the first swelling/deswelling cycle. However, unlike the photocured parts, the printed samples changed from transparent to white during the water absorption process. After the first equilibrium state is reached, both the flower and the jigsaw shape were completely white. It is interesting to note that after the temperature rose and fell, the swollen samples returned to transparency. In addition, at the later stage of the swelling experiment the printed samples began to crack or even break after absorbing water. This was due to accidental damage caused by the repeated wiping motions during the weighing process.

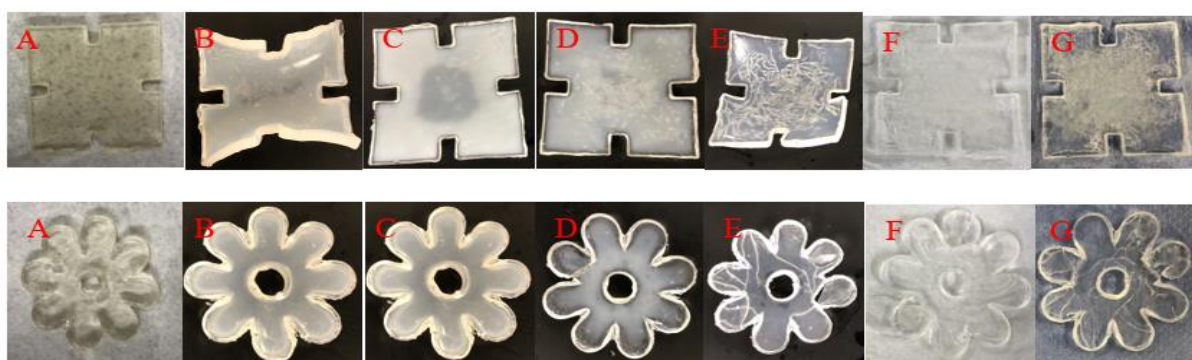


Figure 3-54 The appearance of the 4D printed puzzle and flower samples at times: A 0 hour; B 6 hours; C 24 hours; D 72 hours; E 168 hours; F 240 hours; G 408 hours.

In summary, the flower and puzzle samples manufactured via UV chamber system displayed the same reversible expansion/contraction properties as the disc samples. A smooth surface and excellent appearance were maintained. However, samples with large dimensions require a longer time to reach their maximum capacity. Additionally, 4D printing has been successfully demonstrated in this study. These printed samples were able to demonstrate intelligent and reversible expansion/shrinkage behaviour.

3.3.8 Gel fraction measurement

Gel fraction can be used as a qualitative indicator of the efficiency of network formation (Wu *et al.*, 2010). The greater the gel fraction percentage, the greater the covalent bonding. Gel fraction is the mass fraction of the network material resulting from a network forming polymerisation or crosslinking process. The improved stability of the hydrogels is attributed to the denser crosslink structure of the copolymer network. **Figure 3-55** shows the gel fraction percentages of P(NVCL-DMAAm) hydrogels prepared using different photoinitiators and polymerisation methods. The result is that the different photoinitiators and polymerisation methods have minimal effect on the gel fraction. Thus, the three samples of P(NVCL-DMAAm) were able to maintain a similar gel fraction of about 95%. Only 5% weight loss confirms the excellent quality of the cured and printed products.

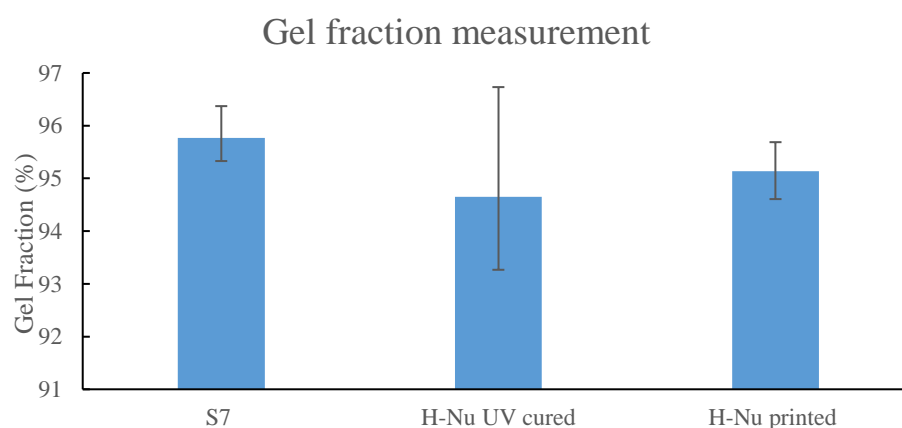


Figure 3-55 The gel fraction of printed samples, S7 and H-Nu UV cured samples. $n=3$, $p>0.05$.

3.3.9 Tensile tests

The tensile tests were also performed on the photopolymerised S7, 3D-printed F2 and photocured samples to investigate the differences between maximum load, tensile strength and tensile modulus. As shown in **Figure 3-56**, there was little difference in all the properties investigated for each sample. H-Nu samples are slightly stronger than both S7 and printed samples. The same trend has also been found in terms of tensile strength where S7 UV-cured samples have a greater tensile strength at limit. In general, tensile properties can be slightly influenced by the type of photoinitiators, and the polymerisation method used.

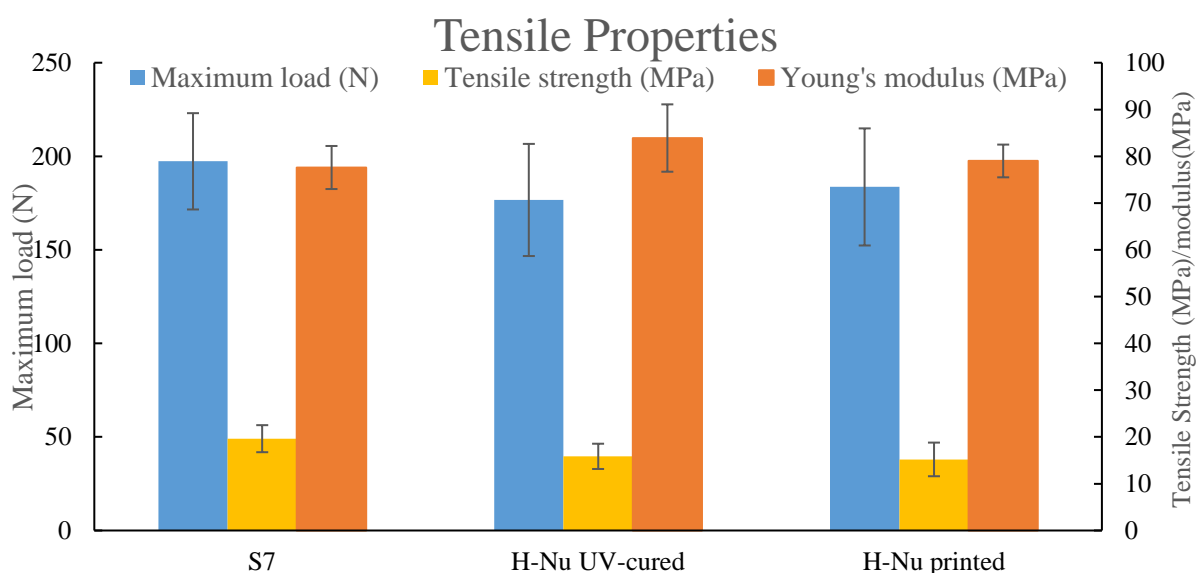


Figure 3-56 The comparison of tensile properties between S7, H-Nu photocured and H-Nu printed samples. $n=5$, $p>0.05$ (maximum load), $p>0.05$ (tensile strength), $p>0.05$ (Young's modulus).

3.3.10 Goniometry

The contact angle provided the level of hydrophobicity of each hydrogel. The hydrophobicity of the 3D printed and UV cured hydrogels was determined using goniometry to measure the angle of a drop of water wetting the surface of the solid xerogel. The S7 copolymer P(NVCL-DMAAm) prepared using 0.1 wt% Irgacure 2959 had a mean contact angle of 67.8° at zero second, dispersing into a drop with a mean contact angle of

45.3 °, characterising it as a hydrophilic material. The same trend was observed with F2 cured samples, which had a mean contact angle of 75.2 ° at zero seconds, spreading into a drop with mean contact angle of 62.3 ° at 115 seconds. However, the F2 3D printed samples had a mean contact angle of 62.6 ° at zero seconds, dispersing into a drop with a mean contact angle of 32.5 ° at 115 seconds. Based on the wettability measurements, SLA increases the hydrophilicity of P(NVCL-DMAAm) compared to UV chamber samples. This coincides with the FTIR findings, where the 3D printed samples show stronger peaks of O-H bonds than the UV polymerised samples. Furthermore, when comparing the two UV cured samples, the Irgacure 2959 sample contact water angle was closer to 0 °, which meant that the mix of H-Nu 400IL reduced the hydrophilicity of P(NVCL-DMAAm) compared to the Irgacure 2959 samples.

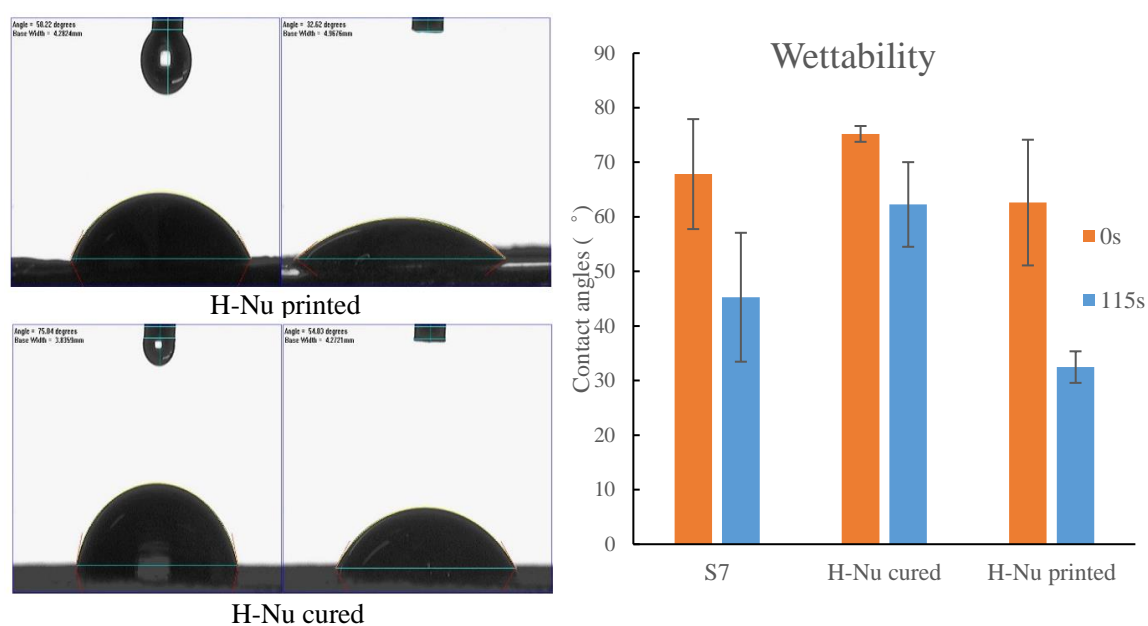


Figure 3-57 (L) The representative contact angles figures of F2 printed and UV-cured samples at 0 and 115 seconds; (R) The comparison of contact angles between S7, F2 UV-cured and 3D printed samples. $n=3$, $p>0.05(0s)$, $p<0.05(115s)$.

3.3.11 Summary

The formulations containing **2 wt% H-Nu 400IL**, **2 wt% PEGDMA**, **30 wt% DMAAm** and **70% wt% NVCL** were developed using a Form 2 SLA 3D printer. The 3D prints exhibited an excellent appearance and were able to respond to temperature pulses across their critical temperatures, showing intelligent and reversible swelling/deswelling behaviour in water media.

In addition, the effect on the material properties of NVCL samples prepared via stereolithography and UV chamber polymerisation has been examined and summarised. Both S7 and F2 samples showed a gel fraction around 95%. The photopolymerised and 3D printed P(70NVCL/30DMAAm) parts were able to demonstrate expected expand/shrink behaviour in water media. Moreover, when viewing the chemical structures and lower critical solution temperatures, there was no significant difference between those items. Overall, the differences between polymerisation methods and photoinitiator types can be significant; although their chemical structures and thermal properties are similar, there was differences recorded with regard to swellability and wettability of samples.

3.4 Use of bilayer structures in UV chamber system to develop shape shifting materials

3.4.1 Preface

The successful development of 4D material has been described in the previous section. The printed objects were able to expand in water at room temperature and shrink when the temperature increased above their LCST. However, the 4D objects developed in the prior section can only change their size when immersed in water. It is difficult to develop new applications with a single volume change behaviour. Therefore, in order to maximize the value of the 4D samples, new intelligent behaviours were also investigated.

Stimuli-responsive hydrogels can undergo a dramatic volume change in response to the external signals such as temperature. Due to the single change behaviour, hydrogels cannot be flexibly converted between multiple configurations as SMPs, although some hydrogels can also be formulated to possess shape memory functions (Wu *et al.*, 2018). It has been reported in the literature that intelligent deformation occurs when a force is generated between two different materials. Generally, the shape-shifting materials are composed of two materials. One is the active layer, made of the stimuli-responsive materials; the other is the passive layer, often made with low stiffness materials. Once triggered by the activation stimulus, the deformation generation on the active layer spurs the passive change, leading to a change in dimensions and curvature (van Manen *et al.*, 2018). Depending on the combination of the two layers, the bilayer structures are able to achieve self-folding, self-curving, self-bending, self-twisting, self-buckling and self-rolling behaviours (Nam & Pei, 2019).

The 3D printer used in this study was not expensive (approximately 3000 euros) and can only apply one material at a time for printing. Therefore, the new shape-shifting behaviours are difficult to develop with this type of 3D printer. From the previous sections,

the hydrogel samples synthesised using S7 formulation via UV chamber system demonstrated reasonable reversible swelling behaviours. Therefore, an attempt to develop new double-layered 4D objects by means of UV chamber system was made. Although other researchers have developed such smart structures and complex deformation mechanisms, few scholars have used NVCL based polymers developed in a UV chamber system. In this section, several commercial flexible materials are selected to combine with the S7 material to form the bilayers. For feasibility purposes, the simple strip and flower shape samples which showed an excellent performance in the former sections were used for trials. The shape-shifting behaviours of double-layered structures were detected by the pulsatile swelling studies.

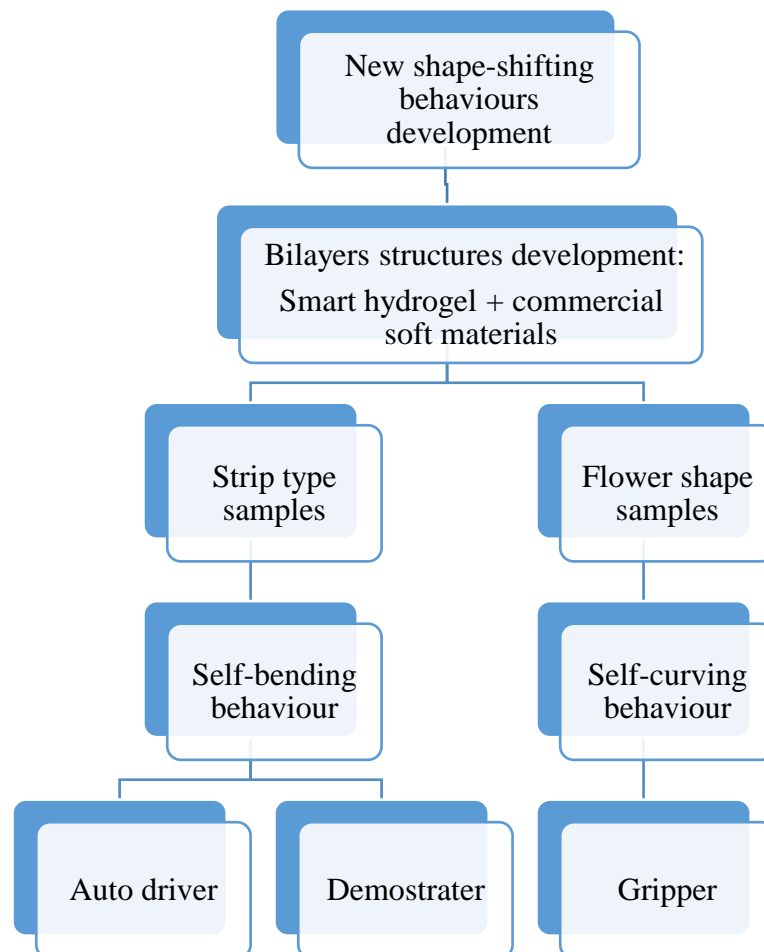


Figure 3-58 Work breakdown structure for the development of the bilayer smart 4D objects.

3.4.2 The development of first-generation bilayer strips

4D objects were successfully prepared by 3D printer in the former section. However, the fact that the samples could only change their dimension resulted in the limited application of the 4D printed samples. The structures being developed in this section are expected to exhibit more complex change behaviours. It is well known that deformation occurs when a force is generated. Stimulus-sensitive materials are capable of generating expansion forces when stimuli are triggered. When a layer of flexible material is overlaid on the stimulus-sensitive material, the force generated by the stimulus-sensitive material can drive and stimulate changes in the flexible material, resulting in changes in planar dimensions and curvature (van Manen *et al.*, 2018). Thus, the idea of creating a bilayer structure was born.

The flexible photopolymers used in this study were purchased from Formlabs company. One of the materials used to prepare the passive layer is known as “Flexible Resin”. Flexible resin is a black legacy formulation of mostly stiff, soft-tough material. The ultimate tensile strength of this material can reach to 7.7-8.5 MPa. The elongation at failure is 75-85%. The other material used for preparing the passive layer is called “Elastic 50A resin”. Elastic resin is a soft and transparent photopolymer resin. 50A stands for the hardness of the materials. The ultimate tensile strength of this material is 3.23 MPa. The elongation is 160%. The Flexible and Elastic resins can both withstand bending, stretching, and compression in repeated cycles without tearing and are able to spring back to their original shape. According to the provided description of the materials, the flexible photopolymers are suitable for prototyping parts normally produced with silicone (Formlabs, 2019). However, the Flexible resin is stiffer than Elastic resin.



Figure 3-59 The Flexible and Elastic 50A resin cartridge obtained from formlabs.

The first trial of bilayer structures was prepared in the shape of a rectangle via a chamber system. The method for creating a bilayer structure was described in section 2.8. The patterns of the strips were designed based on the literature (Janbaz *et al.*, 2016). The patterns and parameters of the first-generation strip models were described in section 2.8.1. The designed strips were expected to have different shape changes. In order to fabricate the bilayer structure via UV chamber system, the five different prototypes of the strips were first printed via Form 2 3D printer using high temperature resin. In previous studies, silicone moulds have demonstrated the ability to accommodate NVCL-based polymers under UV exposure. The cured parts could be perfectly formed and easily separated from the mould. Therefore, a silicone mould was prepared again for bilayer creation. The formulation details of the bilayer structure are shown in **Table 2-8**. Based on the S7 formulation, the liquid base polymer was prepared and pipetted into the prepared mould first. After UV curing for 10 minutes, the flexible and elastic resins were poured on the top of the cured layer and placed into the chamber for another 10 minutes. It is important

to note that air bubbles form when injecting the elastomeric resin into the silicone moulds, which can be removed with a pipette to ensure the quality of the sample.

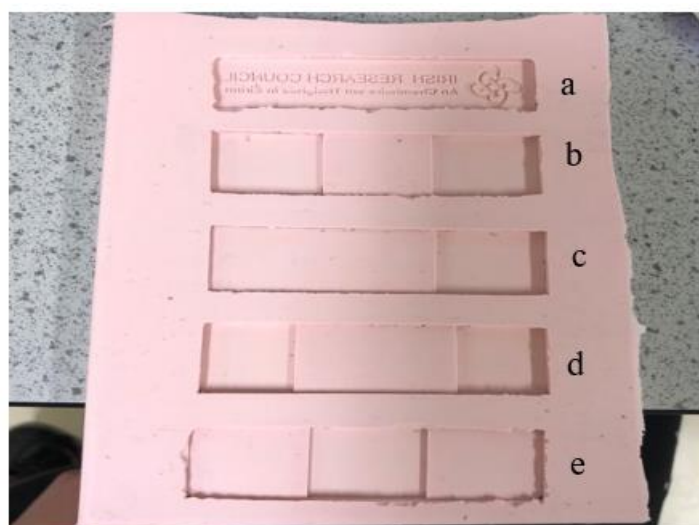


Figure 3-60 *The first-generation strips types of silicone mould.*

The photocured bilayer structures are shown in **Figure 3-61**. Samples of all types of strips were successfully prepared with excellent appearance and adhesion. The elastic resin is transparent and has good photosensitivity, allowing the formation of passive layers of varying thicknesses under UV light. Compared to elastic resin, the black colour of flexible resin makes it easier to distinguish between the active and passive layers. However, once the black resin has cured on the surface, the black layer would block UV radiation and prevents the curing of the flexible photopolymer below.

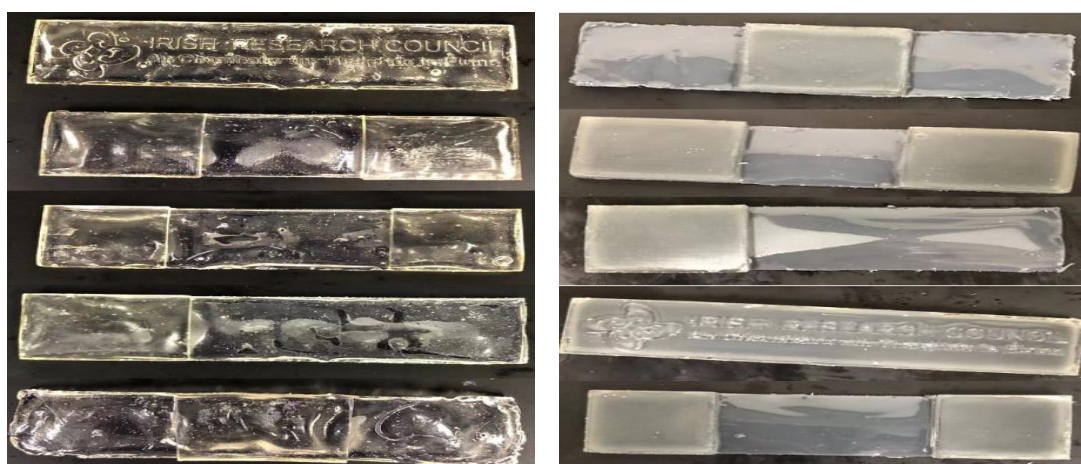


Figure 3-61 *(L) Bilayer strips made using Elastic resin + NVCL; (R) Bilayer strips made using Flexible resin + NVCL.*

3.4.3 Shape shifting behaviours detection of first-generation bilayer strips

The different shapes and types of the bilayer strip structures were successfully fabricated as described in the last section. The purpose of preparing five types of strip shapes was to investigate the effect of different shapes and positions of active layers on the shape shifting behaviour. In parallel, the effect of the different flexible materials used to prepare the passive layers on the quality and shape change behaviour of the samples was also evaluated.

The prepared strips with flexible and elastic layers were placed into large plastic trays to ensure that the samples could be fully submerged in water during the whole experiment. In order to detect the behaviours and shape changes, photographs were taken at specific time intervals as shown in **Figure 3-62** below. In the case of bilayers constructed with flexible resins, no shape changes were displayed. Only a change in the size of the active layer could be observed after 1 hour. In addition, even for the same type of bilayer structure, the exhibited shape-shifting behaviours were different. This phenomenon may have occurred due to the fact that the proportion of active layers was different for each sample. Additionally, as there is no limit to the active structure, there is no guarantee that the expansion of the active layer will act on the flexible layer and cause the flexible layer to change shape. As the swelling ratio increased, the active layer began to peel off the passive layer. After 24 hours, the active layer had almost completely shed from the flexible layer. This may have been caused by the thinness of the flexible layer which could not withstand the rapid expansion of the NVCL layer. Due to the unsatisfactory performances of the flexible bilayers, the pulsatile testing was not performed on these samples.

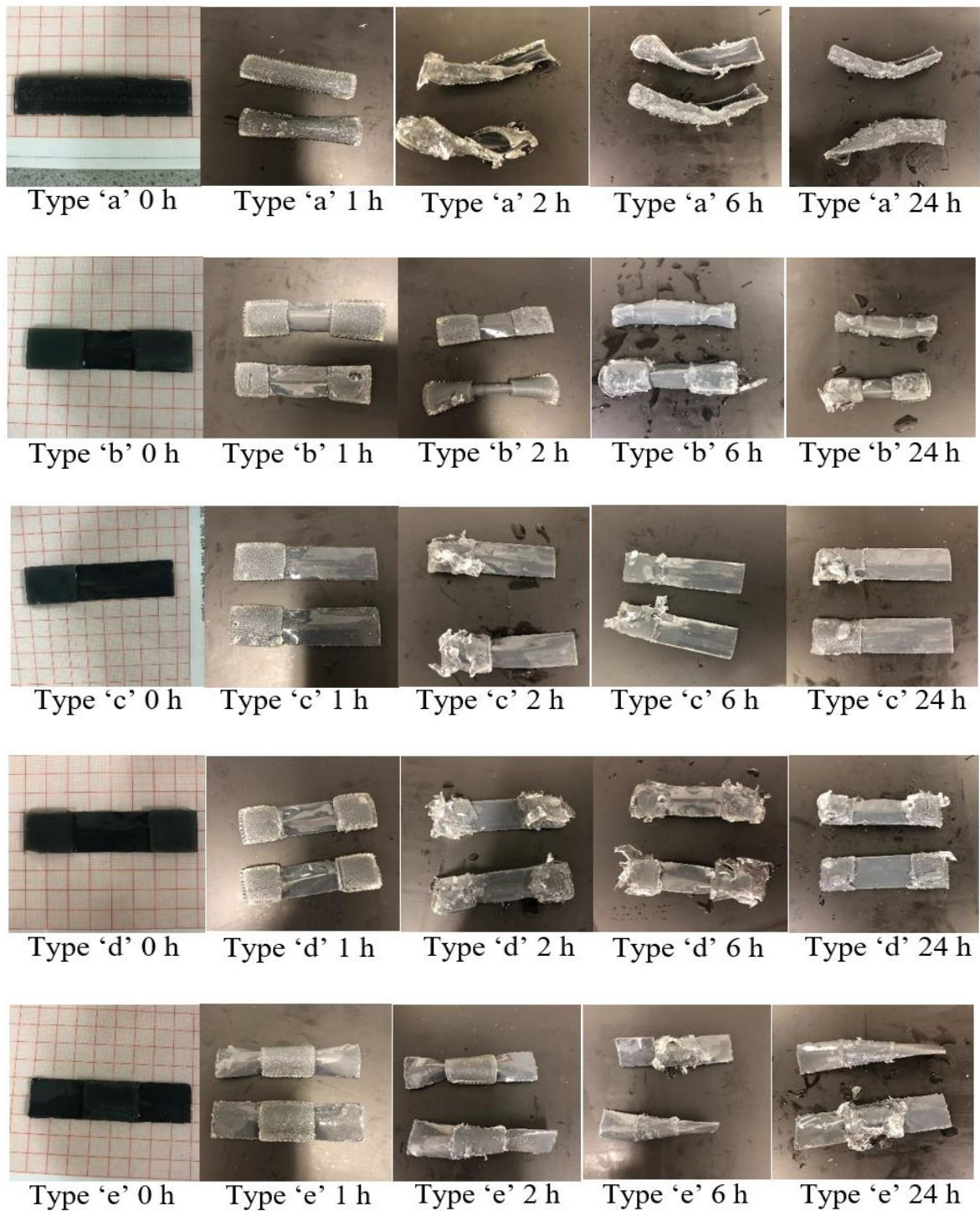
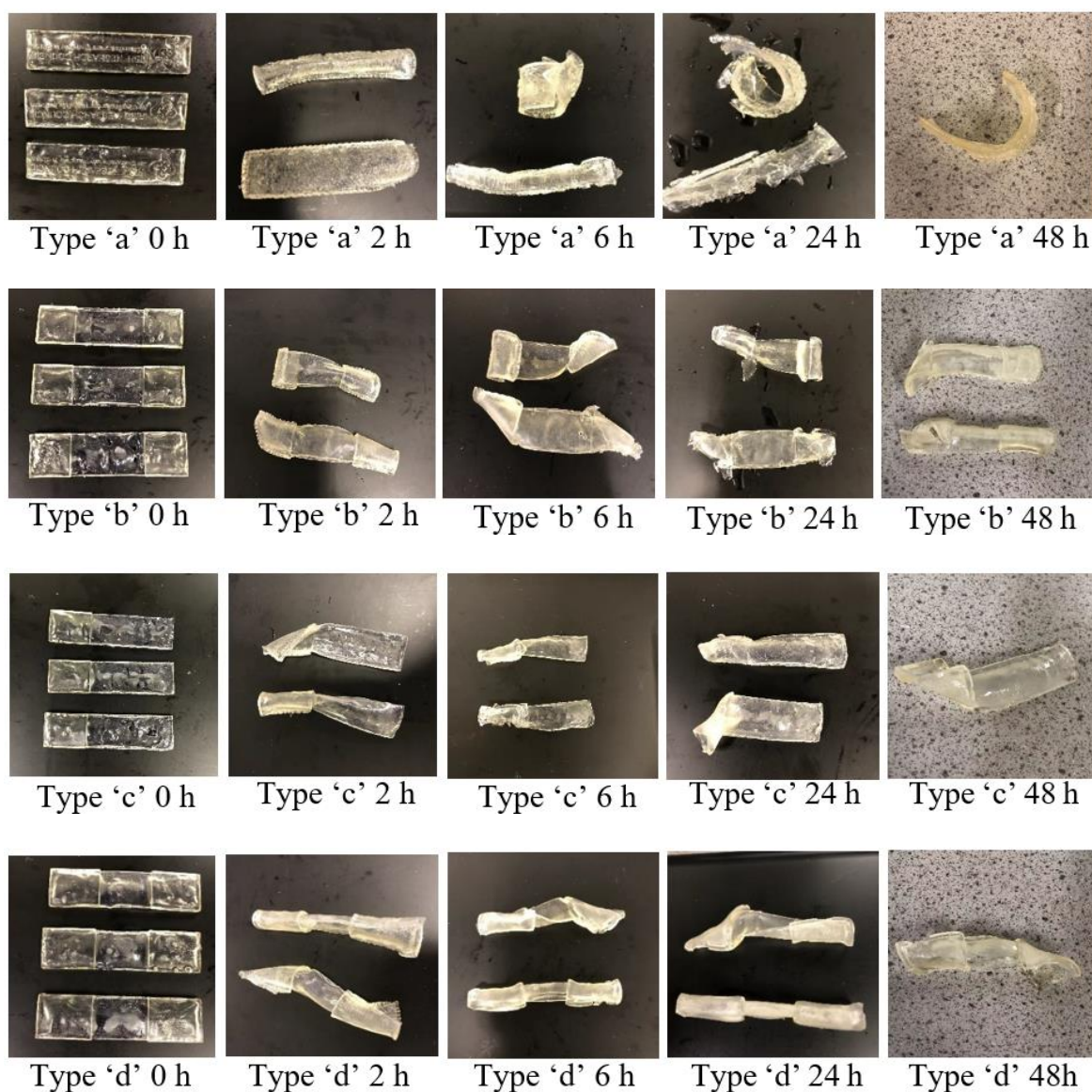


Figure 3-62 At room temperature, the appearances of the different types of flexible bilayer strips at the times: (L-R) 0 hours, 1 hour, 2 hours, 6 hours and 24 hours.

Figure 3-63 demonstrates the shape changing behaviours of those double-layers established with elastic resin. As with the flexible samples, due to the uncontrolled proportions and highly water absorbent NVCL layers, elastic bilayers showed irregular changes in the water environment at room temperature. All types of bilayers folded after

2 hours due to excessive lateral forces as there was no restriction on the direction of swelling of the active layer. Notably, one of the 'a' type bilayer showed self-rolling behaviour after 6 hours. However, shedding still occurred on the samples and became worse as the active substance expanded in size. When the temperature increased, the desired behaviour did not manifest. Although the active layer did not detach extensively after water absorption, the appearance of all samples was almost identical to that of the samples at room temperature.



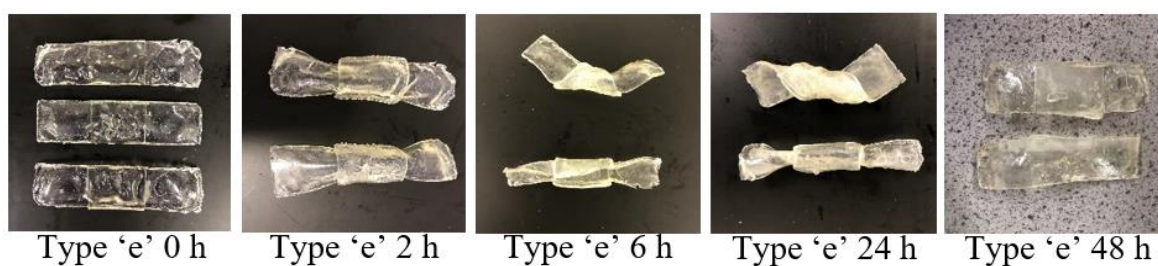


Figure 3-63 The appearances of the different types of elastic bilayer strips at the times: (L-R) 0 hour, 2 hours, 6 hours, 24 hours and 48 hours (oven).

In summary, the flexible and elastic bilayer structures were successfully prepared. Due to the characteristics of the flexible resin, the cured black layer blocks UV light and makes it difficult for the resin below to continue curing. In addition, the elastic resin has greater ductility than the flexible resin. When water is absorbed, the expanding active layer drives changes in the elastic layer, although these changes are irregular. As the designed moulds were unable to control the proportional relationship between the active and passive layers and the direction of expansion of the active layer, the shape change behaviour exhibited by the five strip samples did not fulfil expected responsiveness. Only one sample showed the expected shape change behaviour. Although this sample exhibited poor properties after the active layer reached swelling equilibrium, it did demonstrate the possibility of achieving shape change behaviour using a bilayer strip structure. Therefore, the elastic bilayer structure and the 'a' bilayer design were chosen to continue further shape change behaviour studies. In order to effectively control the direction and proportion of expansion, rectangular based strip structures were be designed.

3.4.4 The development of second-generation bilayer strips

The previous section described how the bilayer could only exhibit random shape change behaviour due to the lack of control over the expansion of the active layer. In order to maintain consistency and to allow shape changes to be reproduced, new strips were designed using the method described in section 2.8.2. Silicone moulds were made for the preparation of the new generation of bilayer structures. In order to control the ratio

between the passive and active layers, one end of these strips was designed in the form of a step. The NVCL solution was first pipetted into the silicone mould until the first step was filled and cured in the UV chamber for 10 minutes. The elastic resin was then poured over the top of the cured active layer and cured under UV light for a further 10 minutes. By using this method, the difference in thickness and ratio between the passive and active layers can be effectively controlled. Furthermore, in order to control the direction of expansion, the stepped side of the strip can be glued to a flat platform prior to immersion in water, so that the behaviour of the shape change can only occur from one side to the other, thus achieving a self-deformation behaviour.

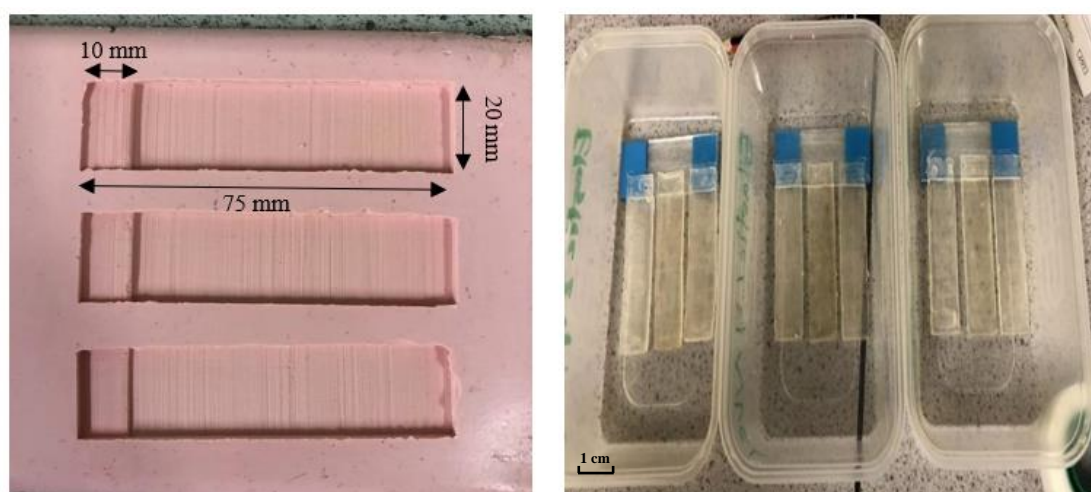


Figure 3-64 (L) *The second-generation silicone mould of strips* & (R) *The scheme of direction control for strips in water.*

The strip samples with ratio between the active and passive layers of 1:2, 1:1 and 2:1 are shown in **Figure 3-65**. All samples were successfully prepared with transparent appearances. All strips were flat. The active and passive layers adhere excellently to each other and the difference in thickness between the active and passive layers can be visually observed.



Figure 3-65 (L) *The thickness of proportioned strip samples & (R) the appearances of proportioned strip samples.*

3.4.5 Shape shifting behaviours detection of second-generation bilayer strips

The aim of this section was to investigate the effect of different proportions of strip on the self-rolling behaviour. In parallel, the possibility of achieving reproducibility of shape changes by controlling the direction and capacity of expansion was being investigated.

The expansion test of the double strips was carried out in triplicate. The stepped side of the strip was stuck to a smooth glass platform by double-sided tape prior to immersion in water. Due to the high density of the glass, it was able to sink to the bottom of the water, allowing the sample to remain fully submerged throughout the experiment. Furthermore, as the passive layer cannot swell in water, it ensures that the sample sticks tightly to the glass platform for the duration of the change. Although the ratio between the active and passive layers was effectively guaranteed, the three strips did not show the expected self-rolling behaviour. As the photographs show, all samples fell off the glass platform after two hours. This phenomenon may have occurred because the tape's adhesion was reduced by contact with water, which caused the strips to separate from the platform when the curling force was generated. It was also observed that, after 2 hours, almost all samples exhibited vertical folding behaviour instead of horizontal rolling. This may be due

to the superior swelling ability of the NVCL samples. Pulsatile testing was not performed on the samples because of the unsatisfactory behaviour of the shape shifting. However, it is worth noting that, after 24 hours, the force generated by the expansion of the active layer did not break the strip. Although the expected change in shape was not achieved, the samples ended up behaving in an almost consistent manner in water. In summary, for the next phase of the research, effective control of the size of the expansion may be a key factor in the successful production of predictable shape changes.

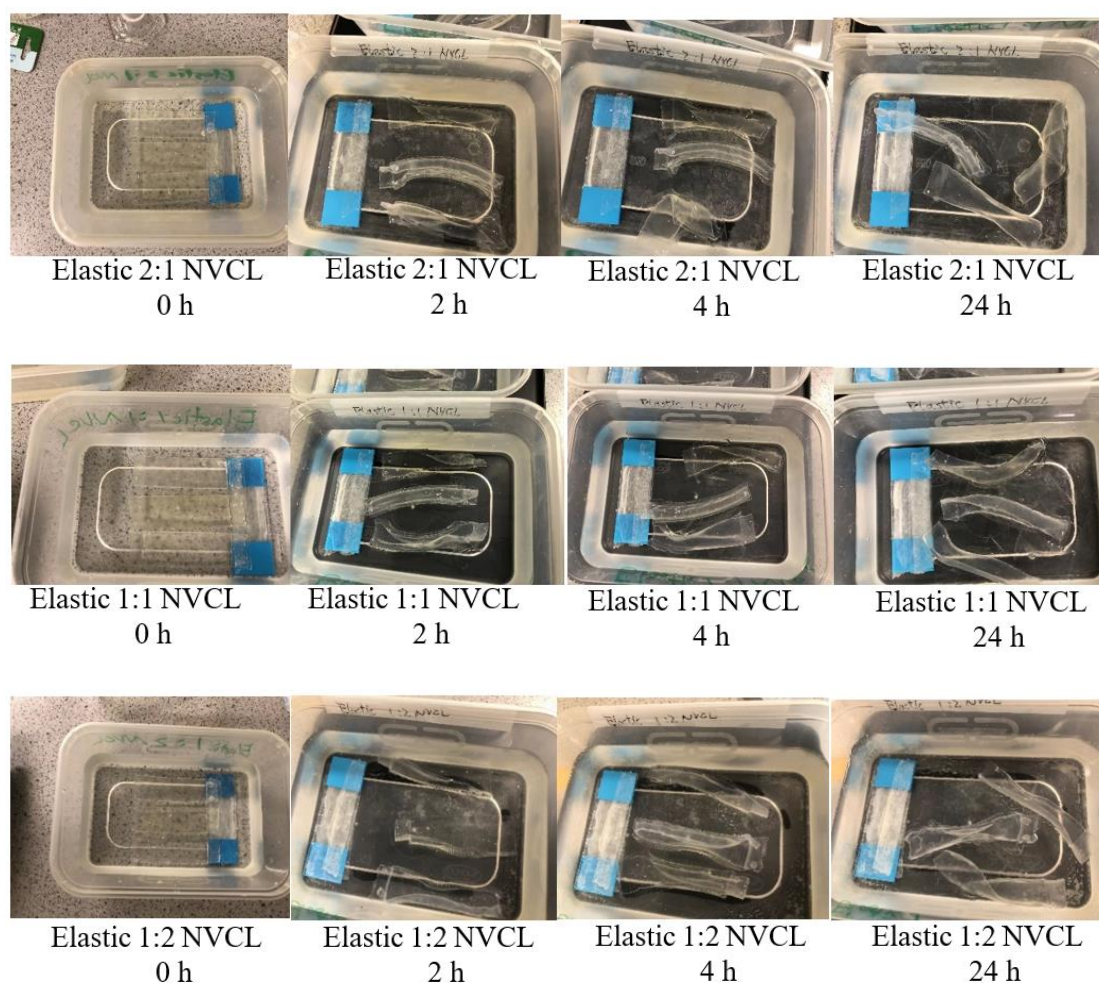


Figure 3-66 At room temperature, the appearances of swollen proportioned bilayer samples at the times: 0 hour, 2 hours, 4 hours and 24 hours.

3.4.6 The development of third-generation bilayer strips

The previous section described the making of the proportioned strips. Although the samples were able to show a consistent pattern of shape change, they did not follow

the intended pattern of change. This may be explained by the excessive expansion capacity of the active layer. Therefore, strips that can effectively control the expansion size were created in this section. The first scheme proposed to control the swelling rate was to modify the formulation used to prepare the active layer. The active layer of the strip was prepared according to the S7 formulation, which has a swelling ratio of 5 when it reaches equilibrium. Compared to other previously formulated formulations, S7 had the lowest swelling ratio and provides relatively good strength and appearance after water absorption. It has been reported in the literature that the swelling rate of samples can be reduced by increasing the amount of crosslinker (Iyer *et al.*, 2008), though this is not something that to undertake in the latter stages of a doctorate, An alternative model for controlling the swelling rate was to reduce the amount of the active layer. In a strip structure, the ratio, position and shape of the active and passive layers can be different. When a significant number of passive layers are combined with a limited number of active layers to form a bilayer structure, the force generated by water absorption and swelling is not sufficient to induce a change in the entire passive layer, thus controlling the swelling rate in another way. In addition, because the direction of the force applied has a strong influence on the final shape change behaviour, the third-generation strip models have been designed to be fully enclosed. The patterns of the third-generation strips are shown in section 2.7.3. The five types of strips were first created via 3D printer using high temperature resin. Using the same method, the silicone mould was prepared and used for new generation bilayer construction. The prototypes and silicone moulds of the five strips are shown in **Figure 3-67**. Even through the amount of active layer is reduced, the active layer of the five types was uniformly positioned on the strips. All the slots used to fill the NVCL solution have been designed to be rectangular. This may have a positive effect on the formation of a regular shape change behaviour.

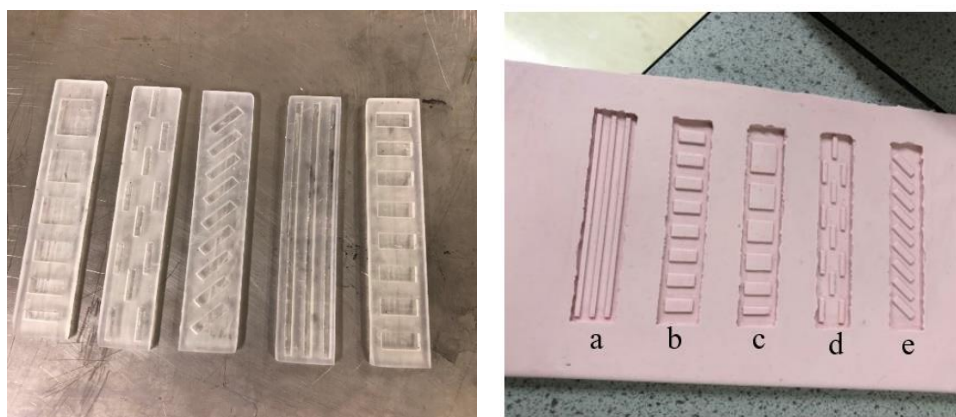


Figure 3-67 (L) The 3D printed strips & (R) The third-generation silicone mould of strips.

Unlike the previous double-layered structure, the elastic resin is first incorporated into the silicone mould. When curing was complete, the cured elastic resin forms a new mould. Subsequently, the prepared NVCL solution is incorporated into the space reserved by the elastic mould. It is important to note that, in order to ensure the quality of the double layer structure, the elastic resin needs to be added to the silicone mould in several stages during curing. This ensures that the shape and detail of each pattern can be reproduced. Furthermore, due to the ductility of the elastomeric resin, the cured elastomeric resin bends to one side, therefore it is necessary to use double-sided tape to attach the elastic mould to the platform in the UV chamber before incorporating the NVCL solution. The appearances of the third-generation photocured bilayer structures are demonstrated in **Figure 3-68**. All samples were successfully produced in the predefined manner. The surfaces of the strips were smooth and slightly yellow in appearance.

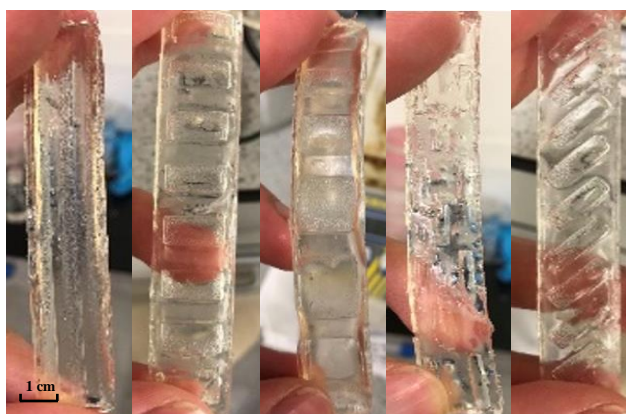


Figure 3-68 The appearances of third-generation bilayer strips.

3.4.7 Shape shifting behaviour detection of third-generation strips

The swelling tests on the double-layer structures was carried out in triplicate. The prepared strips were separately placed into large plastic trays to ensure that the samples could be fully submerged in water throughout the experiment. Almost all self-deformation behaviours developed for hydrogel-based materials exhibit a bending–unbending responsiveness (Li *et al.*, 2017; Zheng *et al.*, 2018; He *et al.*, 2019). The photographs in **Figure 3-69** below were taken at different times and show the shape change behaviour of the 'a' and 'd' type samples in water. For the type 'a' strips, although some samples showed the expected behaviour after 24 hours, consistency of the shape change was an issue. The two strips exhibited two different transformation modes. It was also noticeable that some of the active layers at the sides of the strips were damaged due to the large deformation at the ends of the strips. This may be attributed to the forces generated by the scaled active layer still being too strong, causing the strips to fold laterally rather than longitudinally. In contrast, all strips of type 'd' exhibited the predetermined changes. The orientation and angle of curvature of the samples at any given moment remained generally consistent. After 24 hours, when the expansion of the active layer reached its maximum size, the bilayer strips showed a less noticeable angle of deformation. Additionally, when the temperature was raised above the LCST, the deformed strips failed to return to a perfectly flat formation. This is because the active layer de-swells at high temperature, but the shrunken sample still retains a 200% expansion ratio, so that only a reduction in the bending angle can be observed in the samples.

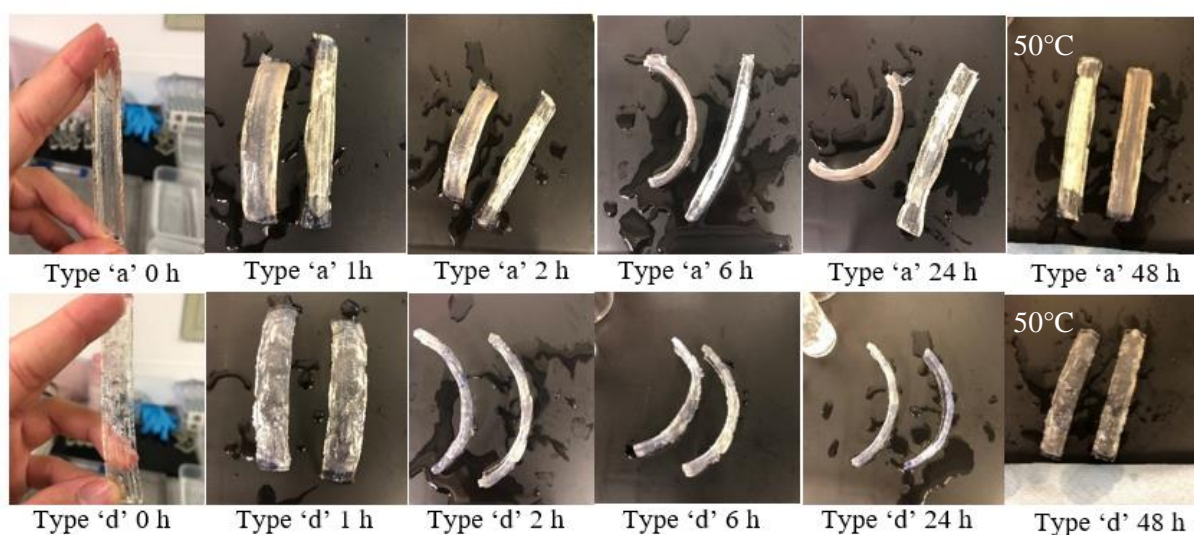


Figure 3-69 The appearances of swollen type 'a' and 'd' bilayer samples at the times (L-R): 0 hour; 1 hour; 2 hours; 6 hours; 24 hours and 48 hours (50°C).

Comparing with the types 'a' and 'd' samples, by specifying and limiting the direction and volume of the expansion, the samples of types 'b', 'c' and 'd' exhibited the better repeatable shape change behaviours as the temperature increased and decreased. The responsiveness of the shape changing has been approved in at least three cycles of the testing, as shown in **Figure 3-70**. The bending behaviour is reflected in the variation of the distance between the two sides of the strip. At room temperature, the type 'b' flat strips started to bend, resulting in a reduction of the distance between the two ends from 85 mm (length of the strip) to about 26 mm. After 6 hours of immersion, the distance reduced to around 5 mm. When the active layers reached equilibrium state, the flat strips were able to curve to a loop (0–2 mm). As the temperature rose to 50 °C, the active layers shrank to a relatively small expansion size, thus reducing the bending angle of the bilayer strips. Due to the fact that the active layer remains in an expanded state, samples cannot fully recover to their original shape. After 48 h immersed at 50 °C (which is shown at 72 hours in the **Figure 3-70**), the distance between the two sides increased to about 48 mm. After 144 hours, when the temperature returned to room temperature, the increased water absorption capacity of the active layer allowed for a second increase in the bending of the bilayer strip

(the distance between the two sides reduces to 2–5 mm). In the bending process, it is worth noting that the hydrogel layer did not separate from the passive layer during the entire pulsatile swelling test, which indicates the integrity and consistency of the shape change behaviour.

The rectangular design on the ‘c’ strip is progressively increasing in size. Different areas of the active layer can exert different forces on the passive layer so self-rolling behaviour was expected to be achieved in water. At room temperature, the strip started to curl due to the expansion of the active layer. However, the ‘c’ type strip failed to achieve the expected responsiveness; instead, it showed similar bending behaviour to the ‘b’ type as the water absorption increased. This may be due to the fact that the active layer does not generate enough force to produce a greater degree of curling in the strip. In the subsequent heating/cooling cycles, the strip exhibited a consistent change in the degree of bending. In the case of type ‘e’ strips, the active layer was designed at an angle of 45 degrees, which was expected to induce the bilayer strips to helix in the 45° direction. As can be seen in the images, type ‘e’ showed a different level of responsiveness than type ‘b’ and ‘c’ samples. At room temperature, though no helical structure is formed, the ‘e’ strip shows a nearly 90° folded posture when the NVCL layer is fully expanded. As the temperature increased to 50°C, the strips reverted to a slightly bent state. The manifestation of this responsiveness offers the possibility of using such hydrogel materials to develop behaviours that are distinct from bending–unbending.

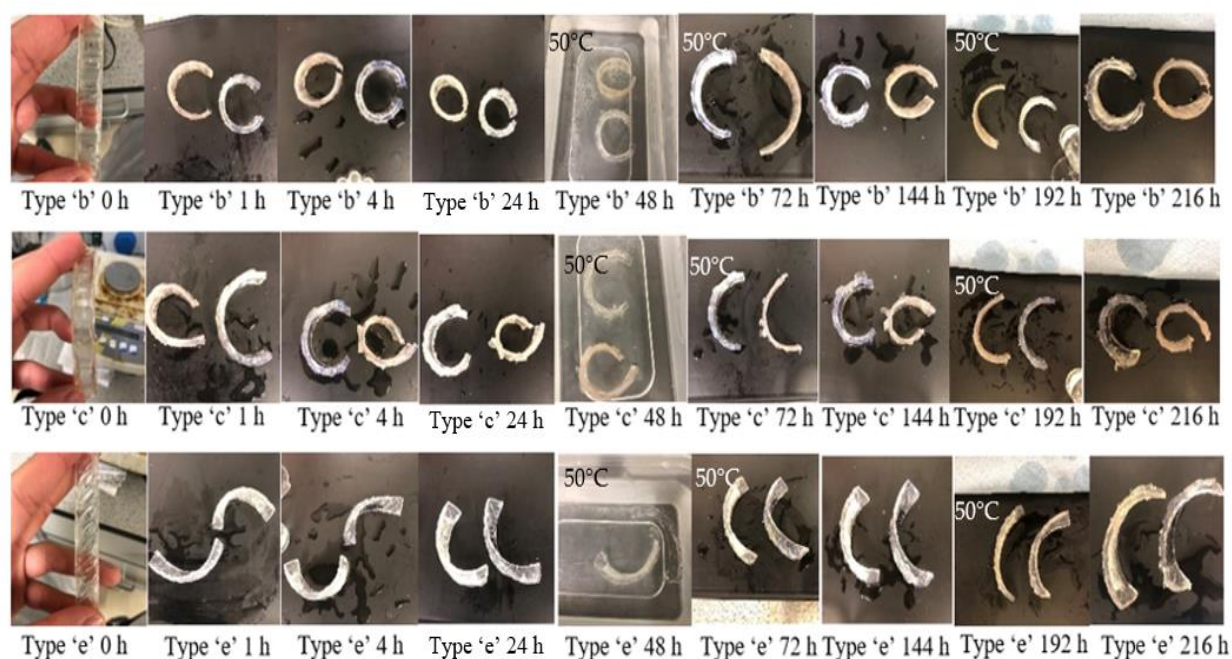


Figure 3-70 The appearances of swollen type 'b', 'c' and 'e' bilayer samples at the times: 0 hour; 1 hour; 4 hours; 24 hours; 48 hours (Oven); 72 hours (Oven); 144 hours; 192 hours (Oven) and 216 hours.

In summary, the idea of creating bilayers was proposed, to allow NVCL smart hydrogels to exhibit different changes in addition to simple dimensional changes. By combining it with an elastic material, simple bilayer strip samples were produced. After these strips had been submerged in water, the active layer prepared by NVCL began to swell. Due to the connection with the elastic layer, the forces generated by the swelling acted and applied to the passive layer, resulting in a different way of changing shape. As a result, five types of bilayer strips were successfully prepared. All samples were able to show transformation behaviour. However, these types of bilayers were difficult to apply in practice due to the following reasons: inconsistent change behaviour (type 'a'), inconspicuous change behaviour (type 'd') and unfinished expected changes (type 'c'). Only the type 'b' and 'e' strips demonstrated the predetermined shape-shifting behaviours. Although the strips were unable to return to their original shape as the temperature rose above LCST, the apparent angular changes throughout the expansion tests demonstrated

the intelligence and value of these strips. Based on the success of the strip models, the next section of this study will attempt to prepare the bilayer structure of the flower models.

3.4.8 The development of bilayer flowers

In order to further examine the feasibility of the bilayer structure, flower shaped samples were prepared. In Section 3.3, the flower shaped NVCL-based hydrogels demonstrated an excellent swelling capacity, which provided the rationale for the preparation of bilayer structures. From the previous bilayer strip models, it can be concluded that the swelling direction of the active layer and the proportional relationship between the active and passive layers all have a significant influence on achieving the desired shape transformation behaviour. The bilayer flower structure created in this section is intended to mimic the flowering process in nature so that a self-curving behaviour is expected to be achieved. As described previously, the flower model was printed on a 3D printer at a thickness of 3 mm. In order to have the same thickness for the passive and active layers, another model with a thickness of 1.5 mm was also prepared. A silicone mould was then produced using the two flowers as models, as is shown in **Figure 3-71**. A silicone mould was then produced using the two flowers as models. The two-layer flower structures were constructed by dropping a prepared NVCL solution into a 1.5 mm thick silicone mould, before being placed in the UV chamber system. In the presence of UV light, the S7 solution was cured. The cured active layer was then placed in the bottom of the 3 mm mould. After that, the elastic resin is pipetted on the top of the active layer until the 3 mm mould was full. This effectively ensured the thickness ratio between the active and passive layers.

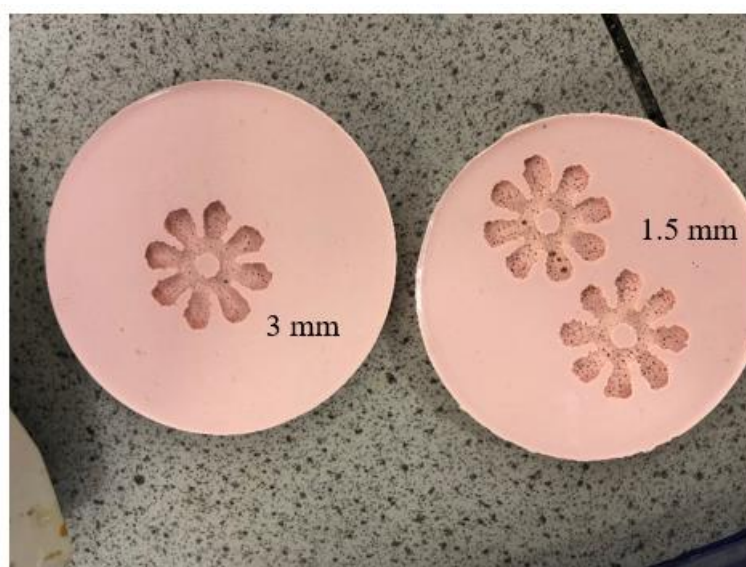


Figure 3-71 The 1.5 mm and 3 mm flower shaped silicone mould.

The bilayer flower samples with a ratio of 1:1 between the active and passive layers were prepared and are shown in **Figure 3-72**. All flower samples were successfully prepared with flat and transparent appearances. The surface of the flower samples was smooth. In addition, the shape and integrity of the ‘petals’ were perfectly maintained. The passive layer was accurately constructed on the top of the active layer, which gives an assurance for the deformation behaviour.

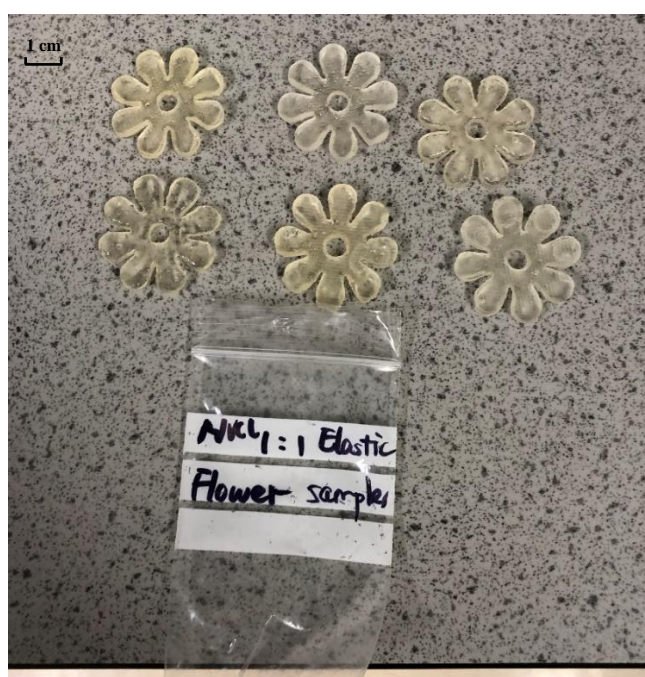


Figure 3-72 The appearances of bilayer flower samples.

3.4.9 Shape shifting behaviours of bilayer flowers

The pulsatile swelling tests were carried out on bilayer flower samples. The dry and flat samples were placed in a large container at 0 hour to ensure there was sufficient water for deformation throughout the experiment. As demonstrated in **Figure 3-73**, at room temperature, the fully opened ‘flowers’ started to curve due to water absorption. The angle of the curve of the ‘flower’ increased as the rate of water absorption increased. After 6 hours, the flower samples closed completely. The self-curving behaviour was displayed. However, as the active layer continued to swell to its equilibrium state, the passive layer was unable to withstand the curving forces generated by the active layer, resulting in damage to the sample. Therefore, the closed flowers were placed at 50 °C after 6 hours, which prevented the swelling rate from increasing. This operation yielded excellent results. After 20 hours, the completely closed flowers were reopened due to the contraction of the active layer. In the subsequent warming and cooling transitions, the double-layered flower samples showed the expected opening and closing process, which successfully simulated the flowering process in nature.

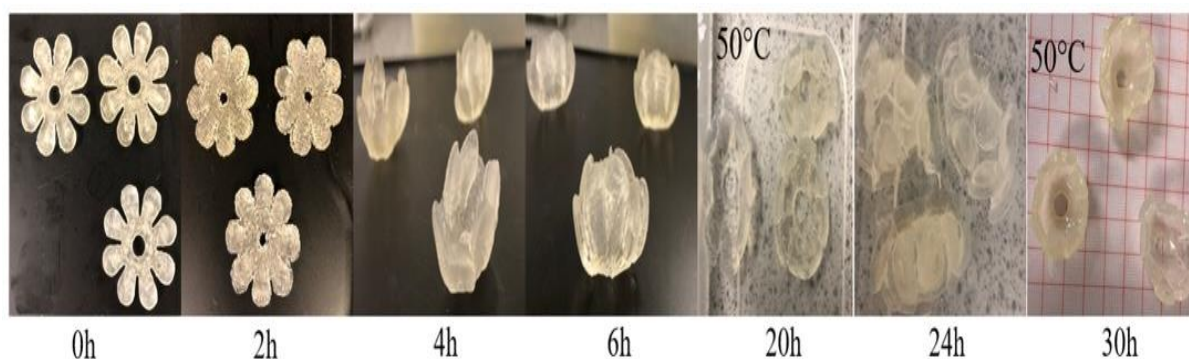


Figure 3-73 The appearance of swollen bilayer flowers samples at the time (L to R): 0 hours, 2 hours, 4 hours, 6 hours, 20 hours (14 hours in oven), 24 hours, 30 hours (6 hours in oven).

In summary, by combining NVCL with an elastic material, simple bilayer strip samples were produced. All samples were able to show transformation behaviour. However, Only the type ‘b’ and ‘e’ strips demonstrated acceptable reproducible

shapeshifting behaviours. Although the strips were unable to return to their original shape as the temperature rises, the apparent angular changes throughout the expansion tests demonstrated the intelligence and potential value of these strips. For the bilayer flower structures, by limiting the expansion time at room temperature, the flower samples prepared in this contribution exhibited predictable and reversible shapeshifting behaviour.

3.4.10 Demonstration I: TUS Demonstration

The bilayer structures produced in this study show promising shapeshifting behaviours. This provides the opportunity to develop practical applications using the bilayer structures.

As shown in **Figure 3-74**, the first application developed in this section was the TUS automatic displayer. At room temperature, it can be observed that the strips exhibit a certain degree of natural bending in water at the beginning of the swelling. This may be caused by the buoyancy of the water. After 24 h, when the active layer of the strips swelled to its maximum size, the double-layered strips underwent a self-bending behaviour, causing the “AIT”, “TUS” and “LIT” symbols to be displayed on the front of the container. When the temperature increased to 50 °C, the active layer of the strip shrunk, leading to a decrease in the expansion volume. Therefore, a decrease in the bending angle of the bilayer strip can be observed. This resulted in the three sets of letters lifting backwards and not being fully presented on the front side of the container. As the temperature returns to ambient, the “AIT”, “TUS” and “LIT” symbols are again displayed on the front side due to the increase of the water uptake. These performances marked the successful development of the automatic demonstration concept, though further finetuning could be carried out in the future to further improve consistency of the system.

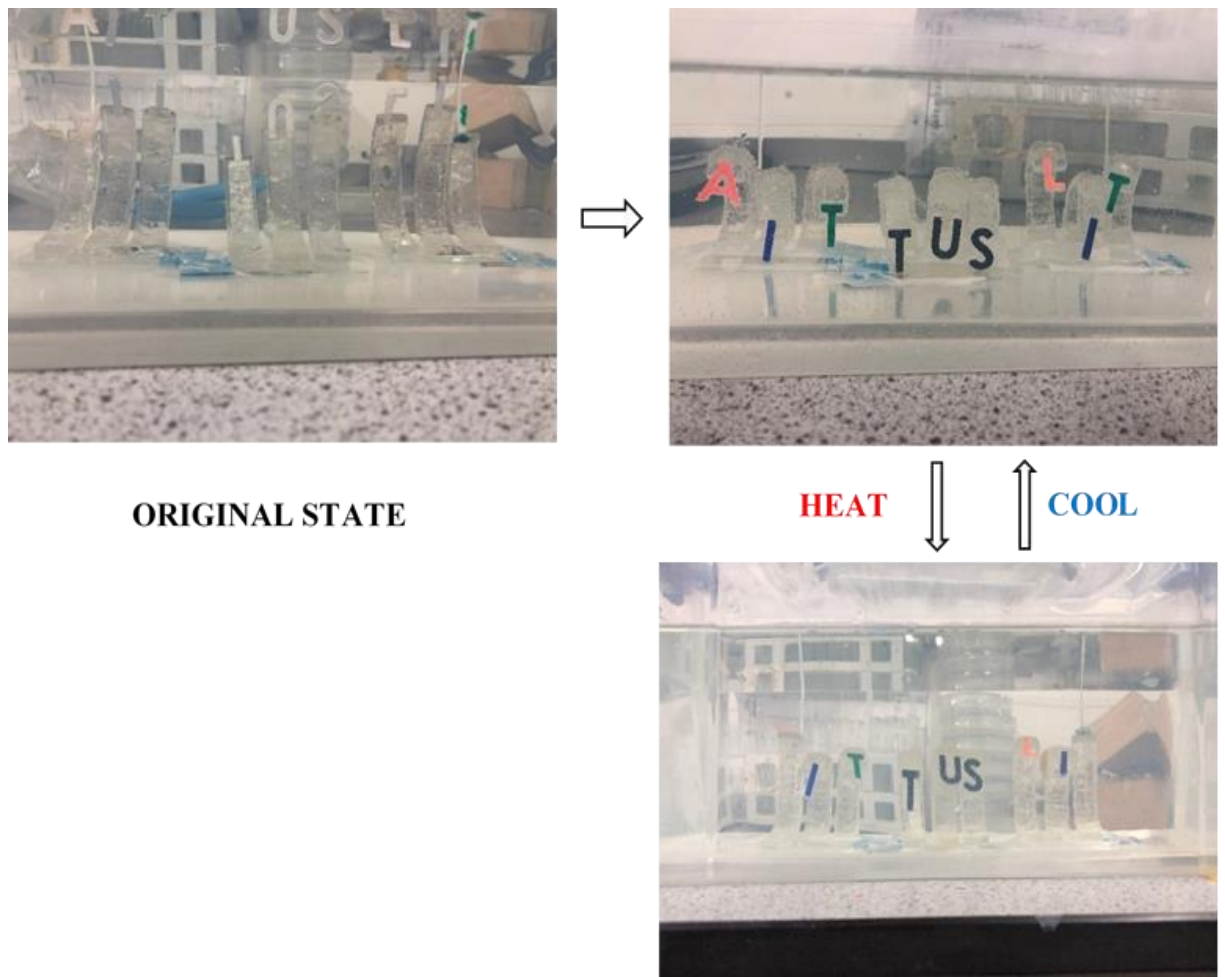


Figure 3-74 The TUS automatic displayers achieved by using self-curving strips.

3.4.11 Demonstration development II: Toy train puller

As shown in **Figure 3-75**, the second demonstrator developed in this section was a toy train puller. At room temperature, it can be observed that the rope was loose in the absence of tension at the beginning of the swelling. The train stopped at 0 cm. As the active layer expands, the self-curving behaviour occurred, thus driving the rope to pull the train. After 24 h, the active layer expanded to its equilibrium state, which resulted in a maximum bending angle of the bilayer strip. This generated a tension force acting on the rope and propelling the train forward. At maximum expansion state, the train was pulled forward to 10 cm. These performances illustrated the successful development of the automatic puller.

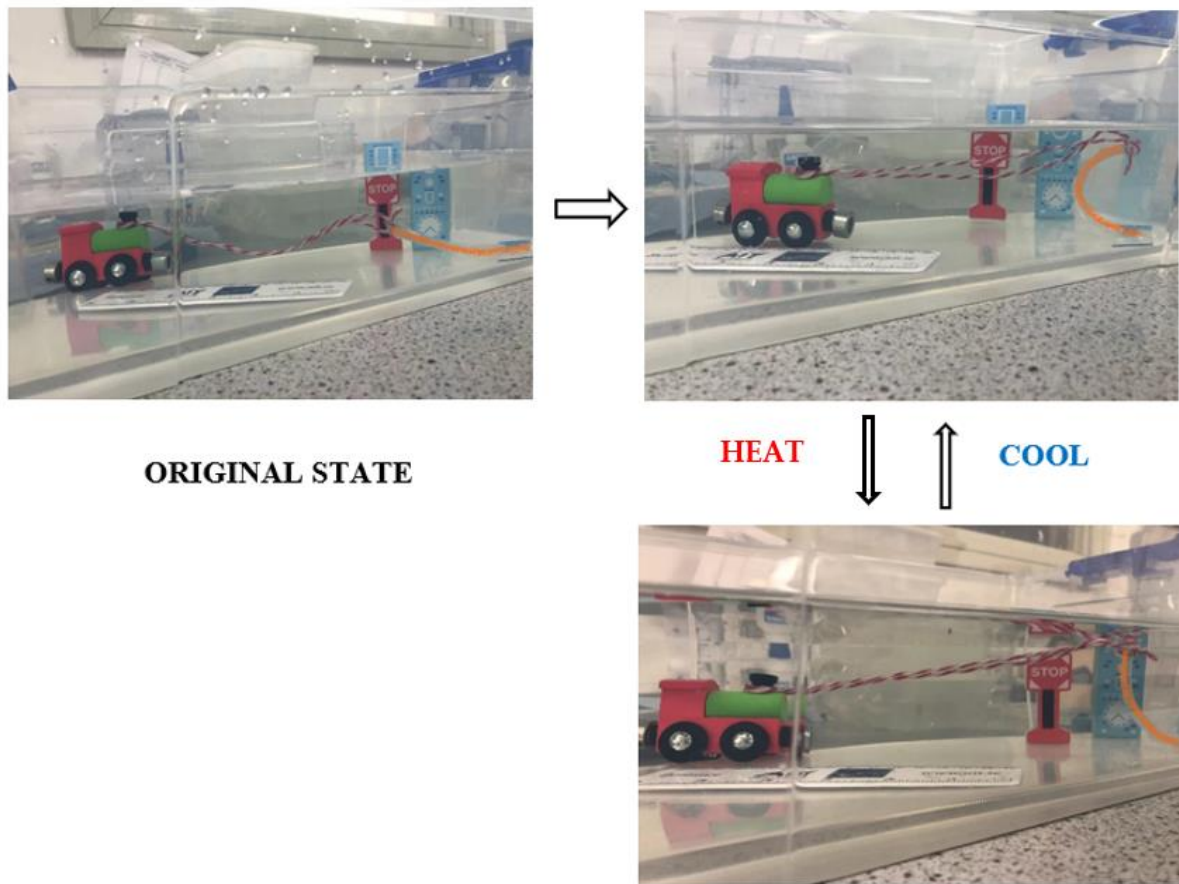


Figure 3-75 The toy train automatic puller achieved by using self-curving strips.

3.4.12 Demonstration development III: Gripper

As shown in **Figure 3-76**, the third application developed in this section was a flower-shaped gripper. At the beginning of the experiment, the bilayer flower was fully opened at the top of the bolt. At room temperature, as the active layer expanded, the ‘petals’ began to bend inward and wrap around the bolt. After 6 h, it was observed that the bolt was wrapped in the petals and could easily grip the bolt. This phenomenon is attributed to the force provided by the water absorption of the active layer, which allowed the petals to close completely. When the temperature was raised to 50 °C, the bolt was released. This was due to the fact that the active layer of the bilayer structure started to shrink, resulting in a reduction in the curvature of the petals. The open petals do not provide enough support to grip the bolt. When the temperature dropped back down to ambient temperature, the angle of the bilayer flower bend increased again and the bolt was again gripped.

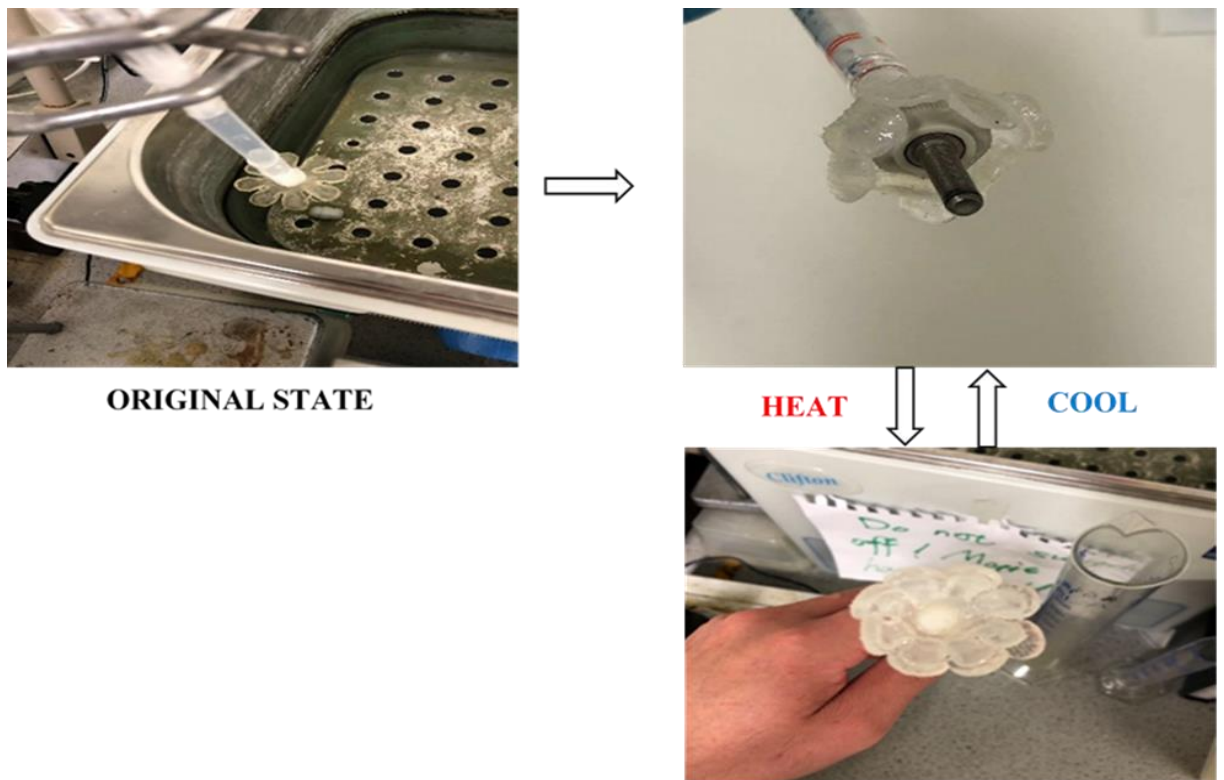


Figure 3-76 *The flower gripper achieved by using bilayer self-curving flowers.*

3.4.13 Summary

In this section, a novel method of constructing bilayer structures has been developed. By combining the NVCL-based polymers and elastic resin, the bilayer strip and flower structures were successfully manufactured via a UV chamber system. In order to achieve the shape shifting behaviours, the appearances and patterns of the samples were continually modified and updated. Finally, by controlling the ratio and amount of active and passive layers and limiting the expansion direction of the active layer, the created strip and flower samples successfully exhibited predictable and reversible shape shifting behaviours. Based on the success of the deformation behaviour of the bilayer structure, three simple and practical demonstrators have been developed for this study.

In terms of strip samples, third generation double-layer strips exhibited controlled self-bending behaviour. By using this type of strip, an automatic demonstrator has been developed. In the presence of water, the TUS letters can appear and disappear on the front side as the temperature rises and falls. Furthermore, a mechanism for pulling a wooden toy locomotive was also made from this strip. As the temperature increases and decreases, the locomotive can be pulled forward and pushed back in the water. In terms of the flower samples, the expected self-curving behaviour has been achieved, which provides the opportunity to develop a gripper using a double layer flower model. As the temperature climbs and drops, a bolt on the bottom of the water was able to be gripped and released, flexibly. These operations not only open up new applications for medical NVCL materials, but also provide a simple and fast method for the preparation of 4D materials.

Chapter 4:

Conclusion & Future work

4 Conclusion and Future work

4.1 Conclusion

The major objective of this research was to achieve advanced 4D printing technology by using temperature-sensitive based polymers. Following a thorough review of the literature, NVCL temperature responsive polymer was chosen. Firstly, it was essential to characterise the polymer and evaluate how the sample reacted with the inclusion of different photoinitiators. Based on the wavelength range of the UV chamber system and 3D printer, three types of photoinitiators were selected to prepare the physically crosslinked PNVCL homopolymers with different feed ratios by photopolymerisation. In a comparison of the homopolymers, all of the Irgacure 2959 samples were transparent and glass-like in appearance after the curing process. However, as the NVCL blended with VA-086 and CQ, the samples could not be cured properly under the UV irradiation. The phase transition temperature of physically crosslinked gels was determined by cloud-point measurement, DSC, UV-spectroscopy and rheology. The 10 wt% and 5 wt% aqueous solutions were prepared. The results illustrated that the greater the concentration of PNVCL in solution, the higher the LCST achieved. In order to possess the lowest cytotoxic potential in the same group sample, **0.1 wt%** was considered for use in the preparation of temperature-sensitive chemically crosslinked hydrogels. The chemically crosslinked hydrogels are able to reach equilibrium swelling ratios at room temperature and shrink at temperatures above their critical temperatures. This capability can be regarded as 4D behaviour. Therefore, in order to attain samples with good water absorption, a chemical crosslinker PEGDMA was used to mix with NVCL at different concentrations. The FTIR spectra of the homopolymers showed the C=C peak disappeared after photopolymerisation, indicating that the NVCL successfully polymerised. The swelling ratios and appearance of the hydrogels were affected by altering the amount of

crosslink agent employed during polymerisation. The chemically crosslinked xerogels which were prepared using **0.1 wt% Irgacure 2959** photoinitiator and **2 wt% PEGDMA** crosslinker exhibited promising water absorption capabilities. However, the samples became soft and flaccid after expansion, which resulted in the structural integrity and disc shape of the sample being easily damaged.

In an effort to further optimise and improve the temperature-responsive properties, using the same method of synthesis as for the homopolymers (UV chamber polymerisation), a series of copolymers comprising NVP or DMAAm and terpolymers comprising of NVP/DMAAm and NVP/NIPAAm at different monomeric feed ratios were fabricated. Similar analytical techniques used in the characterisation of the homopolymers were again utilised in the study of these copolymers and terpolymers. The structural analysis of hydrogels using FTIR again confirmed the presence and polymerisation of the monomers and formation of random copolymers and terpolymers. Alternating the feed ratio of the monomers, using the hydrophilic NVP or DMAAm and hydrophobic NIPAAm resulted in copolymers and terpolymers with distinctive phase transition temperatures. The phase transition temperatures of those samples were again determined by cloud-point measurement, DSC, UV-spectroscopy and rheology. Increases in the feed ratio of the hydrophilic monomer had a significant influence on the LCST which can even be increased to 50 degrees Celsius. The hydrophilicity of hydrogels was analysed by goniometry. The swelling capacities and the thermosensitivity of the hydrogels were examined through pulsatile swelling studies. The copolymer and terpolymer samples were able to respond to temperature pulses across their critical temperatures, showing reversible swelling and deswelling behaviour in distilled water media. However, only the hydrogels which were created using **0.1 wt% Irgacure 2959**, **2 wt% PEGDMA**, **30 wt% DMAAm** and **70 wt% NVCL** were able to maintain their shape and structural integrity. Those hydrogels showed a relatively fast reaction time, suitable swelling and mechanical

properties at both low and high temperatures. The improvement of the mechanical properties was validated by tensile tests. The outstanding reversible swelling properties suggested there was the possibility of changing final shape and applying such a formulation to a 4D printing technique.

In order to further investigate the 4D printing feasibility of preparing a formulation for 4D printing, more complex shaped jigsaw and flower hydrogels were synthesised via UV chamber with candidate formulations. The jigsaw and flower samples showed the same behaviour as the disc samples which were transparent and glass-like in appearance after the curing process. Pulsatile swelling studies showed that these hydrogels were able to respond to temperature pulses across their critical temperatures, showing reversible swelling and deswelling behaviour in water media as disc hydrogels. The hydrogels again attained high equilibrium swelling ratios at room temperature and shrunk at temperatures above their LCSTs. However, when the formulation was made into a resin for use in the Form 2 3D printer, the designed parts failed to construct. Comparing the differences between the SLA and UV chamber, the reason why the homemade resin was unprintable could have been that the amount of photoinitiator in the formulation was low and insufficient to cure the resin with the low intensity UV provided by the printer. Therefore, the candidate formulation had to be modified. A review of the literature showed that H-Nu 400IL photoinitiator possesses a high UV photosensitivity. By increasing the concentration of photoinitiator, optimising the layout of printed objects (deleting the support structures) and increasing the amount of resin content, the 4D objects were ultimately created using **2 wt% H-Nu 400IL**, **2 wt% PEGDMA**, **30 wt% DMAAm** and **70 wt% NVCL**. The 3D prints exhibited an excellent appearance and were able to respond to temperature pulses across their critical temperatures, showing intelligent and reversible swelling/deswelling behaviour in water media. The effects on material properties of NVCL samples prepared via stereolithography and UV chamber polymerisation were also

investigated. When viewing the chemical structures and phase transition temperature, there was no significant difference between those samples.

For the purpose of developing new shape transition behaviours with hydrogel-based polymers, bilayer structures were introduced. By overlaying a layer of cured NVCL polymer on the commercial elastic resin, the bilayer structures were fabricated. The NVCL layer can be regarded as the active layer, and elastic material as the passive layer. Once triggered by the activation stimulus, the deformation generated on the active layer spurs the passive change, leading to the change in dimensions and curvature. The bilayer strips and flowers were constructed via UV chamber system. By controlling the ratio and amount of active and passive layers and limiting the expansion direction of the active layer, the shape-shifting behaviours were implemented and a series of demonstrator produced.

In terms of strip samples, third generation double-layer strips exhibited controlled self-bending behaviour. By using the 'b' type of strips, an automatic demonstrator was developed. In the presence of water, the TUS letters can appear and disappear on the front side as the temperature rises and falls. Furthermore, a system for pulling a wooden toy locomotive was also made from this strip. As the temperature increases and decreases, the locomotive can be automatically pulled forward and pushed back in water. In terms of the flower samples, the expected self-curving behaviour was achieved, which provided the opportunity to develop a gripper using a double layer flower model. As the temperature climbed and then dropped, a bolt at the bottom of the water was able to be gripped and then released flexibly. Although other researchers have developed bilayer structures and complex deformation mechanisms, none have used NVCL based polymers and developed it in a UV chamber system. The findings of this study not only open up new potential applications (such as thermosensitive electrical components, actuators and toys) for medical NVCL materials, but also provide a simple and fast method for the preparation of 4D materials.

4.2 Future Works

The findings in this thesis have comprehensively addressed the primary goals of this project, but there are a number of emerging areas worthy of further examination:

1. The NVCL formulation used to fabricate bilayer structures has a high swelling ratio at room temperature, resulting in damage to the sample as it expands to its maximum size. Future studies can look at optimising this. The swelling rate of the hydrogel could be adjusted with the addition of other additives or by increasing the proportion of crosslinker feed, so that the NVCL polymer can more easily develop more complex deformation behaviours.
2. The changes of 4D printed objects developed in this study can only be displayed in an aqueous medium. In some cases, it is inconvenient to apply this 4D part. Therefore, the exploitation of 4D printing technology through the use of other temperatures or stimuli (such as PH and magnetic etc.) responsive polymers to develop a more sophisticated 4D printing technique could be the focus of future work.
3. The shape shifting behaviours have been successfully achieved. There are many other intelligent behaviours that could be developed in relation to NVCL-based polymers. For example, it may be possible to achieve deformation behaviour in a single hydrogel sample by curing different parts of the same sample under different intensities of UV light. In addition, there are no reports in the literature describing the incorporation of colour change ink or pigment with the stimuli-responsive polymers. The commercial colour change powders are able to change their colour following an environmental change, such as light, temperature or PH. The idea is to synthesise multi-stimuli-responsive polymers that can change their colour and shape to meet various requirements.

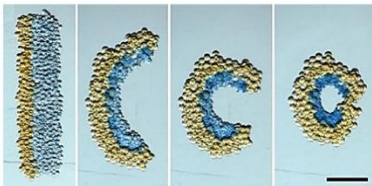

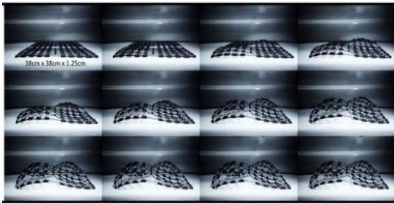
Chapter 5:

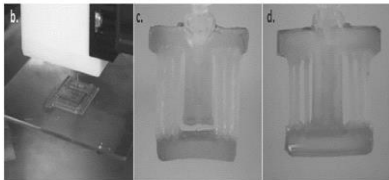
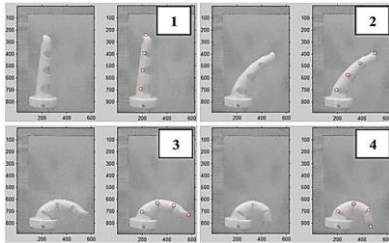
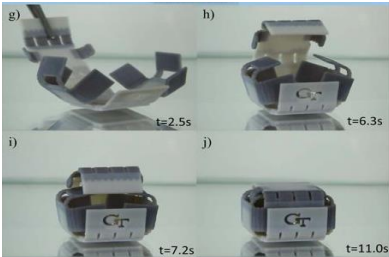
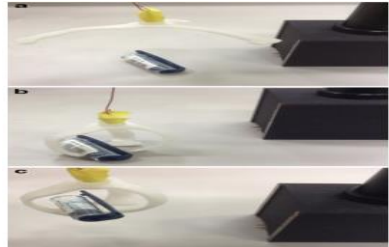
Appendices

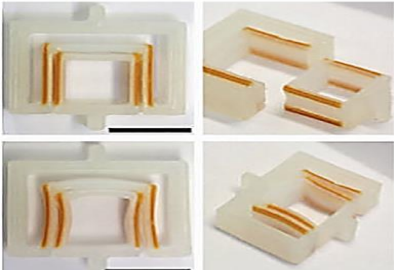
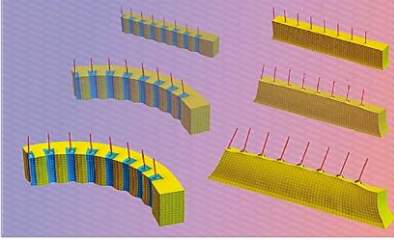
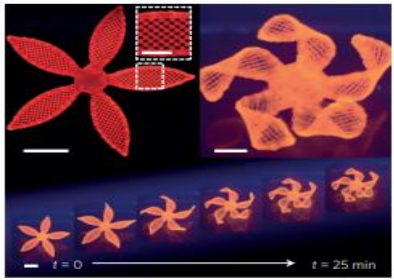
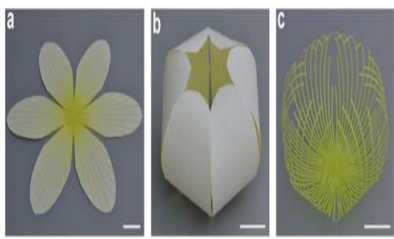
5 Appendices

5.1 Appendix A-Literature Supplement

Summary of the application of 4D printing existing in literature

Material(s)	Stimuli	Reaction time	Printing method	Prototype developed	Function	Reference
Aqueous droplet	Osmosis	Not Mention	Not Mention		Rectangular to circle (tissue engineering)	(Villar <i>et al.</i> 2013)
Rigid and active material	Water	0, 30mins, 24hrs	Multi-material 3D printer		Morph change	(Tibbits <i>et al.</i> , 2014)
Vinyl Caprolatam, PE, Epoxy diacrylate oligomer, Irgacure 819	Water	Not mention	Multi-material 3D printer		Surface curling	(Raviv <i>et al.</i> , 2014)

Alginate/PNIPAAm	Heat and water	1 min	3D-bioplotter		Actuators	(Bakarich <i>et al.</i> , 2015)
Thermoplastic elastomer(TPE)	force	Immediately	FDM		Prosthetic finger	(Mutlu <i>et al.</i> , 2015)
Tangoblack+, Verowhite	Heat	11s	Multi-material 3D printer		Self-lock/3D fold	(Y. Mao <i>et al.</i> , 2015)
SMP PU	Heat	Not mention	FDM		Gripper	(Yang <i>et al.</i> , 2016)

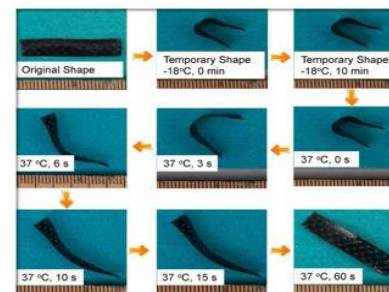
PUA oligomer	magnetic	Not mention	bioprinter		Key-lock connectors	(Kokkinis <i>et al.</i> , 2015)
PNIPAAm/spiro benzopyran (SP)	Heat and light	about 4h	Not mention		Mimic the contraction	(Kuksenok & Balazs, 2016)
Nanoclay, Irgacure 2959, NIPAAm, glucose oxidase, NFC	DI Water	25mins	SLA		Flower closing/opening	(Sydney Gladman <i>et al.</i> , 2016)
Polylactic acid (PLA) Filament	Heat	Not mention	FDM		Morph change	(Zhang & Hu, 2016)

acetone/soybean oil epoxidized acrylate/Irgacure 819

Heat

60s

SLA



Soy scaffolds bending

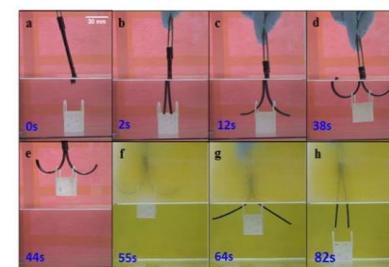
(Miao *et al.*, 2016)

Tangoblack+, Verowhite

Heat

0,2s,12s,38s
0,11s,20s,38s

Multi-material 3D printer



Smart hook

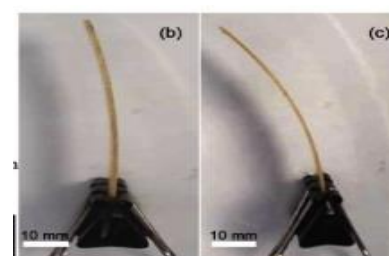
(Jiangtao Wu *et al.*, 2016)

PLA and PHA wood fibre

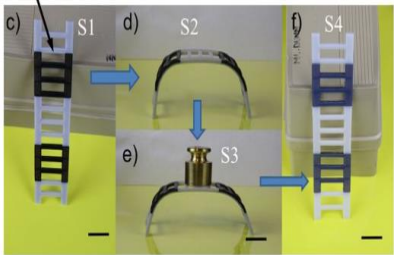
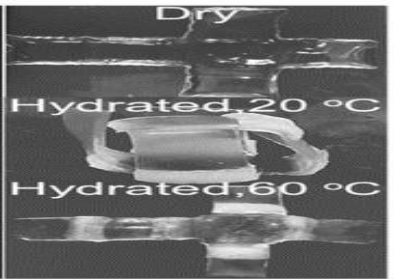
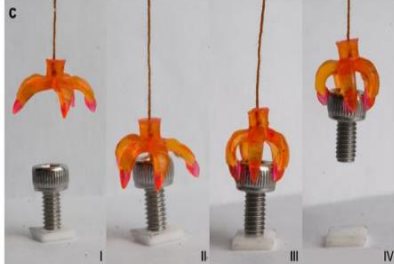
moisture

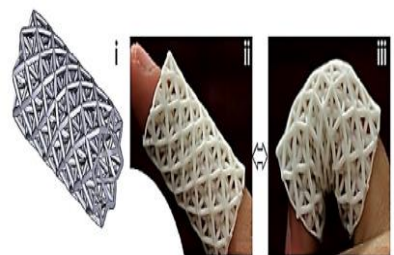
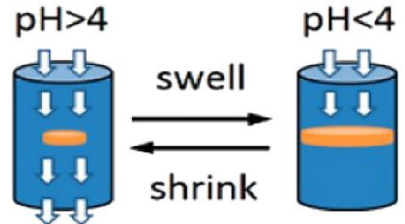
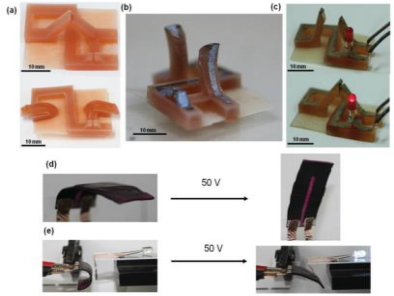
Not mention

FDM



(Le Duigou *et al.*, 2016)
Morph change

Tangoblack+, Verowhite	Heat	10s	Multi-material 3D printer		(Mao <i>et al.</i> , 2016) Load-bearing
PNIPAAm/PHEMA/PEO-PU/BIS	Heat and Water	Not mention	SLA		Fold (Naficy <i>et al.</i> , 2016)
Benzyl methacrylate(BMA)/PEGDMA/BPA/DEGDMA	Heat	around 20 mins	SLA		Gripper (Ge <i>et al.</i> , 2016)

DMAAm/PVP/Methacrylic acid/Methacrylic anhydride	Force	Immediately	micro SLA		(Y. Jiang & Wang, 2016) Twisting & bending
P2VP/ABS	PH	Not mention	FDM		Regulate the flow rate (Nadgorny <i>et al.</i> , 2016)
methacrylate polycaprolactone	Heat and Voltage	14s	SLA		(Zarek <i>et al.</i> , 2016) Power connected

tBA/DEGDA/BA PO	Heat	11s	SLA		Morph change	(Choong <i>et al.</i> , 2017)
SMPs PU filaments	Heat	Not mention	FDM		Self-folding	(Bodaghi <i>et al.</i> , 2017)
PUA/DGEDA/IB OA/Irgacure 184	Water	12s	SLA		Morph change	(T. Zhao <i>et al.</i> , 2018)

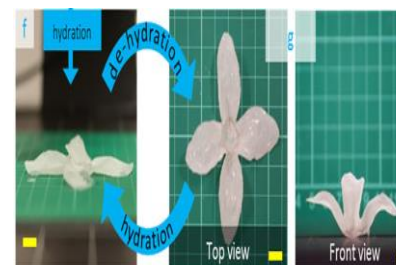
PCLDMA/BASF	Heat	5 min	SLA		Self-repair	(Invernizzi <i>et al.</i> , 2018)
PA66/carbon fibre	Heat	Not mention	fibre and resin printer		Deformation, self-morphing	(Q. Wang <i>et al.</i> , 2018)
PS film	Heat/photo	about 5s	Not mention		Actuators	(Zolfaghari <i>an et al.</i> , 2018)

Composites/clay/
CMC

Water

Not mention

FDM



Morph
change

(Mulakkal
et al., 2018)

5.2 Appendix B –Experimental Figures and Tables

5.2.1 DSC results

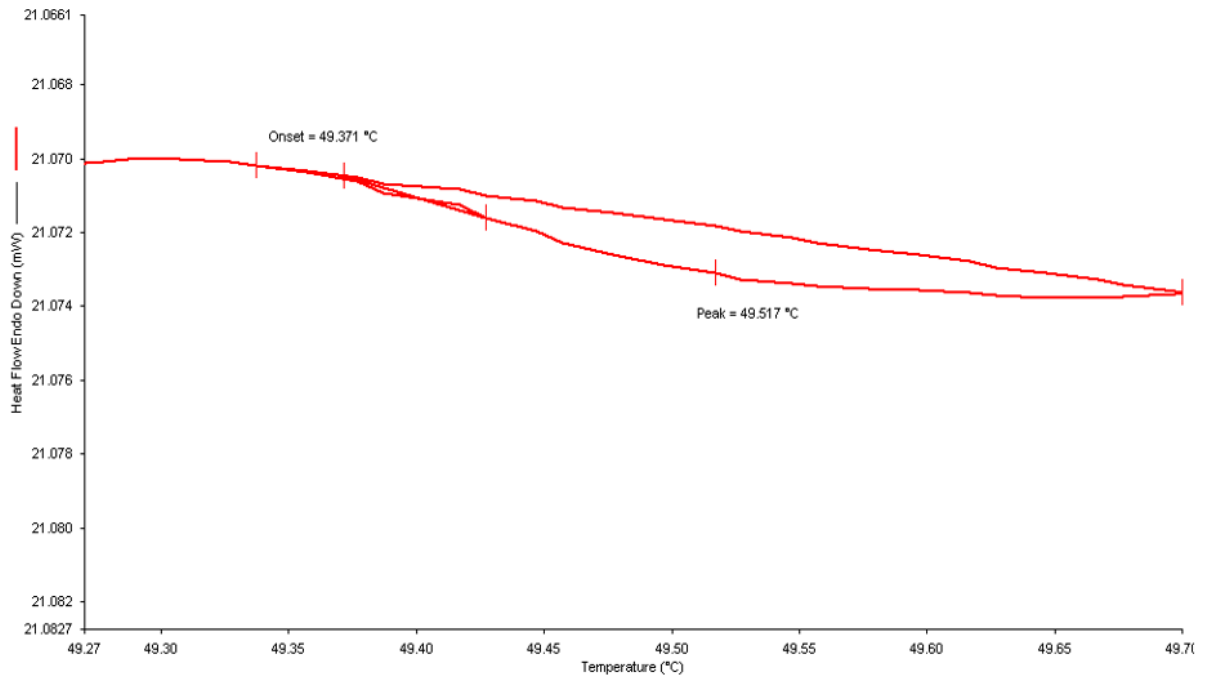


Figure 5-1 DSC graph of S1 PNVCCL based polymer sample.

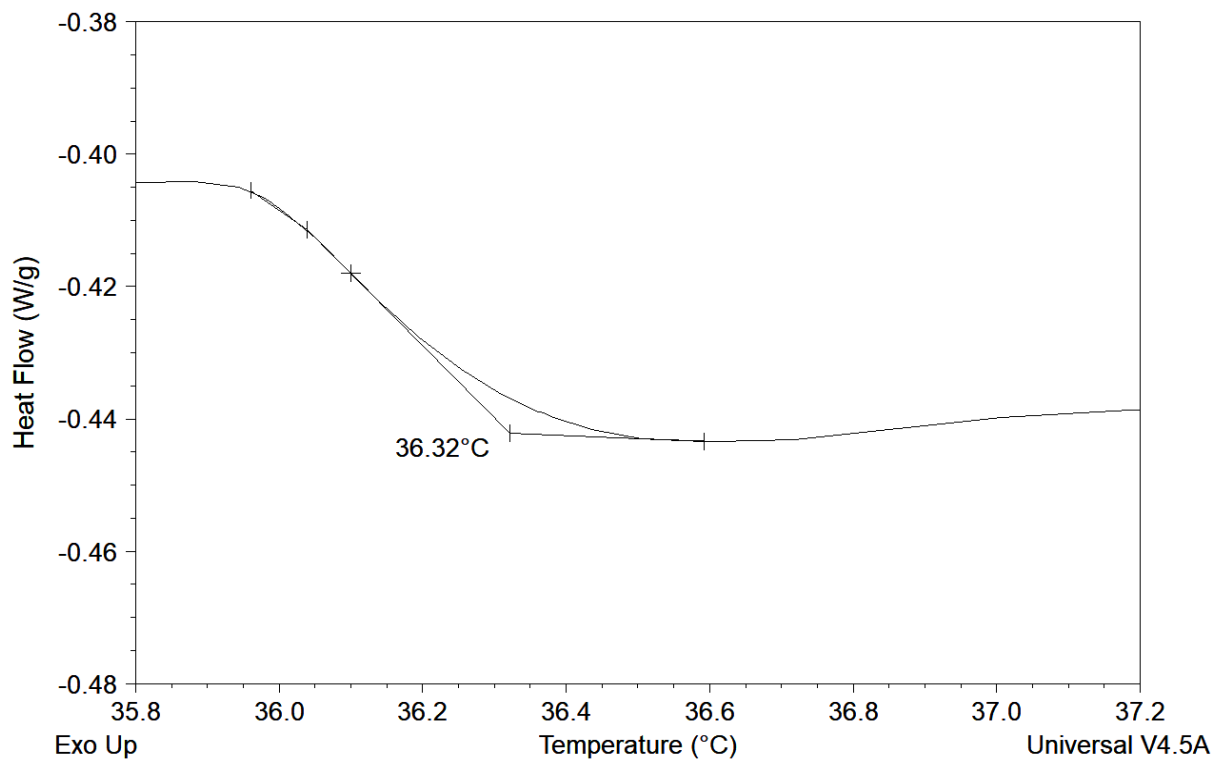


Figure 5-2 DSC graph of S3 PNVCCL based polymer sample.

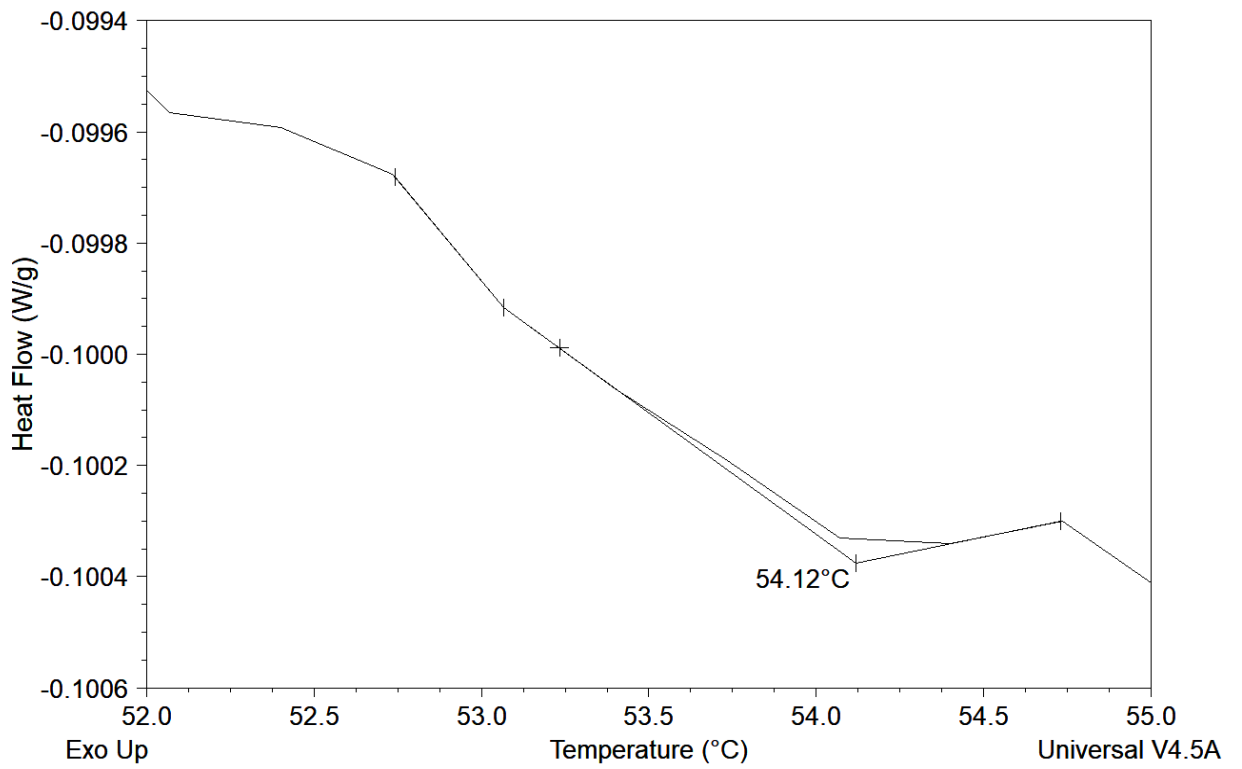


Figure 5-3 DSC graph of S10 PNVCL based polymer sample.

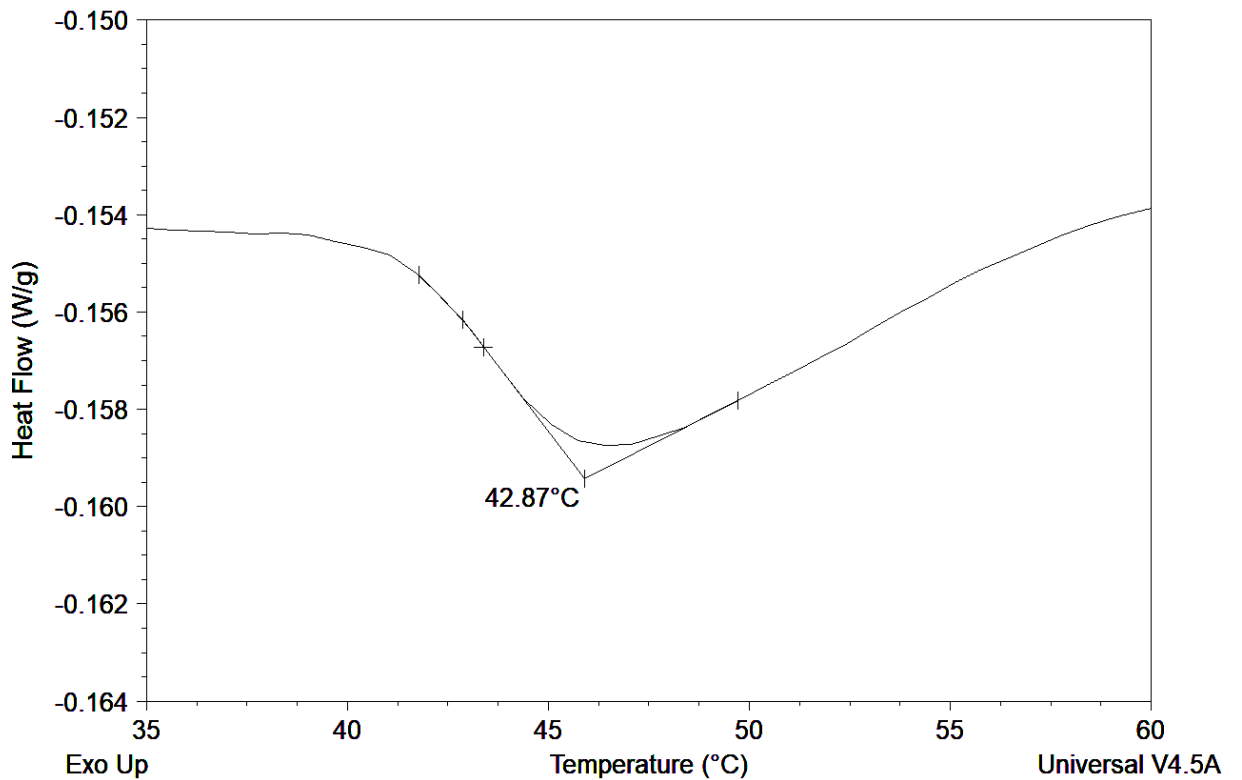


Figure 5-4 DSC graph of S12 PNVCL based polymer sample.

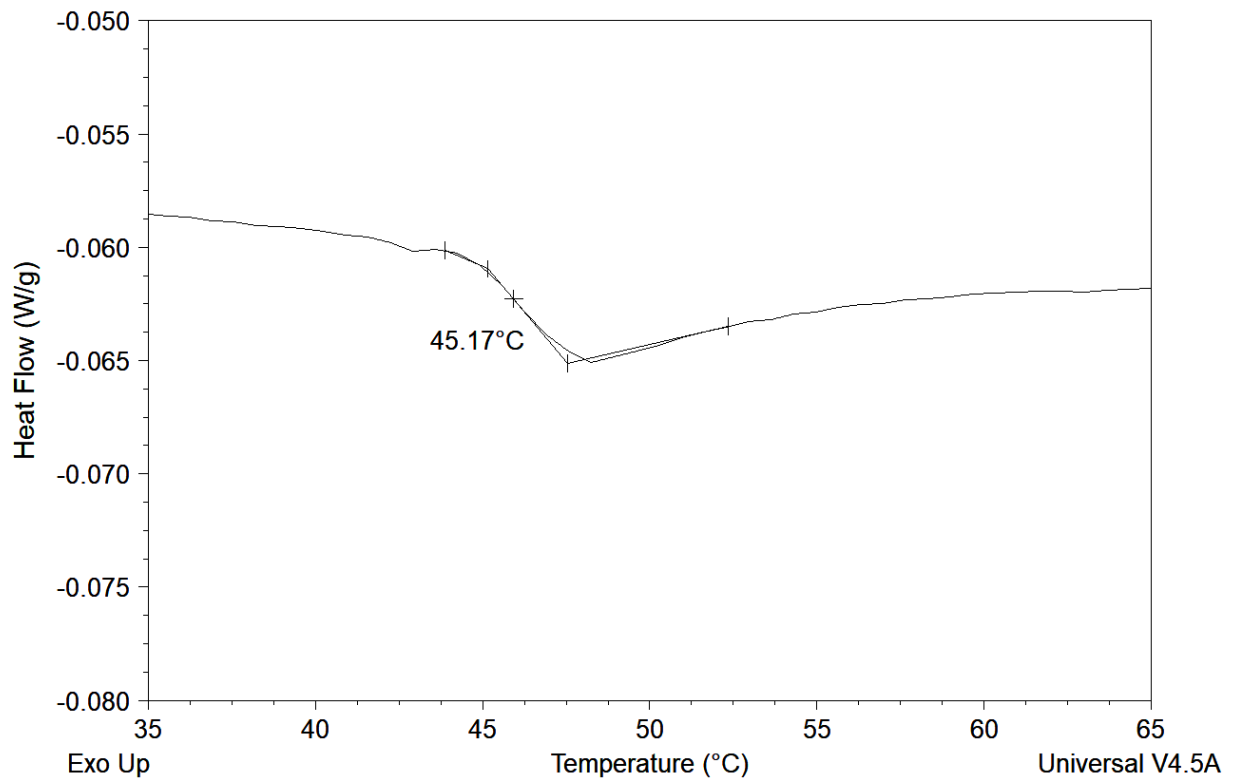


Figure 5-5 DSC graph of S13 PNVC L based polymer sample.

5.2.2 Rheology results

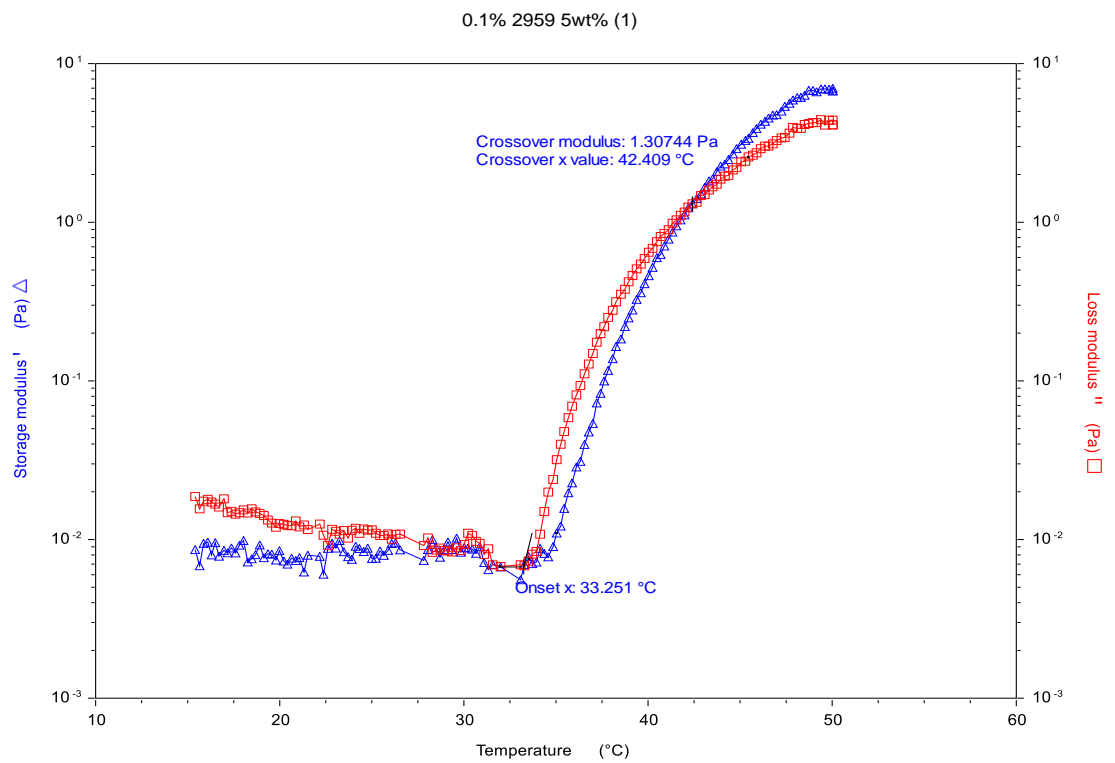


Figure 5-6 The rheology graph shows the phase transition and gelation point of 5 wt% PNVC L sample.

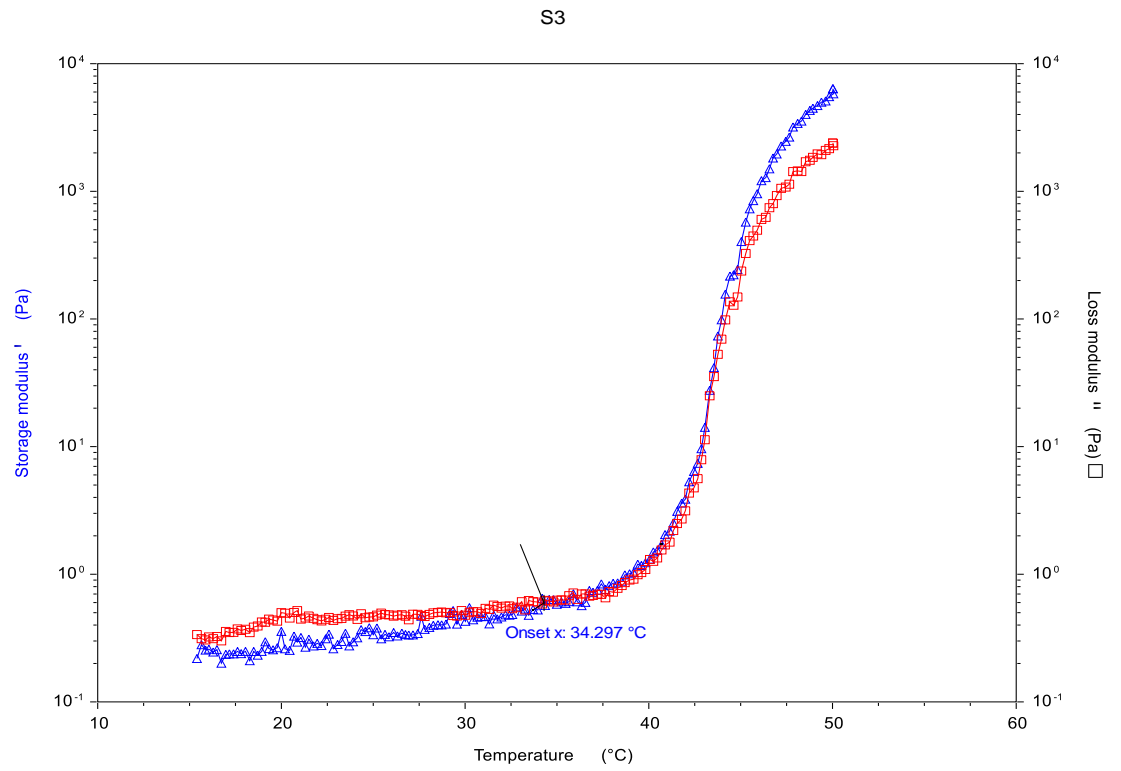


Figure 5-7 The rheology graph shows the phase transition and gelation point of S3 sample.

5.2.3 Swelling studies

Table 5-1 Below and above LCST swelling wt% ratios for the chemically crosslinked samples.

Time (hrs)	0	1	2	6	24	48	72
PNVCL/PEGDMA-Below LCST (Mean)							
0% PEGDMA	1.225	1.531	1.395	1.129	-	-	-
0.1% PEGDMA	1.321	1.586	1.43	1.135	-	-	-
1% PEGDMA	1.443	1.764	1.603	1.263	-	-	-
2% PEGDMA	1.4	1.981	2.2	2.84	6.3	9.23	9.8
5% PEGDMA	0.944	1.317	1.446	2.378	3.014	2.413	1.181
Swelling ratio % (Mean)							
0% PEGDMA	0	25	14	-	-	-	-
0.1% PEGDMA	0	20	8	-	-	-	-
1% PEGDMA	0	22	11	-	-	-	-
2% PEGDMA	0	41.5	57	103	350	559	600
5% PEGDMA	0	28	30	52	139	223	80
PNVCL/PEGDMA-Above LCST (Mean)							
0% PEGDMA	1.084	1.283	1.448	1.57	1.583	1.639	
0.1% PEGDMA	1.354	1.557	1.603	1.483	1.535	1.605	
1% PEGDMA	1.423	1.709	1.804	1.835	1.859	1.984	
2% PEGDMA	1.259	1.554	1.716	1.829	1.877	1.885	
5% PEGDMA	1.273	1.617	1.748	1.89	2.013	1.979	
Swelling ratio % (Mean)							
0% PEGDMA	0	18	34	45	46	51	
0.1% PEGDMA	0	15	18	10	13	18.5	
1% PEGDMA	0	20	27	29	31	39	
2% PEGDMA	0	23	36	45	49	50	
5% PEGDMA	0	27	37	48.5	58	55.5	

Table 5-2 Pulsatile swelling study performed on the PNVCL based polymer samples and swelling wt% ratio in below and above LCST condition.

Time (hrs)	0	1	6	24	48	72	144	168	24(oven)	48	72	24(room)	48	72	96	120	24(oven)	48
Co/terpolymers (Mean)																		
S4	1.51	1.788	1.049	-	-	-	-	-	-	-	-	-	-	-	-	-	-	-
S5	1.41	1.773	3.577	6.251	8.874	9.287	8.971	-	5.602	5.217	4.994	9.01	-	-	9.344	9.463	5.704	5.464
S6	1.36	1.959	3.944	6.797	8.666	12.17	16.60	18.498	10.267	8.553	8.443	-	-	14.3	17.75	-	10.74	10.55
S7	1.18	1.949	3.702	4.915	6.266	6.7	6.041	-	3.642	3.568	3.718	6.008	-	-	6.184	6.262	3.952	3.771
S8	1.39	2.609	5.935	8.792	11.69	14.86	17.73	18.80	7.255	5.822	5.778	-	-	14.43	17.15	-	-	-
S9	1.47	2.27	3.719	5.51	6.948	7.616	7.297	-	4.032	4.173	3.93	6.439	-	-	6.439	6.637	4.448	4.308
Swelling ratio % (Mean)																		
S4	0	18.3	-	-	-	-	-	-	-	-	-	-	-	-	-	-	-	-
S5	0	25.3	153	342	527	556	534	-	296	269	253	537	-	-	560	569	303	286
S6	0	70	189	397	534	791	1115	1253	651	526	518	-	-	946	1198	-	686	672
S7	0	65	213	315	429	435	410	-	208	201	214	407	-	-	422	429	234	218
S8	0	87	325	530	738	965	1170	1247	420	317	314	-	-	934	1129	-	-	-
S9	0	54	152	274	371	416	395	-	173	183	166	337	-	-	350	356	202	192

Time (hrs)	0	1	2	4	6	24	48	72	96	168	192	216	240	264	336	360	384	408
Co/terpolymers (Mean)																		
S15	1.598	2.296	2.812	3.643	4.624	8.448	9.087	9.059	8.917	4.76	4.879	7.318	7.411	4.595	4.884	7.083	7.111	6.966
S17	1.466	2.392	2.66	3.195	3.853	7.508	8.13	8.673	8.772	3.003	3.481	7.864	7.862	3.67	3.58	7.569	7.608	7.443
S19	1.414	2.137	2.437	2.891	3.386	6.697	8.363	8.673	8.764	2.42	2.593	7.984	8.147	2.265	3.048	8.068	8.072	7.977
Swelling ratio% (Mean)																		
S15	0	33	52	83	114	276	326	330	329	137	154	253	265	132	144	249	254	251
S17	0	35	45	64	85	203.5	272	312	325	74	81	276	283	80	79	266	276	272
S19	0	27	38	58	78	209	277	311	326	46	58	297	304	48	59	296	297	291

Table 5-3 Pulsatile swelling study performed on the H-Nu 4D printed and UV-cured samples and swelling wt% ratio in below and above LCST condition.

Time (hrs)	0	1	2	4	6	24	48	72	144	24 (oven)	48	72	24 (room)	96	24 (oven)	48	72	24 (room)	96	120
H-Nu printed and UV cured samples (Mean)																				
Printed flower	2.77 2	5.703	7.241	9.42	10.44 7	11.88 4	11.67 3	11.62 7	11.44	5.975	6.05	6.103	11.20 9	10.96 3	5.689	6.222	6.456	10.88 2	10.82 1	11.01 2
Printed jigsaw	7.04 1	11.72 7	13.80 4	17.33 7	19.95 1	29.57 2	31.83 4	32.10 8	31.86 2	17.07 8	17.45 4	17.21 5	29.92 8	30.69 5	15.79 4	16.48 3	16.58 5	29.53	30.36	30.96
UV cured	1.30 5	2.017	2.423	3.27	3.897	6.269	6.734	6.862	6.877	3.45 ⁽⁷²⁾	3.357 ⁽⁹⁶⁾	-	6.478	6.702 ⁽⁴⁸⁾	3.029	-	3.08 ⁽⁹⁶⁾	6.421	6.623 ⁽⁴⁸⁾	6.646 ⁽⁷²⁾
Swelling ratio % (Mean)																				
Printed flower	0	88	132	197	234	320	326	324	319	123	124	129	306	302	106	126	128	296	294	302
Printed jigsaw	0	67	96	146	183	320	352	356	352.5	143	148	144.5	325	336	124	134	135.5	319	331	340
UV cured	0	57	93.5	156	217	391	417	423	429	164.5	157	-	396	410	130	-	137	395	405	406

Time (hrs)	0	1	2	4	6	24	48	72	144	24 (oven)	48 (80°C)	72	96	72 (room)	96	24 (oven)	48	72	96 (room)	120
Shape of samples (one sample)																				
Disc	1.44 6	2.37 6	2.67 7	3.258	3.987	6.903	7.41	7.386	7.037	3.37	2.85 3	3.462	3.448	6.857	7.106	2.83 9	3.475	3.497	7.138	7.235
Flower	2.02 1	4.15 4	4.94 3	6.8	8.137	11.35 7	11.36 3	11.23 3	10.74 5	5.106	4.35 4	5.269	5.267	10.11 8	10.46 2	4.27 8	5.287	5.227	10.83 6	10.94 9
Jigsaw	4.65 7	8.06 9	9.08 9	10.74 6	13.10 4	24.62 1	26.95 7	26.93 2	25.54 2	13.36 2	9.76	11.78 8	11.68 8	24.01 1	24.90 8	9.78 4	11.65 6	11.73 6	25.25	25.80 2
Swelling ratio % (Mean)																				
Discs	0	130	193	281	339	493	509	504	474	178	124	179	182	461	478	123	178	180	488	495
Flowers	0	106	145	237	299	457	458	451	4128	164	115. 5	160	157	397	414	116	161	156	431	437
Jigsaws	0	78	104	149	201	457	510	511	481	197	115	166	163	444	464	118	161	161	474	485

5.2.4 UV spectroscopy

Table 5-4 UV spectroscopy data for LCST studies on PNVCL and its copolymers.

(°C)	2959 5wt%	2959 10 wt%	0.2 wt% 2959	0.5 wt% 2959	1 wt% 2959	2 wt% 2959	5 wt% 2959	S1	S2	S3	S10	S12	S13
22	0.056	0.49	0.1	0.061	0.046	0.049	0.057	-	-	-	-	-	-
23	0.057	0.48	0.095	0.061	0.047	0.05	0.056	-	-	-	-	-	-
24	0.058	0.478	0.11	0.062	0.047	0.049	0.057	-	-	-	-	-	-
25	0.056	0.462	0.127	0.063	0.048	0.049	0.058	0.077	0.118	0.049	0.046	0.053	0.046
26	0.057	0.461	0.14	0.066	0.048	0.049	0.059	0.079	0.118	0.051	0.046	0.054	0.046
27	0.058	0.449	0.134	0.068	0.048	0.05	0.061	0.081	0.118	0.051	0.046	0.055	0.046
28	0.059	0.495	0.125	0.071	0.049	0.051	0.061	0.084	0.119	0.051	0.047	0.056	0.046
29	0.06	0.474	0.138	0.074	0.049	0.05	0.064	0.086	0.12	0.051	0.046	0.055	0.046
30	0.063	0.466	0.159	0.077	0.049	0.051	0.065	0.089	0.12	0.052	0.046	0.055	0.046
31	0.067	0.458	0.157	0.081	0.051	0.052	0.068	0.093	0.12	0.051	0.047	0.056	0.046
32	0.077	0.473	0.162	0.088	0.053	0.053	0.074	0.097	0.134	0.053	0.047	0.054	0.046
33	1.119	0.448	0.163	0.095	0.055	0.056	0.082	0.101	0.33	0.055	0.047	0.054	0.046
34	1.335	0.454	0.162	0.105	0.06	0.061	0.117	0.104	0.747	0.055	0.046	0.056	0.047
35	1.623	1.462	0.179	0.112	0.08	0.076	2.165	0.11	1.183	0.056	0.046	0.057	0.047
36	1.702	1.424	0.207	0.131	1.989	1.594	2.365	0.116	1.541	0.061	0.046	0.06	0.047
37	1.738	1.543	2.013	1.403	2.239	2.069	2.331	0.12	1.808	0.164	0.046	0.063	0.048
38	1.764	1.791	2.066	2.229	2.117	2.011	2.233	0.126	2.002	0.398	0.046	0.067	0.048
39	1.806	2.1	1.978	2.113	2.23	1.963	2.199	0.133	2.145	0.719	0.046	0.073	0.048
40	1.857	2.016	2.3	2.145	2.147	1.899	2.204	0.136	2.249	1.054	0.046	0.074	0.049
41	1.887	1.965	2.22	2.016	2.099	1.951	2.224	0.145	2.326	1.414	0.046	0.074	0.05
42	1.912	1.96	2.199	2.007	2.103	1.958	2.249	0.152	2.383	1.738	0.047	0.074	0.053

43	1.931	1.948	2.168	1.996	2.122	1.994	2.278	0.162	2.42	1.974	0.046	0.066	0.075
44	1.944	1.95	2.172	2.002	2.151	2.027	2.3	0.169	2.443	2.131	0.046	0.136	0.188
45	1.957	1.95	2.185	2.016	2.162	2.063	2.319	0.178	2.462	2.236	0.046	1.036	0.828
46	1.967	1.94	2.191	2.022	2.167	2.09	2.322	0.19	2.469	2.299	0.046	1.169	1.252
47	1.975	1.929	2.194	2.031	2.167	2.112	2.324	0.194	2.467	2.336	0.046	1.364	1.365
48	1.982	1.911	2.2	2.031	2.175	2.131	2.32	0.209	2.46	2.354	0.046	1.504	1.489
49	1.986	1.883	2.221	2.019	2.192	2.144	2.309	0.216	2.452	2.359	0.047	1.612	1.585
50	1.988	1.85	2.241	2.001	2.2	2.16	2.277	0.228	2.44	2.356	0.047	1.68	1.648

5.2.5 Gel fraction measurement

Table 5-5 Gel fraction results of S7, H-Nu printed and UV-cured samples.

	Printed samples (W_0)	W_t	Gel fraction (%)	S7 (W_0)	W_t	Gel fraction (%)	H-Nu UV cured (W_0)	W_t	Gel fraction (%)
1	2.982	2.824	94.7	4.65	4.421	95.1	1.305 (1.235)	1.235	94.6
2	2.772	2.354	95.7	5.249	4.954	94.4	1.276(1.201)	1.201	94.1
3	7.041	6.097	95	0.789	0.772	97.8	1.063(1.012)	1.012	95.2
Mean			95.1			95.8			94.7

5.2.6 Goniometry

Table 5-6 The contact angles result of PNVCL homopolymers, co/terpolymers, H-Nu printed and UV-cured samples.

10 wt% homopolymer			C3			H-Nu printed		
Time	0s	115s	Time	0s	115s	Time	0s	115s
1	60.41	27.58	1	56.69	46.26	1	51.23	28.84
2	40.6	34.37	2	48.02	38.66	2	78.4	32.62
3	39.9	33.23	3	47.52	35.13	3	58.22	35.92
Mean	47	31.7	Mean	50.7	40	Mean	62.6	32.5

S5			S7			H-Nu cured		
Time	0s	115s	Time	0s	115s	Time	0s	115s
1	69.94	45.91	1	54.83	30.83	1	76.56	72.97
2	84.81	51.98	2	79.38	59.77	2	75.84	54.83
3	79.16	41.67	3	69.29	45.19	3	73.19	59
Mean	78	46.5	Mean	67.8	45.3	Mean	75.2	62.3

S9			S15			S17		
Time	0s	115s	Time	0s	115s	Time	0s	115s
1	86.17	64.53	1	64.34	52.77	1	69.15	58.52
2	82.38	55.6	2	82.91	69.91	2	87.79	55.35
3	83.91	57.42	3	75.2	45.76	3	91.38	62.14
Mean	84.2	59.2	Mean	74.2	56.1	Mean	82.8	58.7

S19		
Time	0s	115s
1	44.77	36.51
2	47.58	38.61
3	68.23	62.61
Mean	53.5	45.9

5.2.7 Tensile tests

Table 5-7 The tensile tests data of P1, C3, S7, H-Nu printed and UV-cured samples.

P1	Maximum load (N)	Tensile strength (MPa)	Elongation at Maximum Load (mm)
1	78.2	8.5	2.9
2	82.5	9.2	2.8
3	80.9	8.9	2.9
4	84.2	8.3	2.9
5	82.2	9.2	3.0
Mean	81.6	8.8	2.9
C3	Maximum load (N)	Tensile strength (MPa)	Elongation at Maximum Load (mm)
1	107.7	11.8	2.5
2	111.6	11.5	2.8
3	126.2	12.4	2.6
4	116.9	11.8	2.1
5	125.8	13.2	2.3
Mean	117.6	12.1	2.5
S7	Maximum load (N)	Tensile strength (MPa)	Elongation at Maximum Load (mm)
1	207.2	20.7	3.1
2	168.6	15.6	1.8
3	173.5	18	2.3
4	340	24.3	2.2
Mean	197.3	19.6	2.3
H-Nu UV-cured	Maximum load (N)	Tensile strength (MPa)	Elongation at Maximum Load (mm)
1	141.4	12.6	0.6
2	210.5	20.2	0.7
3	182.4	17	0.8
4	142.4	13.6	0.6
5	206.6	15.8	0.9
Mean	176.7	15.9	0.7
H-Nu printed	Maximum load (N)	Tensile strength (MPa)	Elongation at Maximum Load (mm)
1	195	15.8	1.4
2	187	14.8	2.3
3	226.7	21.3	1.7
4	179.5	14	1.3
5	129.9	10.1	2
Mean	183.6	15.2	1.8

5.3 Appendix C- Gantt chart workplan and works display and publish during the PhD

5.3.1 Poster

THE SUNDAY TIMES
GOOD UNIVERSITY GUIDE
2018
INSTITUTE OF TECHNOLOGY OF THE YEAR

AIT Research

The Development of Smart 4D Materials: by Utilising Temperature-Sensitive Polymer

Shuo Zhuo, Dr. Joe Geever, Mr. Conor Hayes, Dr. Luke Geever
Material Research Institute, Athlone Institute of Technology, Dublin Road, Athlone, Co. Westmeath.
e-mail: s.zhuo@research.ait.ie, lgeever@ait.ie

Introduction

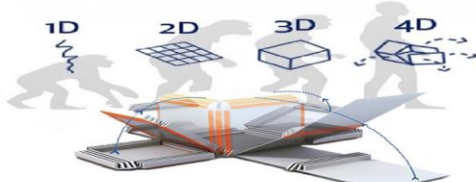


Figure 1 The basic concept for 4D printing [1]

There is more that can be done with 3D printed materials to make them more flexible and more useful: by utilising structures (Smart Polymers) that can transform in a pre-programmed way in response to a stimulus. Very recently given the popular science name of "4D printing", it refers to 3D printed objects that can transform their shape over time, thus giving them an extra dimension.

In this study, a temperature sensitive material, Poly(N-vinylcaprolactam) (PNVCL), was used. PNVCL is responsive to temperature changes near human physiological temperatures and characteristics include biocompatibility, solubility and accepted cytocompatibility [2]; In this work, a novel smart 4D material is being developed, allowing for the possibility of employing PNVCL into various applications.

Results

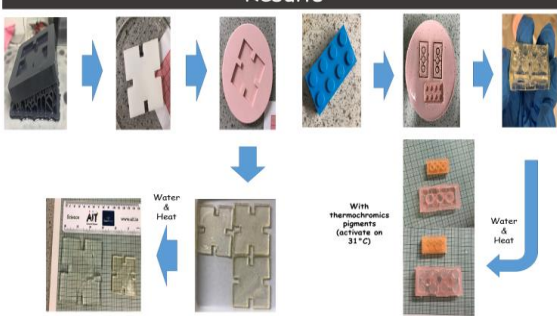


Figure 3 Puzzle model prototype design in our lab and the size changes after immersion in water and heating for 48h

Figure 4 Thermochromic LEGO model prototype and the size and color changes after immersion in water and heating for 48h

Aim

To develop smart 4D objects using PNVCL-based polymers via stereolithography (SLA) 3D printer.

Methods

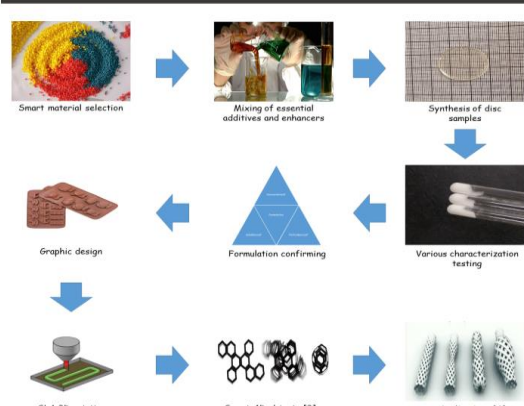


Figure 2 The scheme of 4D printing implementation

4D Printing

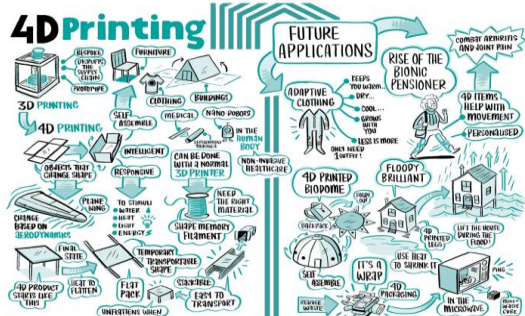


Figure 5 The future applications for 4D printing [9]

Discussion and Conclusion

Based on characterisation testing, the best formulations were determined, which showed tough, flexible and excellent swelling properties.

The models with complex shapes and structures can be perfectly cured and exhibited the intelligent reaction behaviors.

The next phase of research is to design simple and practical models or structures for potential applications.

References

1. <https://jgoffner.com/blog/4d-printing>
2. Cortez-Lemus, Norma A., and Angel Licea-Claverie. 2016. "Poly(N-Vinylcaprolactam), a Comprehensive Review on a Thermoresponsive Polymer Becoming Popular." *Progress in Polymer Science* 53: 1-51. <https://doi.org/10.1016/j.proppolymsci.2015.08.001>
3. <https://www.sculpteo.com/blog/2015/07/22/material-can-change-shape-with-4d-printing/>
4. <https://www.smithsonianmag.com/innovation/Objects-That-Change-Shape-On-Their-Own-180951447/>
5. <http://www.imperial-business-partners.com/tech-foresight/tech-foresight-2038-shifting-realities/attachment/future-of-4d-printing-illustration/>

THE SUNDAY TIMES
GOOD UNIVERSITY GUIDE
2018
INSTITUTE OF TECHNOLOGY OF THE YEAR

AIT Research

Figure 5-8 Best material research institute poster in AIT seminar in 2019.

5.3.2 Publications

- “Lower Critical Solution Temperature Tuning and Swelling Behaviours of NVCL-Based Hydrogels for Potential 4D Printing Applications”
Shuo Zhuo, Elaine Halligan, Billy Shu Hieng Tie, Colette Breheny and Luke M. Geever. - MDPI polymers journal (<https://doi.org/10.3390/polym14153155>).
- “A Development of New Material for 4D Printing and the Material Properties Comparison between the Conventional and Stereolithography Polymerised NVCL Hydrogels”
Shuo Zhuo, Luke M. Geever, Elaine Halligan, Billy Shu Hieng Tie and Colette Breheny. - MDPI Journal of Functional Biomaterials (<https://doi.org/10.3390/jfb13040262>).
- “Strategies for Developing Shape-Shifting Behaviours and Potential Applications of Poly (N-vinyl Caprolactam) Hydrogels”
Shuo Zhuo, Billy Shu Hieng Tie, Gavin Keane and Luke M. Geever. - MDPI polymers journal (<https://doi.org/10.3390/polym15061511>).
- “Liquid-Based 4D Printing of Shape Memory Nanocomposites: A Review”
Mohammad Alsaadi, Eoin P. Hinchy, Conor T. McCarthy, Vicente F. Moritz,
Shuo Zhuo, Evert Fuenmayor and Declan M. Devine. - MDPI Journal of Manufacturing and Materials Processing (<https://doi.org/10.3390/jmmp7010035>).
- “Synthesis of NVCL-NIPAM Hydrogels Using PEGDMA as a Chemical Crosslinker for Controlled Swelling Behaviours in Potential Shapeshifting Applications”
Billy Shu Hieng Tie, Elaine Halligan, **Shuo Zhuo**, Gavin Keane and Luke Geever. - MDPI gels journal (<https://doi.org/10.3390/gels9030248>).

- “Modulation of the Lower Critical Solution Temperature of Thermoresponsive Poly(N-vinylcaprolactam) Utilizing Hydrophilic and Hydrophobic Monomers”

Elaine Halligan, **Shuo Zhuo**, Declan Mary Colbert, Mohamad Alsaadi, Billy Shu Hieng Tie, Gilberto S. N. Bezerra, Gavin Keane and Luke M. Geever. - MDPI polymers journal (<https://doi.org/10.3390/polym15071595>).

Table 5-8 Gantt chart workplan Sept. 2017-June 2022.

The Development of Smart 4D Objects Utilising Temperature Responsive Polymer
Literature Reviews
Reviewing the work has been done in our lab on temperature responsive polymers Background of hydrogels Chemically and physically crosslinking Hydrogels characteristics & preparation Applications of the hydrogels Stimuli sensitive materials Temperature sensitive materials Lower and upper critical solution temperature Shape-shifting strategy N-vinylcaprolactam Photopolymerisation Introduction of 3D printing techniques Stereolithography (SLA) Introduction of 4D printing Current state of art of shape-shifting materials
Development of a formulation in which the sample exhibits the best properties (appearance, swelling size and quality, mechanical strength) and has the potential to be fabricated 4D objects
Photoinitiators selection Crosslinkers selection Silicone mould making Discs samples preparation using different concentrations of Irgacure 2959 (physically crosslinking)

<p>Discs samples preparation using different concentrations of VA-086 (physically crosslinking)</p> <p>Discs samples preparation using different concentration of Camphorquinone (physically crosslinking)</p> <p>Exclude samples by appearance</p> <p>Discs samples preparation using different concentration of PEGDMA (chemically crosslinking)</p> <p>Structure detective of physically and chemically crosslinking homopolymers using FTIR technique</p> <p>Phase transition determination by cloud point analysis</p> <p>Phase transition determination by DSC</p> <p>Phase transition determination by UV-spectroscopy</p> <p>Phase transition determination by Rheology</p> <p>Swelling studies</p> <p>Thesis writing</p>
<p>By incorporating the hydrophilic monomers, to enhance the mechanical properties of the first generation NVCL homopolymer and develop different extension capabilities samples</p>
<p>Literature observation</p> <p>Hydrophilic monomers selection</p> <p>Copolymers/terpolymers preparation using different concentrations of NVP, DMAAm and NIPAAm</p> <p>Exclude samples by appearance</p> <p>FTIR</p> <p>Phase transition determination by cloud point analysis</p> <p>Phase transition determination by DSC</p> <p>Phase transition determination by UV-spectroscopy</p> <p>Phase transition determination by Rheology</p> <p>Pulsatile swelling studies on co/terpolymers</p> <p>Final decision of formulation based on the samples performances, transition temperature and swelling capability</p> <p>Thesis writing</p>
<p>Transfer to PhD in April 2020</p>
<p>To explore shape shifting capabilities through SLA 3D printer</p>
<p>The design of the complex printing patterns</p>

Flower prototype preparation by 3D printing
 Silicone mould making
 The flower shape samples first prepare by photopolymerisation
 First printing attempt: using the best formulation developed in previous work
 Failure analysis & literature observations
 Second printing attempt: increasing amounting of Irgacure 2959
 New photoinitiators selection (BAPO, TPO, H-Nu 400IL)
 Third printing attempt: using the best formulation blends with new photoinitiators and concentrations
 New formulation confirmation
 Enhancement of printing parts (postcure treatment, support structure)
 Printing support design
 Fourth printing attempt: using the new formulation printing with the support
 Structure detection of the photopolymerised flower samples by FTIR
 Structure detection of the printed flower samples by FTIR
 Phase transition determination of the photopolymerised flower samples by DSC
 Phase transition determination of the printed flower samples by DSC
 Pulsatile swelling studies on photopolymerised flower samples (4D behaviour demonstration)
 Pulsatile swelling studies on printed flower samples (4D behaviour demonstration)
 Properties comparison of photopolymerised and printed samples
 More sophisticated models design
 4D printing of sophisticated models
 Thesis writing

To explore shape shifting capabilities through UV chamber system

Literatures observation
 Schemes selection for shape shifting
 Scheme 1: bilayer structures
 Selection of rigid materials for passive layer (Flexible vs Elastic)
 Scheme 2: Hinge structures

Different strips bilayer structure design
Shape shifting behaviours observation by swelling test
Determining the material of the passive layer (Elastic)
Determining the final strip bilayer structure pattern
Tensile tests on elastic material
Self-rolling behaviour development (literature found & samples prepare)
Swelling test on strips bilayer structure samples
Thickness determining for active & passive layer
Self-bending behaviour development on flower samples
Swelling test on flower bilayer structure samples
Demonstration development (Gripper, auto puller)
Thesis writing

Chapter 6:

Bibliography

6 Bibliography

- Ahmad, S., Ahmad, M., Manzoor, K., Purwar, R., & Ikram, S. (2019). A review on latest innovations in natural gums based hydrogels: Preparations & applications. In *International Journal of Biological Macromolecules* (Vol. 136, pp. 870–890). Elsevier. <https://doi.org/10.1016/j.ijbiomac.2019.06.113>
- Ahmad, Z., Salman, S., Khan, S. A., Amin, A., Rahman, Z. U., Al-Ghamdi, Y. O., Akhtar, K., Bakhsh, E. M., & Khan, S. B. (2022). Versatility of Hydrogels: From Synthetic Strategies, Classification, and Properties to Biomedical Applications. In *Gels* (Vol. 8, Issue 3, p. 167). Multidisciplinary Digital Publishing Institute. <https://doi.org/10.3390/gels8030167>
- Ahmed, E. M. (2015). Hydrogel: Preparation, characterization, and applications: A review. *Journal of Advanced Research*, 6(2), 105–121. <https://doi.org/10.1016/j.jare.2013.07.006>
- Ahmed, E. M., Aggor, F. S., Awad, A. M., & El-Aref, A. T. (2013). An innovative method for preparation of nanometal hydroxide superabsorbent hydrogel. *Carbohydrate Polymers*, 91(2), 693–698. <https://doi.org/10.1016/j.carbpol.2012.08.056>
- Akhtar, M. F., Hanif, M., & Ranjha, N. M. (2016). Methods of synthesis of hydrogels ... A review. *Saudi Pharmaceutical Journal*, 24(5), 554–559. <https://doi.org/10.1016/j.jsps.2015.03.022>
- Akin, A., & Işiklan, N. (2016). Microwave assisted synthesis and characterization of sodium alginate-graft-poly(N,N'-dimethylacrylamide). *International Journal of Biological Macromolecules*, 82, 530–540. <https://doi.org/10.1016/j.ijbiomac.2015.10.050>
- Alarcón, C. de las H., Pennadam, S., & Alexander, C. (2005). Stimuli responsive polymers for biomedical applications. *Chem. Soc. Rev.*, 34(3), 276–285. <https://doi.org/10.1039/B406727D>
- Aldana, A. A., Rial-Hermida, M. I., Abraham, G. A., Concheiro, A., & Alvarez-Lorenzo, C. (2017). Temperature-sensitive biocompatible IPN hydrogels based on poly(NIPA-PEGdma) and photocrosslinkable gelatin methacrylate. *Soft Materials*, 15(4), 341–349. <https://doi.org/10.1080/1539445X.2017.1378677>
- Alpaslan, D., Ersen Dudu, T., & Aktas, N. (2021). Synthesis of Smart Food Packaging from Poly (Gelatin-co-Dimethyl Acrylamide) / Citric Acid-Red Apple peel Extract. *Soft Materials*, 19(1), 64–77. <https://doi.org/10.1080/1539445X.2020.1765802>
- An, J., Chua, C. K., & Mironov, V. (2016). A Perspective on 4D Bioprinting. *International Journal of Bioprinting*, 2(0), 3–5. <https://doi.org/10.18063/IJB.2016.01.003>
- Anufrieva, E. V., Gromova, R. A., Kirsh, Y. E., Yanul, N. A., Krakovyak, M. G., Lushchik, V. B., Pautov, V. D., & Sheveleva, T. V. (2001). Complexing properties and structural characteristics of thermally sensitive copolymers of N-vinylpyrrolidone and N-vinylcaprolactam. *European Polymer Journal*, 37(2), 323–328. [https://doi.org/10.1016/S0014-3057\(00\)00109-9](https://doi.org/10.1016/S0014-3057(00)00109-9)
- Asghar, S., Minhas, M. U., Ahmad, M., Khan, K. U., Sohail, M., & Khalid, I. (2018). Hydrophobic–hydrophilic cross-linked matrices for controlled release formulation of Highly water-soluble drug venlafaxine: Synthesis and evaluation studies.

- Advances in Polymer Technology*, 37(8), 3146–3158.
<https://doi.org/10.1002/adv.22085>
- Aswathy, S. H., Narendrakumar, U., & Manjubala, I. (2020). Commercial hydrogels for biomedical applications. *Heliyon*, 6(4), e03719.
<https://doi.org/10.1016/j.heliyon.2020.e03719>
- Ayushi, Kumar Vates, U., Mishra, S., & Jee Kanu, N. (2021). Biomimetic 4D printed materials: A state-of-the-art review on concepts, opportunities, and challenges. *Materials Today: Proceedings*, 47, 3313–3319.
<https://doi.org/10.1016/j.matpr.2021.07.148>
- Babu, V. R., Hosamani, K. M., & Aminabhavi, T. M. (2008). Preparation and in-vitro release of chlorothiazide novel pH-sensitive chitosan-N,N'-dimethylacrylamide semi-interpenetrating network microspheres. *Carbohydrate Polymers*, 71(2), 208–217. <https://doi.org/10.1016/j.carbpol.2007.05.039>
- Back, J. W., De Jong, L., Muijsers, A. O., & De Koster, C. G. (2003). Chemical cross-linking and mass spectrometry for protein structural modeling. In *Journal of Molecular Biology* (Vol. 331, Issue 2, pp. 303–313). Academic Press.
[https://doi.org/10.1016/S0022-2836\(03\)00721-6](https://doi.org/10.1016/S0022-2836(03)00721-6)
- Bakarich, S. E., Gorkin, R., Naficy, S., Gately, R., Panhuis, M. In Het, & Spinks, G. M. (2016). 3D/4D Printing Hydrogel Composites: A Pathway to Functional Devices. *MRS Advances*, 1(8), 521–526. <https://doi.org/10.1557/adv.2015.9>
- Bakarich, S. E., Gorkin, R., Panhuis, M. In Het, & Spinks, G. M. (2015). 4D printing with mechanically robust, thermally actuating hydrogels. *Macromolecular Rapid Communications*, 36(12), 1211–1217. <https://doi.org/10.1002/marc.201500079>
- Baker, A. B., Bates, S. R. G., Llewellyn-Jones, T. M., Valori, L. P. B., Dicker, M. P. M., & Trask, R. S. (2019). 4D printing with robust thermoplastic polyurethane hydrogel-elastomer trilayers. *Materials and Design*, 163, 107544.
<https://doi.org/10.1016/j.matdes.2018.107544>
- Bastani, S., & Mohseni, M. (2015a). UV-Curable Nanocomposite Coatings and Materials. In *Handbook of Nanoceramic and Nanocomposite Coatings and Materials*. Elsevier Ltd. <https://doi.org/10.1016/B978-0-12-799947-0.00007-9>
- Bastani, S., & Mohseni, M. (2015b). UV-Curable Nanocomposite Coatings and Materials. In *Handbook of Nanoceramic and Nanocomposite Coatings and Materials* (pp. 155–182). Elsevier Ltd. <https://doi.org/10.1016/B978-0-12-799947-0.00007-9>
- Bazban-Shotorbani, S., Hasani-Sadrabadi, M. M., Karkhaneh, A., Serpooshan, V., Jacob, K. I., Moshaverinia, A., & Mahmoudi, M. (2017). Revisiting structure-property relationship of pH-responsive polymers for drug delivery applications. In *Journal of Controlled Release* (Vol. 253, pp. 46–63).
<https://doi.org/10.1016/j.jconrel.2017.02.021>
- Beamish, J. A., Zhu, J., Kottke-Marchant, K., & Marchant, R. E. (2010). The effects of monoacrylated poly(ethylene glycol) on the properties of poly(ethylene glycol) diacrylate hydrogels used for tissue engineering. *Journal of Biomedical Materials Research - Part A*, 92(2), 441–450. <https://doi.org/10.1002/jbm.a.32353>
- Belbekhouche, S., Dulong, V., Picton, L., & Le Cerf, D. (2013). Saccharide effect on the LCST property of a polyether: Influence of structure and length. *Colloids and*

- Surfaces A: Physicochemical and Engineering Aspects*, 428, 25–31.
<https://doi.org/10.1016/j.colsurfa.2013.03.022>
- Bernardo, G., Araújo, T., da Silva Lopes, T., Sousa, J., & Mendes, A. (2020). Recent advances in membrane technologies for hydrogen purification. *International Journal of Hydrogen Energy*, 45(12), 7313–7338.
<https://doi.org/10.1016/j.ijhydene.2019.06.162>
- Bhattacharjee, P., & Ahearne, M. (2021). Significance of crosslinking approaches in the development of next generation hydrogels for corneal tissue engineering. In *Pharmaceutics* (Vol. 13, Issue 3, pp. 1–24).
<https://doi.org/10.3390/pharmaceutics13030319>
- Bodaghi, M., Damanpack, A. R., & Liao, W. H. (2017). Adaptive metamaterials by functionally graded 4D printing. *Materials and Design*, 135, 26–36.
<https://doi.org/10.1016/j.matdes.2017.08.069>
- Bordat, A., Boissenot, T., Nicolas, J., & Tsapis, N. (2019). Thermoresponsive polymer nanocarriers for biomedical applications. In *Advanced Drug Delivery Reviews* (Vol. 138, pp. 167–192). Elsevier. <https://doi.org/10.1016/j.addr.2018.10.005>
- Boutris, C., Chatzi, E. G., & Kiparissides, C. (1997). Characterization of the LCST behaviour of aqueous poly(N-isopropylacrylamide) solutions by thermal and cloud point techniques. *Polymer*, 38(10), 2567–2570.
- Brannon-Peppast, L. (1991). EQUILIBRIUM SWELLING HYDROGELS OF pH-SENSITIVE. *Chemical Engineering*, 46(3), 715–722.
- Brighenti, R., & Cosma, M. P. (2022). Mechanics of multi-stimuli temperature-responsive hydrogels. *Journal of the Mechanics and Physics of Solids*, 169, 105045.
<https://doi.org/10.1016/j.jmps.2022.105045>
- Burke, G., Barron, V., Geever, T., Geever, L., Devine, D. M., & Higginbotham, C. L. (2019). Evaluation of the materials properties, stability and cell response of a range of PEGDMA hydrogels for tissue engineering applications. *Journal of the Mechanical Behavior of Biomedical Materials*, 99(July), 1–10.
<https://doi.org/10.1016/j.jmbbm.2019.07.003>
- Bustamante-Torres, M., Romero-Fierro, D., Arcentales-Vera, B., Palomino, K., Magaña, H., & Bucio, E. (2021). Hydrogels classification according to the physical or chemical interactions and as stimuli-sensitive materials. In *Gels* (Vol. 7, Issue 4). Multidisciplinary Digital Publishing Institute (MDPI).
<https://doi.org/10.3390/gels7040182>
- Byun, M., Santangelo, C. D., & Hayward, R. C. (2013). Swelling-driven rolling and anisotropic expansion of striped gel sheets. *Soft Matter*, 9(34), 8264–8273.
<https://doi.org/10.1039/c3sm50627d>
- Caló, E., & Khutoryanskiy, V. V. (2015). Biomedical applications of hydrogels: A review of patents and commercial products. In *European Polymer Journal* (Vol. 65, pp. 252–267). Pergamon. <https://doi.org/10.1016/j.eurpolymj.2014.11.024>
- Can, A., Zhang, Q., Rudolph, T., Schacher, F. H., Gohy, J. F., Schubert, U. S., & Hoogenboom, R. (2015). Schizophrenic thermoresponsive block copolymer micelles based on LCST and UCST behavior in ethanol-water mixtures. *European Polymer Journal*, 69, 460–471. <https://doi.org/10.1016/j.eurpolymj.2015.04.008>

- Cao, Y., & Mezzenga, R. (2020). Design principles of food gels. *Nature Food*, 1(2), 106–118. <https://doi.org/10.1038/s43016-019-0009-x>
- Cao, Z., Liu, W., Gao, P., Yao, K., Li, H., & Wang, G. (2005). Toward an understanding of thermoresponsive transition behavior of hydrophobically modified N-isopropylacrylamide copolymer solution. *Polymer*, 46(14), 5268–5277. <https://doi.org/10.1016/j.polymer.2005.04.050>
- Cendula, P., Kiravittaya, S., Mei, Y. F., Deneke, C., & Schmidt, O. G. (2009). Bending and wrinkling as competing relaxation pathways for strained free-hanging films. *Physical Review B - Condensed Matter and Materials Physics*, 79(8). <https://doi.org/10.1103/PhysRevB.79.085429>
- Chai, Q., Jiao, Y., & Yu, X. (2017). Hydrogels for biomedical applications: Their characteristics and the mechanisms behind them. In *Gels* (Vol. 3, Issue 1, p. 6). Multidisciplinary Digital Publishing Institute. <https://doi.org/10.3390/gels3010006>
- Champeau, M., Heinze, D. A., Viana, T. N., de Souza, E. R., Chinellato, A. C., & Titotto, S. (2020). 4D Printing of Hydrogels: A Review. *Advanced Functional Materials*, 30(31), 1–22. <https://doi.org/10.1002/adfm.201910606>
- Chavda, H., & Patel, C. (2011). Effect of crosslinker concentration on characteristics of superporous hydrogel. *International Journal of Pharmaceutical Investigation*, 1(1), 17. <https://doi.org/10.4103/2230-973X.76724>
- Chen, J., Liu, M., Liu, H., & Ma, L. (2009). Synthesis, swelling and drug release behavior of poly(N,N-diethylacrylamide-co-N-hydroxymethyl acrylamide) hydrogel. *Materials Science and Engineering C*, 29(7), 2116–2123. <https://doi.org/10.1016/j.msec.2009.04.008>
- Chen, M., Zhong, M., & Johnson, J. A. (2016). Light-Controlled Radical Polymerization: Mechanisms, Methods, and Applications. *Chemical Reviews*, 116(17), 10167–10211. https://doi.org/10.1021/ACS.CHEMREV.5B00671/ASSET/IMAGES/LARGE/CR-2015-006712_0045.JPEG
- Chen, W., Sun, B., Biehl, P., & Zhang, K. (2022). Cellulose-Based Soft Actuators. In *Macromolecular Materials and Engineering* (Vol. 307, Issue 6, p. 2200072). John Wiley & Sons, Ltd. <https://doi.org/10.1002/mame.202200072>
- Chen, Yihang, Zhang, S., Cui, Q., Ni, J., Wang, X., Cheng, X., Alem, H., Tebon, P., Xu, C., Guo, C., Nasiri, R., Moreddu, R., Yetisen, A. K., Ahadian, S., Ashammakhi, N., Emaminejad, S., Jucaud, V., Dokmeci, M. R., & Khademhosseini, A. (2020). Microengineered poly(HEMA) hydrogels for wearable contact lens biosensing. *Lab on a Chip*, 20(22), 4205–4214. <https://doi.org/10.1039/d0lc00446d>
- Chen, Ying, Li, J., Lu, J., Ding, M., & Chen, Y. (2022). Synthesis and properties of Poly(vinyl alcohol) hydrogels with high strength and toughness. *Polymer Testing*, 108, 107516. <https://doi.org/10.1016/j.polymertesting.2022.107516>
- Chen, Z., Huang, G., Trase, I., Han, X., & Mei, Y. (2016). Mechanical Self-Assembly of a Strain-Engineered Flexible Layer: Wrinkling, Rolling, and Twisting. *Physical Review Applied*, 5(1), 1–33. <https://doi.org/10.1103/PhysRevApplied.5.017001>
- Chia, H. N., & Wu, B. M. (2015). Recent advances in 3D printing of biomaterials. *Journal of Biological Engineering*, 9(1), 4. <https://doi.org/10.1186/s13036-015-0001-4>

- Choong, Y. Y. C., Maleksaeedi, S., Eng, H., Wei, J., & Su, P. C. (2017). 4D printing of high performance shape memory polymer using stereolithography. *Materials and Design*, 126, 219–225. <https://doi.org/10.1016/j.matdes.2017.04.049>
- Claudio-Rizo, J. A., Escobedo-Estrada, N., Carrillo-Cortes, S. L., Cabrera-Munguía, D. A., Flores-Guía, T. E., & Becerra-Rodriguez, J. J. (2021). Highly absorbent hydrogels comprised from interpenetrated networks of alginate–polyurethane for biomedical applications. *Journal of Materials Science: Materials in Medicine*, 32(6), 1–13. <https://doi.org/10.1007/s10856-021-06544-4>
- Cortez-Lemus, Norma A, & Licea-Claverie, A. (2016). Poly(N-vinylcaprolactam), a comprehensive review on a thermoresponsive polymer becoming popular. *Progress in Polymer Science*, 53, 1–51. <https://doi.org/10.1016/j.progpolymsci.2015.08.001>
- Cortez-Lemus, Norma Aidé, & Licea-Claverie, A. (2018). Preparation of a mini-library of thermo-responsive star (NVCL/NVP-VAc) polymers with tailored properties using a hexafunctional xanthate RAFT agent. *Polymers*, 10(1), 20. <https://doi.org/10.3390/polym10010020>
- Dalton, M. B., Halligan, S. C., Killion, J. A., Wang, W., Dong, Y., Nugent, M. J. D., & Geever, L. M. (2018). The Effect Acetic Acid has on Poly(N-Vinylcaprolactam) LCST for Biomedical Applications. *Polymer - Plastics Technology and Engineering*, 57(12), 1165–1174. <https://doi.org/10.1080/03602559.2017.1373400>
- Dalton, M., Halligan, S., Killion, J., Murray, K. A., & Geever, L. (2014). Smart Thermosensitive Poly (N-vinylcaprolactam) Based Hydrogels for Biomedical Applications. *Advances in Environmental Biology*, 8(824), 1–6.
- Deirram, N., Zhang, C., Kermaniyan, S. S., Johnston, A. P. R., & Such, G. K. (2019). pH-Responsive Polymer Nanoparticles for Drug Delivery. In *Macromolecular Rapid Communications* (Vol. 40, Issue 10). <https://doi.org/10.1002/marc.201800917>
- Demoly, F., Dunn, M. L., Wood, K. L., Qi, H. J., & André, J. C. (2021). The status, barriers, challenges, and future in design for 4D printing. In *Materials and Design* (Vol. 212, p. 110193). Elsevier. <https://doi.org/10.1016/j.matdes.2021.110193>
- Deshmukh, K., Houkan, M. T., AlMaadeed, M. A. A., & Sadasivunid, K. K. (2019). Introduction to 3D and 4D printing technology: State of the art and recent trends. In *3D and 4D Printing of Polymer Nanocomposite Materials: Processes, Applications, and Challenges*. Elsevier Inc. <https://doi.org/10.1016/B978-0-12-816805-9.00001-6>
- Ding, H., Zhang, X., Liu, Y., & Ramakrishna, S. (2019). Review of mechanisms and deformation behaviors in 4D printing. *International Journal of Advanced Manufacturing Technology*, 105(11), 4633–4649. <https://doi.org/10.1007/s00170-019-03871-3>
- Drahansky, M., Paridah, M. ., Moradbak, A., Mohamed, A. ., Owolabi, F. abdulwahab taiwo, Asniza, M., & Abdul Khalid, S. H. . (2016). We are IntechOpen , the world ' s leading publisher of Open Access books Built by scientists , for scientists TOP 1 % . *Intech, i(tourism)*, 13. <https://doi.org/http://dx.doi.org/10.5772/57353>
- Duquette, D., & Dumont, M. J. (2019). Comparative studies of chemical crosslinking reactions and applications of bio-based hydrogels. *Polymer Bulletin*, 76(5), 2683–2710. <https://doi.org/10.1007/s00289-018-2516-6>

- Ebara, M., Kotsuchibashi, Y., Narain, R., Idota, N., Kim, Y.-J., Hoffman, J. M., Uto, K., & Aoyagi, T. (2014). Smart biomaterials. In *Science* (pp. 9–65).
[https://doi.org/10.1016/0958-2118\(92\)80030-Z](https://doi.org/10.1016/0958-2118(92)80030-Z)
- Eeckman, F., Moës, A. J., & Amighi, K. (2004). Synthesis and characterization of thermosensitive copolymers for oral controlled drug delivery. *European Polymer Journal*, 40(4), 873–881. <https://doi.org/10.1016/j.eurpolymj.2003.11.010>
- El-Husseiny, H. M., Mady, E. A., Hamabe, L., Abugomaa, A., Shimada, K., Yoshida, T., Tanaka, T., Yokoi, A., Elbadawy, M., & Tanaka, R. (2022). Smart/stimuli-responsive hydrogels: Cutting-edge platforms for tissue engineering and other biomedical applications. In *Materials Today Bio* (Vol. 13, p. 100186). Elsevier.
<https://doi.org/10.1016/j.mtbio.2021.100186>
- Elastic 50A Elastic 50A Resin for Soft Flexible Parts Wearables and consumer goods prototyping Medical models and devices Compliant features for robotics Special effects props and models.* (2019).
- Fajardo, A. R., Fávoro, S. L., Rubira, A. F., & Muniz, E. C. (2013). Dual-network hydrogels based on chemically and physically crosslinked chitosan/chondroitin sulfate. *Reactive and Functional Polymers*, 73(12), 1662–1671.
<https://doi.org/10.1016/j.reactfunctpolym.2013.10.003>
- Fallon, M., Halligan, S., Pezzoli, R., Geever, L., & Higginbotham, C. (2019). Synthesis and characterisation of novel temperature and pH sensitive physically cross-linked poly(N-vinylcaprolactam-co-itaconic acid) hydrogels for drug delivery. *Gels*, 5(3), 41. <https://doi.org/10.3390/gels5030041>
- Ferraz, C. C., Varca, G. H. C., Ruiz, J. C., Lopes, P. S., Mathor, M. B., Lugão, A. B., & Bucio, E. (2014). Radiation-grafting of thermo- and pH-responsive poly(N-vinylcaprolactam-co-acrylic acid) onto silicone rubber and polypropylene films for biomedical purposes. *Radiation Physics and Chemistry*, 97, 298–303.
<https://doi.org/10.1016/j.radphyschem.2013.12.027>
- Förch, R., Schönherr, H., & Jenkins, A. T. A. (2009). Contact angle goniometry. In *Surface Design: Applications in Bioscience and Nanotechnology* (3rd ed., pp. 471–473). Wiley.
- Frazar, E. M., Shah, R. A., Dziubla, T. D., & Hilt, J. Z. (2020). Multifunctional temperature-responsive polymers as advanced biomaterials and beyond. In *Journal of Applied Polymer Science* (Vol. 137, Issue 25, p. 48770). John Wiley & Sons, Ltd.
<https://doi.org/10.1002/app.48770>
- Furyk, S., Zhang, Y., Ortiz-Acosta, D., Cremer, P. S., & Bergbreiter, D. E. (2006). Effects of end group polarity and molecular weight on the lower critical solution temperature of poly(N-isopropylacrylamide). *Journal of Polymer Science, Part A: Polymer Chemistry*, 44(4), 1492–1501. <https://doi.org/10.1002/pola.21256>
- Gaballa, H. A., Geever, L. M., Killion, J. A., & Higginbotham, C. L. (2013). Synthesis and characterization of physically crosslinked N-vinylcaprolactam, acrylic acid, methacrylic acid, and N,N-dimethylacrylamide hydrogels. *Journal of Polymer Science, Part B: Polymer Physics*, 51(21), 1555–1564.
<https://doi.org/10.1002/polb.23369>
- Gao, B., Yang, Q., Zhao, X., Jin, G., Ma, Y., & Xu, F. (2016). 4D Bioprinting for Biomedical Applications. *Trends in Biotechnology*, 34(9), 746–756.
<https://doi.org/10.1016/j.tibtech.2016.03.004>

- García-Peñas, A., Biswas, C. S., Liang, W., Wang, Y., Yang, P., & Stadler, F. J. (2019). Effect of hydrophobic interactions on lower critical solution temperature for poly(N-isopropylacrylamide-co-dopamine methacrylamide) copolymers. *Polymers*, *11*(6), 991. <https://doi.org/10.3390/polym11060991>
- Ge, Q., Sakhaei, A. H., Lee, H., Dunn, C. K., Fang, N. X., & Dunn, M. L. (2016). Multimaterial 4D Printing with Tailorable Shape Memory Polymers. *Scientific Reports*, *6*(1), 31110. <https://doi.org/10.1038/srep31110>
- Geever, L. M., Devine, D. M., Nugent, M. J. D., Kennedy, J. E., Lyons, J. G., Hanley, A., & Higginbotham, C. L. (2006). Lower critical solution temperature control and swelling behaviour of physically crosslinked thermosensitive copolymers based on N-isopropylacrylamide. *European Polymer Journal*, *42*(10), 2540–2548. <https://doi.org/10.1016/j.eurpolymj.2006.06.002>
- Gibson, I., Rosen, D. W., & Stucker, B. (2010). Photopolymerization Processes. In *Additive Manufacturing Technologies* (pp. 78–119). Springer US. https://doi.org/10.1007/978-1-4419-1120-9_4
- Gil, E. S., & Hudson, S. M. (2004). Stimuli-responsive polymers and their bioconjugates. In *Progress in Polymer Science (Oxford)* (Vol. 29, Issue 12, pp. 1173–1222). <https://doi.org/10.1016/j.progpolymsci.2004.08.003>
- Góis, J. R., Serra, A. C., & Coelho, J. F. J. (2016). Synthesis and characterization of new temperature-responsive nanocarriers based on POEOMA-b-PNVCL prepared using a combination of ATRP, RAFT and CuAAC. *European Polymer Journal*, *81*, 224–238. <https://doi.org/10.1016/j.eurpolymj.2016.06.011>
- González-Ayón, M. A., Licea-Claverie, A., & Sañudo-Barajas, J. A. (2020). Different strategies for the preparation of galactose-functionalized thermo-responsive nanogels with potential as smart drug delivery systems. *Polymers*, *12*(9), 2150. <https://doi.org/10.3390/POLYM12092150>
- Gonzalez-Urias, A., Licea-Claverie, A., Sañudo-Barajas, J. A., & González-Ayón, M. A. (2022). NVCL-Based Hydrogels and Composites for Biomedical Applications: Progress in the Last Ten Years. In *International Journal of Molecular Sciences* (Vol. 23, Issue 9, p. 4722). Multidisciplinary Digital Publishing Institute. <https://doi.org/10.3390/ijms23094722>
- Goodridge, R. D., Shofner, M. L., Hague, R. J. M., McClelland, M., Schlea, M. R., Johnson, R. B., & Tuck, C. J. (2011). Processing of a Polyamide-12/carbon nanofibre composite by laser sintering. *Polymer Testing*, *30*(1), 94–100. <https://doi.org/10.1016/j.polymertesting.2010.10.011>
- Guo, Y., Gao, Z., Liu, Y., Huang, Z., Chai, C., & Hao, J. (2019). Multiple Cross-Linking-Dominated Metal-Ligand Coordinated Hydrogels with Tunable Strength and Thermosensitivity [Research-article]. *ACS Applied Polymer Materials*, *1*(9), 2370–2378. <https://doi.org/10.1021/acsapm.9b00490>
- Hager, M. D., Bode, S., Weber, C., & Schubert, U. S. (2015). Shape memory polymers: Past, present and future developments. *Progress in Polymer Science*, *49–50*, 3–33. <https://doi.org/10.1016/j.progpolymsci.2015.04.002>
- Halligan, S. C., Dalton, M. B., Murray, K. A., Dong, Y., Wang, W., Lyons, J. G., & Geever, L. M. (2017). Synthesis, characterisation and phase transition behaviour of temperature-responsive physically crosslinked poly (N-vinylcaprolactam) based

- polymers for biomedical applications. *Materials Science and Engineering C*, 79, 130–139. <https://doi.org/10.1016/j.msec.2017.03.241>
- Halligan, S., Murray, K., Hopkins, M., Rogers, I., Lyons, J., Vrain, O., & Geever, L. (2020). Enhancing and controlling the critical attributes of poly (N-vinylcaprolactam) through electron beam irradiation for biomedical applications. *Journal of Applied Polymer Science*, 137(18), 1–10. <https://doi.org/10.1002/app.48639>
- Haq, M. A., Su, Y., & Wang, D. (2017). Mechanical properties of PNIPAM based hydrogels: A review. *Materials Science and Engineering: C*, 70, 842–855. <https://doi.org/10.1016/J.MSEC.2016.09.081>
- He, S., J. Yaszemski, M., Yasko, A. W., Engel, P. S., & Mikos, A. G. (2000). Injectable biodegradable polymer composites based on poly(propylene fumarate) crosslinked with poly(ethylene glycol)-dimethacrylate. *Biomaterials*, 21(23), 2389–2394. [https://doi.org/10.1016/S0142-9612\(00\)00106-X](https://doi.org/10.1016/S0142-9612(00)00106-X)
- He, X., Sun, Y., Wu, J., Wang, Y., Chen, F., Fan, P., Zhong, M., Xiao, S., Zhang, D., Yang, J., & Zheng, J. (2019). Dual-stimulus bilayer hydrogel actuators with rapid, reversible, bidirectional bending behaviors. *Journal of Materials Chemistry C*, 7(17), 4970–4980. <https://doi.org/10.1039/c9tc00180h>
- Hennink, W. E., & van Nostrum, C. F. (2012). Novel crosslinking methods to design hydrogels. *Advanced Drug Delivery Reviews*, 64(SUPPL.), 223–236. <https://doi.org/10.1016/j.addr.2012.09.009>
- Hoare, T. R., & Kohane, D. S. (2008). Hydrogels in drug delivery: Progress and challenges. In *Polymer* (Vol. 49, Issue 8, pp. 1993–2007). Elsevier. <https://doi.org/10.1016/j.polymer.2008.01.027>
- Hoffman, A. S. (2012). Hydrogels for biomedical applications. In *Advanced Drug Delivery Reviews* (Vol. 64, Issue SUPPL., pp. 18–23). Elsevier. <https://doi.org/10.1016/j.addr.2012.09.010>
- Hoffman, A. S. (2013). Stimuli-responsive polymers: Biomedical applications and challenges for clinical translation. In *Advanced Drug Delivery Reviews* (Vol. 65, Issue 1, pp. 10–16). Elsevier. <https://doi.org/10.1016/j.addr.2012.11.004>
- Hoogenboom, R. (2014). Temperature-responsive polymers: Properties, synthesis and applications. In *Smart Polymers and their Applications*. Woodhead Publishing Limited. <https://doi.org/10.1533/9780857097026.1.15>
- Hu, Y., Wang, Z., Jin, D., Zhang, C., Sun, R., Li, Z., Hu, K., Ni, J., Cai, Z., Pan, D., Wang, X., Zhu, W., Li, J., Wu, D., Zhang, L., Chu, J., Hu, Y. L., Wang, Z. Y., Sun, R., ... Wang, X. W. (2019). *Botanical-Inspired 4D Printing of Hydrogel at the Microscale*. <https://doi.org/10.1002/adfm.201907377>
- Huang, Q., Guo, L., & Marinescu, I. D. (2015). Grind/Lap of Ceramics with UV-Bonded Diamond Wheels. In *Handbook of Ceramics Grinding and Polishing* (Second Edi). Elsevier Inc. <https://doi.org/10.1016/b978-1-4557-7858-4.00010-8>
- Hughes, C., Gaunt, L., Brown, M., Clarke, N. W., & Gardner, P. (2014). Assessment of paraffin removal from prostate FFPE sections using transmission mode FTIR-FPA imaging. *Analytical Methods*, 6(4), 1028–1035. <https://doi.org/10.1039/c3ay41308j>

- Hwa, L. C., Rajoo, S., Noor, A. M., Ahmad, N., & Uday, M. B. (2017). Recent advances in 3D printing of porous ceramics: A review. *Current Opinion in Solid State and Materials Science*. <https://doi.org/10.1016/j.cossms.2017.08.002>
- Idris, A., Man, Z., Maulud, A. S., & Khan, M. S. (2017). Effects of phase separation behavior on morphology and performance of polycarbonate membranes. *Membranes*, 7(2), 21. <https://doi.org/10.3390/membranes7020021>
- Invernizzi, M., Turri, S., Levi, M., & Suriano, R. (2018). 4D printed thermally activated self-healing and shape memory polycaprolactone-based polymers. *European Polymer Journal*, 101, 169–176. <https://doi.org/10.1016/j.eurpolymj.2018.02.023>
- Ionov, L. (2014). Hydrogel-based actuators: Possibilities and limitations. *Materials Today*, 17(10), 494–503. <https://doi.org/10.1016/j.mattod.2014.07.002>
- Iyer, G., Tillekeratne, L. M. V., Coleman, M. R., & Nadarajah, A. (2008). Equilibrium swelling behavior of thermally responsive metal affinity hydrogels, Part I: Compositional effects. *Polymer*, 49(17), 3737–3743. <https://doi.org/10.1016/j.polymer.2008.06.037>
- Jakubiak, J., Allonas, X., Fouassier, J. P., Sionkowska, A., Andrzejewska, E., Linden, L. Å., & Rabek, J. F. (2003). Camphorquinone-amines photoinitiating systems for the initiation of free radical polymerization. *Polymer*, 44(18), 5219–5226. [https://doi.org/10.1016/S0032-3861\(03\)00568-8](https://doi.org/10.1016/S0032-3861(03)00568-8)
- Janbaz, S., Hedayati, R., & Zadpoor, A. A. (2016). Programming the shape-shifting of flat soft matter: From self-rolling/self-twisting materials to self-folding origami. *Materials Horizons*, 3(6), 536–547. <https://doi.org/10.1039/c6mh00195e>
- Jiang, X., Guo, Q., He, Y., Li, H., & Xie, T. (2018). Using light to control the floatability of solid particles in aqueous solution of a Gemini surfactant. *Colloids and Surfaces A: Physicochemical and Engineering Aspects*. <https://doi.org/10.1016/j.colsurfa.2018.05.060>
- Jiang, Y., & Wang, Q. (2016). Highly-stretchable 3D-architected Mechanical Metamaterials. *Scientific Reports*, 6(1), 34147. <https://doi.org/10.1038/srep34147>
- Kabac, J. (2017). The influence of a radical structure on the kinetics of photopolymerization. *Journal of Polymer Science, Part A: Polymer Chemistry*, 55(9), 1575–1589. <https://doi.org/10.1002/pola.28525>
- kayla matthews. (2016). *3D Printing Evolves to 4D: Here's What We Know So Far*. Technology Explained. <http://www.makeuseof.com/tag/3d-printing-evolves-4d-heres-know-far/>
- Kenessova, Z. A., Mun, G. A., Bakytzhanuly, B., Rakhmetullayeva, R. K., Yessirkepova, A. N., Samenova, N. O., & Urkimbayeva, P. I. (2019). Radiation-Chemical Synthesis of Crosslinked Films Based on N-Vinylcaprolactam Copolymers. *Bulletin of Experimental Biology and Medicine*, 167(5), 685–688. <https://doi.org/10.1007/s10517-019-04599-6>
- Khalid, M. Y., Arif, Z. U., Noroozi, R., Zolfagharian, A., & Bodaghi, M. (2022). 4D printing of shape memory polymer composites: A review on fabrication techniques, applications, and future perspectives. *Journal of Manufacturing Processes*, 81(February), 759–797. <https://doi.org/10.1016/j.jmapro.2022.07.035>
- Khansari, M. M., Sorokina, L. V., Mukherjee, P., Mukhtar, F., Shirdar, M. R., Shahidi, M., & Shokuhfar, T. (2017). Classification of Hydrogels Based on Their Source: A

- Review and Application in Stem Cell Regulation. *Jom*, 69(8), 1340–1347.
<https://doi.org/10.1007/s11837-017-2412-9>
- Khoo, Z. X., Teoh, J. E. M., Liu, Y., Chua, C. K., Yang, S., An, J., Leong, K. F., & Yeong, W. Y. (2015). 3D printing of smart materials: A review on recent progresses in 4D printing. *Virtual and Physical Prototyping*, 10(3), 103–122.
<https://doi.org/10.1080/17452759.2015.1097054>
- Killion, J. A., Geever, L. M., Devine, D. M., Kennedy, J. E., & Higginbotham, C. L. (2011). Mechanical properties and thermal behaviour of PEGDMA hydrogels for potential bone regeneration application. *Journal of the Mechanical Behavior of Biomedical Materials*, 4(7), 1219–1227.
<https://doi.org/10.1016/j.jmbbm.2011.04.004>
- Killion, J. A., Kehoe, S., Geever, L. M., Devine, D. M., Sheehan, E., Boyd, D., & Higginbotham, C. L. (2013). Hydrogel/bioactive glass composites for bone regeneration applications: Synthesis and characterisation. *Materials Science and Engineering C*, 33(7), 4203–4212. <https://doi.org/10.1016/j.msec.2013.06.013>
- Kim, J. J., & Park, K. (1998). Smart hydrogels for bioseparation. *Bioseparation*, 7(4–5), 177–184. <https://doi.org/10.1023/a:1008050124949>
- Kokkinis, D., Schaffner, M., & Studart, A. R. (2015). Multimaterial magnetically assisted 3D printing of composite materials. *Nature Communications*, 6(1), 8643.
<https://doi.org/10.1038/ncomms9643>
- Kowalska, A., Sokolowski, J., & Bociong, K. (2021). The photoinitiators used in resin based dental composite—a review and future perspectives. In *Polymers* (Vol. 13, Issue 3, pp. 1–17). Multidisciplinary Digital Publishing Institute.
<https://doi.org/10.3390/polym13030470>
- Kozanoğlu, S. (2008). Polymerization and Characterization of N-vinyl caprolactam. In *Thesis*. <https://doi.org/10.1017/CBO9781107415324.004>
- Kuang, X., Roach, D. J., Wu, J., Hamel, C. M., Ding, Z., Wang, T., Dunn, M. L., & Qi, H. J. (2019). Advances in 4D Printing: Materials and Applications. In *Advanced Functional Materials* (Vol. 29, Issue 2). Wiley-VCH Verlag.
<https://doi.org/10.1002/adfm.201805290>
- Kuksenok, O., & Balazs, A. C. (2016). Stimuli-responsive behavior of composites integrating thermo-responsive gels with photo-responsive fibers. *Materials Horizons*, 3(1), 53–62. <https://doi.org/10.1039/c5mh00212e>
- Kurečić, M., Majda, S. S., & Karin, S. K. (2012). Uv Polymerization of Poly (N-Isopropylacrylamide) Hydrogel. *Materiali in Tehnologije*, 46(1), 87–91.
- Laupheimer, M., Preisig, N., & Stubenrauch, C. (2015). The molecular organogel n-decane/12-hydroxyoctadecanoic acid: Sol-gel transition, rheology, and microstructure. *Colloids and Surfaces A: Physicochemical and Engineering Aspects*, 469, 315–325. <https://doi.org/10.1016/j.colsurfa.2015.01.039>
- Le Duigou, A., Castro, M., Bevan, R., & Martin, N. (2016). 3D printing of wood fibre biocomposites: From mechanical to actuation functionality. *Materials and Design*, 96, 106–114. <https://doi.org/10.1016/j.matdes.2016.02.018>
- Lee, A. Y., An, J., & Chua, C. K. (2017). Two-Way 4D Printing: A Review on the Reversibility of 3D-Printed Shape Memory Materials. *Engineering*, 3(5), 663–674.
<https://doi.org/10.1016/J.ENG.2017.05.014>

- Lee, B., Jiao, A., Yu, S., You, J. B., Kim, D. H., & Im, S. G. (2013). Initiated chemical vapor deposition of thermoresponsive poly (N-vinylcaprolactam) thin films for cell sheet engineering. *Acta Biomaterialia*, 9(8), 7691–7698. <https://doi.org/10.1016/j.actbio.2013.04.049>
- Lee, J.-Y., An, J., & Chua, C. K. (2017). Fundamentals and applications of 3D printing for novel materials. *Applied Materials Today*, 7, 120–133. <https://doi.org/10.1016/j.apmt.2017.02.004>
- Lee, S. C., Kwon, I. K., & Park, K. (2013). Hydrogels for delivery of bioactive agents: A historical perspective. *Advanced Drug Delivery Reviews*, 65(1), 17–20. <https://doi.org/10.1016/j.addr.2012.07.015>
- Lee, T. H., & Jho, J. Y. (2018). Temperature-Responsive Actuators Fabricated with PVA/PNIPAAm Interpenetrating Polymer Network Bilayers. *Macromolecular Research*, 26(7), 659–664. <https://doi.org/10.1007/s13233-018-6084-2>
- Lemanowicz, M., Gierczycki, A., Kuźnik, W., Sancewicz, R., & Imiela, P. (2014). Determination of Lower Critical Solution Temperature of thermosensitive flocculants. *Minerals Engineering*, 69, 170–176. <https://doi.org/10.1016/j.mineng.2014.07.022>
- Lewandowska, K. (2014). Miscibility and interactions in chitosan and polyacrylamide mixtures. *Progress on Chemistry and Application of Chitin and Its Derivatives*, 19(1–2), 65–72. <https://doi.org/10.15259/PCACD.19.07>
- Li, J., Jia, X., & Yin, L. (2021). Hydrogel: Diversity of Structures and Applications in Food Science. In *Food Reviews International* (Vol. 37, Issue 3, pp. 313–372). <https://doi.org/10.1080/87559129.2020.1858313>
- Li, Xiaomo, Zhong, H., Li, X., Jia, F., Cheng, Z., Zhang, L., Yin, J., An, L., & Guo, L. (2014). Synthesis of attapulгите/N-isopropylacrylamide and its use in drug release. *Materials Science and Engineering C*, 45, 170–175. <https://doi.org/10.1016/j.msec.2014.08.056>
- Li, Xue, Cai, X., Gao, Y., & Serpe, M. J. (2017). Reversible bidirectional bending of hydrogel-based bilayer actuators. *Journal of Materials Chemistry B*, 5(15), 2804–2812. <https://doi.org/10.1039/C7TB00426E>
- Liu, F., & Urban, M. W. (2010). Recent advances and challenges in designing stimuli-responsive polymers. *Progress in Polymer Science (Oxford)*, 35(1–2), 3–23. <https://doi.org/10.1016/j.progpolymsci.2009.10.002>
- Liu, Jiayu, Erol, O., Pantula, A., Liu, W., Jiang, Z., Kobayashi, K., Chatterjee, D., Hibino, N., Romer, L. H., Kang, S. H., Nguyen, T. D., & Gracias, D. H. (2019). Dual-Gel 4D Printing of Bioinspired Tubes. *ACS Applied Materials and Interfaces*, 11(8), 8492–8498. <https://doi.org/10.1021/acsami.8b17218>
- Liu, Juan, Su, C., Chen, Y., Tian, S., Lu, C., Huang, W., & Lv, Q. (2022). Current Understanding of the Applications of Photocrosslinked Hydrogels in Biomedical Engineering. In *Gels* (Vol. 8, Issue 4, p. 216). Multidisciplinary Digital Publishing Institute. <https://doi.org/10.3390/gels8040216>
- Liu, Juan, Zheng, H., Poh, P. S. P., Machens, H. G., & Schilling, A. F. (2015). Hydrogels for engineering of perfusable vascular networks. *International Journal of Molecular Sciences*, 16(7), 15997–16016. <https://doi.org/10.3390/ijms160715997>

- Liu, L., Bai, S., Yang, H., Li, S., Quan, J., Zhu, L., & Nie, H. (2016). Controlled release from thermo-sensitive PNVCL-co-MAA electrospun nanofibers: The effects of hydrophilicity/hydrophobicity of a drug. *Materials Science and Engineering C*, 67, 581–589. <https://doi.org/10.1016/j.msec.2016.05.083>
- Liu, T., Zhou, T., Yao, Y., Zhang, F., Liu, L., Liu, Y., & Leng, J. (2017). Stimulus methods of multi-functional shape memory polymer nanocomposites: A review. In *Composites Part A: Applied Science and Manufacturing* (Vol. 100, pp. 20–30). <https://doi.org/10.1016/j.compositesa.2017.04.022>
- Liu, Ye, Wang, R., & Chung, T. S. (2001). Chemical cross-linking modification of polyimide membranes for gas separation. *Journal of Membrane Science*, 189(2), 231–239. [https://doi.org/10.1016/S0376-7388\(01\)00415-X](https://doi.org/10.1016/S0376-7388(01)00415-X)
- Liu, Yuanfen, Ran, Y., Ge, Y., Raza, F., Li, S., Zafar, H., Paiva-Santos, A. C., Yu, C., Sun, M., Zhu, Y., Li, F., & Wu, Y. (2022). pH-Sensitive Peptide Hydrogels as a Combination Drug Delivery System for Cancer Treatment. *Pharmaceutics*, 14(3). <https://doi.org/10.3390/pharmaceutics14030652>
- Liu, Yuyan, Han, C., Tan, H., & Du, X. (2010). Thermal, mechanical and shape memory properties of shape memory epoxy resin. *Materials Science and Engineering A*, 527(10–11), 2510–2514. <https://doi.org/10.1016/j.msea.2009.12.014>
- Lusina, A., & Cegłowski, M. (2022). Molecularly Imprinted Polymers as State-of-the-Art Drug Carriers in Hydrogel Transdermal Drug Delivery Applications. *Polymers*, 14(3). <https://doi.org/10.3390/polym14030640>
- M. M. Otrokov, I. I. Klimovskikh, F. Calleja, A. M. S., O. Vilkov, A. G. Rybkin, D. Estyunin, S. Mu, J. H. D., A. L. Vázquez de Parga, R. Miranda, H. O., & F. Guinea, J. I. Cerdá, E. V. Chulkov, A. A. (2018). *Ac ce pte d M us. III*, 0–13.
- Maeda, Y., Nakamura, T., & Ikeda, I. (2002). Hydration and Phase Behavior of Poly (N -vinylcaprolactam) and Poly (N -vinylpyrrolidone) in Water. *Macromolecules*, 32, 217–222. <https://doi.org/10.1021/ma011034+>
- Mahltig, B. (2016). Smart hydrophobic and soil-repellent protective composite coatings for textiles and leather. In *Smart Composite Coatings and Membranes: Transport, Structural, Environmental and Energy Applications*. Elsevier Ltd. <https://doi.org/10.1016/B978-1-78242-283-9.00010-5>
- Maitra, J., & Shukla, V. K. (2014). Cross-linking in Hydrogels - A Review. *American Journal of Polymer Science*, 4(2), 25–31. <https://doi.org/10.5923/j.ajps.20140402.01>
- Manapat, J. Z., Chen, Q., Ye, P., & Advincula, R. C. (2017). 3D Printing of Polymer Nanocomposites via Stereolithography. *Macromolecular Materials and Engineering*, 302(9), 1–13. <https://doi.org/10.1002/mame.201600553>
- Mao, H., Qiu, Z., Xie, B., Wang, Z., Shen, Z., & Hou, W. (2016). *Development and Application of Ultra-High Temperature Drilling Fluids in Offshore Oilfield Around Bohai Sea Bay Basin, China*. <https://doi.org/10.4043/26384-ms>
- Mao, S., Johir, M. A. H., Onggowarsito, C., Feng, A., Nghiem, L. D., & Fu, Q. (2022). Recent developments of hydrogel based solar water purification technology. In *Materials Advances* (Vol. 3, Issue 3, pp. 1322–1340). Royal Society of Chemistry. <https://doi.org/10.1039/d1ma00894c>

- Mao, Y., Ding, Z., Yuan, C., Ai, S., Isakov, M., Wu, J., Wang, T., Dunn, M. L., & Qi, H. J. (2016). 3D Printed Reversible Shape Changing Components with Stimuli Responsive Materials. *Scientific Reports*, 6(1), 24761. <https://doi.org/10.1038/srep24761>
- Mao, Y., Yu, K., Isakov, M. S., Wu, J., Dunn, M. L., & Jerry Qi, H. (2015). Sequential Self-Folding Structures by 3D Printed Digital Shape Memory Polymers. *Scientific Reports*, 5(1), 13616. <https://doi.org/10.1038/srep13616>
- Marsili, L., Dal Bo, M., Berti, F., & Toffoli, G. (2021). Chitosan-based biocompatible copolymers for thermoresponsive drug delivery systems: On the development of a standardization system. In *Pharmaceutics* (Vol. 13, Issue 11, p. 1876). Multidisciplinary Digital Publishing Institute. <https://doi.org/10.3390/pharmaceutics13111876>
- Martínez-Pellitero, S., Castro, M. A., Fernández-Abia, A. I., González, S., & Cuesta, E. (2017). Analysis of influence factors on part quality in micro-SLA technology. *Procedia Manufacturing*, 13, 856–863. <https://doi.org/10.1016/j.promfg.2017.09.143>
- Martinez, P. R., Goyanes, A., Basit, A. W., & Gaisford, S. (2017). Fabrication of Drug-Loaded Hydrogels with Stereolithographic 3D Printing. *International Journal of Pharmaceutics*. <https://doi.org/10.1016/j.ijpharm.2017.09.003>
- Melchels, F. P., Feijen, J., & Grijpma, D. W. (2010). A review on stereolithography and its applications in biomedical engineering. In *Biomaterials* (Vol. 31, Issue 24, pp. 6121–6130). <https://doi.org/10.1016/j.biomaterials.2010.04.050>
- Meng, H., & Li, G. (2013). A review of stimuli-responsive shape memory polymer composites. *Polymer (United Kingdom)*, 54(9), 2199–2221. <https://doi.org/10.1016/j.polymer.2013.02.023>
- Messing, R., & Schmidt, A. M. (2011). Perspectives for the mechanical manipulation of hybrid hydrogels. *Polym. Chem.*, 2(1), 18–32. <https://doi.org/10.1039/C0PY00129E>
- Miao, S., Zhu, W., Castro, N. J., Nowicki, M., Zhou, X., Cui, H., Fisher, J. P., & Zhang, L. G. (2016). 4D printing smart biomedical scaffolds with novel soybean oil epoxidized acrylate. *Scientific Reports*, 6(1), 27226. <https://doi.org/10.1038/srep27226>
- Michalik, R., & Wandzik, I. (2020). A mini-review on chitosan-based hydrogels with potential for sustainable agricultural applications. *Polymers*, 12(10), 1–16. <https://doi.org/10.3390/polym12102425>
- Moad, G. (2017). RAFT polymerization to form stimuli-responsive polymers. *Polym. Chem*, 8. <https://doi.org/10.1039/c6py01849a>
- Mohammed, M. N., Yusoh, K. Bin, & Shariffuddin, J. H. B. H. (2018). Poly(N-vinyl caprolactam) thermoresponsive polymer in novel drug delivery systems: A review. *Materials Express*, 8(1), 21–34. <https://doi.org/10.1166/mex.2018.1406>
- Mokhtar, S. M. A., Alvarez de Eulate, E., Yamada, M., Prow, T. W., & Evans, D. R. (2021). Conducting polymers in wearable devices. *MEDICAL DEVICES & SENSORS*, 4(1), e10160. <https://doi.org/10.1002/mds3.10160>
- Momeni, F., M.Mehdi Hassani.N, S., Liu, X., & Ni, J. (2017). A review of 4D printing. *Materials and Design*, 122, 42–79. <https://doi.org/10.1016/j.matdes.2017.02.068>

- Mondschein, R. J., Kanitkar, A., Williams, C. B., Verbridge, S. S., & Long, T. E. (2017). Polymer structure-property requirements for stereolithographic 3D printing of soft tissue engineering scaffolds. In *Biomaterials* (Vol. 140, pp. 170–188). Elsevier. <https://doi.org/10.1016/j.biomaterials.2017.06.005>
- Mulakkal, M. C., Trask, R. S., Ting, V. P., & Seddon, A. M. (2018). Responsive cellulose-hydrogel composite ink for 4D printing. *Materials & Design*, *160*, 108–118. <https://doi.org/10.1016/j.matdes.2018.09.009>
- Murray, K. A., Kennedy, J. E., McEvoy, B., Vrain, O., Ryan, D., Cowman, R., & Higginbotham, C. L. (2013). Effects of gamma ray and electron beam irradiation on the mechanical, thermal, structural and physicochemical properties of poly (ether-block-amide) thermoplastic elastomers. *Journal of the Mechanical Behavior of Biomedical Materials*, *17*, 252–268. <https://doi.org/10.1016/j.jmbbm.2012.09.011>
- Mutlu, R., Alici, G., Panhuis, M. In Het, & Spinks, G. (2015). Effect of flexure hinge type on a 3D printed fully compliant prosthetic finger. *IEEE/ASME International Conference on Advanced Intelligent Mechatronics, AIM, 2015-Augus*, 790–795. <https://doi.org/10.1109/AIM.2015.7222634>
- Nadgorny, M., Xiao, Z., Chen, C., & Connal, L. A. (2016). Three-Dimensional Printing of pH-Responsive and Functional Polymers on an Affordable Desktop Printer. *ACS Applied Materials and Interfaces*, *8*(42), 28946–28954. <https://doi.org/10.1021/acsami.6b07388>
- Naficy, S., Gately, R., Gorkin, R., Xin, H., & Spinks, G. M. (2017). 4D Printing of Reversible Shape Morphing Hydrogel Structures. *Macromolecular Materials and Engineering*, *302*(1), 1–9. <https://doi.org/10.1002/mame.201600212>
- Nagase, K., Yamato, M., Kanazawa, H., & Okano, T. (2018). Poly(N-isopropylacrylamide)-based thermoresponsive surfaces provide new types of biomedical applications. *Biomaterials*, *153*, 27–48. <https://doi.org/10.1016/J.BIOMATERIALS.2017.10.026>
- Nam, S., & Pei, E. (2019). A taxonomy of shape-changing behavior for 4D printed parts using shape-memory polymers. *Progress in Additive Manufacturing*, *4*(2), 167–184. <https://doi.org/10.1007/s40964-019-00079-5>
- Nastysyn, S., Stetsyshyn, Y., Raczowska, J., Nastishin, Y., Melnyk, Y., Panchenko, Y., & Budkowski, A. (2022). Temperature-Responsive Polymer Brush Coatings for Advanced Biomedical Applications. *Polymers*, *14*(19). <https://doi.org/10.3390/polym14194245>
- Neffe, A. T., Loebus, A., Zaupa, A., Stoetzel, C., Müller, F. A., & Lendlein, A. (2011). Gelatin functionalization with tyrosine derived moieties to increase the interaction with hydroxyapatite fillers. *Acta Biomaterialia*, *7*(4), 1693–1701. <https://doi.org/10.1016/j.actbio.2010.11.025>
- Niaki, M. K., Torabi, S. A., & Nonino, F. (2019). Why manufacturers adopt additive manufacturing technologies: The role of sustainability. *Journal of Cleaner Production*, *222*, 381–392. <https://doi.org/10.1016/j.jclepro.2019.03.019>
- Nigro, V., Angelini, R., Bertoldo, M., Bruni, F., Ricci, M. A., & Ruzicka, B. (2017). Dynamical behavior of microgels of interpenetrated polymer networks. *Soft Matter*, *13*(30), 5185–5193. <https://doi.org/10.1039/c7sm00739f>
- Nizardo, N. M., Alimin, D. F., & Lestari, M. L. A. D. (2022). Synthesis and characterization of dual-responsive poly(N-vinylcaprolactam-co-N-

- methylolacrylamide) nanogels. *https://Doi.Org/10.1080/15685551.2022.2086412*, 25(1), 155–164. <https://doi.org/10.1080/15685551.2022.2086412>
- Nowak, D., Ortyl, J., Kamińska-Borek, I., Kukuła, K., Topa, M., & Popielarz, R. (2017). Photopolymerization of hybrid monomers, part I: Comparison of the performance of selected photoinitiators in cationic and free-radical polymerization of hybrid monomers. *Polymer Testing*. <https://doi.org/10.1016/j.polymertesting.2017.10.020>
- Occhetta, P., Visone, R., Russo, L., Cipolla, L., Moretti, M., Rasponi, M., Moretti, M., & Rasponi, M. (n.d.). *VA-086 Methacrylate Gelatine Photopolymerizable Hydrogels: a Parametric Study for Highly Biocompatible 3D Cell Embedding*. <https://doi.org/10.1002/jbm.a.35346/abstract>
- Ohm, C., Brehmer, M., & Zentel, R. (2010). Liquid crystalline elastomers as actuators and sensors. *Advanced Materials*, 22(31), 3366–3387. <https://doi.org/10.1002/adma.200904059>
- Oliver, K., Seddon, A., & Trask, R. S. (2016). Morphing in nature and beyond: a review of natural and synthetic shape-changing materials and mechanisms. In *Journal of Materials Science* (Vol. 51, Issue 24, pp. 10663–10689). Springer. <https://doi.org/10.1007/s10853-016-0295-8>
- Ortega-García, A., Martínez-Bernal, B. G., Ceja, I., Mendizábal, E., Puig-Arévalo, J. E., & Pérez-Carrillo, L. A. (2022). Drug Delivery from Stimuli-Responsive Poly(Nisopropylacrylamide-co-N-isopropylmethacrylamide)/Chitosan Core/Shell Nanohydrogels. *Polymers*, 14(3), 522. <https://doi.org/10.3390/polym14030522>
- Otero, T. F., & Valero, L. (2017). Bending Monolayer Artificial Muscle. *ChemElectroChem*, 4(12), 3276–3282. <https://doi.org/10.1002/celec.201700713>
- Pagonis, K., & Bokias, G. (2004). Upper critical solution temperature—type cononsolvency of poly(N,N-dimethylacrylamide) in water—organic solvent mixtures. *Polymer*, 45(7), 2149–2153. <https://doi.org/10.1016/j.polymer.2004.01.063>
- Pan, X., Tasdelen, M. A., Laun, J., Junkers, T., Yagci, Y., & Matyjaszewski, K. (2016). Photomediated controlled radical polymerization. In *Progress in Polymer Science* (Vol. 62, pp. 73–125). Pergamon. <https://doi.org/10.1016/j.progpolymsci.2016.06.005>
- Park, J. J., Park, D. M., Youk, J. H., Yu, W. R., & Lee, J. (2010). Functionalization of multi-walled carbon nanotubes by free radical graft polymerization initiated from photoinduced surface groups. *Carbon*, 48(10), 2899–2905. <https://doi.org/10.1016/j.carbon.2010.04.024>
- Park, K. R., & Nho, Y. C. (2003). Synthesis of PVA/PVP hydrogels having two-layer by radiation and their physical properties. *Radiation Physics and Chemistry*, 67(3–4), 361–365. [https://doi.org/10.1016/S0969-806X\(03\)00067-7](https://doi.org/10.1016/S0969-806X(03)00067-7)
- Patel, A., & Mequanint, K. (2011). Synthesis and characterization of polyurethane-block-poly(2-hydroxyethyl methacrylate) hydrogels and their surface modification to promote cell affinity. *Journal of Bioactive and Compatible Polymers*, 26(2), 114–129. <https://doi.org/10.1177/0883911511398713>
- Pei, E. (2014). 4D Printing: dawn of an emerging technology cycle. *Assembly Automation*, 34(4), 310–314. <https://doi.org/10.1108/AA-07-2014-062>

- Pelosi, C., Guazzelli, E., Calosi, M., Bernazzani, L., Tiné, M. R., Duce, C., & Martinelli, E. (2021). Investigation of the lcst-thermo-responsive behavior of novel oligo(Ethylene glycol)-modified pentafluorostyrene homopolymers. *Applied Sciences (Switzerland)*, *11*(6), 2711. <https://doi.org/10.3390/app11062711>
- Pereira, R. F., & Bártolo, P. J. (2015). 3D Photo-Fabrication for Tissue Engineering and Drug Delivery. *Engineering*, *1*(1), 090–112. <https://doi.org/10.15302/J-ENG-2015015>
- Pietsch, C., Hoogenboom, R., & Schubert, U. S. (2010). PMMA based soluble polymeric temperature sensors based on UCST transition and solvatochromic dyes. *Polymer Chemistry*, *1*(7), 1005–1008. <https://doi.org/10.1039/c0py00162g>
- Qiu, Y., & Park, K. (2012). Environment-sensitive hydrogels for drug delivery. In *Advanced Drug Delivery Reviews* (Vol. 64, Issue SUPPL., pp. 49–60). Elsevier. <https://doi.org/10.1016/j.addr.2012.09.024>
- Quoika, P. K., Podewitz, M., Wang, Y., Kamenik, A. S., Loeffler, J. R., & Liedl, K. R. (2020). Thermosensitive Hydration of Four Acrylamide-Based Polymers in Coil and Globule Conformations. *Journal of Physical Chemistry B*, *124*(43), 9745–9756. <https://doi.org/10.1021/acs.jpcc.0c07232>
- Raimi-Abraham, B. T., Mahalingam, S., Edirisinghe, M., & Craig, D. Q. M. (2014). Generation of poly(N-vinylpyrrolidone) nanofibres using pressurised gyration. *Materials Science and Engineering C*, *39*(1), 168–176. <https://doi.org/10.1016/j.msec.2014.02.016>
- Ramírez-Jiménez, A., Montoya-Villegas, K. A., Licea-Claverie, A., & González-Ayón, M. A. (2019). Tunable thermo-responsive copolymers from DEGMA and OEGMA synthesized by RAFT polymerization and the effect of the concentration and saline phosphate buffer on its phase transition. *Polymers*, *11*(10), 1657. <https://doi.org/10.3390/polym11101657>
- Ratner, B. D., & Zhang, G. (2020). A History of Biomaterials. In *Biomaterials Science* (Fourth Edi). Elsevier. <https://doi.org/10.1016/b978-0-12-816137-1.00002-7>
- Raviv, D., Zhao, W., McKnelly, C., Papadopoulou, A., Kadambi, A., Shi, B., Hirsch, S., Dikovsky, D., Zyracki, M., Olguin, C., Raskar, R., & Tibbitts, S. (2014). Active printed materials for complex self-evolving deformations. *Scientific Reports*, *4*(1), 7422. <https://doi.org/10.1038/srep07422>
- Ribas-Massonis, A., Cicujano, M., Duran, J., Besalú, E., & Poater, A. (2022). Free-Radical Photopolymerization for Curing Products for Refinish Coatings Market. In *Polymers* (Vol. 14, Issue 14, p. 2856). Multidisciplinary Digital Publishing Institute. <https://doi.org/10.3390/polym14142856>
- Roth, P. J., & Lowe, A. B. (2017). Stimulus-responsive polymers. *Polym. Chem.*, *8*(1), 10–11. <https://doi.org/10.1039/C6PY90169G>
- Roy, D., Cambre, J. N., & Sumerlin, B. S. (2010). Future perspectives and recent advances in stimuli-responsive materials. In *Progress in Polymer Science (Oxford)* (Vol. 35, Issues 1–2, pp. 278–301). Pergamon. <https://doi.org/10.1016/j.progpolymsci.2009.10.008>
- Saba, N., Jawaid, M., & Sultan, M. T. H. (2018). An overview of mechanical and physical testing of composite materials. In *Mechanical and Physical Testing of Biocomposites, Fibre-Reinforced Composites and Hybrid Composites* (pp. 1–12). Elsevier. <https://doi.org/10.1016/B978-0-08-102292-4.00001-1>

- Sánchez, J., Dax, D., Tapiero, Y., Xu, C., & Willför, S. (2021). Bio-Based Hydrogels With Ion Exchange Properties Applied to Remove Cu(II), Cr(VI), and As(V) Ions From Water. *Frontiers in Bioengineering and Biotechnology*, 9, 327. <https://doi.org/10.3389/fbioe.2021.656472>
- Saritha, D., & Boyina, D. (2021). A concise review on 4D printing technology. *Materials Today: Proceedings*, 46, 692–695. <https://doi.org/10.1016/j.matpr.2020.12.016>
- Sarwan, T., Kumar, P., Choonara, Y. E., & Pillay, V. (2020). Hybrid Thermo-Responsive Polymer Systems and Their Biomedical Applications. In *Frontiers in Materials* (Vol. 7, p. 73). Frontiers Media S.A. <https://doi.org/10.3389/fmats.2020.00073>
- Saxena, A. K. (2010). Synthetic biodegradable hydrogel (PleuraSeal) sealant for sealing of lung tissue after thoracoscopic resection. *Journal of Thoracic and Cardiovascular Surgery*, 139(2), 496–497. <https://doi.org/10.1016/j.jtcvs.2008.11.003>
- Scherzinger, C., Schwarz, A., Bardow, A., Leonhard, K., & Richtering, W. (2014). Cononsolvency of poly-N-isopropyl acrylamide (PNIPAM): Microgels versus linear chains and macrogels. *Current Opinion in Colloid and Interface Science*, 19(2), 84–94. <https://doi.org/10.1016/j.cocis.2014.03.011>
- Schmaljohann, D. (2006). Thermo- and pH-responsive polymers in drug delivery. In *Advanced Drug Delivery Reviews* (Vol. 58, Issue 15, pp. 1655–1670). <https://doi.org/10.1016/j.addr.2006.09.020>
- Shahrubudin, N., Koshy, P., Alipal, J., Kadir, M. H. A., & Lee, T. C. (2020). Challenges of 3D printing technology for manufacturing biomedical products: A case study of Malaysian manufacturing firms. *Heliyon*, 6(4), e03734. <https://doi.org/10.1016/j.heliyon.2020.e03734>
- Sharma, A., & Singholi, A. K. S. (2019). A comprehensive review of materials used for 4D printing. In *Lecture Notes in Mechanical Engineering*. Springer Singapore. https://doi.org/10.1007/978-981-13-6469-3_69
- Shin, J., Braun, P. V., & Lee, W. (2010). Fast response photonic crystal pH sensor based on templated photo-polymerized hydrogel inverse opal. *Sensors and Actuators, B: Chemical*, 150(1), 183–190. <https://doi.org/10.1016/j.snb.2010.07.018>
- Singh, A., Sharma, P. K., Garg, V. K., & Garg, G. (2010). Hydrogels: A review. *International Journal of Pharmaceutical Sciences Review and Research*, 4(2), 97–105.
- Singh, S., Rajkumar, B., Gupta, V., & Bhatt, A. (2017). Current photo-initiators in dental materials. *International Journal of Applied Dental Sciences*, 3(1), 17–20.
- Skylar Tibbits. (n.d.). *Skylar Tibbits: The emergence of "4D printing"* | TED Talk. 2013. Retrieved 21 May 2018, from https://www.ted.com/talks/skylar_tibbits_the_emergence_of_4d_printing
- Soni, H., Bhopal, D. H. S., & Author, C. (2021). Hydrogels as Effective drug Delivery Systems. *J Anat Physiol*, 2(2), 17–21.
- Sood, A. K., Ohdar, R. K., & Mahapatra, S. S. (2010). Parametric appraisal of mechanical property of fused deposition modelling processed parts. *Materials and Design*, 31(1), 287–295. <https://doi.org/10.1016/j.matdes.2009.06.016>

- Stojkov, G., Niyazov, Z., Picchioni, F., & Bose, R. K. (2021). Relationship between structure and rheology of hydrogels for various applications. In *Gels* (Vol. 7, Issue 4, p. 255). Multidisciplinary Digital Publishing Institute. <https://doi.org/10.3390/gels7040255>
- Stoychev, G., Kirillova, A., & Ionov, L. (2019). Light-Responsive Shape-Changing Polymers. *Advanced Optical Materials*, 7(16), 1–30. <https://doi.org/10.1002/adom.201900067>
- Strandman, S., & Zhu, X. X. (2015). Thermo-responsive block copolymers with multiple phase transition temperatures in aqueous solutions. *Progress in Polymer Science*, 42, 154–176. <https://doi.org/10.1016/j.progpolymsci.2014.10.008>
- Stuart, M. A. C., Huck, W. T. S., Genzer, J., Müller, M., Ober, C., Stamm, M., Sukhorukov, G. B., Szleifer, I., Tsukruk, V. V., Urban, M., Winnik, F., Zauscher, S., Luzinov, I., & Minko, S. (2010). Emerging applications of stimuli-responsive polymer materials. *Nature Materials*, 9(2), 101–113. <https://doi.org/10.1038/nmat2614>
- Studart, A. R. (2015). Biologically inspired dynamic material systems. *Angewandte Chemie - International Edition*, 54(11), 3400–3416. <https://doi.org/10.1002/anie.201410139>
- Su, M., Ruan, L., Dong, X., Tian, S., Lang, W., Wu, M., Chen, Y., Lv, Q., & Lei, L. (2023). Current state of knowledge on intelligent-response biological and other macromolecular hydrogels in biomedical engineering: A review. In *International Journal of Biological Macromolecules* (Vol. 227, pp. 472–492). Elsevier. <https://doi.org/10.1016/j.ijbiomac.2022.12.148>
- Sun, H. B., Takada, K., Kawata, S., Oberlerchner, J. T., Rosenau, T., Potthast, A., Hina, S., Zhang, Y., Wang, H., Vaughan, A. D., Duke, S. R., Sun, H. B., Kawata, S., & Polat, O. (2008). REACTION ANALYSIS OF TEMPLATED POLYMER SYSTEMS Except. *Applied Physics Letters*, 36(September), 1–92. <https://doi.org/10.1007/b94405>
- Sun, H., Kabb, C. P., Sims, M. B., & Sumerlin, B. S. (2019). Architecture-transformable polymers: Reshaping the future of stimuli-responsive polymers. In *Progress in Polymer Science* (Vol. 89, pp. 61–75). Pergamon. <https://doi.org/10.1016/j.progpolymsci.2018.09.006>
- Sydney Gladman, A., Matsumoto, E. A., Nuzzo, R. G., Mahadevan, L., & Lewis, J. A. (2016). Biomimetic 4D printing. *Nature Materials*, 15(4), 413–418. <https://doi.org/10.1038/nmat4544>
- Száráz, I., & Forsling, W. (2000). A spectroscopic study of the solvation of 1-vinyl-2-pyrrolidone and poly(1-vinyl-2-pyrrolidone) in different solvents. *Polymer*, 41(13), 4831–4839. [https://doi.org/10.1016/S0032-3861\(99\)00705-3](https://doi.org/10.1016/S0032-3861(99)00705-3)
- Takeuchi, A. (2020). Mixing entropy of exact equiatomic high-entropy alloys formed into a single phase. *Materials Transactions*, 61(9), 1717–1726. <https://doi.org/10.2320/matertrans.MT-M2020141>
- Taylor, D., & Dua, R. (2020). Intelligent Hydrogels in Diagnostics and Therapeutics. In *Intelligent Hydrogels in Diagnostics and Therapeutics*. <https://doi.org/10.1201/9781003036050>
- Thompson, M. C., Barad, B. A., Wolff, A. M., Sun Cho, H., Schotte, F., Schwarz, D. M. C., Anfinrud, P., & Fraser, J. S. (2019). Temperature-jump solution X-ray scattering

- reveals distinct motions in a dynamic enzyme. *Nature Chemistry*, *11*(11), 1058–1066. <https://doi.org/10.1038/s41557-019-0329-3>
- Tibbits, S., McKnelly, C., Olguin, C., Dikovsky, D., & Hirsch, S. (2014). 4d Printing and Universal Transformation. *ACADIA 14 Design Agency: Proceedings of the 34th Annual Conference of the Association for Computer Aided Design in Architecture*, 539–548.
- Ullah, F., Othman, M. B. H., Javed, F., Ahmad, Z., & Akil, H. M. (2015). Classification, processing and application of hydrogels: A review. *Materials Science and Engineering C*, *57*, 414–433. <https://doi.org/10.1016/j.msec.2015.07.053>
- Unagolla, J. M., & Jayasuriya, A. C. (2020). Hydrogel-based 3D bioprinting: A comprehensive review on cell-laden hydrogels, bioink formulations, and future perspectives. In *Applied Materials Today* (Vol. 18, p. 100479). Elsevier Ltd. <https://doi.org/10.1016/j.apmt.2019.100479>
- van Manen, T., Janbaz, S., & Zadpoor, A. A. (2018). Programming the shape-shifting of flat soft matter. *Materials Today*, *21*(2), 144–163. <https://doi.org/10.1016/j.mattod.2017.08.026>
- Vandenhoute, M., Snoeck, D., Vanderleyden, E., De Belie, N., Van Vlierberghe, S., & Dubruel, P. (2017). Stability of Pluronic®F127 bismethacrylate hydrogels: Reality or utopia? *Polymer Degradation and Stability*, *146*, 201–211. <https://doi.org/10.1016/j.polymdegradstab.2017.10.003>
- Varaprasad, K., Raghavendra, G. M., Jayaramudu, T., Yallapu, M. M., & Sadiku, R. (2017). A mini review on hydrogels classification and recent developments in miscellaneous applications. *Materials Science and Engineering C*, *79*, 958–971. <https://doi.org/10.1016/j.msec.2017.05.096>
- Vihola, H., Laukkanen, A., Tenhu, H., & Hirvonen, J. (2008). Drug release characteristics of physically cross-linked thermosensitive poly(N-vinylcaprolactam) hydrogel particles. *Journal of Pharmaceutical Sciences*, *97*(11), 4783–4793. <https://doi.org/10.1002/jps.21348>
- Vihola, H., Marttila, A. K., Pakkanen, J. S., Andersson, M., Laukkanen, A., Kaukonen, A. M., Tenhu, H., & Hirvonen, J. (2007). Cell-polymer interactions of fluorescent polystyrene latex particles coated with thermosensitive poly(N-isopropylacrylamide) and poly(N-vinylcaprolactam) or grafted with poly(ethylene oxide)-macromonomer. *International Journal of Pharmaceutics*, *343*(1–2), 238–246. <https://doi.org/10.1016/j.ijpharm.2007.04.020>
- Volkov, A. G., Foster, J. C., Ashby, T. A., Walker, R. K., Johnson, J. A., & Markin, V. S. (2010). *Mimosa pudica*: Electrical and mechanical stimulation of plant movements. *Plant, Cell and Environment*, *33*(2), 163–173. <https://doi.org/10.1111/j.1365-3040.2009.02066.x>
- Wang, Q., Tian, X., Huang, L., Li, D., Malakhov, A. V., & Polilov, A. N. (2018). Programmable morphing composites with embedded continuous fibers by 4D printing. *Materials and Design*, *155*, 404–413. <https://doi.org/10.1016/j.matdes.2018.06.027>
- Wang, X., Jiang, M., Zhou, Z., Gou, J., & Hui, D. (2017). 3D printing of polymer matrix composites: A review and prospective. *Composites Part B: Engineering*, *110*, 442–458. <https://doi.org/10.1016/j.compositesb.2016.11.034>

- Wang, Yifei, Xie, T., Yang, J., Lei, M., Fan, J., Meng, Z., Xue, M., Qiu, L., Qi, F., & Wang, Z. (2019). Fast screening of antibiotics in milk using a molecularly imprinted two-dimensional photonic crystal hydrogel sensor. *Analytica Chimica Acta*, *1070*, 97–103. <https://doi.org/10.1016/j.aca.2019.04.031>
- Wang, Yuting, Zhang, S., & Wang, J. (2021). Photo-crosslinkable hydrogel and its biological applications. *Chinese Chemical Letters*, *32*(5), 1603–1614. <https://doi.org/10.1016/j.ccllet.2020.11.073>
- Ward, I. M. (2009). Polymers: Chemistry and Physics of Modern Materials, 3rd edition, by J.M.G. Cowie and V. Arrighi. *Contemporary Physics*, *50*(6), 670–670. <https://doi.org/10.1080/00107510902992270>
- Wegrzynowska-Drzymalska, K., Grebicka, P., Mlynarczyk, D. T., Chelminiak-Dudkiewicz, D., Kaczmarek, H., Goslinski, T., & Ziegler-Borowska, M. (2020). Crosslinking of chitosan with dialdehyde chitosan as a new approach for biomedical applications. *Materials*, *13*(15), 1–27. <https://doi.org/10.3390/ma13153413>
- Wilke, P., Coger, V., Nachev, M., Schachschal, S., Million, N., Barcikowski, S., Sures, B., Reimers, K., Vogt, P. M., & Pich, A. (2015). Biocompatible microgel-modified electrospun fibers for zinc ion release. *Polymer*, *61*, 163–173. <https://doi.org/10.1016/j.polymer.2015.01.078>
- Wu, A., Ruan, Z., & Wang, J. (2022). Rheological behavior of paste in metal mines. In *International Journal of Minerals, Metallurgy and Materials* (Vol. 29, Issue 4, pp. 717–726). <https://doi.org/10.1007/s12613-022-2423-6>
- Wu, J. J., Huang, L. M., Zhao, Q., & Xie, T. (2018). 4D Printing: History and Recent Progress. In *Chinese Journal of Polymer Science (English Edition)* (Vol. 36, Issue 5, pp. 563–575). <https://doi.org/10.1007/s10118-018-2089-8>
- Wu, Jiangtao, Yuan, C., Ding, Z., Isakov, M., Mao, Y., Wang, T., Dunn, M. L., & Qi, H. J. (2016). Multi-shape active composites by 3D printing of digital shape memory polymers. *Scientific Reports*, *6*(1), 24224. <https://doi.org/10.1038/srep24224>
- Wu, Jie, Wei, W., Wang, L.-Y., Su, Z.-G., & Ma, G.-H. (2007). A thermosensitive hydrogel based on quaternized chitosan and poly(ethylene glycol) for nasal drug delivery system. *Biomaterials*, *28*(13), 2220–2232. <https://doi.org/10.1016/j.biomaterials.2006.12.024>
- Wu, Y.-H., Park, H. B., Kai, T., Freeman, B. D., & Kalika, D. S. (2010). Water uptake, transport and structure characterization in poly(ethylene glycol) diacrylate hydrogels. *Journal of Membrane Science*, *347*(1–2), 197–208. <https://doi.org/10.1016/j.memsci.2009.10.025>
- Wu, Y. H., Park, H. B., Kai, T., Freeman, B. D., & Kalika, D. S. (2010). Water uptake, transport and structure characterization in poly(ethylene glycol) diacrylate hydrogels. *Journal of Membrane Science*, *347*(1–2), 197–208. <https://doi.org/10.1016/j.memsci.2009.10.025>
- Wurm, F. R., Boyer, C., & Sumerlin, B. S. (2021). Progress on Stimuli-Responsive Polymers. In *Macromolecular Rapid Communications* (Vol. 42, Issue 18). <https://doi.org/10.1002/marc.202100512>
- Xia, S., Song, S., & Gao, G. (2018). Robust and flexible strain sensors based on dual physically cross-linked double network hydrogels for monitoring human-motion. *Chemical Engineering Journal*, *354*, 817–824. <https://doi.org/10.1016/j.cej.2018.08.053>

- Xia, Y., He, Y., Zhang, F., Liu, Y., & Leng, J. (2021). A Review of Shape Memory Polymers and Composites: Mechanisms, Materials, and Applications. In *Advanced Materials* (Vol. 33, Issue 6). <https://doi.org/10.1002/adma.202000713>
- Xiao, P., Zhang, J., Dumur, F., Tehfe, M. A., Morlet-Savary, F., Graff, B., Gigmes, D., Fouassier, J. P., & Lalevée, J. (2015). Visible light sensitive photoinitiating systems: Recent progress in cationic and radical photopolymerization reactions under soft conditions. *Progress in Polymer Science*, *41*(C), 32–66. <https://doi.org/10.1016/j.progpolymsci.2014.09.001>
- Xie, F., Zhang, T., Bryant, P., Kurusingal, V., Colwell, J. M., & Laycock, B. (2019). Degradation and stabilization of polyurethane elastomers. In *Progress in Polymer Science* (Vol. 90, pp. 211–268). <https://doi.org/10.1016/j.progpolymsci.2018.12.003>
- Yagci, Y., Jockusch, S., & Turro, N. J. (2010). Photoinitiated polymerization: Advances, challenges, and opportunities. In *Macromolecules* (Vol. 43, Issue 15, pp. 6245–6260). <https://doi.org/10.1021/ma1007545>
- Yang, Y., Chen, Y., Wei, Y., & Li, Y. (2016). 3D printing of shape memory polymer for functional part fabrication. *International Journal of Advanced Manufacturing Technology*, *84*(9–12), 2079–2095. <https://doi.org/10.1007/s00170-015-7843-2>
- Zainal, S. H., Mohd, N. H., Suhaili, N., Anuar, F. H., Lazim, A. M., & Othaman, R. (2021). Preparation of cellulose-based hydrogel: A review. In *Journal of Materials Research and Technology* (Vol. 10, pp. 935–952). Elsevier. <https://doi.org/10.1016/j.jmrt.2020.12.012>
- Zarek, M., Layani, M., Cooperstein, I., Sachyani, E., Cohn, D., & Magdassi, S. (2016). 3D Printing of Shape Memory Polymers for Flexible Electronic Devices. *Advanced Materials*, *28*(22), 4449–4454. <https://doi.org/10.1002/adma.201503132>
- Zhang, F., Wei, M., Viswanathan, V. V., Swart, B., Shao, Y., Wu, G., & Zhou, C. (2017). 3D printing technologies for electrochemical energy storage. In *Nano Energy* (Vol. 40, pp. 418–431). <https://doi.org/10.1016/j.nanoen.2017.08.037>
- Zhang, J. T., Huang, S. W., Xue, Y. N., & Zhuo, R. X. (2005). Poly(N-isopropylacrylamide) nanoparticle-incorporated PNIPAAm hydrogels with fast shrinking kinetics. *Macromolecular Rapid Communications*, *26*(16), 1346–1350. <https://doi.org/10.1002/marc.200500298>
- Zhang, Jing, & Xiao, P. (2018). 3D printing of photopolymers. *Polymer Chemistry*, *9*(13), 1530–1540. <https://doi.org/10.1039/c8py00157j>
- Zhang, Jinnan, Cui, Z., Field, R., Moloney, M. G., Rimmer, S., & Ye, H. (2015). Thermo-responsive microcarriers based on poly(N-isopropylacrylamide). *European Polymer Journal*, *67*, 346–364. <https://doi.org/10.1016/j.eurpolymj.2015.04.013>
- Zhang, Qilu, & Hoogenboom, R. (2015). Polymers with upper critical solution temperature behavior in alcohol/water solvent mixtures. *Progress in Polymer Science*, *48*, 122–142. <https://doi.org/10.1016/j.progpolymsci.2015.02.003>
- Zhang, Quan, Zhang, K., & Hu, G. (2016a). Smart three-dimensional lightweight structure triggered from a thin composite sheet via 3D printing technique. *Scientific Reports*, *6*(November 2015), 1–8. <https://doi.org/10.1038/srep22431>
- Zhang, Quan, Zhang, K., & Hu, G. (2016b). Smart three-dimensional lightweight structure triggered from a thin composite sheet via 3D printing technique. *Scientific Reports*, *6*(1), 22431. <https://doi.org/10.1038/srep22431>

- Zhang, Z., Chen, Z., Wang, Y., Chi, J., Wang, Y., & Zhao, Y. (2019). Bioinspired Bilayer Structural Color Hydrogel Actuator with Multienvironment Responsiveness and Survivability. *Small Methods*, 3(12), 1–7. <https://doi.org/10.1002/smtd.201900519>
- Zhao, Q., Qi, H. J., & Xie, T. (2015). Recent progress in shape memory polymer: New behavior, enabling materials, and mechanistic understanding. *Progress in Polymer Science*, 49–50, 79–120. <https://doi.org/10.1016/j.progpolymsci.2015.04.001>
- Zhao, T., Yu, R., Li, X., Cheng, B., Zhang, Y., Yang, X., Zhao, X., Zhao, Y., & Huang, W. (2018). 4D printing of shape memory polyurethane via stereolithography. *European Polymer Journal*, 101, 120–126. <https://doi.org/10.1016/j.eurpolymj.2018.02.021>
- Zhao, Z., Wu, J., Mu, X., Chen, H., Qi, H. J., & Fang, D. (2017). Origami by frontal photopolymerization. *Science Advances*, 3(4), 1–8. <https://doi.org/10.1126/sciadv.1602326>
- Zheng, J., Xiao, P., Le, X., Lu, W., Théato, P., Ma, C., Du, B., Zhang, J., Huang, Y., & Chen, T. (2018). Mimosa inspired bilayer hydrogel actuator functioning in multi-environments. *Journal of Materials Chemistry C*, 6(6), 1320–1327. <https://doi.org/10.1039/c7tc04879c>
- Zolfagharian, A., Kaynak, A., Khoo, S. Y., & Kouzani, A. (2018). Pattern-driven 4D printing. *Sensors and Actuators, A: Physical*, 274, 231–243. <https://doi.org/10.1016/j.sna.2018.03.034>